Chapter 8: Anthropogenic and Natural Radiative Forcing

Coordinating Lead Authors: Gunnar Myhre (Norway), Drew Shindell (USA)

Lead Authors: François-Marie Bréon (France), William Collins (UK), Jan Fuglestvedt (Norway), Jianping Huang (China), Dorothy Koch (USA), Jean-François Lamarque (USA), David Lee (UK), Blanca Mendoza (Mexico), Teruyuki Nakajima (Japan), Alan Robock (USA), Graeme Stephens (USA), Toshihiko Takemura (Japan), Hua Zhang (China)

Contributing Authors: Olivier Boucher (France), Stig B. Dalsøren (Norway), John Daniel (USA), Piers Forster (UK), Claire Granier (France), Joanna Haigh (UK), Jed O. Kaplan (Switzerland), Brian, O'Neill (USA), Glen Peters (Norway), Julia Pongratz (Germany), Venkatachalam Ramaswamy (USA), Leon Rotstayn (Australia), Paul Young (USA), Jean-Paul Vernier (USA)

Review Editors: Daniel Jacob (USA), A.R. Ravishankara (USA), Keith Shine (UK)

Date of Draft: 5 October 2012

Notes: TSU Compiled Version

Table of Contents

Executive Summary

As in previous IPCC assessments, AR5 uses the radiative forcing[1] (RF) concept, but it also introduces adjusted forcing[2] (AF). Knowledge of RF is essential to understanding human and natural influence on climate in the past and future. The RF concept has been used for many years and in previous IPCC assessments for comparing the strength of the various mechanisms affecting Earth's radiation balance and thus causing climate change. AF is used to characterize some of the more complex forcing agents that involve rapid adjustment of some components of the atmosphere that are assumed constant in the RF concept. Whereas in the RF concept all surface and tropospheric conditions are kept fixed, the AF calculations presented here allow all variables to respond to perturbations except for the ocean and sea ice. The AF and RF values are significantly different for anthropogenic aerosols due to their influence on clouds and on snow cover. The changes to clouds caused by aerosols are rapid adjustments and occur on a time scale much faster than responses of the ocean (even the upper layer) to forcing. RF and AF are estimated over the industrial era from 1750 to 2011 if other periods are not explicitly stated. [8.1; Figure 8.1]

The total anthropogenic RF over the industrial era has a best estimate of 2.4 ± 0.6 W m^{-2} and the AF is 2.2 ± 0.9 W m^{-2} [3]. It is *virtually certain* that the anthropogenic RF is positive. The total anthropogenic RF is 50% higher compared to AR4 (2005) due primarily to reductions in estimated aerosol RF but also to continued growth in greenhouse gas RF. The total AF value is weaker than total RF and has greater uncertainty due to its inclusion of additional impacts on clouds. [8.5.1; Figure 8.17]

RF from the well-mixed greenhouse gases (WMGHG) has increased by 0.20 ± 0.02 W m^{-2} (8%) since AR4 (2005) due to increased concentrations. The RF of WMGHG is 2.83 ± 0.28 W m^{-2}. Of the 0.20 W m^{-2} increase since AR4, 0.01 W m^{-2} is due to updates in the RF calculations and the rest due to concentration changes, mainly from increases in CO_2. The industrial era RF for CO_2 alone is 1.82 ± 0.18 W m^{-2} and is *virtually certain* the strongest component causing a positive RF since 1750. Over the last 15 years, CO_2 has clearly been the dominant contributor to the increase in RF from the WMGHG, with RF of CO_2 having an average growth rate slightly less than 0.3 (0.27 ± 0.03) W m^{-2} per decade. [8.3.2; Figure 8.6]

WMGHG other than CO_2 show a weak increase in RF since AR4 (2005). A small growth in the CH_4 concentration has increased its RF by 2% compared to the AR4 (2005) value to 0.48 ± 0.05 W m^{-2}. N_2O has increased by 6% since AR4 (2005) and has a RF of 0.17 ± 0.02 W m^{-2}. N_2O concentrations continue to rise while those of CFC-12, the third largest WMGHG contributor to RF for several decades, are falling due to phase-out of this chemical under the Montreal Protocol. Since 2011 N_2O has become the third largest WMGHG contributor to RF. The RF from all halocarbons (0.36 W m^{-2}) is very similar to the value in AR4 (2005), with a reduced RF from CFCs but increases from many of their replacements. Four of the halocarbons (CFC-11, CFC-12, CFC-113, and HCFC-22) account for around 85% of the total halocarbon RF. The first three of these compounds have declining RF over the last five years but their combined decrease is compensated for by the increased RF from HCFC-22. Since AR4 (2005) the RF from all HFCs has increased by 78% and has a RF of 0.02 W m^{-2}. There is *high confidence* that the growth rate in RF from all WMGHG is weaker over the last decade than in the 1970s and 1980s owing to a reduced rate of increase in the non-CO_2 RF. [8.3.2; Figure 8.6]

Short-lived GHG contribute substantially to RF. The total RF due to changes in ozone is 0.30 ± 0.20 W m^{-2}, with RF due to tropospheric ozone of 0.40 ± 0.20 W m^{-2} and due to stratospheric ozone of –0.10 ± 0.15 W m^{-2}. Ozone is not emitted directly into the atmosphere; but is formed by photochemical reactions. Tropospheric ozone RF is largely attributed to anthropogenic emissions of methane, carbon monoxide, volatile organics and nitrogen oxides, while stratospheric ozone RF results primarily from ozone depletion by halocarbons. However, there is now *robust evidence* for substantial links between the changes in tropospheric and stratospheric ozone. Estimates are now also provided attributing RF to emitting compounds with ozone depleting substances (ODS) causing ozone RF of –0.20 (–0.30 to 0.0) W m^{-2} and tropospheric

[1] Change in net irradiance at the tropopause after allowing for stratospheric temperatures to readjust to radiative equilibrium, while holding surface and tropospheric temperatures and state variables fixed at the unperturbed values.
[2] Change in net irradiance at the TOA after allowing for atmospheric temperatures, water vapour, clouds and land albedo to adjust, but with all or a portion of surface conditions unchanged.
[3] Uncertainties are given associated with best estimates of RF. The uncertainty values represent the 5–95% (90%) confidence range.

ozone precursors causing ozone RF of 0.50 ± 0.20 W m^{-2}. There is *medium evidence* that tropospheric ozone also has a detrimental impact on vegetation physiology, and therefore on its CO_2 uptake, but there is a *low confidence* on quantitative estimates of this effect. RF for stratospheric water vapour from CH_4 oxidation is 0.07 ± 0.05 W m^{-2}. Recent observations indicate a reduction in the stratospheric water vapour abundance, but this is *very likely* not linked to CH_4 oxidation and is therefore not treated as a RF mechanism. The RF estimates of the short-lived GHG are very similar to estimates in AR4. [8.2; 8.3.3; Figure 8.8]

The uncertainty in the effect of aerosols is large, but slightly reduced since AR4. For the various aerosol effects, the RF initiated by aerosol-radiation-interactions, formerly referred to as *direct aerosol effect*, is given a best estimate of –0.40 ± 0.30 W m^{-2}, RF of aerosol-cloud-interactions is –0.3 (–0.7 to 0) W m^{-2}, and black carbon (BC) on snow and ice is 0.04 (0.02 to 0.09) W m^{-2}. A total aerosol-cloud-interaction is also quantified in terms of the AF concept with an estimate of –0.4 (–0.9 to 0) W m^{-2}. The total aerosol effect is estimated as RF of –0.7 and AF of –0.9 (–1.5 to –0.3) W m^{-2}. The new RF estimates of aerosol are weaker than in AR4 owing to improved knowledge of aerosols rather than changes in aerosol abundances. The large uncertainty in aerosol RF and AF is the dominant contributor to overall net industrial era forcing uncertainty. Despite the large uncertainty range, there is a *high confidence* that aerosols have offset a substantial portion of WMGHG forcing. [8.3.4; 8.5.1; Figure 8.17]

There is *robust evidence* that anthropogenic land use change has increased the land surface albedo, which leads to a RF of –0.15 ± 0.1 W m^{-2}. There is still a large spread of estimates due to different assumptions for the albedo of natural and managed surfaces and for land use changes before 1750. Land use change causes additional modifications that are not radiative but impact the surface temperature. These are more uncertain and they are difficult to quantify, but tend to offset the impact of albedo changes. As a consequence, there is *low agreement* on the sign of the net change in global mean temperature as a result of land use change. [8.3.5]

Satellite observations of total solar irradiance (TSI) changes since 1978 spanning 3 solar cycle minima show a RF of –0.04 ± 0.02 W m^{-2}. There is some diversity in the estimated trends of the composites of various satellite data, but a downward trend in TSI over this time period is *very likely*. Secular trends of TSI before the start of satellite observations rely on a number of indirect proxies. The best estimate of RF from TSI changes over the industrial era is 0.04 ± 0.06 W m^{-2}, which includes greater RF up to 1980 and then a decrease. This RF estimate is substantially weaker than the AR4 estimate due to the addition of the latest solar cycle and inconsistencies in how solar RF has been estimated in earlier IPCC assessments. The recent solar minimum was unusually low and long-lasting and several projections indicate lower TSI for the forthcoming decades. However, current abilities to project solar irradiance are extremely limited so that there is *very low confidence* concerning future solar forcing. [8.4.1; Figure 8.13; Figure 8.14]

The RF of stratospheric aerosols is well understood and can have a large impact on the climate for years to decades after volcanic eruptions. There have been no major volcanic eruptions since Mt. Pinatubo in 1991, but several smaller eruptions have caused a RF of about –0.1 ± 0.03 W m^{-2} during the 2000 to 2010 period. These small eruptions have led to better understanding of the dependence of climate impacts on the amount of material and time of the year of high-latitude injections. Emissions of CO_2 from volcanic eruptions are at least 100 times smaller than anthropogenic emissions, and inconsequential for climate on time scales of a century or less. [8.4.2; Figure 8.15; Figure 8.18]

The most rapid rate of increase in total anthropogenic AF has been since 1970. Time evolution of the total anthropogenic AF shows a substantial increase from 1750 to around 1930, primarily during the late 19th and early 20th centuries, with only a modest change over the next decades out to 1970. There is a *very high confidence* that there has been a strong increase in the total anthropogenic AF since 1970, fuelled by the continuous increase in WMGHG concentration. There is still *low agreement* on the magnitude of the aerosol AF, which is the primary factor in the uncertainty of the total anthropogenic forcing and its time evolution. [8.5.2; Figure 8.18]

There is *very high confidence* that natural forcing is a small fraction of the anthropogenic forcing. In particular, over the past three decades (since 1980), *robust evidence* from satellite observations of the TSI and volcanic aerosols demonstrate a near-zero (–0.04 W m^{-2}) change in the natural forcing compared to the anthropogenic AF increase of ~1.0 ± 0.3 W m^{-2}. [8.5.2; Figure 8.19]

Research since AR4 has improved the confidence level for some of the forcing mechanisms. Among the forcing agents, there is a *very high confidence* only for the WMGHG RF. Five forcing agents are given a confidence level of '*high'* and three '*medium'*, while an additional three are assigned '*low'* and two effects assigned a confidence level of '*very low'*. Relative to AR4, the level of scientific understanding[4] has been elevated for six forcing agents due to *improved evidence* and *agreement.* [8.5.1; Figure 8.16]

Forcing can also be attributed to emissions, rather than to the resulting concentration changes. Changes in CO_2 are the largest single contributor to historical RF from either the perspective of atmospheric concentration changes or the impact net emissions. The relative importance of other forcing agents varies with the perspective chosen. Methane emissions *very likely* have a much larger forcing (~1.0 W m^{-2} over the industrial era) than methane concentration increases (~0.5 W m^{-2}) due to several indirect effects through atmospheric chemistry. In addition, emissions of carbon monoxide *very likely* have a clear positive forcing, while emissions of nitrogen oxides *likely* have a net negative forcing but uncertainties are large. Emissions of ozone-depleting halocarbons likely cause a net positive forcing as their direct radiative effect is larger than the impact of the stratospheric ozone depletion that they induce. [8.5.1; Figure 8.17; FAQ8.2]

Variation in late 21st century forcing between the RCP scenarios is dominated by CO_2. Differences between RCP scenarios are relatively small for year 2030 but become very large for 2100. Results based on the RCP scenarios show a strong reduction in the aerosols and a substantial weakening of the negative total aerosol AF. Nitrate aerosols are an exception to this reduction with a substantial increase which is a robust feature among available models. [8.5.3; Figure 8.20; Figure 8.21]

While the WMGHG are well mixed in the atmosphere and therefore show a fairly homogeneous forcing, other agents such as aerosols, ozone and land use changes are highly heterogeneous spatially. Industrial era RF initiated by aerosol-radiation-interactions showed a maximum values over eastern North America and Europe during the early 20th century, with large values extending to East and Southeast Asia, South America and central Africa by 1980. Since then, however, the magnitude has decreased over eastern North America and Europe due to pollution control and the peak forcing has shifted to South and East Asia primarily as a result of economic growth and the resulting increase in emissions in those areas. Aerosol AF shows similar behaviour for locations with maximum negative forcing, but also shows substantial positive forcing over some deserts and the Arctic. In contrast, whole atmosphere ozone forcing increased throughout the 20th century, and has peak positive amplitudes around 15°N–30°N but negative values over Antarctica. [8.6.2; Figure 8.24]

Different metrics can be used to quantify and communicate the relative and absolute contributions to climate change of emissions of different substances, and of emissions from regions/countries or sources/sectors. In the case of forcing driven by emissions changes, metrics are especially valuable for an assessment of various mitigation options. They account for the radiative efficiency of the various substances, their lifetime in the atmosphere, and can include the timescale of the response. Up through AR4, the most common metric has been the global warming potential (GWP) that integrates RF out to a particular time horizon. Several alternative are available in the literature. There is now increasing focus on the Global Temperature change Potential (GTP), which is based on the change in global surface temperature at a chosen point in time. Both the GWP and the GTP use a time horizon, the choice of which is highly subjective. Short-lived species, such as black carbon, or intermediate lifetime species, such as methane, show a significant relative contribution for short time horizons, but their impacts become progressively less for longer time horizons. One may imagine and define a large number of other metrics, down the driver-response-impact chain. No single metric can accurately compare all consequences (i.e., responses in climate parameters over time) of different emissions, and the choice of metric therefore depends strongly on the particular impact being investigated and the context in which it is applied. It is important to note that the metrics do not define the policies or goals, but facilitate evaluation and implementation of multi-component policies to meet particular goals. The GWP has received much criticism and there are serious limitations and inconsistencies related to the treatment of indirect effects and feedbacks. The uncertainty in the GWP increases with time horizon and for GWP_{100} the uncertainty is larger than 50%. Several studies also point out

[4] Level of understanding is not standard in AR5, but confidence level for the forcing agent has been converted approximately to level of understanding for a comparison with previous IPCC reports.

that this metric is not well suited for target based policies. All choices of metric, even 'traditional' or 'widely-used' metrics, contain implicit value judgements. [8.7.1]

Forcing and temperature response can also be attributed to sectors. From this perspective and with the GTP metric, a single year's worth of current global emissions from the power generation and industrial sectors have the largest contributions to warming over the next 25–100 years. Livestock, household cooking and heating, on-road transportation, and agriculture are also relatively large contributors to warming, especially over shorter time horizons (~20 years). [8.7.2; Figure 8.33]

8.1 Radiative Forcing

There are a variety of ways to facilitate understanding how various drivers contribute to climate change. In principle, observations of the climate response to a single factor could directly show the impact of that factor, or climate models could be used to study the impact of any single factor. In practice, however, it is usually difficult to find measurements that are only influenced by a single cause, and it is computationally prohibitive to simulate the response to every individual factor of interest. Hence metrics intermediate between cause and effect are used to provide estimates of the climate impact of individual factors, with applications both in science and policy. Radiative forcing (RF) is one of the most widely used metrics, with most other metrics based upon RF. In this chapter, we discuss RF from natural and anthropogenic components during the industrial period, presenting values for 1750–2011 unless otherwise stated, and projected values through 2100. In this section, we present the various definitions of forcing used in this chapter, and discuss the utility and limitations of radiative forcing. Emission metrics designed to facilitate rapid evaluation of the climate effects of particular emissions are discussed in Section 8.7.

8.1.1 The Radiative Forcing Concept

RF is the net change in the energy balance of the Earth system due to some imposed perturbation. It is usually expressed in watts per square meter averaged over a particular period of time and quantifies the energy imbalance that occurs when the imposed change takes place. Though usually difficult to observe, calculated RF provides a simple quantitative basis for comparing some aspects of the eventual climate responses to different imposed agents, and hence is widely used in the scientific community. Forcing is often presented as the value due to changes between two particular times, such as preindustrial to present-day, but the time-evolution of forcing provides a more complete picture.

8.1.1.1 Defining Radiative Forcing

Alternative definitions of RF have been developed, each with its own advantages and limitations. The instantaneous RF refers to an instantaneous change in net (down minus up) radiative flux (solar plus longwave; in W m^{-2}) due to an imposed change. This forcing is usually defined in terms of flux changes at the top of the atmosphere (TOA) or at the tropopause, with the latter being a better indicator of the response in the lower atmosphere in cases when they differ.

Climate change takes place when the system responds in order to counteract the flux changes, and all such responses are explicitly excluded from this definition of forcing. The assumed relation between a sustained RF and the equilibrium global mean surface temperature response (ΔT) is $\Delta T = \lambda RF$ where λ is the equilibrium climate sensitivity parameter. The relationship between RF and ΔT is an expression of the energy balance of the climate system and a simple reminder that the steady state global mean climate response to a given forcing is determined both by the forcing and the responses inherent in λ.

Implicit in the concept of RF is the proposition that the change in net irradiance at the tropopause or TOA can be separated from all responses to the energy flux changes. These are not in fact always cleanly separable and thus some ambiguity exists in what may be considered a forcing versus what is part of the response.

In both the TAR and AR4, the term radiative forcing (RF, as distinct from instantaneous RF; also called stratospherically-adjusted RF) was defined as the change in net irradiance at the tropopause after allowing for stratospheric temperatures to readjust to radiative equilibrium, while holding surface and tropospheric temperatures and state variables such as water vapor and cloud cover fixed at the unperturbed values[5]. RF is generally more indicative of the surface and tropospheric temperature responses than instantaneous RF, especially for agents such as carbon dioxide or ozone change that substantially alter stratospheric temperatures.

[5] except for the impact of aerosols on cloud albedo due to changes in droplet size with constant cloud liquid water which was considered an RF in AR4 and is called the RF due to aerosol-cloud interactions (RF_{aci}) in Chapter 7 and Section 8.3.4.

To be consistent with TAR and AR4, RF is hereafter taken to mean the stratospherically-adjusted radiative forcing. For many forcing agents the RF gives a very useful and appropriate way to compare the relative importance of their potential climate effect. Instantaneous RF or RF are not necessarily accurate indicators of the eventual temperature response for all forcing agents, however. Rapid adjustments in the troposphere can either enhance or reduce the flux perturbations, leading to substantial differences in the forcing driving long-term climate change. This is the case for cloud responses to heating by absorbing aerosols or cloud changes in response to aerosols acting as nucleation sites, for example. In much the same way that allowing for the relatively rapid adjustment of stratospheric temperatures provides a more useful characterization of the forcing due to stratospheric constituent changes, inclusion of rapid tropospheric adjustments has the potential to provide more useful characterization for drivers in the lower atmosphere.

A forcing encompassing rapid adjustments facilitates calculation of forcings that do not fit cleanly into the RF concept. For example, aerosol forcing is in part due to the influence of aerosols themselves on radiative fluxes. However, especially for absorbing aerosol, changes in the temperature distribution above the surface occur due to a variety of effects, including cloud response to changing atmospheric stability (Hansen et al., 2005; Section 7.3.5.2), and cloud absorption effects (Jacobson, 2012), that affect fluxes but are not strictly part of RF. Similar adjustments take place for many forcings, including CO_2.

Aerosols also alter cloud properties via microphysical interactions leading to indirect forcings (see Section 7.4). Although these adjustments are complex and not fully quantified, they occur both on the microphysical scale of the cloud particles as well as on a more macroscopic scale involving whole cloud systems (e.g., Penner et al., 2006; Quaas et al., 2009). A portion of these adjustments occurs over a short period, on cloud-life cycle time scales, and is not part of a feedback from the surface temperature changes. Previously these adjustments have been termed ‘fast feedbacks’ (e.g., Gregory et al., 2004), while in AR5 they will be denoted ‘rapid adjustments’ to emphasize their distinction from feedbacks involving surface temperature changes. Traditional climate feedbacks are also sometimes divided into fast and slow components (though with much longer timescales for both categories; see Chapters 9 and 12).

Several measures of forcing have been introduced that attempt to include rapid adjustments. One example includes rapid adjustment of tropospheric temperature, water vapor and clouds induced by the RF of CO_2 (Gregory and Webb, 2008; Gregory et al., 2004), and the separation of rapid and slow responses is discussed further by Andrews et al. (2010). Furthermore, studies have demonstrated the utility of including rapid adjustment in comparison of forcing agents, especially in allowing quantification of forcing due to aerosol-induced changes in cloud lifetime that are not amenable to characterization by RF (Lohmann et al., 2010; Rotstayn and Penner, 2001).

In this chapter, we emphasize a forcing definition that accounts for the complicating effects of rapid adjustments to allow quantification of additional forcing agents. This forcing is the adjusted forcing (AF), which is the change in net TOA irradiance after allowing for atmospheric temperatures, water vapour, clouds and land albedo to adjust, but with all or a portion of surface conditions unchanged. The primary methods in use for such calculation are (1) fixing sea surface temperatures (SSTs) and sea ice cover and allowing all other parts of the system to respond (e.g., (Hansen et al., 2005)) or (2) analyzing the transient global mean surface temperature response to an instantaneous perturbation and using the regression of the response extrapolated back to the start of the simulation to derive the implied forcing (Gregory et al., 2004). The regression technique has an uncertainty range of about 10% for a single simulation due to internal variability in the transient climate, while given a similar length simulation the fixed-SST uncertainty is much smaller. Analysis of both techniques shows that the fixed-SST method yields a smaller spread across models, even when neglecting the uncertainty in the regression fitting procedure (Andrews et al., 2012a). Hence for practical purposes, we emphasize the fixed-SST technique here. This AF has been shown to provide a better estimate of the ultimate temperature change than either instantaneous RF or RF (Hansen et al., 2002; Hansen et al., 2005). We note, however, that there is a small low bias in the AF using this technique as land temperature response is included. It is possible to correct for this bias in the global mean forcing, but it will also introduce gradients in land-sea temperatures that could cause small artificial climate responses. Despite the low bias in fixed-SST AF, results from the regression technique for a multi-model analysis of the forcing due to CO_2 are 7% lower (Andrews et al., 2012a) though this is within the uncertainty range of the calculation.

The conceptual relation between instantaneous RF, RF and AF is illustrated in Figure 8.1 and it implies the adjustments to the instantaneous RF involve effects of processes that occur more rapidly than the time scale of the response of the global mean surface temperature to the forcing. However, as our definition is a pragmatic one based in part on technical advantages of the particular technique, there is no a priori timescale defined for adjustments to be rapid. The majority take place on timescales of seasons or less, but there is a spectrum of adjustment times. Changes in snow cover, for example, may take place over many years. The AF thus represents that part of the instantaneous RF that is maintained over long timescales and more directly contributes to the steady-state climate response. The RF can be considered a more limited version of AF. Since the atmospheric temperature has been allowed to adjust, AF would be identical if calculated at the tropopause instead of the TOA.

Using the RF concept, the climate sensitivity parameter can vary substantially across different forcing agents (Forster et al., 2007). The response to RF from a particular agent relative to RF from CO_2 has been termed the efficacy (Hansen et al., 2005). By including many of the rapid adjustments that differ across agents, the AF concept leads to more uniform climate sensitivity across forcing agents. For example, the influence of clouds on the interaction of aerosols with sunlight and the effect of aerosol heating on cloud formation can lead to very large differences in the impact of black carbon RF as a function of altitude, but the response to AF is nearly uniform with altitude (Hansen et al., 2005). Hence as we use AF in this chapter when it differs significantly from RF, efficacy is not used hereafter. For inhomogeneous forcings, the climate sensitivity parameter may also depend upon the horizontal forcing distribution, especially with latitude, however.

A combination of RF and AF will be used in this chapter with RF provided to keep consistency with TAR and AR4, and AF used to allow quantification of more complex forcing agents and provide a more useful metric than RF in some cases.

8.1.2 Limitations of Radiative Forcing

Both the RF and AF concepts have strengths and weaknesses in addition to those discussed above. Dedicated model simulations that are required to diagnose the AF can be more computationally demanding than those for instantaneous RF or RF as many years are required to reduce meteorological variability. The presence of meteorological variability can also make it difficult to isolate the AF of small forcings that are easily isolated in the pair of calculations within a single experiment performed for RF (Figure 8.1). However, in many cases the AF and RF are nearly equal. In particular, using fixed-SST simulations, Hansen et al. (2005) found that AF is virtually identical to RF for increased CO_2, tropospheric ozone and solar irradiance, and within 6% for methane, N_2O, stratospheric aerosols, and for the direct effect of reflective aerosols. A study of six GCMs found a substantial inter-model variation in the rapid tropospheric adjustment to CO_2 using regression analysis in slab ocean models, though the ensemble mean result was that the adjustments caused less than 5% change to the RF (Andrews and Forster, 2008). Part of the large uncertainty range arises from the greater noise inherent in regression analyses of single runs in comparison with fixed-SST experiments. Lohmann et al. (2010) also report a small increase in the forcing from CO_2 using AF instead of RF base on the fixed-SST technique, while finding no substantial difference for methane, direct aerosol forcing or aerosol indirect effects on cloud albedo. In the fixed-SST simulations of Hansen et al. (2005), AF was substantially greater than RF for stratospheric ozone (~50%, though that forcing is small), ~20% less for the atmospheric effects of black carbon (BC) aerosols (not including aerosol-cloud microphysical interactions), and nearly 300% greater for the forcing due to BC snow albedo forcing (Hansen et al., 2007). The various studies demonstrate that RF provides a good estimate of AF in most cases, as the differences are very small, with the notable exceptions of BC-related forcings, along with stratospheric ozone. AF provides better characterization of those effects, as well as allowing quantification of a broader range of effects including aerosol indirect effects on cloud lifetime. Hence while RF and AF are generally quite similar for well-mixed greenhouse gases, AF typically provides a more useful indication of climate response for near-term climate forcers (see Box 8.1).

[START BOX 8.1 HERE]

Box 8.1: Grouping Forcing Compounds by Common Properties

As many compounds cause RF when their atmospheric concentration is changed, it can be useful to refer to groups of compounds with similar properties. Here we discuss two primary groupings: well-mixed greenhouse gases (WMGHGs) and near-term climate forcers (NTCFs).

We define as 'well-mixed' those greenhouse gases that are sufficiently mixed throughout the troposphere that concentration measurements from a few remote surface sites can characterise the climate-relevant atmospheric burden; although these gases may still have local variation near sources and sinks and even hemispheric gradients. Emission metrics (forcing per unit emission) for these gases thus do not depend on the geographic location of the emission. These gases, or a subset of them, have sometimes been referred to as 'long-lived greenhouse gases', but the physical property that causes the above common characteristics is more directly associated with their mixing within the atmosphere. WMGHGs include CO_2, N_2O, CH_4, SF_6, and many halogenated species. Conversely, ozone and water vapour are not WMGHGs.

We define 'Near-term climate forcers' as those compounds whose impact on climate occurs primarily within the first decade after their emission. This set of compounds is primarily composed of those with short lifetimes in the atmosphere compared to WMGHGs. However, the common property that is of greatest interest to a climate assessment is the timescale over which their impact on climate is felt. Thus this set of compounds includes methane, which is a WMGHG, as well as ozone, aerosols and some halogenated species that are not WMGHGs. These compounds do not accumulate in the atmosphere at decadal to centennial timescales, and so their effect on climate is predominantly in the near-term following their emission.

[END BOX 8.1 HERE]

Whereas the global mean AF provides a useful indication of the eventual change in global-mean surface temperature, it does not reflect regional climate changes. This is especially the case for the inhomogeneously distributed forcings because they activate climate feedbacks based on their regional distribution. For example, forcings over Northern Hemisphere middle and high latitudes induce snow and ice albedo feedbacks more than forcings at lower latitudes or in the Southern Hemisphere (e.g., Shindell and Faluvegi, 2009). Spatial variation in the strength of climate feedbacks means that the response to quasi-homogeneous forcings is also inhomogeneous, so that the pattern of eventual response depends on both the pattern of forcing and the distribution of feedbacks/sensitivity (Section 8.6). The seasonal and diurnal cycles of insolation also affect the radiative forcing of agents that act on shortwave radiation. For example, volcanic aerosols in the polar night have no radiative forcing in the shortwave (although they still have a small longwave forcing).

In the case of agents that strongly absorb incoming solar radiation (such as BC, and to a lesser extent organic carbon (OC) and ozone) the TOA forcing provides little indication of the change in radiation reaching the surface which can force local changes in evaporation and alter regional and general circulation patterns (e.g., Ramanathan and Carmichael, 2008; Wang et al., 2009). Hence the forcing at the surface, or the atmospheric heating, defined as the difference between surface and tropopause/TOA forcing, might also be useful metrics. Global mean precipitation changes can be related separately to atmospheric RF and to a slower response to global mean temperature changes (Andrews et al., 2010; Ming et al., 2010). Relationships between surface forcing and localized aspects of climate response have not yet been clearly quantified, however.

In general, most widely used definitions of RF and most forcing-based metrics are intended to yield the eventual temperature response, and most analyses to date have explored the global mean temperature response only. These metrics do not explicitly include impacts such as changes in precipitation, surface sunlight available for photosynthesis, extreme events, etc, or regional temperatures, which can differ greatly from the global mean. Hence although they are quite useful for understanding the factors driving global mean temperature change, they provide only an imperfect and limited perspective on the factors driving broader climate change. Additionally, basing the metric solely on radiative perturbations does not allow comparison of non-radiative forcings, such as effects of land cover change on evapotranspiration or physiological impacts of CO_2 and O_3 except where these cause further impacts on radiation such as through cloud cover changes (Andrews et al., 2012b).

[INSERT FIGURE 8.1 HERE]

Figure 8.1: Cartoon comparing (a) instantaneous RF, (b) RF, which allows stratospheric temperature to adjust, (c) flux change when the surface temperature is fixed over the whole Earth, (d) AF, the adjusted forcing which allows atmospheric and land temperature to adjust while ocean conditions are fixed, and (e) the equilibrium response to the climate forcing agent. The methodology for calculation of each type of forcing is also outlined. dT_o represents the land temperature response, while dT_s is the full surface temperature response. Updated from Hansen et al. (2005).

8.1.3 Attribution of Radiative Forcing to Concentration or Emission Changes

Analysis of forcing due to observed or modelled concentration changes between preindustrial, defined here as 1750, and present provides an indication of the importance of different forcing agents to climate change during this period. Such analyses have been a mainstay of climate assessments. This type of analysis has the advantage that observational data are available to accurately quantify the concentration changes for several of the largest forcing components. Atmospheric concentration changes, however, are the net result of variations in emissions of multiple compounds and any climate changes that have influenced processes such as wet removal, atmospheric chemistry or the carbon cycle. Characterizing forcing according to concentration changes thus mixes multiple root causes along with climate feedbacks. Policy decisions are better informed by analysis of forcing attributable to emissions, which the IPCC first presented in AR4. These analyses can be applied to historical emissions changes in a 'backward-looking' perspective, or to current or projected future emissions in a 'forward-looking' view (see Section 8.7).

Such calculations typically necessitate more model simulations, and require careful consideration of which processes are included, especially when comparing results to concentration-based forcings. In particular, simulation of concentration responses to emissions changes requires incorporating models of the carbon cycle and atmospheric chemistry (gas and aerosol phases). Dynamic vegetation models can also be included. The requisite expansion of the modelling realm for emissions-based forcing should in principle be consistent for all drivers. For example, if the CO_2 concentration responses to CO_2 emissions include the impact of CO_2-induced climate changes on carbon uptake, then the effect of climate changes caused by any other emission on carbon uptake should also be included. If instead the response of carbon uptake to climate change is excluded, perhaps on the grounds that it could be considered a feedback, then forcing due to CO_2 concentration changes attributable to all emissions (CO_2 directly, others indirectly) may not equal the forcing due to observed CO_2 concentration changes. Similarly, if the effects of atmospheric CO_2 concentration change on carbon uptake are included, the effects of other atmospheric composition or deposition changes on carbon uptake should be included as well. Comparable issues are present for other forcing agents. In practice, the modelling realm used in various studies of forcing attributable to emissions has not always been consistent. The issue of modelling realm applies to the calculation of AF as well. Ideally, all known rapid adjustments would be included, but in practice calculations for CO_2 have to date largely been performed with models that exclude atmospheric chemistry and dynamic vegetation. Calculations of aerosol AF are of course based on modelling that includes atmospheric chemistry, but also neglects vegetation responses. In this chapter, we endeavour to clarify which processes have been included in the various estimates of forcing attributed to emissions (Section 8.7).

RF or AF estimates based on either historical emissions or concentrations provide valuable insight into the relative and absolute contribution of various drivers to historical climate change. Scenarios of changing future emissions and land use are also developed based on various assumptions about socio-economic trends and societal choices. The forcing resulting from such scenarios is used to understand the drivers of potential future climate changes (Sections 8.5.3 and 8.6). As with historical forcings, the actual impact on climate depends on both the temporal and spatial structure of the forcings and the rate of response of various portions of the climate system.

8.2 Atmospheric Chemistry

8.2.1 Introduction

Most radiatively active compounds in the Earth's atmosphere are chemically active, meaning that atmospheric chemistry plays a large role in determining their burden and residence time. In the atmosphere, a gaseous chemically active compound can be affected by 1) interaction with other species (including aerosols and water) in its immediate vicinity and 2) interaction with solar radiation (photolysis). Finally, physical processes (wet removal and dry deposition) act on some chemical compounds (gas or aerosols) to further

define their residence time in the atmosphere. Atmospheric chemistry is therefore a strongly interacting and highly variable system, leading to nonlinearities (Kleinman et al., 2001) and a wide range of timescales of importance (Isaksen et al., 2009).

This section will assess updates in understanding of processes, modelling and observations since AR4 Section 2.3, on all reactive species contributing to RF. Note that aerosols, including processes responsible for the formation of aerosols, are described in further detail in Section 7.3.

8.2.2 Global Chemistry Modelling in CMIP5

While several CMIP5 modeling groups performed simulations with interactive chemistry (i.e., computed simultaneously within the climate model), there were still a significant number of models that used as input pre-computed distributions of radiatively active gases and/or aerosols. In order to assess the distributions of chemical species and their respective RF, many research groups participated in the Atmospheric Chemistry and Climate Model Intercomparison Project (ACCMIP), Table 8.1; (Lamarque et al., 2012).

In all CMIP5/ACCMIP chemistry models, anthropogenic and biomass burning emissions are specified for all model simulations. More specifically, a single set of historical anthropogenic and biomass burning emissions (Lamarque et al., 2010) and one for each of the RCPs (van Vuuren et al., 2011) were used (Figure 8.2). This was designed to increase the comparability of simulations. However, because of the uncertainty in underlying fuel usage and emission factors (e.g., Bond et al., 2007; Lu et al., 2011), there is a considerable range in the estimates and time evolution of recent anthropogenic emissions (Granier et al., 2011). Historical reconstructions of biomass burning (wildfires and deforestation) also exhibit quite large uncertainties (Ito and Penner, 2005; van der Werf et al., 2010; Kasischke and Penner, 2004; Schultz et al., 2008). Finally, it is important to recognize that RCP biomass burning projections are only crudely represented, with no feedback between climate change and fires (Bowman et al., 2009; Thonicke et al., 2010; Pechony and Shindell, 2010). Evaluation of multiple models driven by these emissions thus provides a useful estimate of the uncertainty due to representation of physical and chemical processes in models, but does not incorporate uncertainty in emissions.

[INSERT FIGURE 8.2 HERE]

Figure 8.2: Time evolution of global anthropogenic and biomass burning emissions 1850–2100 used in CMIP5/ACCMIP following each RCP; blue (RCP2.6), light blue (RCP4.5), orange (RCP6.0) and red (RCP8.5). BC stands for black carbon (in Tg(C) yr^{-1}), OC for organic carbon (in Tg(C) yr^{-1}), NMVOC for non-methane volatile organic compounds (in Tg(C) yr^{-1}) and NO_X for nitrogen oxides (in Tg(NO_2) yr^{-1}). Other panels are in Tg(species) yr^{-1}. Historical (1850–2000) values are from (Lamarque et al., 2010). RCP values are from (van Vuuren et al., 2011). Regional estimates for Africa, China, India, North America, South America and Western Europe are shown in Supplementary Material.

The ACCMIP simulations (Table 8.1) were defined to provide information on the long-term changes in atmospheric composition with a few, well-constrained atmospheric simulations. The models have been extensively evaluated against observations (Bowman et al., 2012; Lee et al., 2012; Shindell et al., 2012d; Stevenson et al., 2012; Voulgarakis et al., 2012; Young et al., 2012). Research groups involved in global three-dimensional chemistry-climate modelling were openly invited to participate to this project; however, because of the nature of the simulations (pre-industrial, present-day and future climates), only a limited number of chemistry-transport models (models which require a full definition of the meteorological fields needed to simulate physical processes and transport) participated in the ACCMIP project, which instead drew primarily from the same GCMs as CMIP5 (see Lamarque et al., 2012) for a list of the participating models and their configurations).

Table 8.1: List of ACCMIP experiments.

Historical simulations									
Emissions/configuration	1850	1890	1910	1930	1950	1970	1980	1990	2000
Emissions and SSTs/GHGs for given year	C	1	1	C	1	1	C	1	C
Year 2000 emissions/1850 SSTs & GHGs				1			1		C

Future simulations				
Emissions/configuration	2010	2030	2050	2100
RCP2.6		C	1	C
RCP4.5	1	1	1	1
RCP6.0	C	C	1	C
RCP8.5		C	1	C
Year 2000 emissions/2100 RCP8.5 SSTs & GHGs		C		C

Notes:
C = Core
1 = Tier 1
Blank = not requested.
While RCP6.0 was listed as core, only a smaller subset of models performed those simulations compared to RCP2.6 and RCP8.5 (Lamarque et al., 2012).

8.2.3 Chemical Processes and Trace Gas Budgets

8.2.3.1 Tropospheric Ozone

The RF from tropospheric ozone is strongly height- and latitude-dependent (Lacis and Hansen, 1974; Worden et al., 2008). Consequently, to compute the forcing since pre-industrial times, it is necessary to estimate its full three-dimensional distribution, which can only be obtained through simulations using global models. It is also well established that ozone detrimentally affects plant productivity (Ashmore, 2005), albeit estimating its impact on chemistry and climate, while possible significant, is still limited to a few studies (Sitch et al., 2007; UNEP, 2011).

Tropospheric ozone is a by-product of the oxidation of carbon monoxide, methane and non-methane hydrocarbons in the presence of nitrogen oxides. Ozone production is usually limited by the supply of HO_x ($OH + HO_2$) and NO_X ($NO + NO_2$) (Seinfeld and Pandis, 2006). Because of the catalytic role of nitrogen oxides in ozone production, tropospheric ozone chemistry is strongly nonlinear in its dependence on nitrogen oxides (Seinfeld and Pandis, 2006). As emissions of these precursors have increased (Figure 8.2), tropospheric ozone has increased since pre-industrial times (Volz and Kley, 1988; Marenco et al., 1994) and over the last decades (Parrish et al., 2009; Cooper et al., 2010; Logan et al., 2012), but with important regional variations (Section 2.2). Ozone's major loss pathways in the troposphere are through 1) photolysis (to O^1D, followed by reaction with water vapour) and 2) reaction with HO_2 (Seinfeld and Pandis, 2006) . The former pathway leads to couplings between stratospheric ozone (photolysis rate being a function of the overhead ozone column) and climate change (through water vapour). Observed surface ozone abundances typically range from less than 10 ppb over the tropical Pacific Ocean to more than 100 ppb downwind of highly emitting regions. The lifetime of ozone in the troposphere varies strongly with season and location: it may be as little as 1 day in the tropical boundary layer, or as much as 1 year in the upper troposphere. The global mean lifetime of ozone is approximately 25 days (Stevenson et al., 2006).

For present (circa 2000) conditions, the various components of the budget of global mean tropospheric ozone are estimated from the ACCMIP simulations and other model simulations since AR4 (Table 8.2). In particular, most recent models define a globally and annually averaged tropospheric ozone burden of ≈330 ± 50 Tg (or equivalently 31 Dobson Units (DU); 1 Dobson Unit corresponds to 2.69×10^{16} ozone molecules for every square centimetre of area at the base of an atmospheric column and approximately equals 10.7 Tg). Differences in the definition of the tropopause lead to inter-model variations of approximately 10% (Wild, 2007). The multi-model mean estimate of global annual tropospheric ozone burden has not significantly changed since the ACCENT-PhotoComp estimates (344 ± 39 Tg) (Stevenson et al., 2006), and is in reasonable agreement with satellite-based OMI-MLS (Ziemke et al., 2011) and TES (Osterman et al., 2008) climatologies.

Table 8.2: Summary of tropospheric ozone global budget model and observation estimates for present conditions. Focus is on modelling studies published since AR4.

Burden Tg	Prod Tg yr^{-1}	Loss Tg yr^{-1}	Dep Tg yr^{-1}	STE Tg yr^{-1}	Reference
			Modelling Studies		
332 ± 22	N/A	N/A	N/A	N/A	Young et al., 2012; ACCMIP
323	N/A	N/A	N/A	N/A	Archibald et al., 2011
330	4876	4520	916	560	Kawase et al., 2011
312	4289	3881	829	421	Huijnen et al., 2010
334	3826	3373	1286	662	Zeng et al., 2008
324	4870	4570	801	502	Wild and Palmer, 2008
372	5042	4507	884	345	Horowitz, 2006
349	4384	3972	808	401	Liao et al., 2006
344 ± 39	5110 ± 606	4668 ± 727	1003 ± 200	552 ± 168	Stevenson et al., 2006; ACCENT
292	4758	4157	1278	677	Hauglustaine et al., 2005
314 ± 33	4465 ± 514	4114 ± 409	949 ± 222	529 ± 105	Wild, 2007 (summary of post-2000 studies)
N/A	N/A	N/A	N/A	515	Hsu and Prather, 2009
N/A	N/A	N/A	N/A	655	Hegglin and Shepherd, 2009
			Observational Studies		
344					Li et al., 1995; taken from Wild, 2007
333					Fortuin and Kelder, 1998
327					Logan, 1999
325					Ziemke et al., 2011; value is from 60S to 60N
319–351					Osterman et al., 2008; 60S–60N

To establish credibility in simulating the recent atmospheric composition, model simulations for present-day conditions or the recent past are evaluated (Figure 8.3) against frequent ozonesonde measurements (Logan, 1999; Tilmes et al., 2011) and additional surface, aircraft and satellite measurements. The ACCMIP model simulations indicate a reasonable representation of tropospheric ozone, especially when the multi-model ensemble mean (or median) is considered, albeit with significant biases. The overall spread in model results is slightly smaller than the ACCENT-AR4 simulations, most likely coming from the use of different anthropogenic and biomass burning emission datasets but also possibly from a smaller set of models. A similar multi-model mean but with a larger spread is found for the CMIP5 models (Eyring et al., 2012). Overall, our estimate of tropospheric ozone burden for year 2000 conditions has not substantially changed since AR4. (Skeie et al., 2011a) calculate a 5% increase in burden from 2000 to 2010.

[INSERT FIGURE 8.3 HERE]

Figure 8.3: Comparisons between observations and simulations for the monthly mean ozone for ACCMIP results (Young et al., 2012). ACCENT refers to the model results in (Stevenson et al., 2006).

Estimates of the ozone chemical sources and sinks are however more uncertain, with a net chemical production (production *minus* loss) of approximately 300 Tg yr^{-1} (Table 8.2). As noted in (Stevenson et al., 2006; Wu et al., 2007), since TAR and to some extent AR4, there has been a continual increase in the overall modelled production and loss contributions owing in part to the inclusion of additional hydrocarbon chemistry. In the ACCENT-AR4 model simulations, deposition of ozone to the surface was estimated to be in the range of 902 ± 255 Tg yr^{-1}. No results are available from ACCMIP due to inconsistencies in models reporting those quantities (Young et al., 2012). Finally, transport across the tropopause represents a net influx of ozone into the troposphere of 636 ± 273 Tg yr^{-1} based on the ACCENT-AR4 results. Additional model estimates (Hegglin and Shepherd, 2009; Hsu and Prather, 2009) fall within that range, as do estimates based on observations (Gettelman et al., 1997; Murphy and Fahey, 1994).

Similar to AR4, global chemistry-climate models used in ACCMIP provide an estimated tropospheric ozone increase (Figure 8.4) from 1850 to 2000 of approximately 95 Tg (8.9 ± 0.8 DU). It is important to note that,

while the standard deviation among model estimates for the absolute 1850 and 2000 burdens is more than 50 Tg, the changes in the ozone fields due to the changes in emissions and environmental conditions between 1850 and 2000 are more consistent between models. Attribution simulations (Stevenson et al., 2012) indicate unequivocally that changes in ozone precursor emissions are responsible for the increase between 1850 and 2000.

In most studies 'pre-industrial' does not represent any specific year but is usually assumed to correspond to 1750s levels. Using the Lamarque et al. (2010) emissions, the ACCMIP models (Young et al., 2012) are unable to reproduce the low levels of ozone observed at Montsouris 1876–1886 (Volz and Kley, 1988); additional information from Schönbein paper analysis is controversial (Marenco et al., 1994) and therefore assessed to be of qualitative use only. Parrella et al. (2012) were able to get good agreement with the Montsouris observations by adding bromine chemistry to their model. However, their pre-industrial to present day ozone change (approximately 115 Tg, using different emissions than the ACCMIP models) is not significantly affected by the presence of bromine chemistry. The main uncertainty in estimating the pre-industrial to present-day change in ozone therefore remains the lack of constraint on emission trends because of the very incomplete knowledge of pre-industrial ozone concentrations, of which no new information is available. On shorter time scales (decades since present), models also have a difficult time reproducing observed trends (Section 2.2), although a recent evaluation of ozonesonde observations question the reliability of some of those over long periods, especially in association with Brewer-Mast measurements (Logan et al., 2012).

The uncertainty on pre-industrial conditions is not confined to ozone but applies to aerosols as well (e.g., Schmidt et al., 2012). Furthermore, the CMIP5 and ACCMIP simulations have used a single set of anthropogenic and biomass burning emissions (Lamarque et al., 2010). Furthermore, the historical estimates were constructed independently from the land use-land cover change (Hurtt et al., 2011) used for the carbon cycle simulations. All these point to the need of additional studies that would expand the range of simulated tropospheric chemistry changes during the historical and future periods.

[INSERT FIGURE 8.4 HERE]

Figure 8.4: (a) Time evolution of global tropospheric ozone burden (in $Tg(O_3)$) from 1850 to 2100 from ACCMIP results. In bottom panel (b), time evolution of global tropospheric ozone burden (in $Tg(O_3)$) differenced to 1850. The box, whiskers, line and dot show the interquartile range, full range, median and mean burdens and differences, respectively. The green line indicates the range of observational estimates (Table 8.2). Adapted from Young et al. (2012).

8.2.3.2 Stratospheric Ozone and Water Vapour

Stratospheric ozone has experienced significant depletion since the 1970s due to bromine and chlorine-containing compounds (Solomon, 1999). Most of the ozone loss is associated with the long-lived bromine and chlorine containing compounds (chlorofluorocarbons and substitutes) released by human activities, in addition to nitrous oxide. This is in addition to a background level of natural emissions of short-lived halogens from oceanic and volcanic sources.

With the advent of the Montreal Protocol, emissions of CFCs and replacements have strongly declined (Montzka et al., 2011a) and signs of ozone stabilization and even possibly recovery have already occurred (Mader et al., 2010; Salby et al., 2012). A further consequence is that N_2O emissions now dominate all other emissions in terms of ozone depleting potential (Ravishankara et al., 2009). Chemistry-climate models with resolved stratospheric chemistry and dynamics recently provided an estimated global mean total ozone column recovery to 1980 levels to occur in 2032 (for the multi-model mean) under the A1B scenario (Eyring et al., 2010b). Increases in the stratospheric burden and acceleration of the stratospheric circulation leads to an increase in the stratosphere-troposphere flux of ozone (Shindell et al., 2006c; Hegglin and Shepherd, 2009; Zeng et al., 2010). This is also seen in recent RCP8.5 simulations (Figure 8.10), with the impact of increasing tropospheric burden (Kawase et al., 2011; Lamarque et al., 2011; Young et al., 2012). However, observationally-based estimates of recent trends in age of air (Engel et al., 2009; Stiller et al., 2012) are not in agreement with the acceleration of the stratospheric circulation found in model simulations, possibly due to inherent difficulties with extracting trends from SF6 (Garcia et al., 2011).

Oxidation of methane in the stratosphere (see Section 8.2.3.3) is a significant source of water vapour and hence this process contributes an anthropogenic forcing (see Section 8.3).

8.2.3.3 Methane

The concentration of CH_4 has increased by 2.5 times since pre-industrial times (Table 2.12) with some projections indicating a further doubling by 2100 (Figure 8.5). Present CH_4 emissions have an estimated total of 479–706 $TgCH_4\,yr^{-1}$ (see Table 6.7).

[INSERT FIGURE 8.5 HERE]

Figure 8.5: Time evolution of global-averaged mixing ratio of long-lived species1850–2100 following each RCP; blue (RCP2.6), light blue (RCP4.5), orange (RCP6.0) and red (RCP8.5). Based on Meinshausen et al. (2011b).

The main sink of CH_4 is through its reaction with the hydroxyl radical OH in the troposphere, A primary source of tropospheric OH is initiated by the photodissociation of O_3, followed by reaction with water vapour (creating sensitivity to humidity, cloud cover and solar radiation) (Seinfeld and Pandis, 2006), The other primary source of OH is through secondary reactions (Lelieveld et al., 2008). A recent estimate of the CH_4 tropospheric chemical lifetime with respect to OH constrained by methyl chloroform surface observations is 11.2 ± 1.3 years (Prather et al., 2012). In addition, bacterial uptake provides an additional small, less constrained loss, with another small loss in the stratosphere. Halogen chemistry in the troposphere also contributes to some tropospheric methane loss (Allan et al., 2007).

The ACCMIP estimate for present CH_4 lifetime with respect to tropospheric OH varies quite widely (9.8 ± 1.6 years (Voulgarakis et al., 2012), with a multi-model mean similar to prior studies nt with methyl chloroform trend estimates (Montzka et al., 2011b; see Section 2.4.1.1.2).

A partial explanation for the range in CH_4 lifetime changes can be found in the degree of representation of chemistry in chemistry-climate models. Indeed, Archibald et al. (2010) showed that the response of OH to increasing nitrogen oxides strongly depends on the treatment of hydrocarbon chemistry in a model.

The chemical coupling between OH and CH_4 leads to a significant amplification of the emission impact; i.e., increasing CH_4 emissions decreases tropospheric OH which in turn increases the CH_4 lifetime and therefore its burden. The calculated OH feedback, $\delta\ln(OH)/\delta(\ln(CH_4))$ was estimated in Chapter 4 of TAR to be –0.32, leading to a 0.32% decrease in OH for a 1% increase in CH_4. A multi-model study (Fiore et al., 2009) provides a slightly smaller value (–0.25 ± 0.03) while ACCMIP (from 2 models only) provides –0.17 and –0.23 (Voulgarakis et al., 2012; see Figure 8.SM.1).

8.2.3.4 Nitrous Oxide

Nitrous oxide (N_2O) in 2010 has a surface concentration 19% above its 1750 level (Table 2.12 and Section 2.4.1.1.3). Increases in N_2O deplete mid- to upper-stratospheric ozone and impact tropospheric chemistry through increase in stratosphere-troposphere exchange of ozone (from an increase in mid-latitude lower stratospheric ozone) and odd nitrogen species (Prather and Hsu, 2010). Anthropogenic emissions represent around 30–45% of the present-day global total, and are mostly from agricultural (fertilizer) and fossil-fuel activities. Natural emissions come mostly from microbial activity in the soil. The main sink for N_2O is through photolysis and oxidation reactions in the stratosphere, leading to an estimated lifetime of 131 ± 10 years (Prather et al., 2012), slightly larger than previous estimates (Prather and Hsu, 2010; Montzka et al., 2011a).

8.2.3.5 Halogenated Species

Halogenated species can be strong greenhouse gases. Those containing chlorine and bromine also deplete stratospheric ozone and are referred to as ozone depleting substances (ODSs). Most of those compounds do not have natural emissions and, because of the implementation of the Montreal Protocol, total emissions of ODSs have sharply decreased since the 1990s (Montzka et al., 2011a). For CFCs, PFCs and SF6 the main loss is through photolysis in the stratosphere. The CFC substitutes (hydrochlorofluorocarbons, HCFCs, and

hydrofluorocarbons, HFCs) are destroyed by OH oxidation in the troposphere. Their global concentration has steadily risen over the recent past (see Section 2.4.1.1.4).

8.2.3.6 Aerosols

Aerosol particles are present in the atmosphere with size ranges from a few nanometres to tens of micrometres. They are the results of direct emission (primary aerosols: black carbon, primary organic, sea-salt, dust) into the atmosphere or as products of chemical reactions (secondary inorganic aerosols (SIA): sulphate, nitrate, ammonium, and secondary organic aerosols (SOA)) occurring in the atmosphere. SIA are the products of reactions involving sulphur dioxide, ammonia and nitric oxide emissions. SOA are the result of chemical reactions of non-methane hydrocarbons (and their products) with the hydroxyl radical (OH), ozone, nitrate (NO_3) or photolysis (Hallquist et al., 2009). Thus although many hydrocarbons in the atmosphere are of biogenic origin, anthropogenic pollutants have strong impacts on their conversion to SOA. There is tremendous complexity and still much uncertainty in the processes involved in the formation of secondary-organic aerosols (Carslaw et al., 2010; Hallquist et al., 2009). Additional information can be found in Section 7.3.2.

Once generated, the size and composition of aerosol particles can be modified by additional chemical reactions, condensation or evaporation of gaseous species and coagulation (Seinfeld and Pandis, 2006). It is this set of processes that defines their physical, chemical and optical properties, and hence their impact on radiation and clouds, with large regional and global differences (Section 7.3.3). Furthermore, their distribution is affected by transport and deposition, defining a residence time in the troposphere of usually a few days (Textor et al., 2006; also see FAQ.7.1).

8.3 Present-Day Anthropogenic Radiative Forcing

Human activity has caused a variety of changes in different forcing agents in the atmosphere or land surface. A large number of greenhouse gases have had a substantial increase over the industrial era and some of these gases are entirely of anthropogenic origin. Some of the gases are directly emitted to the atmosphere whereas other greenhouse gases are secondary products from human emitted species and the lifetime of these different gases vary substantially. Atmospheric aerosols have diverse and complex influences on the climate. Human activity has modified the land cover and changed the surface albedo. This section discusses all known anthropogenic forcing agents of non-negligible importance and their quantification in terms of RF or AF based on changes in abundance over the 1750–2011 period.

8.3.1 Changes in our Understanding of the Spectral Properties of WMGHG and Radiative Transfer Codes

RF estimates are performed with a combination of radiative transfer codes typical for GCMs as well as more detailed radiative transfer codes. Physical properties are needed in the radiative transfer codes such as absorption data for gases. HITRAN (High Resolution Transmission; Rothman, 2010) is widely used in radiative transfer models and the current edition is HITRAN 2008 (Rothman et al., 2009). Some researchers studied the difference among different editions of HITRAN databases for diverse uses (Feng and Zhao, 2009; Feng et al., 2007; Fomin and Falaleeva, 2009; Kratz, 2008). Model calculations have shown that modifications of the spectroscopic characteristics tend to have a modest effect on the determination of RF estimates of order 2–3% of the calculated RF at the tropopause attributed to the combined doubling of CO_2, N_2O and CH_4. These results showed that even the largest overall RF induced by differences among the HITRAN databases is considerably smaller than the range reported for the modelled RF estimates, thus, the line parameter updates to the HITRAN database are not a significant source for discrepancies in the RF calculations appearing in the IPCC reports. It is found that the differences among the continuum formulations tend to be comparable to the differences among the various HITRAN databases; but use of the older continuum formula produces significantly larger flux differences, thus, replacement of the older continuum is warranted (Kratz, 2008). Differences in absorption data from various HITRAN versions and updates on the water vapour continuum are *very likely* a small contributor to the uncertainty in RF of WMGHG.

Line-by-line (LBL) models using the HITRAN dataset as an input are the benchmark of radiative transfer models. The accuracy given by LBL is important to evaluate the calculated RF by diverse models. Some researchers compared different LBL models (Collins et al., 2006; Zhang et al., 2005) and line-wing cutoff, line-shape function and gas continuum absorption treatment effect on LBL calculations (Fomin and Falaleeva, 2009; Zhang et al., 2008). The agreement between LBL codes have been investigated in many studies and found to generally to be within a few percent (e.g., Collins et al., 2006; Forster et al., 2011a; Iacono et al., 2008) and to compare well to observed radiative fluxes under controlled situations (Oreopoulos et al., 2012). Forster et al. (2011a) evaluated global mean radiatively important properties of chemistry climate models (CCMs) and found that the combined long-lived greenhouse gas global annual mean instantaneous RF at the tropopause is within 30% of LBL models for all CCM radiation codes tested. The accuracies of the LW RF due to CO_2, tropospheric ozone and water vapour increase are generally very good and within 10% for most of the participation models, but problems remained in simulating RF for stratospheric water vapour and ozone changes with errors between 3% and 200% compared to LBL models. The agreement among the LW LBL codes where within 5%, except for stratospheric water vapour changes with large differences (90% for SW and 40% for LW).

Most intercomparison studies on RF of greenhouse gases are for clear-sky and aerosol free conditions; the introduction of clouds would greatly complicate the targets of research and are usually omitted in the intercomparison exercises of GCM radiation codes and LBL codes (e.g., Collins et al., 2006; Iacono et al., 2008). It is shown that cloud can greatly reduce the magnitude of radiative forcing due to greenhouse gases by about 25% (Forster et al., 2005; Zhang et al., 2011); but the influence of clouds on the diversity in RF is found to be within 5% in detailed 4 radiative transfer schemes with realistic cloud distributions (Forster et al., 2005). Differences in the RF estimates of WMGHG between LBL and radiative transfer codes used in GCMs can be substantial (30%), but they are small (5%) between the LBL codes. Estimates of WMGHG RF are based on the LBL codes or the radiative transfer codes compared and validated against LBL models and the uncertainty range in the RF of WMGHG of 10% is retained. We underscore that uncertainty in RF calculations in many GCMs is substantially higher.

8.3.2 Well-mixed Greenhouse Gases

AR4 assessed the RF from 1750 to 2005 of the well-mixed greenhouse gases (WMGHGs) to be 2.63 W m^{-2}. The four most important gases were CO_2, CH_4, CFC-12 and N_2O in that order. Halocarbons contributed 0.337 W m^{-2} to the total. Uncertainties (90% confidence ranges) were assessed to be approximately 10% for the WMGHGs. The major changes to the science since AR4 are the updating of the atmospheric concentrations, the inclusion of new species (NF_3 and SO_2F_2) and discussion of AF for CO_2. Since AR4 N_2O has overtaken CFC-12 as the third most important greenhouse gas.

A contribution to the uncertainty in the anthropogenic forcing of WMGHGs comes from the choice of the baseline date (1750) representing the division between natural and anthropogenic driven changes. The trends in the major WMGHGs (CO_2, CH_4, N_2O) were not flat in 1750 but were varying, partly due to changing climate and partly due to anthropogenic emissions (agriculture, residential waste, wood fuel and biomass burning).

8.3.2.1 CO_2

The atmospheric mixing ratio of CO_2 has increased globally by about 112 ppm from 1750 (before large scale industrialisation) to 390.5 ppm in 2011 (Section 2.4.1.1). Here we assess the RF due to changes in atmospheric concentration rather than attributing it to anthropogenic emissions. Section 6.3.2.6 describes how only a fraction of the historical CO_2 emissions have remained in the atmosphere. The impact of land use change on CO_2 from 1850 to 2000 was assessed in AR4 to be 12–35 ppm (0.17–0.51 W m^{-2}).

Using the simple formula from Ramaswamy et al. (2001), the CO_2 radiative forcing (as defined in Section 8.1) from 1750 to 2011 is 1.82 W m^{-2}. The uncertainties in the total forcing from Ramaswamy et al. (2001) are approximately 10%. As discussed in Section 8.3.1, the 10% uncertainty is retained for AR5.

Table 8.3 shows the concentrations and RF in AR4 (2005) and 2011 for the most important WMGHGs. Figure 8.6 shows the time evolution of RF and its rate of change. Since AR4 the RF of CO_2 has increased by

0.16 W m^{-2} and continues the rate noted in AR4 of almost 0.3 W m^{-2} per decade. As shown in Figure 8.6(c) the rate of increase in the RF from the WMGHGs over the last 15 years has been dominated by CO_2. Since AR4 CO_2 has accounted for 82% of the RF increase. The interannual variability in the rate of increase in the CO_2 RF is largely due to variation in the natural land uptake whereas the trend is driven by increasing anthropogenic emissions (see Figure 6.8 in Section 6.3.1).

[INSERT FIGURE 8.6 HERE]

Figure 8.6: (a) Radiative forcing from the major well-mixed greenhouse gases and groups of halocarbons from 1850 to 2011 (data currently from NASA GISS http://data.giss.nasa.gov/modelforce/ghgases/). (b) Radiative forcing from the minor well-mixed greenhouse gases from 1850 to 2011. (c) Rate of change in forcing from the major well-mixed greenhouse gases and groups of halocarbons from 1850 to 2011.

As described in Section 8.1.1 CO_2 can also affect climate through physical effects on lapse rates and clouds, leading to an adjusted forcing (AF) that will be different from the RF. Andrews et al. (2012a) calculated an AF for 4 × CO_2 of 7.0 W m^{-2} with a 20% uncertainty, however they did not present RF using the same models. As described in Section 8.1, analysis of earlier models revealed substantial spread in AF/RF ratios for CO_2 but no clear systematic difference between AF and RF (Forster and Taylor, 2006). It is therefore not possible to conclude with the current information whether the AF for CO_2 is higher or lower than the RF. Therefore we assess the ratio AF/RF to be 1.0 with and uncertainty of 20%. We have medium confidence in this based on our understanding that the physical processes responsible for the differences between AF and RF are small enough to be covered within the 20% uncertainty.

There are additional effects mediated through plant physiology, reducing the conductance of the plant stomata and hence the transpiration of water. Andrews et al. (2012b) find a physiological enhancement of the adjusted forcing by 3.5% due mainly to reductions in low cloud. This is smaller than a study with an earlier model by Doutriaux-Boucher et al. (2009) which found a 10% effect. Longer-term impacts of CO_2 on vegetation distributions also affect climate (Andrews et al., 2012b; O'ishi et al., 2009) but we class these as feedbacks rather than rapid responses.

8.3.2.2 CH_4

Globally-averaged surface methane concentrations have risen from 722 ± 4 ppb in 1750 to 1803 ppb by 2011 (Section 2.4.1.1.2). Over that timescale the rise has been predominantly due to changes in anthropogenic-related methane. Anthropogenic emissions of other compounds have also affected methane concentrations by changing its removal rate (Section 8.2.3.3). Using the formula from Ramaswamy et al. (2001) the RF for methane from 1750 to 2011 is 0.48 W m^{-2}, with an uncertainty of ±10% as assessed in Section 8.3.1. This increase of 0.011 W m^{-2} since AR4 is due to the 29 ppb increase in the methane mixing ratio driven by a combination of increase in net natural and anthropogenic emissions and change in oxidising capacity, but the various contributions are not well quantified. Recent trends in methane and their causes are discussed in Sections 2.4.1.1.2 and 6.3.3.1.

In this section only the direct forcing from changing methane concentrations is addressed. Methane emissions can also have indirect effects on climate through impacts on CO_2, stratospheric water vapour, ozone, sulphate aerosol, and vegetation (Boucher et al., 2009; Collins et al., 2010; Shindell et al., 2009). These are covered in Sections 8.3.3, 8.5.1 and 8.7.7.

8.3.2.3 N_2O

Concentrations of nitrous oxide have risen from 270 ppb in 1750 to 324 ppb in 2011, an increase of 5 ppb since 2005 (Section 2.4.1.1.3). N_2O now has the third largest forcing of the anthropogenic gases, at 0.17 W m^{-2}. Only the direct RF from changing nitrous oxide concentrations is included, and indirect effects of N_2O emissions on stratospheric ozone are not taken into account here.

8.3.2.4 Other WMGHGs

RF of the other WMGHG are shown in Figure 8.6 (b). The contribution of groups of halocarbons to the rate of change of RF is shown in Figure 8.6 (c). Between 1970 and 1990 halocarbons made a significant

contribution to the rate of change of RF. Since the Montreal Protocol, the rate of change of RF from halocarbons has been much less, but still positive (total RF of 0.36 W m^{-2} in 2011 compared to 0.35 W m^{-2} in 2005) as the growth of HCFCs and HFCs (0.010 and 0.009 W m^{-2} since 2005) more than compensates for the decline in the CFC RF (–0.008 W m^{-2} since 2005).

8.3.2.4.1 CFCs and HCFCs

The CFCs and HCFCs contribute approximately 11% of the WMGHG RF. Although emissions have been drastically reduced for CFCs, their long lifetimes mean this takes time to affect their concentrations. The RF from CFCs has declined since 2005 (mainly due to a reduction in the concentrations of CFC-11 and CFC-12), whereas the RF from HCFCs is still rising (mainly due to HCFC-22).

8.3.2.4.2 HFCs

The RF of HFCs is 0.02 W m^{-2} and has close to doubled since AR4 (2005 concentrations). HFC-134a is the dominant contributor to RF of the HFCs with a RF of 0.01 W m^{-2}.

8.3.2.4.3 PFCs and SF6

These gases have lifetimes of thousands to tens of thousands of years (Table 8.A.1), therefore emissions essentially accumulate in the atmosphere on the timescales considered here. They currently contribute 0.3% of the total WMGHG RF.

8.3.2.4.4 New species

Nitrogen Trifluoride is used in the electronics industry and sulfuryl fluoride is used as a fumigant. Both have rapidly increasing emissions and high GWPs, but currently contribute only 0.0001 W m^{-2} and 0.0003 W m^{-2} to anthropogenic RF, respectively (Andersen et al., 2009; Muhle et al., 2009; Weiss et al., 2008).

Table 8.3: Present-day concentrations (in ppt except where specified) and RF (in W m^{-2}) for the measured WMGHGs. Concentration data are averages of NOAA and AGAGE observations where available. CO_2 concentrations are the average of NOAA and SIO. See Table 2.12 for more details of the data sources. The data for 2005 (the time of the AR4 estimates) are also shown. Some of the concentrations vary slightly from those reported in AR4 due to averaging different data sources. Radiative efficiencies for the minor gases are taken from Hodnebrog et al. (2012). Uncertainties in the RF are dominated by the uncertainties in the radiative efficiencies.

	Concentrations (ppt)		Radiative efficiency (m W m^{-2} ppt^{-1})	Radiative forcing [a] (W m^{-2})	
Species	*2011*	*2005*		*2011*	*2005*
CO_2 (ppm)	390	379	1.37×10^{-5} [e]	1.82	1.66
CH_4 (ppb)	1803	1774	3.63×10^{-4} [e]	0.48	0.47 [f]
N_2O (ppb)	324	319	3.03×10^{-3} [e]	0.170	0.162
CFC-11	238	251	0.26 ± 0.03	0.062	0.065
CFC-12	528	542	0.32 ± 0.03	0.169	0.173
CFC-13	2.7		0.25 ± 0.03	0.0007	
CFC-113	74.3	78.6	0.30 ± 0.03	0.0223	0.0236
CFC-115	8.37	8.36	0.21 ± 0.02	0.0018	0.0018
HCFC-22	213	168	0.20 ± 0.02	0.0426	0.0336
HCFC-141b	21.4	17.6	0.15 ± 0.02	0.0032	0.0027
HCFC-142b	21.1	15.4	0.19 ± 0.02	0.0040	0.0030
HFC-23	24.0	18.8	0.18 ± 0.02	0.0043	0.0034
HFC-32	4.92	1.15	0.11 ± 0.02	0.0005	0.0001
HFC-125	9.58	3.69	0.22 ± 0.02	0.0021	0.0008
HFC-134a	62.5	34.3	0.16 ± 0.02	0.0100	0.0055
HFC-143a	12.04	5.65	0.16 ± 0.02	0.0019	0.0009
HFC-152a	6.42	3.47	0.09 ± 0.02	0.0006	0.0003
SF_6	7.28	5.64	0.57 ± 0.06	0.0041	0.0032
CF_4	79.0	75.0	0.10 ± 0.01	0.0039	0.0035

C_2F_6	4.16	3.66	0.26 ± 0.03	0.0011	0.0010
CH_3CCl_3	6.31	18.30	0.07 ± 0.01	0.0004	0.0013
CCl_4	85.7	92.5	0.18 ± 0.02	0.0154	0.0166
CFCs				0.262[b]	0.271[c]
HCFCs				0.0498	0.0392
Montreal Gases [d]				0.328	0.328
Halocarbons				0.357	0.348[g]
Total				2.83	2.64

Notes:
(a) Pre-industrial values are zero except for CO_2 (278 ppm), CH_4 (722 ppb), N_2O (270 ppb), and CF_4 (40 ppt).
(b) Total includes 0.007 W m^{-2} to account for CFC-114, Halon-1211 and Halon-1301.
(c) Total includes 0.009 W m^{-2} forcing (as in AR4) to account for CFC-13, CFC-114, CFC-115, Halon-1211 and Halon-1301.
(d) Defined here as CFCs+HCFCs+CH_3CCl_3+CCl_4
(e) The radiative efficiencies for CO_2, CH_4 and N_2O are incremental efficiencies starting from 2011 values.
(f) The value for the 1750 methane concentrations has been updated from AR4 in this report, thus the 2005 methane RF is slightly lower than reported in AR4.
(g) Estimates for halocarbons given in the table may have changed from estimates reported in AR4 due to updates in radiative efficiencies and concentrations.

8.3.3 Ozone and Stratospheric Water Vapour

AR4 assessed the radiative forcing from tropospheric ozone to be 0.35 W m^{-2} from multi-model studies with a high 95th percentile of 0.65 W m^{-2} to allow for the possibility of model underestimates of the pre-industrial tropospheric ozone levels. The stratospheric ozone RF was assessed from observational trends from 1979 to 1998 to be –0.05 ± 0.1 W m^{-2} with the 90% confidence range increased to reflect uncertainty in the trend prior to 1979 and since 1998. The RF from stratospheric water vapour generated by methane oxidation was assessed to be +0.07 ± 0.05 W m^{-2} based on Hansen et al. (2005).

Since AR4 there have been a few individual studies of tropospheric or stratospheric ozone forcing, a multimodel study of stratospheric ozone radiative forcing in the 2010 WMO stratospheric ozone assessment, and the ACCMIP multimodel study of tropospheric and tropospheric + stratospheric chemistry models. There is now greater understanding of how tropospheric ozone precursors can affect stratospheric ozone, and how ODSs can affect tropospheric ozone. We assess the total ozone RF to be +0.30 ± 0.2 W m^{-2}. This can be split according to altitude or by forcing agent (Shindell et al., 2012d). We assess these contributions to be +0.40 ± 0.2 W m^{-2} for tropospheric ozone, –0.10 ± 0.15 W m^{-2} for stratospheric ozone (Table 8.4), or alternatively 0.50 ± 0.2 W m^{-2} from ozone precursors, –0.20 (–0.3 to 0.0) m^{-2} from ODSs. Climate change has influenced ozone levels, and is typically included in RF estimates as those are based on modelled concentration changes, but the available literature provides insufficiently evidence for the sign and magnitude of the impact and we therefore refrain from giving an estimate.

The disagreement between tropospheric chemistry models and purported 19th century ozone observations is not yet resolved, but addition of bromine chemistry may help in the next generation of models. There is little new information since AR4 on the radiative forcing from water vapour formed from the stratospheric oxidation of methane.

Unlike for the well-mixed greenhouse gases the estimate of the tropospheric and stratospheric ozone concentration changes are almost entirely model based for the full pre-industrial to present-day interval (though observations are available for recent decades, especially for the stratosphere).

8.3.3.1 Tropospheric Ozone

Ozone is formed in the troposphere by photochemical reactions of natural and anthropogenic precursor species (Section 8.2.3.1). Changes in stratospheric ozone depleting substances (ODSs) can also affect tropospheric ozone either by transport across the tropopause or modification of photolysis rates. Changes in

climate have also affected tropospheric ozone concentrations through changes in chemistry, natural emissions and transport from the stratosphere (Isaksen et al., 2009).

The most recent estimates of the tropospheric ozone radiative forcing come from multi-model studies under the ACCMIP project (Conley et al., 2012; Lamarque et al., 2012; Stevenson et al., 2012). These global chemistry-climate models used in ACCMIP (Table 8.4) provide an estimated tropospheric ozone increase (Figure 8.4) over 1850 to 2000 of approximately 98 Tg (see Figure 8.7). It is important to note that, while the standard deviation among model estimates for the 1850 and 2000 estimate is more than 20 Tg, the ozone field responds quite similarly in the different models to the changes in emissions and environmental conditions between 1850 and 2000. The average tropospheric ozone radiative forcing from 1850 to 2000 is 0.34 W m^{-2} (Conley et al., 2012; Stevenson et al., 2012). Skeie et al. (2011a) found a tropospheric ozone radiative forcing between 1750 and 1850 of 0.04 W m^{-2}, and similarly a 0.02W m^{-2} increase between 2000 and 2010, so we add these to the ACCMIP results to give 0.40 W m^{-2} over the period 1750 to 2010. The best estimate of tropospheric ozone forcing is taken as the average of the ACCMIP models and the Søvde et al. result, giving 0.40 ± 0.20 W m^{-2}, where the uncertainty is given for the 5–95% confidence range and is greater than the range derived from the model studies to account for uncertainty in preindustrial emissions. The tropospheric ozone RF is sensitive to the assumed 'pre-industrial' levels. As described in Section 8.2.3.1 late 19th and early 20th century observations are lower than the ACCMIP models for the same period, however we assess that those observations are so uncertain that we maintain the use of the inter-model RF distribution to determine the 95th percentile confidence limit. The overall *confidence* in the tropospheric ozone RF is assessed as high.

The time evolution of the tropospheric ozone forcing is shown in Figure 8.8, along with the other short-lived gases. There is a noticeable acceleration in the forcing after 1950 and a deceleration in the 1990s.

It is useful to calculate a normalised radiative forcing (NRF) which is a radiative forcing per change in ozone column in W m^{-2} DU^{-1} or W mol^{-1}. The NRF is sensitive to the vertical profile of the ozone change and to the latitudinal profile to a smaller extent. Calculations from Stevenson et al. (2012), Søvde et al. (2011) give a NRF of 0.041 ± 0.005 W m^{-2} DU^{-1} (83 W mol^{-1}) slightly lower than the value of 0.042 W m^{-2} DU^{-1} (94 W mol^{-1}) in TAR (Ramaswamy et al., 2001).

[INSERT FIGURE 8.7 HERE]

Figure 8.7: Time evolution of tropospheric ozone column (in DU) from 1850 to 2005 from ACCMIP results and (Kawase et al., 2011). The OMI-MLS (Ziemke et al., 2011) and TES (Osterman et al., 2008) satellite-based climatologies are also shown, along with the ACCENT-AR4 results.

A small number of studies have looked at attributing the ozone changes between the anthropogenically emitted species. Søvde et al. (2011) report a tropospheric ozone RF of 0.38 W m^{-2}, 0.44 W m^{-2} from ozone precursors and –0.06 W m^{-2} from the impact of stratospheric ozone depletion on the troposphere. Shindell et al. (2012a) calculate that ODSs are responsible for between –0.08 and –0.10 W m^{-2} of the tropospheric ozone RF. Stevenson et al. (2012) estimate a tropospheric ozone RF of 0.40 W m^{-2} from 1750 to 2010 of which 0.19 W m^{-2} is due to methane emissions, 0.12 W m^{-2} from NO_X emissions, 0.06 W m^{-2} from CO, and 0.04 W m^{-2} from VOCs. These results were calculated by holding emissions of all precursors at year 2000 levels and reducing them individually to 1850 levels. Due to the non-linearity of the chemistry, starting from pre-industrial conditions and increasing precursor emissions singly may give a different result. Note that as well as inducing an ozone forcing, these ozone precursor species can also strongly effect the concentrations of methane and aerosols, adding extra terms (both positive and negative) to their total indirect forcings. The multi-model simulations performed in Stevenson et al. (2012) are line with the an earlier model estimate in Shindell et al. (2005) used in AR4 (Figure 2.21 and Table 2.13).

Tropospheric ozone can also affect the natural uptake of carbon dioxide (see Section 8.2.3.1) and it is found that this indirect effect could have contributed to about 0.2–0.4 W m^{-2} of the total CO_2 RF (Section 8.3.2.1) (Sitch et al., 2007). This would roughly double the overall importance of tropospheric ozone in terms of RF.

[INSERT FIGURE 8.8 HERE]

Figure 8.8: Time evolution of the radiative forcing from tropospheric and stratospheric ozone from 1850 to 2010. Tropospheric ozone data are from Skeie et al. (2011a) scaled to give 0.40 W m^{-2} at 2010, stratospheric ozone RF follow Effective Equivalent Stratospheric Chlorine (Daniel et al., 2010) scaled to give –0.10 W m^{-2} at 2010.

Table 8.4: Contributions of tropospheric and stratospheric ozone changes to radiative forcing from 1750 to 2010.

	Troposphere				Stratosphere		
	LW	SW	Total	NRF W m^{-2} DU^{-1}	LW	SW	Total
AR4 (Forster et al., 2007)			0.35 (–0.1, +0.3)				–0.05 ± 0.1
Shindell et al. (2006c)			0.37				–0.03
WMO (Forster et al., 2011b)							–0.03 ± 0.2 +0.03
Søvde et al. (2011)			0.45 (REF)	40			–0.12 (REF)
			0.38 (R2)	39			–0.12 (R2)
Skeie et al. (2011a) [a]			0.44 ± 0.13	38			–0.15 ± 0.14
ACCMIP [b]	0.32 ± 0.08	0.09 ± 0.02	0.40 ± 0.10	42 ± 5	–0.14 ± 0.3	0.09 ± 0.16	–0.05 ± 0.2
AR5			0.40 ± 0.20	42 ± 5			–0.10 ± 0.15

Notes:
[a] Here we have included both the impacts of tropospheric precursors and ODSs on tropospheric ozone in Skeie et al. (2011a).
[b] The ACCMIP tropospheric ozone RFs are from an average of 2 radiative transfer schemes (Conley et al., 2012; Stevenson et al., 2012) . The values have been increased by 20% in the LW and SW (total of 0.06 W m^{-2}) to account for changes before 1850 and since 2010. The stratospheric ozone values are from Conley et al. (2012) only.

8.3.3.2 Stratospheric Ozone

The decreases in stratospheric ozone since the pre-industrial era have a positive radiative forcing in the short wave (increasing the flux into the troposphere) and a negative radiative forcing in the long-wave. This leaves a residual forcing that is the difference of two larger terms. In the lower stratosphere the long wave effect tends to be larger, whereas in the upper stratosphere the short wave dominates. Thus whether stratospheric ozone depletion has contributed an overall net positive or negative forcing depends on the vertical profile of the change (Forster and Shine, 1997).WMO (2010) assessed the RF from 1979 to 2005 from observed ozone changes (Randel and Wu, 2007) and results from 16 models for the 1970s average to 2004. The observed and model mean ozone changes gave RF of different signs (see Table 8.4). The ACCMIP study also included some models with stratospheric chemistry with an estimate of –0.05 ± 0.2 W m^{-2}. The results from these are in good agreement with the model studies from WMO (2010). Forster et al. (2007) calculated a forcing of –0.05 W m^{-2} from observations over the period 1979–1998 and increased the uncertainty to 0.10 W m^{-2} to encompass changes between the pre-industrial period and 2005. Assuming the forcing follows the equivalent effective stratospheric chlorine these values would be increased by around 30% to account for depletion before 1979 and recovery since 1998 (Cionni et al., 2011; Hansen et al., 2002; Skeie et al., 2011a). The stratospheric ozone forcing roughly follows the trajectory of the changes in the stratospheric equivalent chlorine loading. It starts to decline in the 1960s, reaches a minimum in the late 1990s and has started to recover since then (Figure 8.8). The RF from stratospheric ozone changes is here assessed to –0.10 ± 0.15 and is a stronger negative value than AR4. RF is stronger due taking into account changes prior to 1979 as well as the fact that several models underestimate the stratospheric ozone reduction.

Other than the direct radiative forcing, stratospheric ozone depletion can indirectly affect regional surface temperatures and sea ice by altering circulation patterns such as the Southern Annular Mode (WMO, 2010). These are discussed in more detail in Chapters 11, 12 and 14.

It should be noted that the total direct radiative forcing from ODSs (0.33 W m^{-2} in Section 8.3.2) is substantially compensated for by their effect on both stratospheric and tropospheric ozone (–0.20 (–0.30 to 0.0) W m^{-2} in AR5; see also Shindell et al., 2012d).

8.3.3.3 Stratospheric Water

Stratospheric water vapour is dependent upon the amount entering from the tropical troposphere and chemical production from the oxidation of methane. Changes to the latter can be considered as an anthropogenic forcing. This contrasts with tropospheric water vapour which is almost entirely controlled by the balance between evaporation and precipitation (see FAQ 8.1). Stratospheric water vapour can also vary through changes in dynamics (Solomon et al., 2010) and through volcanic emission (Joshi and Jones, 2009), neither of which can be considered an anthropogenic forcing.

Myhre et al. (2007) used observations of the vertical profile of methane to deduce a contribution from oxidation of anthropogenic methane of 0.083 W m^{-2} which compares with the value of 0.07 W m^{-2} from calculations in a 2D model in Hansen et al. (2005). Both these values are consistent with the AR4 which obtained the stratospheric water vapour forcing by scaling the methane direct forcing by 15%. Thus the time evolution of this forcing is also obtained by scaling the methane forcing by 15%. The best estimate and uncertainty range from AR4 of 0.07 ± 0.05 W m^{-2} remain unchanged and the large uncertainty range is partly remaining due to large differences found in the intercomparison studies of change in stratospheric water vapour (see Section 8.4.1).

Water vapour is directly emitted into the stratosphere by aircraft. Contributions from the current civilian aircraft fleet are very small. Lee et al. (2009; 2010) estimate an anthropogenic contribution in 2005 of 0.003 W m^{-2} but with low confidence.

8.3.4 Aerosols and Cloud Effects

8.3.4.1 Introduction and Summary of AR4

In AR4 (Forster et al., 2007), RF estimates were provided for three aerosol effects. These were the RF of aerosol-radiation interaction (previously denoted as direct aerosol effect), RF of the aerosol-cloud interaction (previously denoted as the cloud albedo effect), and the impact of BC on snow and ice surface albedo. See Chapter 7 and Figure 7.2 for an explanation of the change in terminology between AR4 and AR5. The RF of aerosol-radiation interaction is scattering and absorption of shortwave and longwave radiation by atmospheric aerosols. Several different aerosol types from various sources are present in the atmosphere. Most of the aerosols primarily scatter solar radiation, but some components absorb solar radiation to various extents with black carbon as the most absorbing component. RF of aerosols in the troposphere is often calculated at the TOA since it is similar to tropopause values (Forster et al., 2007). An increase in the quantity of scattering aerosols exerts a negative RF, whereas increasing the amount of strongly absorbing components give a positive RF, which also depends on the underlying albedo. A best estimate RF of –0.5 ± 0.4 W m^{-2} was given in AR4 for the change in the net aerosol-radiation interaction between 1750 and 2005 and a medium to low level of scientific understanding (LOSU).

An increase in the hygroscopic aerosol abundance may enhance the concentration of cloud condensation nuclei (CCN). This may increase the cloud albedo and under the assumption of fixed cloud water content it is referred to RF of aerosol-cloud interaction (previously denoted as cloud albedo effect, see Chapter 7 and Figure 7.2). For the RF of aerosol-cloud interaction a best estimate of –0.7 W m^{-2} (range from –1.8 to –0.3) was given in AR4 and a low LOSU.

Black carbon in the snow or ice can lead to a decrease of the surface albedo. This leads to a positive RF. In AR4 this mechanism was given a best RF estimate of 0.1 ± 0.1 W m^{-2} and a low LOSU.

Impacts on clouds from the AF of aerosol-cloud interaction (including both effects previously denoted as cloud lifetime and cloud albedo effect) and the AF of aerosol-radiation interaction (including both effects previously denoted as direct aerosol effect and semi-direct effect) were not strictly in accordance with the RF concept, because they involve tropospheric changes in variables other than the forcing agent at least in the available model estimates, so no best RF estimates were provided in AR4 (see Section 8.1). However, the AF of aerosol-cloud interaction and the AF of aerosol-radiation interaction were included in the discussion of total aerosol effect in Chapter 7 in AR4 (Denman et al., 2007). The mechanisms influenced by

anthropogenic aerosol including the aerosol cloud interactions are discussed in detail in this assessment in Section 7.5 and summarized in the subsections below.

8.3.4.2 RF of the Aerosol-Radiation Interaction by Component

Based on a combination of global aerosol models and observation-based methods, the best RF estimate of the aerosol-radiation interaction in AR5 is –0.40 ± 0.30 W m^{-2}. This estimate is thus weaker than in AR4 and with a somewhat reduced uncertainty range. Compared to AR4 the estimate and uncertainty are more robust since the agreement between estimates from various sources is much better (see Chapter 7.5). The main source of the model estimate is based on updated simulations in AeroCom (http://aerocom.met.no/aerocomhome.html), which is an intercomparison exercise of a large set of global aerosol models that includes extensive evaluation against measurements.

The RF of aerosol-radiation interaction is separated into 7 components in this report; namely sulphate, BC from fossil fuel and biofuel, OA from fossil fuel and biofuel, BC and OA combined from biomass burning (BB), nitrate, SOA, and mineral dust. BC and OA from biomass burning are combined due to the joint sources, whereas treated separately for fossil fuel and biofuel since there is larger variability in the ratio of BC to OA in the fossil fuel and biofuel emissions. This approach is consistent with TAR and AR4. Table 8.5 compares the best RF estimates of the aerosol-radiation interaction for various components in this report with values in SAR, TAR and AR4. In magnitude the sulphate and BC from use of fossil fuel and biofuel dominate. It is important to note that the BB RF is small in magnitude but consists of larger, offsetting terms in magnitude from OA and BC. The changes in the RF estimates of the aerosol-radiation interaction of the various components have been rather modest compared to AR4, with largest changes for BC from fossil fuel and biofuel and for nitrate (see Section 7.5). SOA is a new component compared to AR4. Anthropogenic SOA precursors contribute only modestly to the anthropogenic change in SOA. The increase in SOA is mostly from biogenic precursors and enhanced partitioning of SOA into existing particles from anthropogenic sources and changes in the atmospheric oxidation (Carlton et al., 2010). This change in SOA is therefore of anthropogenic origin, but natural emission of SOA precursors are important (Hoyle et al., 2011).

Note that the best estimate and the uncertainty for the total is not equal to the sum of the aerosol components since the total is estimated based on combination of methods, whereas the estimates for the components rely mostly on model estimates.

Table 8.5: Global and annual mean RF of aerosol-radiation interaction between 1750 and 2010 of 7 aerosol components. Values and uncertainties from SAR, TAR, AR4 and AR5 are provided when available.

	Global Mean Radiative Forcing (W m^{-2})				
	SAR	TAR	AR4	AR5	Comment
Sulphate aerosol	–0.40 [2x]	–0.40 [2x]	–0.40 [±0.20]	–0.40 [±0.20]	Estimate unchanged
BC aerosol from fossil fuel and biofuel	+0.10 [3x]	+0.20 [2x]	+0.20 [±0.15]	+0.30 [±0.20]	Re-evaluated to be stronger
Primary OA aerosol from fossil fuel and biofuel	Not estimated	–0.10 [3x]	–0.05 [±0.05]	–0.04 [±0.04]	Re-evaluated to be slightly weaker
Biomass burning	–0.20 [3x]	–0.20 [3x]	+0.03 [±0.12]	–0.0 [±0.10]	Re-evaluated
Secondary organic aerosols	Not estimated	Not estimated	Not estimated	–0.06 [±0.20]	Newly estimated
Nitrate	Not estimated	Not estimated	–0.10 [±0.10]	–0.15[±0.10]	Re-evaluated to be stronger
Dust	Not estimated	–0.60 to +0.40	–0.10 [±0.20]	–0.10 [±0.20]	Estimate unchanged
Total	Not estimated	Not estimated	–0.50 [±0.40]	–0.40 [±0.30]	Re-evaluated to be weaker and better constrained

Notes:
For the AR4 and AR5 columns the 90% uncertainty values are provided in brackets. The [2x] and [3x] provided for the uncertainties in SAR and TAR represent a factor of 2 and 3 relative uncertainty, respectively.

The RF of the aerosol-radiation interaction at some time periods is more uncertain than the current RF. Improvements in the observations of aerosols have been substantial with availability of remote sensing from the ground-based optical observational network AERONET and the launch of the MODIS and MISR instruments (starting in 2000) as well as other satellite data. This has contributed to constrain the current RF by aerosol observations. The aerosol observations are very limited backward in time, although there is growing constraint coming from new ice and lake core records, and uncertainties in the emission of aerosols and their precursors used in the global aerosol modeling are larger previously than for current condition. Emissions of carbonaceous aerosols are particularly uncertain in the 1800s due to a significant biofuel source in this period, in contrast to the SO_2 emissions that were very small until the end of the 1800s. The uncertainty in the biomass burning emissions increases backward in time. Note that, for 1850, the biomass burning emissions from Lamarque et al. (2010) are quite different from the previous estimates. For the other aerosol components 1750 emissions are negligible. Figure 8.9 shows an example of the time evolution of the RF of aerosol-radiation interaction as a total and separated into six aerosol components. From 1950 to 1990 there was a strengthening of the total RF of the aerosol-radiation interaction, mainly due to a strong enhancement of the sulphate RF. After 1990 the change has been small with even a weakening of the aerosol-radiation interaction RF, mainly due to a stronger BC RF as a result of increased emissions in East Asia.

[INSERT FIGURE 8.9 HERE]

Figure 8.9: Time evolution of RF of the aerosol-radiation interaction (total as well as by components). Multi-model results for 1930, 1980, and 2000 from ACCMIP are combined with higher temporal results from the GISS-E2 and Oslo-CTM2 models. Solid lines show the mean of individual model results and one standard deviation among the ACCMIP models are shown for 1930, 1980 and 2000. The 2010 values have been scaled to the best estimates given in Table 8.7. Note that time evolution for mineral dust is not included and the total is estimated based on the total of the six other aerosol components.

8.3.4.3 Aerosol Cloud Interactions

The RF due to aerosol cloud interactions (RFaci), formerly known as the first indirect aerosol forcing, is estimated to be –1 W m^{-2} being an average over all published estimates. This estimate is slightly more negative than the estimate of RFaci in AR4 where the reported value of –0.7 W m^{-2} was obtained from putting more emphasis of the newest results at that time (Forster et al., 2007). However, when RFaci is rescaled to conform with observational constraints from satellite data (Figure 7.19), the RFaci has a reduced magnitude (–0.3 W m^{-2}) reflecting the fact that most estimates of RFaci using satellite-based observations are systematically smaller in magnitude than the estimates derived from GCM calculations.

Adjusted forcings (AF, see Section 8.1) add the radiative effects from rapid adjustments onto the RF. These include rapid adjustments, such as changes to the cloud lifetime, changes in lapse-rate due to absorbing aerosols and aerosol microphysical effects on mixed-phase, ice and convective clouds (Figure 8.1). AF can be caused by aerosol-radiation interactions (ari,) or by aci or as the sum of ari and aci.

The AFari includes the semi-direct effect (see Section 7.3.5) and the rapid adjustments are principally caused by cloud changes. Existing estimates of AFari rely on global models but these models are known to inadequately represent some of the important relevant cloud processes (see Section 7.3.5). As a result the response of models differs and there is low confidence in determining the sign and magnitude of the rapid adjustments at the global scale. Overall a best estimate for this rapid adjustment is taken to be –0.1 W m^{-2}, with 5–95% uncertainty range of –0.3 to +0.1 W m^{-2}. The uncertainties are added in quadrature to the estimate of RFari to give an assessment for AFari of -0.5 ± 0.4 W m^{-2}.

The physical basis for our understanding of aerosol indirect forcing in low stratiform warm clouds has progressed significantly since AR4 (Section 7.4). There are different rapid adjustments that contribute to the AF through changes in cloud condensate, cloud cover, cloud phase or precipitation efficiency (Section 7.4) and thus adjustments extend to a range of different cloud types (e.g., convection, cirrus). Given the difficulties in representing relevant aerosol properties, clouds, and aerosol-cloud interactions in climate models as discussed in Section 7.4 there remain large uncertainties in quantification of the AFaci even for

low stratiform clouds and there is little consensus on the magnitude and sign of adjustments to other cloud types.

The first GCM estimates of AFari+aci only included aci in liquid stratiform clouds. Its mean value of –1.5 W m^{-2} is only slightly less negative than the mean AFaci suggesting that ari play a secondary role once aci are considered. One persistent shortcoming of global model estimates is the tendency to only treat aerosol-cloud interactions in terms of large-scale, but not convective clouds. Thus estimates of the AFaci are incomplete and confounded by remaining model biases in representing clouds in large-scale models. For these reasons, and because lifetime effects depend critically on the interplay of uncertainly parameterized physical processes, global-model based estimates of lifetime effects remain uncertain. With these shortcomings in mind, a best estimate and a 5–95% range for AFari+aci of –0.9 (–1.5 to –0.3) W m^{-2} (Section 7.5.3) being a combination of global model estimates, inverse estimates of AFari+aci and satellite-based estimates. This estimate is significantly weaker than the AR4 estimate but is consistent with several new lines of evidence as discussed in Section 7.5.3.

8.3.4.4 Black Carbon Deposition in Snow and Ice

Because absorption by ice is very weak at visible and UV wavelengths, black carbon in snow makes the snow darker and increases absorption. This is not enough darkening to see by eye, but it is enough to be important for climate (Clarke and Noone, 1985; Warren and Wiscombe, 1980). In AR4 this mechanism was given a best estimate of 0.1 W m^{-2} and a low LOSU. Since AR4, however, several studies have re-examined this issue and find that the RF may be weaker than the estimates of (Hansen and Nazarenko, 2004) and AR4 (Flanner et al., 2007; Koch et al., 2009a; Lee et al., 2012; Rypdal et al., 2009). The anthropogenic BC on snow/ice is assessed to have a positive global and annual mean RF of +0.04 W m^{-2}, with a 0.02–0.09 W m^{-2} 5–95% uncertainty range (see further description in Section 7.5).

The BC concentration in the Arctic atmosphere is observed to be declining since 1990, at least in the Western Hemisphere portion (Sharma et al., 2004), which should lead to less deposition of BC on the snow surface. A large-area field campaign (Huang et al., 2011) found that the BC content of snow in northeast China is comparable to values found in Europe (20–800 ppb). The steep drop off in BC content of snow with latitude in northeast China may indicate that a small fraction of the BC emitted in China in the winter is exported northward to the Arctic (Huang et al., 2011). Figure 8.10 shows the time evolution of RF due to BC on snow and ice mainly based on a multi-model study by Lee et al. (2012). The RF of BC on snow shows rather stable values in the first part of last century, with an increase up to 1980 and thereafter a decline with values in 2010 lower than at 1900. Based on the observations and climate model simulations, the RF due to BC on snow has very likely weakened since 1980.

[INSERT FIGURE 8.10 HERE]

Figure 8.10: Time evolution of RF due to BC on snow and ice. The simulations are mainly based on the ACCMIP multi-model study by Lee et al. for the years 1850, 1930, 1980, and 2000. Additional simulations with one model were performed for the years 1750, 1950, 1970, 1990 and 2010. The 2010 value is scaled to the AR5 best estimate (from Lee et al., 2012).

8.3.4.5 Contrails and Contrail-Induced Cirrus

AR4 assessed the RF of contrails (persistent linear contrails) as +0.01 [–0.007, +0.02] W m^{-2} and provided no estimate for contrail induced cirrus. In AR5, Chapter 7 gives a best estimate of RF of contrails of +0.02 [±0.01] W m^{-2} and an AF estimate of the combined contrails and contrail induced cirrus of +0.05 (0.02 to 0.15) W m^{-2}. Since AR4, the optical depth of contrails has been better constrained by observations and the evidence for contrail induced cirrus has been increased due to observational studies (see further details 7.2.5).

8.3.5 Land Surface Changes

8.3.5.1 Introduction

Anthropogenic land cover change has a direct impact on the Earth radiation budget through a change in the surface albedo. It also impacts the climate through modifications in the surface roughness, latent heat flux, and river runoff. In addition, human activity may change the water cycle through irrigation and power plant cooling, and also generate direct input of heat to the atmosphere by consuming energy. Land use change, and in particular deforestation, also has significant impacts on WMGHG concentration, which are discussed in Chapter 6.

AR4 referenced a large number of RF estimates resulting from a change in land cover albedo. It discussed the uncertainties due to the reconstruction of historical vegetation, the characterization of present day vegetation and the surface radiation processes. On this basis, AR4 gave a best estimate of RF relative to 1750 due to land use related surface albedo at $–0.2 \pm 0.2$ W m$^{–2}$ with a level of scientific understanding at medium-low.

8.3.5.2 Land Cover Changes

Hurtt et al. (2006) estimates that 42–68% of the global land surface was impacted by land use activities (crop, pasture, wood harvest) during the 1700–2000 period. Until the mid-20th century most land use change took place over the temperate regions of the Northern hemisphere. Since then, reforestation is observed in Western Europe and North America as a result of land abandonment, while deforestation is concentrated in the tropics. After a rapid increase of the rate of deforestation during the 1980s and 1990s, satellite data indicate a slowdown in the past decade (FAO, 2010).

Since AR4, Pongratz et al. (2008) and Kaplan et al. (2011) extended existing reconstructions on land use back in time to the past millennium, accounting for the progress of agriculture technique, historical events such as the black death or war invasions. As agriculture was already widespread over Europe and South-Asia by 1750, the RF, that is defined with respect to this date, is weaker than the radiative flux change form the state of natural vegetation cover (see Figure 8.11). Deforestation in Europe and Asia during the last millennium led to a significant regional negative forcing. Betts et al. (2007) and Goosse et al. (2006) argue that it probably contributed to the 'Little Ice Age', together with natural solar and volcanic activity components, before the increase in greenhouse gas concentration led to temperature similar to those experienced in the early part of the second millennium. There is still significant uncertainty in the anthropogenic land cover change, and in particular its time evolution (Gaillard et al., 2010).

8.3.5.3 Surface Albedo and Radiative Forcing

Surface albedo is the ratio between reflected and incident solar radiation at the surface. It varies with the surface cover. Most forests are darker (i.e., lower albedo) than grasses and croplands, which are darker than barren land and desert. As a consequence, deforestation tends to increase the Earth albedo (negative RF) while cultivation of some bright surfaces may have the opposite effect. Deforestation also leads to a large increase in surface albedo in case of snow cover as low vegetation is more easily covered by snow that reflects sunlight much more than vegetation does.

The pre-industrial impact of the Earth albedo increase due to land use change, including the reduced snow masking by tall vegetation, is estimated to be on the order of –0.05 W m$^{–2}$ (Pongratz et al., 2009). Since then, the increase in world population and agriculture development led to additional forcing. Based on reconstruction of land use since the beginning of the industrial era, Betts et al. (2007) and Pongratz et al. (2009) computed spatially and temporally distributed estimates of the land use radiative forcing. They estimate that the present day flux change due to albedo change from vegetation is on the order of –0.2 W m$^{–2}$ (range –0.21 to –0.24). The RF, defined with respect to 1750, is in the range –0.17 to –0.18 W m$^{–2}$. A slightly stronger value (–0.22 W m$^{–2}$) was found by Davin et al. (2007) for the period 1860–1992.

[INSERT FIGURE 8.11 HERE]

Figure 8.11: Change in TOA SW flux [W m$^{–2}$] following the change in albedo as a result of anthropogenic Land Use Change for three periods (1750, 1900 and 1992 from top to bottom). By definition, the RF is with respect to 1750. The lower right inset shows the globally averaged impact of the surface albedo change to the TOA SW flux (left scale) as well as the corresponding RF (right scale) after normalization to the 1750 value. Based on simulations by Pongratz et al. (2009).

In recent years, the availability of global scale MODIS data (Schaaf et al., 2002) has improved surface albedo estimates (Rechid et al., 2009). These data have been used by Myhre et al. (2005a) and Kvalevag et al. (2010). They argue that the observed albedo difference between natural vegetation and croplands is less than usually assumed in climate simulations, so that the RF due to land use change is weaker than in estimates that do not use the satellite data. On the other hand, Nair et al. (2007) show observational evidence of an underestimate of the surface albedo change in land use analysis in southwest Australia. Overall, there is still a significant range of RF estimates for the albedo component of land use forcing. This is mostly due to the range of albedo change as a result of land use change, as shown in an inter-comparison of 7 atmosphere-land models (de Noblet-Ducoudre et al., 2012).

Deforestation has a direct impact on the atmospheric CO_2 concentration, and therefore contributes to the WMGHG RF as quantified in Section 8.3.2. Conversely, afforestation is a climate mitigation strategy to limit the CO_2 concentration increase. Several authors have compared the radiative impact of deforestation/afforestation that results from the albedo change with the greenhouse effect of CO_2 released/sequestered. Pongratz et al. (2010) shows that the historic land use change has had a warming impact (i.e., greenhouse effect dominates) at the global scale and over most regions with the exception of Europe and India. Bala et al. (2007) results show latitudinal contrast where the greenhouse effect dominates for low latitude deforestation while the combined effect of albedo and evapotranspiration impact does at high-latitude. These results are also supported by Bathiany et al. (2010). Similarly, Lohila et al. (2010) shows that the afforestation of boreal peatlands results in a balanced RF between the albedo and greenhouse effect. Overall, because of the opposite impacts, the potential of afforestation to limit climate change is limited (Arora and Montenegro, 2011) while it may have undesired impacts on the atmospheric circulation (Swann et al., 2012).

8.3.5.4 Other Impacts of Land Cover Change on the Earth's Albedo

Burn scars resulting from agriculture practices, uncontrolled fires or deforestation (Bowman et al., 2009) have a lower albedo than unperturbed vegetation (Jin and Roy, 2005). On the other hand, at high latitude, burnt areas are more easily covered by snow, which may result in an overall increase of the surface albedo. Myhre et al. (2005b) estimates a global radiative effect due to African fires of 0.015 W m^{-2}.

Over semi-arid areas, the development of agriculture favours the generation of dust. Mulitza et al. (2010) demonstrates a very large increase of dust emission and deposition in the Sahel concomitant with the development of agriculture in this area. This suggests that a significant fraction of the dust that is transported over the Atlantic, which impacts the Earth albedo, has an anthropogenic origin. There is no full estimate of the resulting RF, however. The dust RF estimate in Section 8.3.4.2 includes both land use contributions and change in wind-driven emissions. Both dust and biomass burning aerosol may impact the Earth surface albedo as these particles can be deposed on snow, which has a large impact on its absorption, in particular for soot. This is discussed in Section 8.3.4.4.

Urban areas have an albedo that is 0.01–0.02 smaller than adjacent croplands (Jin et al., 2005), but several authors, e.g. Oleson et al. (2010), argue that there is the potential for a strong increase through white roof coating with the objective of mitigating the heat island effect. Local effects can be very large, as shown by Campra et al. (2008) that reports a 0.09 increase in albedo and –20 W m^{-2} RF over a province in southeastern Spain, a consequence of greenhouse horticulture development.

8.3.5.5 Impacts of Surface Change on Climate

Davin et al. (2007) argues that the climate sensitivity to land use forcing is lower than that for other forcings, due to its spatial distribution but also the role of non-radiative processes. Indeed, in addition to the impact on the surface albedo, land use change also modifies the evaporation and surface roughness, with counterbalancing consequences on the lower atmosphere temperature. There is increasing evidence that the impact of land use on evapotranspiration – a non RF on climate – is comparable to, but of opposite sign than, the albedo effect, so that RF is not as useful a metric as it is for gases and aerosols. For instance, Findell et al. (2007) climate simulations show a negligible impact of land use change on the global mean temperature, although there are some significant regional changes. The AF concept may be more appropriate for land use change, although no quantitative estimates are available yet.

Numerical climate experiments demonstrate that the impact of land use on climate is much more complex than just the RF. This is due in part to the very heterogeneous nature of land use change (Barnes and Roy, 2008), but mostly due to the impact on the hydrological cycle through evapotranspiration, root depth, and cloudiness (van der Molen et al., 2011). As a consequence, the forcing on climate is not purely radiative and the net impact on the surface temperature may be either positive or negative depending on the latitude (Bala et al., 2007). Davin and de Noblet-Ducoudre (2010) analyses the impact on climate of large-scale deforestation; the albedo cooling effect dominates for high latitude whereas reduced evapotranspiration dominates in the tropics. This latitudinal trend is confirmed by observations of the temperature difference between open land and nearby forested land (Lee et al., 2011).

Irrigated areas have continuously increased during the 20st century although a slowdown has been observed in recent decades (Bonfils and Lobell, 2007). There is clear evidence that irrigation leads to local cooling of several degrees (Kueppers et al., 2007). Irrigation also affects cloudiness and precipitation (Puma and Cook, 2010). In the United States, DeAngelis et al. (2010) found that irrigation in the Great Plains in the summer produced enhanced precipitation in the Midwest 1,000 km to the northeast.

8.3.5.6 Conclusions

There is still a rather wide range of estimates of the albedo change due to anthropogenic land use change, and its RF. Although most published studies provide an estimate close to –0.2 W m^{-2}, there is convincing evidence that it may be somewhat weaker as the albedo difference between natural and anthropogenic land cover may have been overestimated. In addition, non-radiative impact of land use have a similar magnitude, and may be of opposite sign, as the albedo effect (though these are not part of RF). A comparison of the impact of land use change according to seven climate models showed a wide range of results (Pitman et al., 2009), partly due to difference in the implementation of land cover change, but mostly due to different assumptions. There is no agreement on the sign of the temperature change induced by anthropogenic land use change. It is very likely that land use change led to an increase of the Earth albedo with a RF of –0.15 ± 0.10 W m^{-2}, but a net cooling of the surface – accounting for processes that are not limited to the albedo – is about as likely as not.

8.4 Natural Radiative Forcing Changes: Solar and Volcanic

Several natural drivers of climate change operate on multiple timescales. Solar variability takes place at many timescales as the radiant energy output of the Sun changes. Changes in the astronomical alignment of the Sun and Earth induce cyclical changes in RF, but this is substantial only at millennial and longer timescales. Volcanic forcing is highly episodic, but can have dramatic, rapid impacts on climate. Asteroid impacts are rare, but are thought to have played a large role in several climate change events in Earth's history. This section discusses solar and volcanic forcings, the two dominant natural contributors of climate change since the preindustrial time.

8.4.1 Solar Irradiance

In earlier IPCC reports the forcing was estimated as the instantaneous RF at TOA. However, due to wavelength-albedo dependence, solar activity-wavelength dependence and absorption within the stratosphere and the resulting stratospheric adjustment, the RF is reduced to 78% of the TOA instantaneous RF. This factor has an uncertainty of ~5% along the solar cycle (SC), but it may be different for the long-term (Gray et al., 2009) and also it is model dependent (Gregory et al., 2004; Hansen et al., 2005). AR4 gives an 11-years running mean instantaneous TOA RF between 1750 and the present of 0.12 W m^{-2} with a range of estimates of 0.06–0.3W m^{-2}, equivalent to a RF of 0.09 W m^{-2} with a range of 0.05–0.23 W m^{-2} used here. For a consistent treatment of all forcing agents, hereafter we use RF while numbers quoted from AR4 will be provided both as RF and instantaneous RF at TOA.

8.4.1.1 Observed Variations of TSI

8.4.1.1.1 Satellite measurements

The recent measurements of The Total Irradiance Monitor (TIM) on the Solar Radiation and Climate Experiment (SORCE) indicate a TSI of 1360.8 ± 0.5 W m^{-2} during 2008 (Kopp and Lean, 2011) which is 4.46 W m^{-2} lower than the Physikalisch-Meteorologisches Observatorium Davos (PMOD) TSI composite (Frohlich, 2006) during 2008. The TIM measurements are validated by irradiance comparisons to a NIST-calibrated cryogenic radiometer in the new TSI Radiometer Facility (Kopp and Lean, 2011). Such calibration linked to national standards laboratory references for end-to-end accuracy with quantified uncertainties makes an absolute calibration of TSI possible and indicates that TIM´s TSI are presently the best measurements. Given the TIM lower measurements, the general circulation models are calibrated to incorrectly higher values, although it is generally considered that a few tenths of a percent change in the absolute TSI value is of minimal consequences for climate simulations because of the larger uncertainties in cloud properties that have a greater effect on the radiative balance. As the maximum-to-minimum TSI percentage change is well-constrained from observations, and historical variations are calculated as percentage changes relative to modern values, a revision of the TSI affects RF by the same percentage as it affects TSI. The downward revision of TIM TSI with respect to PMOD, being 0.3%, thus has a negligible impact on RF.

Since 1978, several independent space-based instruments have directly measured the TSI. Three main composite series were constructed, referred to as the Active Cavity Radiometer Irradiance Monitor (ACRIM) (Willson and Mordvinov, 2003), the Royal Meteorological Institute of Belgium (RMIB) (Dewitte et al., 2004) and the PMOD (Frohlich, 2006). There are two major differences between ACRIM and RMIB relative to PMOD. The first is the rapid drift in calibration between PMOD and both ACRIM and RMIB before 1981. This arises because all three composites employ the Hickey-Frieden (HF) radiometer data for this interval. Re-evaluation of the early HF degradation has been implemented by PMOD but not by ACRIM and RMIB. The second one is the bridging of the gap between the end of ACRIM I (mid-1989) and the beginning of ACRIM II (late 1991) observations, as it is possible that a change in HF occurred during this gap. This possibility is neglected in ACRIM and thus its TSI increases by more than 0.5 W m^{-2} during SC 22. These differences lead to different long-term TSI trends in these composites: ACRIM rises until 1996 and subsequently declines, RMIB has an upward trend through 2008 and PMOD shows a decline since 1985 which unlike the other two composites, follows the solar-cycle-averaged sunspot number (Lockwood, 2010). Moreover, the ACRIM trend implies that the TSI on time scales longer than the solar cycle (SC) is positively correlated with the galactic cosmic ray (GCR) variation (opposite to the known anti-correlation of GCR with TSI along the SC) predicting a decline in TSI throughout most of the 20th century (the opposite to most TSI reconstructions produced to date, see 8.4.1.2). Furthermore, extrapolating the ACRIM TSI long-term drift would imply a brighter Sun in the Maunder minimum (MM) than now, again opposite to most TSI reconstructions (Lockwood and Frohlich, 2008). Finally, analysis of instrument degradation and pointing issues (Frohlich, 2006, 2009) and independent modeling based on solar magnetograms (Wenzler et al., 2006) confirm the need for correction of HF, and we conclude that PMOD is more accurate than the other composites.

TSI variations of ~0.1% were observed between the maximum and minimum of the 11-year SC in PMOD (Frohlich, 2006), and were also obtained in a recent average of the three composites mentioned above (Kopp and Lean, 2011). This variation is mainly due to a compensation between relatively dark sunspots, bright faculae and bright network elements (Foukal et al., 2006). A declining trend since 1986 in PMOD measurements is evidenced in the lower TSI seen during the SC 23 (1996–2008) minimum compared to the previous two minima (see also Figure 8.12): the mean TSI for September 2008 was 1365.26 ± 0.16 W m^{-2}, for 1996 was 1365.45 ± 0.10 W m^{-2} and for 1986 was 1365.57 ± 0.01 W m^{-2} (Frohlich, 2009). Thus, considering the last three solar minima PMOD values, between 1986 and 2008 there is a negative RF of –0.04 ± 0.02 W m^{-2}. Between 1986 and 2011, an interval that includes a substantial portion of the SC variation, a positive RF of 0.01 ± 0.005 W m^{-2} is calculated.

[INSERT FIGURE 8.12 HERE]

Figure 8.12: Annual average **c**omposites of measured Total Solar Irradiance: The Active Cavity Radiometer Irradiance Monitor (ACRIM) (Willson and Mordvinov, 2003), the Physikalisch-Meteorologisches Observatorium Davos (PMOD) (Frohlich, 2006) and the Royal Meteorological Institute of Belgium (RMIB) (Dewitte et al., 2004). These composites are matched at the year 2003 to the annual average of the Total Solar Irradiance Monitor (TIM) (Kopp and Lean, 2011) measurements that are also shown.

8.4.1.2 TSI Variations since Preindustrial Time

While the year 1750 is used as the nominal year of the preindustrial atmosphere, this was a year of solar activity maximum. To avoid trends caused by comparing different portions of the solar cycle, we analyze TSI changes using multi-year running means. We use a recent TSI reconstruction by Vieira et al. (2011), extending previous work by Krivova et al. (2010), that is based on physical modeling of the evolution of solar surface magnetic flux and its relationship with both sunspots and cosmogenic isotopes. This provides a more comprehensive reconstruction than other models (see the time series in Table 8.SM.1 in the Supplementary Material). The best estimate gives a 7-year running mean RF between the minima of 1745 and 2008 of ~0.04 W m^{-2}. A range of –0.02 to 0.10 W m^{-2} is obtained from the RF of several up-dated reconstructions using also the past to present minima (Delaygue and Bard, 2011; Krivova et al., 2010; Steinhilber et al., 2009; Velasco-Herrera et al., 2012; Wang et al., 2005). Hence we adopt this value and range for AR5. This RF is almost half of that in AR4, in part because the AR4 estimate was based on the previous solar cycle minimum while the AR5 estimate includes the drop of TSI in 2008 compared to the previous two SC minima (see 8.4.1.1.1). Concerning the uncertainty range, in AR4 the upper limit corresponded to the reconstruction of Lean (2000), based on the reduced brightness of non-cycling Sun-like stars assumed typical of a Maunder minimum state. The use of such stellar analogs was based on the work of Baliunas an Jastrow (1990), but more recent surveys have not reproduced their results and suggest that the selection of the original set was flawed (Hall and Lockwood, 2004; Wright, 2004); the lower limit from 1750 to present is due to the increase in the amplitude of the 11-year cycle only. Thus the RF and uncertainty range have been obtained much differently in AR5 compared to AR4. Maxima to maxima RF give a higher estimate than minima to minima RF, but the latter is more relevant for changes in solar activity. Given the *low agreement* and *medium evidence*, this RF value has a *low confidence level* (although *confidence* is higher for the last three decades). Figure 8.13 shows several TSI reconstructions modeled using sunspot numbers (Velasco-Herrera et al., 2012; Wang et al., 2005), cosmogenic isotopes (Delaygue and Bard, 2011; Steinhilber et al., 2009) or both (Vieira et al., 2011).

For the MM-to-present AR4 gives a RF range of 0.1–0.28 W m^{-2}, equivalent to 0.08–0.22 W m^{-2} with the RF definition used here. The reconstructions in Schmidt et al. (2011) indicate a MM-to-present RF range of 0.08–0.18 W m^{-2}, which is within the AR4 range although narrower. As we discussed above, the estimates based on irradiance changes in Sun-like stars are not included in this range because they are now considered incorrect. A more detailed explanation of this is found in the Supplementary Material.

[INSERT FIGURE 8.13 HERE]

Figure 8.13: Reconstructions of Total Solar Irradiance between 1750 and 1975: Wang et al. (2005) with and without an independent change in the background level of irradiance (annual resolution series), Steinhilber et al. (2009; 5-year time resolution series), Vieira et al. (2011; annual resolution series), Delaygue and Bard (2011; 5-year time resolution series) and Velasco-Herrera et al. (2012; annual resolution series). The series are set to match PMOD at the year 1976 (PMOD is already matched to TIM at the year 2003).

8.4.1.3 Attempts to Estimate Future Centennial Trends of TSI

Cosmogenic isotope and sunspot data (Rigozo et al., 2001; Usoskin et al., 2003) reveal that currently the Sun is in a grand activity maximum that began ~1920. However, SC 23 showed a previously unseen activity decline (McComas et al., 2008; Russell et al., 2010; Smith and Balogh, 2008). Most current estimations suggest that the forthcoming solar cycles will have lower TSI than the previous ones (Abreu et al., 2008; Lockwood et al., 2009; Rigozo et al., 2010; Russell et al., 2010; Velasco-Herrera et al., 2012). Recent estimates of the RF between the modern minimum in 2008 and this 21st century minimum indicate a negative RF of about 0.04–0.07 W m^{-2} (Jones et al., 2012; Velasco-Herrera et al., 2012). However, much more evidence is needed and at present we have a very low confidence concerning future solar forcing estimates.

Nevertheless, if there is such a diminished solar activity, there is a high confidence that the TSI RF variations will be much smaller than the projected increased forcing due to GHG (see Section 12.3.1).

8.4.1.3.1 Impacts of UV variations on the stratosphere

Ozone is the main gas involved in stratospheric radiative heating. Ozone production rate variations are largely due to solar UV irradiance changes (HAIGH, 1994), with observations showing statistically

significant variations in the upper stratosphere of 2–4% along the SC (Soukharev and Hood, 2006). UV variations may also produce transport-induced ozone changes due to indirect effects on circulation (Shindell et al., 2006a). Additionally, statistically significant evidence for an 11-year variation in stratospheric temperature and zonal winds is attributed to UV radiation (Frame and Gray, 2010). The direct UV heating of the background ozone is dominant and over twice as large as the ozone forcing in the upper stratosphere and above, while indirect solar and terrestrial radiation through the SC-induced ozone change is dominant below about 5 hPa (Shibata and Kodera, 2005). The RF due to solar-induced ozone changes is a small fraction of the solar RF discussed in 8.4.1.1.1 (Gray et al., 2009).

8.4.1.4 Variations in Spectral Irradiance

Solar spectral irradiance (SSI) variations in the far (120–200 nm) and middle (200–300 nm) ultraviolet (UV) are the primary driver for heating, composition, and dynamic changes of the middle atmosphere, and although these wavelengths compose a small portion of the incoming radiation they have relatively large variations between the maximum and minimum of the SC compared to the corresponding TSI changes. In the stratosphere there are important UV variations, as this region has the potential to affect the troposphere and therefore climate (Gray et al., 2010), the UV may actually have a more significant impact on climate than what the sole TSI suggests. Although this indicates that metrics based only on TSI are not appropriate, UV measurements present several controversial issues and modeling is not yet robust.

8.4.1.4.1 Satellite measurements

AR4, based on multiple space measurements made in the past 30 years (Brueckner et al., 1993; Rottman et al., 1993). Rottman (2006) reported changes along the SC of ~1.3% at 200 to 300 nm and ~0.2% at 315 to 400 nm. The Spectral Irradiance Monitor (SIM) on board of SORCE (Harder et al., 2009) indicates over the SC 23 declining phase measurements that are rather inconsistent with prior knowledge, indicating that additional validation and uncertainty estimates are needed (DeLand and Cebula, 2012; Lean and DeLand, 2012). A wider exposition can be found in the Supporting Material.

8.4.1.4.2 Reconstructions of preindustrial UV variations

The Krivova et al. (2010) reconstruction is based on what is known about spectral properties of sunspots and the relationship between TSI and magnetic fields, the authors interpolated backwards to the year 1610 based on sunspots and magnetic information. The Lean (2000) model is based on historical sunspot number and area and is scaled using the Upper Atmosphere Research Satellite (UARS) on board of the Solar Stellar Irradiance Comparison Experiment (SOLSTICE) measurements. The results show smoothed 11-years UV SSI changes between 1750 and the present of ~25% at ~120 nm, ~8% at 130–175 nm, ~4% at 175–200 nm, and ~0.5% at 200–350 nm. Thus, the UV SSI appears to have generally increased over the past four centuries with larger trends at shorter wavelengths. As few reconstructions are available, these values have *very low confidence*.

8.4.1.5 The Effects of Galactic Cosmic Rays on Clouds

Changing cloud amount or properties modify the Earth's albedo and therefore affect climate. It has been hypothesized that galactic cosmic rays (GCR) create atmospheric ions which facilitates aerosol nucleation and new particle formation with a further impact on the cloud formation (Kazil et al., 2012; Pierce and Adams, 2009). High solar activity means a stronger heliospheric magnetic field and thus a more efficient screen against GCR, then under the hypothesis underlined above, the reduced GCR flux would promote less clouds amplifying the warming effect expected from high solar activity. There is evidence from laboratory, field and modeling studies that ionization from GCR may enhance aerosol nucleation in the free troposphere (Kirkby et al., 2011; Merikanto et al., 2009; Mirme et al., 2010). However there is *high confidence* (*medium evidence* and *high agreement)* that the GCR-ionization mechanism is too weak to influence global concentrations of cloud condensation nuclei or their change over the last century or during a SC in a climatically-significant way (Erlykin and Wolfendale, 2011; Harrison and Ambaum, 2010; Snow-Kropla et al., 2011). A detailed exposition is found in Section 7.4.5.

8.4.2 Volcanic Radiative Forcing

8.4.2.1 Introduction

Volcanic eruptions that inject substantial amounts of SO_2 into the stratosphere are the dominant natural cause of climate change on the annual and multi-decadal time scales, and can explain much of the preindustrial climate change of the last millennium (Brovkin et al., 2010; Legras et al., 2010; Miller et al., 2012; Schneider et al., 2009). While volcanic eruptions inject both mineral particles (called ash or tephra) and sulphate aerosol precursors into the atmosphere, it is the sulphate aerosols, which because of their small size are effective scatterers of sunlight and have long lifetimes, that are responsible for RF important for climate. The emissions of CO_2 from volcanic eruptions are at least 100 times smaller than anthropogenic emissions, and inconsequential for climate on century time scales (Gerlach, 2011). To be important for climate change, sulphur must be injected into the stratosphere, as the lifetime of aerosols in the troposphere is only about one week, while sulphate aerosols in the stratosphere from tropical eruptions have a lifetime of about one year, and those from high-latitude eruptions last several months. Most stratospheric injections are from explosive eruptions that directly put sulphur into the stratosphere, but Bourassa et al. (2012) showed that sulphur injected into the upper troposphere can then be lifted into the stratosphere over the next month or two by large scale Asian summer monsoon circulation. Robock (2000), AR4 (Forster et al., 2007) and Timmreck (2012) provide summaries of this relatively well understood forcing agent.

There have been no large volcanic eruptions with a detectable climatic response since the 1991 Mt. Pinatubo eruption, but several moderate high latitude eruptions have led to a better understanding of their effects. For example, new work has also produced a better understanding of the hydrological response to volcanic eruptions (Anchukaitis et al., 2010; Trenberth and Dai, 2007), better long-term records of past volcanism, and better understanding of the effects of very large eruptions.

There are several ways to measure both the SO_2 precursor and sulphate aerosols in the stratosphere, using balloons, airplanes, and both ground- and satellite-based remote sensing. Both the infrared and ultraviolet signals sensed by satellite instruments can measure SO_2, and stratospheric aerosol measurements by space-based sensors have been made on a continuous basis since 1978 by a number of instruments employing solar and stellar occultation, limb scattering, limb emission, and lidar strategies (Kravitz et al., 2011; Solomon et al., 2011; Thomason and Peter, 2006).

Forster et al. (2007), described four mechanisms by which volcanic forcing influences climate: direct RF; differential (vertical or horizontal) heating, producing gradients and circulation; interactions with other modes of circulation, such as El Niño/Southern Oscillation (ENSO); and ozone depletion with its effects on stratospheric heating, which depends on anthropogenic chlorine. However, stratospheric ozone would increase with a volcanic eruption under low-chlorine conditions. In addition, the enhanced diffuse light from volcanic aerosol clouds impacts vegetation and hence the carbon cycle (Mercado et al., 2009) and indirect effects of sulfate aerosols on clouds in the troposphere can also be important (Schmidt et al., 2010).

8.4.2.2 Recent Eruptions

The background stratospheric aerosol concentration has had an upward trend for the past decade (Hofmann et al., 2009; Nagai et al., 2010). The decadal trend, while small, was produced by a number of small eruptions, with possibly a small contribution from tropospheric pollution (Siddaway and Petelina, 2011; Vernier et al., 2011), and had a small, but important impact on RF (Solomon et al., 2011). Two recent high-latitude eruptions, of Kasatochi Volcano (52.1°N, 175.3°W) on August 8, 2008 and of Sarychev Volcano (48.1°N, 153.2°E) on June 12–16, 2009, each injected ~1.5 Tg SO_2 into the stratosphere, but did not produce detectable climate response. Their eruptions, however, led to better understanding of the dependence of the amount of material and time of year of high-latitude injections to produce climate impacts (Haywood et al., 2010; Kravitz et al., 2010; Kravitz et al., 2011). The RF from high-latitude eruptions is a function of seasonal distribution of insolation and the 3–4 month lifetime of high-latitude volcanic aerosols. Kravitz and Robock (2011) showed that high-latitude eruptions must inject at least 5 Tg SO_2 into the lower stratosphere in the spring or summer, and much more in fall or winter, to have a detectible climatic response.

On April 14, 2010 the Eyjafjallajökull volcano in Iceland (63.6°N, 19.6°W) began an explosive eruption phase that shut down air traffic in Europe for 6 days and continued to disrupt it for another month. The climatic impact of Eyjafjallajökull was about 10,000 times less than that of Pinatubo, however, and was

therefore undetectable amidst the chaotic weather noise in the atmosphere (Robock, 2010). 2011 saw the continuation of a number of small eruptions with significant tropospheric SO_2 and ash injections, including Puyehue-Cordón Caulle in Chile, Nabro in Eritrea, and Grimsvötn in Iceland. None have been shown to have produced an important RF, but the June 13, 2011 Nabro eruption produced the largest stratospheric aerosol cloud since the 1991 Pinatubo eruption (Bourassa et al., 2012). The mean volcanic radiative forcing over the period 2000–2010 has been estimated to be about –0.1 W m^{-2} (Solomon et al., 2011).

Figure 8.14 shows a reconstruction of volcanic aerosol optical depth since 1750 and Figure 8.15 shows observations since 1985.

[INSERT FIGURE 8.14 HERE]

Figure 8.14: Two volcanic reconstructions of aerosol optical depth (at 550 μm) as developed for the Paleoclimate Model Intercomparison Project (top), with a comparison to the updated estimates of Sato et al. (1993). Updated from Schmidt et al. (2011).

[INSERT FIGURE 8.15 HERE]

Figure 8.15: (a) Monthly mean extinction ratio (525 nm) profile evolution in the tropics [20°N–20°S] from January 1985 to June 2010 derived from (left) SAGE II extinction in 1985–2005 and (right) CALIOP scattering ratio in 2006–2011, after removing clouds below 18 km based on their wavelength dependence (SAGE II) and depolarization properties (CALIOP) compared to aerosols. Black contours represent the extinction ratio in log-scale from 0.1 to 100. The position of each volcanic eruption occurring during the period is displayed with its first two letters on the horizontal axis, where tropical eruptions are noted in red. The eruptions were Nevado del Ruiz (Ne), Augustine (Au), Chikurachki (Ch), Kliuchevskoi (Kl), Kelut (Ke), Pinatubo (Pi), Cerro Hudson (Ce), Spur (Sp), Lascar (La), Rabaul (Ra), Ulawun (Ul), Shiveluch (Sh), Ruang (Ru), Reventador (Ra), Manam (Ma), Soufrière Hills (So), Tavurvur (Ta), Chaiten (Ch), Okmok (Ok), Kasatochi (Ka), Fire/Victoria (Vi*), Sarychev (Sa), Merapi (Me), Nabro (Na). Updated from Figure 1 from Vernier et al. (2011). (b) Mean stratospheric Aerosol Optical Depth in the tropics [20°N–20°S] between 20 and 30 km since 1985 from the Stratospheric Aerosol and Gas Experiment (SAGE) II (black line), the Global Ozone Monitoring by Occultation of Stars (GOMOS) (red line), and CALIOP (blue line). Updated from Figure 5, Vernier et al. (2011).

8.4.2.3 Records of Past Volcanism and Effects of Very Large Eruptions

While the effects of volcanic eruptions on climate are largest in the two years following a large stratospheric injection, and the winter warming effect in the Northern Hemisphere has been supported by long-term records (Fischer et al., 2007), there is new work on memory in the ocean heat content and sea level. Work with climate models has quantified these effects (Ottera et al., 2010; Stenchikov et al., 2009), and found an impact on North Atlantic Ocean circulation a decade later (Zanchettin et al., 2010) that warms the ocean. This is in contrast to Zhong et al. (2011) and Miller et al. (2012), who found a mechanism in the North Atlantic that produces long-term cooling. Lacking observations of this process, the long-term interactions of volcanic forcing with ocean feedbacks is not well-understood, but models indicate that the Atlantic Meridional Overturning Circulation could first be stronger from temperature effects and then weaker from salinity impacts.

New work on the mechanisms by which a supereruption (Self and Blake, 2008) could force climate has focused on the 74,000 BP eruption of the Toba volcano (2.5°N, 99.0°E). Robock et al. (2009) used simulations of up to 900 times the 1991 Pinatubo sulphate injection to show that the forcing is not linear as a function of the injection after a substantial part of the solar radiation is blocked. The results agreed with a previous simulation by Jones et al. (2005). They also showed that chemical interactions with ozone had small impacts on the forcing and that the idea of Bekki et al. (1996) that water vapour would limit and prolong the growth of aerosols was not supported. Timmreck et al. (2010) however, incorporating the idea of Pinto et al. (1989) that aerosols would grow and therefore both have less RF per unit mass and fall out of the atmosphere more quickly, found much less of a radiative impact from such a large stratospheric input.

8.4.2.4 Future Effects

How well can we predict the next climatically-important eruption? Ammann and Naveau (2003) and Stothers (2007) suggested an 80-year periodicity in past eruptions, but the data record is quite short and imperfect. While the period 1912–1963 CE was unusual for the past 500 years in having no large volcanic eruptions, and the period 1250–1300 CE had the most globally climatically-significant eruptions in the past 1500 years

(Gao et al., 2008), current knowledge only allows us to predict such periods on a statistical basis, assuming that the recent past distributions are stationary. Ammann and Naveau (2003), Gusev (2008), and Deligne et al. (2010) studied these statistical properties and Ammann and Naveau (2010) showed how they could be used to produce a statistical distribution for future simulations. Although the future forcing from volcanic eruptions will only depend on the stratospheric aerosol loading for most forcing mechanisms, the future effects on reducing ozone will diminish as ozone depleting substances diminish in the future (Eyring et al., 2010c).

8.4.2.5 Volcanic Eruptions as Analogues

Volcanic eruptions provide a natural experiment of a stratospheric aerosol cloud that can serve to inform us of the impacts of the proposed production of such a cloud as a means to control the climate, which is one method of geoengineering (Rasch et al., 2008; see Section 7.5). For example, Trenberth and Dai (2007) showed that the Asian and African summer monsoon, as well as the global hydrological cycle, was weaker for the year following the 1991 Pinatubo eruption, which is consistent with climate model simulations (Robock et al., 2008), and MacMynowski et al. (2011) showed that because the climate system response of the hydrological cycle is rapid, forcing from volcanic eruptions, which typically last about a year, can serve as good analogues for longer-lived forcing. The formation of sulphate aerosols, their transport and removal, their impacts on ozone chemistry, their RF, and the impacts on whitening skies, ecology because of more diffuse radiation, climate, astronomy, and remote sensing, as well as the beautiful sunsets, all also serve as good analogues for geoengineering proposals. However, volcanic eruptions cannot be used to test the long-term impacts of a permanent stratospheric cloud.

Volcanic eruptions also serve as an analogue that supports climate model simulations of the transport and removal of stratospheric soot aerosols, their impacts on ozone chemistry, their RF, and the climate response. The effect of a nuclear explosion is smoke from fires which could be lofted into the stratosphere and cause surface cooling and a reduction of stratospheric ozone (Mills et al., 2008). The use of the current global nuclear arsenal still has the potential to produce continental temperatures below freezing in summer (Robock et al., 2007a; Toon et al., 2008), and the use of 'only' 100 nuclear weapons could produce climate change unprecedented in recorded human history (Robock et al., 2007b).

8.5 Synthesis (Global Mean Temporal Evolution)

The RF can be used to quantify the various agents that drive climate change over the industrial era or the various contributions to future climate change. There are multiple ways in which RF can be attributed to underlying causes, each providing various perspectives on the importance of the different factors driving climate change. This section evaluates the RF with respect to emitted component and with respect to the ultimate atmospheric concentrations. The uncertainties in the RF agents vary and the confidence levels for these are presented in this section. Finally, this section shows historical and scenarios of future time evolution of RF.

8.5.1 Summary of Radiative Forcing by Species and Uncertainties

Table 8.6 has an overview of the RF agents considered here and each of them is given a confidence level for the change in RF over the industrial era at the present day. The confidence level is based on the evidence (robust, medium, and limited) and the agreement (high, medium, and low; see further description in Chapter 1). The confidence level of the forcing agents goes beyond the numerical values available in estimates and is an assessment for a particular forcing agent to have a real value encompassing the estimated range. Some of the RF agents have robust evidence such as WMGHG with well documented increase based on high precision measurements and contrails as additional clouds which can be seen by direct observations. However, for some RF agents the evidence is more limited regarding their existence such as aerosol influence on cloud cover. The consistency in the findings for a particular forcing agent decides the evaluation of the evidence. A combination of different methods, e.g., observations and modeling, and thus the understanding of the processes causing the forcing is important for this evaluation. The agreement is a qualitative judgment of the difference between the various estimates for a particular RF agent. Figure 1.12 in Chapter 1 shows how the combined evidence and agreement results in five levels for the confidence level. The colour codes used in Figure 1.12 for the confidence level are adopted in Table 8.6.

Table 8.6: Confidence level for the RF estimate associated with each forcing agents for the 1750–2011 period. The confidence level is based on the evidence and the agreement and given in the table. The basis for the confidence level and change since AR4 is provided. An asterisk is added to the RF agents with substantially greater confidence level over the period 1980–2011, compared to over the whole industrial era.

	Evidence	Agreement	Confidence Level	Basis for Uncertainty Estimates	Change in Understanding Since AR4
WMGHG	Robust	High	Very high	Uncertainty assessment of measured trends from different observed data sets and differences between radiative transfer models	No major change
Tropospheric Ozone	Robust	Medium	High	Observed trends of ozone in the troposphere and differences between model estimates of RF	No major change
Stratospheric Ozone	Robust	Medium	High	Observed trends in stratospheric and total ozone and differences between estimates of RF	No major change
Stratospheric Water Vapour from CH_4	Robust	Low	Medium	Similarities in independent methods to estimate the RF	Elevated due to more studies
RF of Aerosol-Radiation Interactions	Robust	Medium	High	A large set of observations and similarities in independent estimates of RF	Elevated due to improved understanding
RF of Aerosol-Cloud Interactions	Medium	Low	Low	Observational data and the spread in the model and observational based estimates of RF	No major change
Aerosol-Cloud Interactions beyond RF	Limited	Low	Very low	Observational evidence and spread in model estimates of RF	No major change
Aerosol-Radiation Interactions beyond RF	Limited	Low	Very low	Observational evidence and spread in model estimates of RF	No major change
Surface Albedo (Land Use)	Robust	Medium	High	Estimates of deforestation for agricultural purposes and spread in model estimates of RF	Elevated due to the availability of high quality satellite data
Surface Albedo (BC Aerosol on Snow and Ice)	Robust	Low	Medium	Observations of snow samples and link between BC content in snow and albedo as well as spread in model estimates of RF	Elevated due to improved knowledge from observations and models
Contrails	Robust	Medium	High	Observed contrails and spread in model estimates of RF	Elevated due to improved understanding
Contrail Induced Cirrus	Medium	Low	Low	Observations of a few events of contrail induced cirrus	Elevated due to additional studies
Solar Irradiance*	Medium	Low	Low	Satellite information over last decades and spread in reconstructions based on proxy data	No major change
Volcanic Aerosol*	Robust	Low	Medium	Observations of recent volcanic eruptions and reconstructions of past eruptions	Elevated due to improved understanding

Evidence is robust for several of the RF agents because of long term observations of trends over the indutrial era and well defined links between atmospheric or land surfaced changes and radiative effect. Evidence is medium for a few agents where the anthropogenic changes or the link between the forcing agent and radiative effect are less certain. Medium evidence can be assigned in cases where observations or modelling provide a diversity of information and thus not a consistent picture for a given forcing agents. Limited evidence is given for two RF agents related to clouds where model studies in some cases indicate changes but direct observations of clouds alterations are scarce. High agreement is only given for the WMGHG where the relative uncertainties in the RF estimates are much smaller than for the other RF agents. Low agreement can either be due to large diversity in estimates of the magnitude of the forcing or from the fact that the method to estimate the forcing has a large uncertainty. Stratospheric water vapour is an example of the latter with modest difference in the few available estimates but a known large uncertainty in the radiative transfer calculations (see further description in Section 8.3.1).

Figure 8.16 shows the development in the level of scientific understanding (LOSU) over the last 4 IPCC assessments of the various RF mechanisms. The LOSU terminiology is not regularly used in AR5, but for comparison with previous IPCC assessments the confidence level is converted approximately to LOSU. The figure shows a general increased LOSU but also that more RF mechanisms have been included over time. The LOSU values for the aerosol-radiation interaction (RF), surface albedo, contrails and volcanic aerosols have been raised and are now at the same ranking as those for change in stratospheric and tropospheric ozone. This is due to an increased understanding of key parameteres and their uncertainties for the elevated RF agents, e.g., for contrails the optical depth is better constrained (see Section 8.3.4). For tropospheric and stratospheric ozone changes research has shown further complexities with changes primarily influencing the troposphere or the stratosphere being linked to some extent (see Section 8.3.3). The aerosol-radiation interaction and aerosol-cloud interaction beyond RF are given a *very low confidence* level and had a similar ranking in AR4.

[INSERT FIGURE 8.16 HERE]

Figure 8.16: Level of scientific understanding (LOSU) of the RF mechanisms in the 4 last IPCC assessments. The LOSU terminology is not regularly used in AR5, but for comparison with previous IPCC assessments the confidence level is converted approximately to LOSU. The thickness of the bars represents the relative magnitude of the current RF (with a minimum value for clarity of presentation). LOSU for the RF mechanisms was not available in the first IPCC Assessment (Houghton et al., 1990).

Table 8.7 shows the best estimate of the RF for the various RF agents. Since TAR the RF due to WMGHG has increased by 16% and 8% since AR4. This is mainly due to increased concentrations (see Section 8.3.2), whereas the other changes for the anthropogenic RF agents compared to AR4 are due to re-evaluations and in some cases from improved understanding. An increased number of studies, additional observational data, and better agreement between models and observations can be the causes for such re-evaluations. The best estimates for RF of aerosol-radiation interactions, RF of aerosol-cloud interaction, BC on snow, and solar irradiance are all weaker than in AR4, otherwise the modifications to the best estimates are rather small. For the RF of aerosol-radiation interaction and BC on snow the changes in the estimates are based on additional new studies since AR4 (see Sections 8.3.4 and 7.5). For the change in the estimate of the solar irradiance it is a combination on how the RF is calculated, new evidence showing some larger earlier estimates were incorrect, and a downward trend over the last solar cycles in the solar activity that has been taken into account (see Section 8.4.1). The AF of aerosol-radiation interaction and aerosol-cloud interaction have larger uncertainties than their associated RF estimates. The uncertainties for AF of CO_2 increase also compared to RF (see Section 8.3.2). For the other GHG we do not have sufficient information to include an AF uncertainty to each of these forcing agents. However, for these forcing mechanisms the RF uncertainties are larger than for the WMGHG and thus unlikely that rapid adjustments changes the uncertainties substantially.

Figure 8.17a shows a bar chart of the RF agents listed in Table 8.7 over the 1750–2011 period. Solid bars are given for RF, whereas AF values for CO_2, aerosol-radiation interactions, aerosol-cloud interaction, and total anthropogenic forcing are given as additional hatched bars. An important assumption is that different forcing mechanisms can be treated additively to calculate the total forcing (see Boucher and Haywood, 2001; Haywood and Schulz, 2007). The allowance of rapid adjustment for the aerosol cloud interaction results in important differences in the forcing as evidenced in the figure. The strengthening in the forcing from the RF of aerosol-cloud interaction to AF of aerosol-cloud interaction broadens the shape of the probability density function (PDF) and shifts the PDF to slightly stronger values (see further description in Sections 8.3.4.3 and

7.4). The AF of aerosol-radiation interaction increases the uncertainty and best estimate compared to the RF of aerosol-radiation interaction (see further discussion in Sections 8.3.4.4 and 7.5). Total anthropogenic RF and AF calculated from Monte Carlo simulations are shown in Figure 8.17b, with a best estimate of 2.41 W m^{-2} and 2.24 W m^{-2}, respectively for RF and AF. For each of the forcing agents a PDF is generated based on uncertainties provided in Table 8.7. The combination of the individual RF agents to derive total anthropogenic forcing follows the same approach as in AR4 (Forster et al., 2007) which is based on the method in Boucher and Haywood (2001). The PDF of the GHGs (sum of WMGHG, ozone, and stratospheric water vapour) has a much more narrow shape than the PDF for the aerosols due to the much lower uncertainty. Therefore, the large uncertainty in the aerosol forcing is the cause for the large uncertainty in the total anthropogenic RF and AF. The probability for a negative total anthropogenic forcing is *exceptionally unlikely* even if rapid adjustments (quantified by AF) are taken into account for the aerosol effects. Compared to AR4 the total anthropogenic RF is more strongly positive and the probability for negative RF is much weaker. This is caused by a combination of growth in GHG concentration, and thus strengthening in RF of WMGHG, and weaker RF estimates of aerosols (aerosol-radiation interaction and aerosol-cloud interaction) as a result of new assessments of these effects.

Table 8.7: Summary table of RF estimates for AR5 and comparison with the 3 previous IPCC assessment reports. AF values for AR5 are included [PLACEHOLDER FOR FINAL DRAFT: AR5 values].

	Global Mean Radiative Forcing (W m^{-2})					AF (W m^{-2})
	SAR (1750–1993)	*TAR (1750–1998)*	*AR4 (1750–2005)*	*AR5 (1750–2011)*	*Comment*	*AR5*
Well-mixed Greenhouse Gases (CO_2, CH_4, N_2O, and Halocarbons)	2.45 [15%]	2.43 [10%]	2.63 [±0.26]	2.83 [±0.28]	Change due to increase in concentrations	2.83 [±0.57]
Tropospheric Ozone	+0.40 [50%]	+0.35 [43%]	+0.35 [–0.1, +0.3]	+0.40 [±0.20]	Slightly modified estimate	
Stratospheric Ozone	–0.1 [2x]	–0.15 [67%]	–0.05 [±0.10]	–0.10 [±0.15]	Re-evaluated to stronger estimate	
Stratospheric Water Vapour from CH_4	Not estimated	+0.01 to +0.03	+0.07 [±0.05]	+0.07 [±0.05]	No major change	
Aerosol-Radiation Interactions	Not estimated	Not estimated	–0.50 [±0.40]	–0.4 [±0.3]	Re-evaluated to be weaker and smaller uncertainty range	–0.5 [±0.4]
Aerosol-Cloud Interactions	0 to –1.5 (sulphate only)	0 to –2.0 (all aerosols)	–0.70 [–1.1, +0.4] (all aerosols)	–0.3 [–0.7 to 0.0]	Re-evaluated to be weaker	–0.4 [–0.9 to 0.0]
Surface Albedo (Land Use)	Not estimated	–0.20 [100%]	–0.20 [±0.20]	–0.15 [±0.10]	Re-evaluated to be slightly weaker	
Surface Albedo (BC aerosol on Snow and Ice)	Not estimated	Not estimated	+0.10 [±0.10]	+0.04 [0.02 to 0.09]	Re-evaluated to be weaker	
Contrails	Not estimated	0.02 [3.5x]	0.01 [–0.007, +0.02]	0.02 [±0.01]	Re-evaluated to be stronger	
Combined Contrails and Contrail Induced Cirrus	Not estimated	0 to +0.04	Not estimated	Not estimated	Best estimate unchanged	0.05 [0.02 to 0.15]
Solar Irradiance	+0.30 [67%]	+0.30 [67%]	+0.12 [–0.06, +0.18]	0.04 [±0.05]	Re-evaluated to be weaker	
Total Anthropogenic	Not estimated	Not estimated	1.6 [–1.0, +0.8]	2.41 [±0.60]	Stronger positive due to changes in various forcing agents	2.24 [±0.87]

Notes:

For the AR5 column the 90% uncertainty values are given in brackets either as a ± uncertainty or a range, whereas in the AR4 column the numbers in brackets must be added to the best estimate to obtain the 5 to 95% confidence range. The [2x] and [3x] provided for the uncertainties in SAR and TAR represent a factor of 2 and 3 relative uncertainty, respectively.

[INSERT FIGURE 8.17 HERE]

Figure 8.17: (a) Bar chart for RF (solid) and AF (hatched) for the period 1750–2011, where the total anthropogenic RF and AF are derived from panel b. (b) Probability density function (PDF) of total GHG RF, aerosol forcing, and total anthropogenic forcing. The GHG consists of WMGHG and ozone, and stratospheric water vapour. The PDFs are generated based on uncertainties provided in Table 8.7. The combination of the individual RF agents to derive total anthropogenic forcing are done by Monte Carlo simulations and based on the method in Boucher and Haywood (2001). PDF of the RF from surface albedo changes is included in the total anthropogenic forcing, but not shown as a separate PDF. The AF for GHG other than CO_2 and surface albedo change from land use change are assumed to be equal to their best estimate RF values, but with larger uncertainties. (c) RF bar chart based on emitted compounds (gases, aerosols or aerosol precursors) or other changes. Note that in this figure nitrate aerosols is only associated with NO_X emissions but ammonia (NH_3) is also important for the formation of this aerosol type. SOA has not been included since the formation depends on a variety of factors not currently sufficiently quantified.

Figure 8.17c shows the RF over the industrial era (1750–2011) by emitted compounds (see Table 8.SM.2 in the Supplementary Material for actual numbers). It is more complex to view the RF by emitted species than by compositional change (Figure 8.17a) since the number of emitted compounds and changes leading to RF is larger than the compounds and changes causing RF. The main reason for this is the indirect effect of several compounds and in particular components involved in atmospheric chemistry (see Section 8.2). CO_2 is the dominant positive RF both by abundance and by emitter. Emissions of CH_4, CO, and NMVOC all leads to CO_2 as one end product and is the reason why the RF of direct CO_2 emissions is slightly lower than the RF of abundance change of CO_2. For CH_4 the contribution from emission is twice as large as that from the CH_4 concentration change, 0.97 W m^{-2} versus 0.48 W m^{-2}, respectively. This is because emissions of CH_4 leads to ozone production, stratospheric water vapour, CO_2 (as mentioned above), and importantly affects its own lifetime (Section 8.2). Actually, emissions of CH_4 would lead to a stronger RF via the direct methane greenhouse effect (0.65 W m^{-2}) than from the RF from abundance change of CH_4 (0.48 W m^{-2}). Emissions of CO (0.23 W m^{-2}) and NMVOC (0.11 W m^{-2}) have only indirect effect on RF through ozone production, CH_4 and CO_2 and thus a warming effect. Emissions of NO_X on the other have both indirect effects that lead to positive RF through ozone production and also effects that lead to negative RF through reduction of CH_4 lifetime and thus its concentration and through contributions to nitrate aerosol formation. The overall effect of anthropogenic emissions of NO_X is a negative RF. Emissions of ammonia also contribute to nitrate aerosol formation, with a very small offset due to compensating changes in sulfate aerosols. Additionally indirect effects on sulfate are not included here as model results show large divergences in these responses (though they are typically small). Impacts of emissions other than CO_2 on the carbon cycle via changes in atmospheric composition (ozone or aerosols) are also not shown due to the limited amount of available information.

Emissions of BC have a positive RF through aerosol-radiation interactions and BC on snow (around 0.54 W m^{-2}). The emissions from the various compounds are co-emitted; this is in particular the case for BC and OC from biomass burning aerosols. The net RF of biomass burning emissions for aerosol-radiation interactions is close to zero, but with rather strong positive RF from BC and negative RF from OC (see Sections 8.3.4 and 7.5). The RF of aerosol-cloud interactions is caused by primary emissions of BC, OC, and dust as well as secondary produces aerosol from emissions of SO_2, NO_X and NH_3. However, quantification of the contribution from the various components to the RF of aerosol-cloud interactions has not been attempted in this assessment (see Section 7.5).

8.5.2 Time Evolution of Historical RF

The time evolution of global mean forcing is shown in Figure 8.18 for the whole industrial era. Over all time periods during the industrial era CO_2 and other WMGHG have been the dominant term, except for shorter periods with strong volcanic eruptions. The time evolution shows a nearly continuous increase in the magnitude of anthropogenic RF. This is the case both for CO_2 and other WMGHG as well as several individual aerosol components. The RF from CO_2 and other WMGHG has increased continuously with a

somewhat larger growth for CO_2 since the 1960s. The total aerosol AF (ari and aci used in this assessment) has the strongest negative forcing (except from episodic volcanic aerosols for short time periods), with a strengthening in the magnitude similar to many of the other anthropogenic forcing mechanisms with time. The global mean RF of aerosol-radiation interactions was rather weak until 1950 and has strengthened in the latter half of the last century and in particular in the period between 1950 and 1980. The RF of aerosol-radiation interaction by aerosol component is shown in Section 8.3.4 (Figure 8.9).

While there is *high confidence level* for a substantial enhancement in the negative aerosol forcing in the period 1950–1980, there is much more uncertainty in the global mean aerosol forcing over the last two decades (1990–2010). Over the last two decades there has been a strong geographic shift in aerosol and aerosol precursors emissions, and there are some uncertainties in these emissions (Granier et al., 2011). In addition to the regional changes in the aerosol forcing there is also likely a competition between various aerosol effects. Emission data indicate a small increase in the BC emissions (Granier et al., 2011) but model studies also indicate a weak enhancement of other aerosol types. Therefore, the net aerosol forcing depends on the balance between absorbing and scattering aerosols for the aerosol-radiation interaction as well as balance between the changes in the aerosol-radiation interaction and aerosol-cloud interactions. In the ACCMIP models, for example, the RF from aerosol-radiation interaction becomes less negative during 1980 to 2000, but total aerosol AF becomes more negative (Shindell et al., 2012d). There is very low confidence level for the recent trend in the total aerosol forcing, even the sign, however; there is a *high confidence level* that aerosol forcing during this period has a much smaller magnitude relative to WMGHG RF compared to the 1950–1980 period.

The volcanic RF has a very irregular temporal pattern and for certain years has a strongly negative RF. There has not been a major volcanic eruption in the past decade, but some weaker eruptions give a current RF that is slightly negative (see Section 8.4.2).

Table 8.8 shows anthropogenic and natural RF over some specified time periods and RF values are shown both for exact years and 5-years means. Over the three decades from 1980 to 2010 the total anthropogenic RF has steadily increased to 1.0 W m^{-2}. The natural RF agents of solar and volcanic show year to year variation and this is particularly large for volcanic aerosols. Their net effect has been a near zero RF over the past three decades (depending slightly on how RF is calculated since a major volcanic eruption occurred in 1982). Likewise the natural RF has been close to zero since 1950 with an anthropogenic RF of 1.6 W m^{-2}. The 2000–2010 natural RF is negative with contributions both from solar and volcanic aerosols, whereas the anthropogenic RF continues to strengthen as in the previous decades. For anthropogenic RF the difference in specific years or 5-years mean is small, whereas for the natural it can make a large difference if major volcanic eruptions are included in the 5-years running mean as for the 1980–2010 and 1990–2010 time periods.

Table 8.8: Anthropogenic and natural RF (W m^{-2}) given for changes over four time periods (2008 numbers used so far for 2010). Numbers in parenthesis are 5-year means (for 2010 so far 3-year mean).

Time Period	Anthropogenic RF	Natural RF
1950–2010	1.55 (1.55)	–0.07 (–0.06)
1980–2010	0.97 (0.97)	–0.04 (0.25)
1990–2010	0.64 (0.63)	0.00 (0.83)
2000–2010	0.38 (0.36)	–0.15 (–0.12)

Table 8.9 shows a comparison of the decadal change in the anthropogenic and WMGHG RF for four time periods. The mean decadal WMGHG RF over 1950–2010 is 0.3 W m^{-2}, which is a factor 10 larger than between 1750 and 1900. The difference between WMGHG and anthropogenic RF is smallest for the 1980–2010 period and largest for the period 1750–1900 in relative terms, while it is smallest in the two earliest periods and largest during 1950–1980 in absolute terms.

Table 8.9: Rate of change in RF (W m^{-2} / decade) for three time periods.

Time Period	Anthropogenic RF	WMGHG RF
1750–1900	0.014	0.030
1900–1950	0.073	0.089
1950–1980	0.19	0.28
1980–2010	0.30	0.33

The major contribution to the uncertainties in the time evolution of the anthropogenic forcing is associated with the aerosols (see Section 8.5.1). Despite this, anthropogenic AF is *very likely* considerably more positive than the natural RF over the time periods shown in Table 8.8. This is in particular the case after 1980, where satellite data are available that provide important time series to constrain the natural RF mechanisms.

[INSERT FIGURE 8.18 HERE]

Figure 8.18: Time evolution of RF for anthropogenic and natural RF mechanisms. Bar with the RF estimate at present associated with uncertainty ranges are given to the right part of the figure. For aerosol the RF of aerosol-radiation interaction and total aerosol AF are shown.

Figure 8.19 shows a RF bar chart for the period 1980–2011. Compared to the whole industrial era period the dominance of the CO_2 is larger for this recent period both with respect to other WMGHG and the total anthropogenic RF. The forcing of aerosols is rather weak leading to a very strong positive AF for the 1980–2011 period.

[INSERT FIGURE 8.19 HERE]

Figure 8.19: Bar chart for RF (solid) and AF (hatched) for the period 1980–2011, where the total anthropogenic AF are derived from Monte-Carlo simulations similar to Figure 17b. Total aerosol AF (ari + aci) is shown.

8.5.3 Future Radiative Forcing

Projections of global mean RF are assessed based on results from multiple sources: the ACCMIP initiative (see Section 8.2 and Tables 8.1 and 8.2) provides analysis of the RF due to aerosols and ozone (Shindell et al., 2012d), while WMGHG, land use and stratospheric water RFs are taken from the RCP database (Meinshausen et al., 2011a). As the ACCMIP project provided the largest set of projected forcings at 2030 and 2100, we hereafter highlight forcings at those times. While understanding the relative contributions of various processes to the overall effect of aerosols on forcing is useful, we emphasize the total aerosol AF, which includes all aerosol direct and indirect effects (e.g., it is AFari + AFaci), as this is the most indicative of the aerosol forcing driving climate change. We also present traditional aerosol RF (RFari in this report, previously called aerosol direct forcing) but do not examine further the various components of aerosol AF. Aerosol forcing estimates, both mean and uncertainty ranges, are derived from the 10 ACCMIP models, 8 of which are also CMIP5 models. We analyze forcing during the 21st century (relative to 2000), and hence the WMGHG forcing changes are in addition to persistent forcing from historical WMGHG increases.

Analysis of forcing at 2030 shows that under RCP2.6, aerosol RFari is positive relative to 2000 but small (~0.05 W m^{-2}) due to offsetting impacts from sulfate and nitrate. Total ozone (tropospheric and stratospheric) forcing is near zero, and hence WMGHG forcing dominates changes over this time period (Figure 8.20). WMGHG forcing is dominated by increasing CO_2, as declining methane and increasing N_2O have nearly offsetting small contributions to forcing. Aerosol AF was not evaluated for this RCP under ACCMIP, and values cannot be readily inferred from aerosol RFari as these are not directly proportional. Under RCP8.5, aerosol RFari in 2030 is weakly negative due to nitrate, aerosol AF is positive with a fairly small value and large uncertainty range, total ozone forcing is positive but small (~0.1 W m^{-2}), and thus WMGHG forcing again dominates with a value exceeding 1 W m^{-2}. As with RCP2.6, WMGHG forcing is dominated by CO_2, but under this scenario the other WMGHGs all contribute additional positive forcing. Going to 2100, ozone forcing diverges in sign between the two scenarios, consistent with changes in the tropospheric ozone burden (Figure 8.4) which are largely attributable to projected methane emissions, but is small in either case. Ozone RF includes a positive RF from stratospheric ozone recovery owing to reductions in anthropogenic halocarbon emissions in either scenario, though changes in tropospheric precursors dominate the RF. ACCMIP values differ substantially from the RCP database ozone RF. Under RCP2.6, the

ACCMIP models show almost zero ozone RF over 2000–2030, with roughly –0.20 W m^{-2} forcing at 2100 versus 2000, while the RCP database shows a forcing of about 0.20 W m^{-2} at 2030 and –0.10 W m^{-2} at 2100. Under RCP8.5, the ACCMIP models find 2030 ozone forcing of 0.1 W m^{-2} and 2100 forcing of 0.22 W m^{-2}, while the RCP database again shows larger positive forcing at 2030 (0.3 W m^{-2}) than at 2100 (0.1 W m^{-2}).

The two scenarios are much more consistent in their trends in aerosol RFari by component. There is positive RFari due to reductions in sulfate aerosol. This largely offset by negative RFari by primary carbonaceous aerosols and especially by nitrate, leaving net aerosol RFari values that are very small in both scenarios. Nitrate aerosols continue to increase as ammonia emissions rise steadily due to increased use of agricultural fertilizer even as all other aerosol precursor emissions decrease (Figure 8.2) and less sulfate aerosol allows more formation of nitrate aerosols in the future (Bauer et al., 2007; Bellouin et al., 2011). The comparable RFari values in the RCP database are substantially different. Under RCP2.6, net RFari at 2030 relative to 2000 is very small (<0.05 W m^{-2}) in the RCP database and the ACCMIP models, but at 2100 the RCP value is nearly 0.3 while the ACCMIP value is 0.01 W m^{-2}. Under RCP8.5, there are again substantial differences, especially at 2100 when the RCP database has a forcing of about 0.2 W m^{-2} while the ACCMIP models have RFari of about –0.1 W m^{-2}. The difference in both cases is almost entirely due to nitrate, which gives a small positive forcing in the RCP database but a substantial negative in the ACCMIP models (Figure 8.20). Aerosol AF is likely similar at this time in all scenarios given their similarity in having greatly reduced emissions of all aerosols and aerosol precursors other than ammonia. Aerosol AF shows a large positive value at 2100 relative to 2000, nearly returning to its 1850 levels (the 2100 versus 1850 AF represents a decrease in AF of 91% relative to the 2000 versus 1850 value), as is expected given the RCP emissions. Thus although some models project large increases in nitrate RF in the future, the reduction in overall aerosol loading appears to lead to such a strong reduction in aerosol AF that the impact of aerosols becomes very small under these RCPs. Of course the projections of drastic reductions in aerosol and aerosol and ozone precursor emissions may be overly optimistic as they assume virtually all nations in the world become wealthy and hence implement policies that have historically been implemented only by wealthy nations.

While aerosol AF becomes less negative by nearly 1 W m^{-2} from 2000 to 2100, this change is still small compared with the increased WMGHG forcing under RCP8.5, which is roughly 6 W m^{-2} during this time (Figure 8.20). Roughly 5 W m^{-2} of this WMGHG forcing comes from CO_2, with substantial additional forcing from increases in both methane and nitrous oxide and only a very small negative forcing from reductions in halocarbons. Under RCP2.6, the WMGHG forcing is only about 0.5 W m^{-2} during this time, as relatively strong decreases in methane and halocarbon forcing offset roughly 40% of the increased CO_2 forcing, which is itself far less than under RCP8.5. Hence under this scenario, the projected future forcing due to aerosol reductions is actually much stronger than the WMGHG forcing. Viewing the timeseries of the various forcings, however, indicates that aerosol AF is returning to its preindustrial levels, so that net forcing relative to 1850 (or 1750) becomes increasingly dominated by WMGHGs regardless of scenario during the 21st century (Figure 8.21). As the forcing is so heavily dominated by WMGHGs at 2100, all the scenarios show net forcing values at that time that are fairly close to the scenarios' target values. Forcing due to land use (via albedo only) and stratospheric water vapor changes are not shown separately as their projected values under the four RCPs are quite small: 0.00 to –0.09 and 0.10 to –0.03 W m^{-2}, respectively.

The total adjusted forcing due to all causes has been independently estimated based on the transient response in the CMIP5 models and a linear forcing-response relationship derived through regression of the response to an instantaneous increase in CO_2 (Forster et al., 2012). This estimate produces values for the total projected 2030 and 2100 forcings that are slightly smaller than the results obtained from the ACCMIP models (or the RCP targets). Examining the subset of models included in both this regression analysis and in ACCMIP shows that the ACCMIP subset show forcings on the low side of the mean value obtained from the full set of CMIP5 analyzed, indicated that the discrepancy between the methods is not related to analysis of a different set of models. Instead, it may reflect non-linearities in the response to forcing that are not represented by the regression analysis of the response to abrupt CO_2 increase experiments (Long and Collins, 2012).

Natural forcings will also change in the future. The magnitudes are difficult to project (see Section 8.4), but are likely to be small at multi-decadal scales, although episodic volcanic forcing could be large. For example, recent estimates of the potential variation in solar forcing produced decadal-scale changes of 0.05 W m^{-2} or less throughout the 21st century relative to the 2000s (Velasco-Herrera et al., 2012; see Section 8.4.1.3).

[INSERT FIGURE 8.20 HERE]

Figure 8.20: Radiative forcing relative to 2000 due to anthropogenic composition changes based on ACCMIP models for aerosols (with aerosol AF scaled to match the best estimate of present-day forcing) and total ozone and RCP WMGHG forcings. Ranges are one standard deviation in the ACCMIP models and assessed relative uncertainty for WMGHGs and stratospheric water vapor. Carbonaceous aerosols refers to primary carbonaceous, while SOA are secondary organic aerosols. Note that 2030 AF for RCP2.6 was not available, and hence the total shown for that scenario is not perfectly comparable to the other total values.

[INSERT FIGURE 8.21 HERE]

Figure 8.21: Global mean forcing with symbols indicating the times at which ACCMIP simulations were performed (solid lines with circles are net, long dashes with squares are ozone, short dashes with diamonds are aerosol, dash-dot are WMGHG, colors indicate the RCPs with red for RCP8.5, orange RCP6.0, light blue RCP4.5, and dark blue RCP2.6). RCPs 2.6, 4.5 and 6.0 net forcings at 2100 are approximate values using aerosol AF projected for RCP8.5 (modified from Shindell et al., 2012d).

8.6 Geographic Distribution of Radiative Forcing

8.6.1 Spatial Distribution of Current Radiative Forcing

The RF spatial pattern of the various RF mechanisms varies substantially (Ramaswamy et al., 2001). The WMGHGs such as CO_2 have a rather homogenous spatial RF pattern, with largest forcing in the tropics, decreasing modestly toward the poles. CO_2 forcing is also largest in warm and dry regions and smaller in moist regions and in high-altitude regions (Taylor et al., 2011). For the short-lived components their concentration spatial pattern and therefore their RF pattern are highly inhomogeneous, and again meteorological factors such as temperature, humidity, clouds, and surface albedo influence how concentration translates to RF.

Figure 8.22 shows the RF spatial distribution of the major NTCFs together with standard deviation among the ACCMIP models (Shindell et al., 2012d). These models used unified anthropogenic emissions of aerosol and ozone precursors, so that the model diversity in RF is due only to differences in model chemical and climate features and natural emissions, and would be larger if uncertainty in the anthropogenic emissions were also included. In general, the confidence in geographical distribution is less than for global mean, due to uncertainties in chemistry, transport and removal of species.

The aerosol direct effect RF (first row) is greatest in the NH and near populated and biomass burning regions. The standard deviation for the net aerosol forcing is largest over regions where vegetation changes are largest (e.g., South Asia and central Africa), due to uncertainties in biomass burning aerosol optical properties and to treatment of secondary organic aerosols. Carbonaceous aerosol forcing (second row), is greatest in South and East Asia and can be negative in biomass burning regions due to large non-absorbing organic components. Absorbing aerosols also have enhanced positive forcing when they overlie high albedo surfaces such as cryosphere, desert or clouds, with as much as 50% of BC RF resulting from BC above clouds (Zarzycki and Bond, 2010).

Figure 8.23 compares the aerosol RFs for ACCMIP, which are representative of the CMIP5 experiments, with those from the AeroCom model intercomparison which includes fifteen models that used unified meteorology and are more extensively compared to measurements (e.g., Koch et al., 2009b; Koffi et al., 2012). The forcing results are very similar, establishing the representativeness and validity of the ACCMIP aerosol simulations.

The net adjusted aerosol forcing (Figure 8.22; third row), includes both direct and indirect effects. The spatial pattern correlates with the aerosol direct effect (top), except with stronger effect in the outflow regions over oceans. The flux change is larger in the NH than the SH (e.g., by nearly a factor of 3; Ming et al., 2007). Cloud indirect and semi-direct effects may enhance or reduce cloud cover depending on the region, cloud dynamics and aerosol loading (e.g., Koch and Del Genio, 2010; Persad et al., 2012; Randles and Ramaswamy, 2008). In general, the ocean-land forcing pattern differs from that reported in AR4, where the cloud indirect effects were larger over land than ocean (Forster et al., 2007), and this continues to be a source of uncertainty. Since AR4, Quaas et al. (2009) showed in satellite retrievals that the correlation

between AOD changes and droplet number changes is stronger over oceans than over land and that models tend to overestimate the strength of the relation over land. Penner et al. (2011) showed that satellite retrievals, due to their dependence on present-day conditions, may underestimate the indirect effect, especially over land, although this model analysis may overestimate the cloud condensation nucleus to AOD relation (Quaas et al., 2011). Wang and Penner (2009) also showed that if models include boundary layer nucleation and increase the fraction of sulphur emitted as a primary particle, the effect over land is increased relative to over ocean. The aerosol AF standard deviation is large in biomass burning regions, as for the direct effect, and in regions where cloud effects differ (e.g., northern North America, northeast Asia, Amazonia). Due to uncertainties around cloud responses to aerosols, the spread is much larger than for the RF alone, although the relative standard deviation is no larger for AF than for RF (Shindell et al., 2012d).

For components that primarily scatter radiation, the radiative forcing at the surface is similar to the RF (according to the definition in Section 8.1.1). However for components that absorb radiation in the atmosphere the (direct) radiation reaching the surface is reduced (Andrews et al., 2010; Forster et al., 2007; Ramanathan and Carmichael, 2008). This absorption of incoming solar radiation alters the vertical temperature profile in the atmospheric column and can thus change atmospheric circulation and cloud formation. The aerosol atmospheric absorption (Figure 8.22, last row), or the difference between AF at the TOA and at the surface, has spatial pattern that to lowest order tracks the carbonaceous aerosol forcing, but is also affected by cloud changes, where e.g., cloud loss could enhance atmospheric absorption. Atmospheric absorption patterns thus mirror the indirect pattern, with larger forcing often over continents. The largest standard deviation similarly overlies land masses in the NH.

Ozone RF is calculated using the methodology described in Shindell et al. (2012d), but applied to the larger set of models in ACCMIP including gas-phase only models (Stevenson et al., 2012). The net ozone RF (Figure 8.22; fourth row) is largest at low latitudes, and is more positive in the NH than the SH. Pollution in the NH accounts for positive tropospheric forcing; Loss of stratospheric ozone has caused negative SH polar forcing. Model standard deviation is largest in the polar regions where lower stratosphere/upper troposphere changes differ in the models (Stevenson et al., 2012).

Overall, the *confidence* in aerosol and ozone RF spatial patterns is medium, and in aerosol AF patterns is low due to exacerbated uncertainty in cloud responses.

[INSERT FIGURE 8.22 HERE]

Figure 8.22: Spatial pattern of ACCMIP models preindustrial to present-day forcings, mean values (left) and standard deviation (right) for aerosols and ozone. Values above are the average of the model area-weighted global means, with the area weighted mean of the standard deviation of models at each point provided in parenthesis. Shown are net aerosol RF (top, 10 models), carbonaceous aerosol RF (2nd row, 7 models), net AF (3rd row, 8 models), ozone (4th row, 11 models), atmospheric absorption (bottom, 5 models). Note that RF and AF means are shown with different color scales, and standard deviation color scales vary among rows.

[INSERT FIGURE 8.23 HERE]

Figure 8.23: Spatial pattern of ACCMIP and 15 AeroCom models preindustrial to present-day RF, mean values (left) and standard deviation (right). Values above are the average of the model area-weighted global means, with the area weighted mean of the standard deviation of models at each point provided in parenthesis.

8.6.2 Spatial Evolution of Radiative Forcing and Response over the Industrial Era

8.6.2.1 Regional Forcing Changes During Industrial Era

The magnitude but not the spatial distribution of the WMGHG RF has changed over the industrial era. However the RF spatial distributions for the short-lived components has shifted with emissions, due to the timing of regional developments and implementation of pollution standards. Figure 8.24 shows how the distributions of aerosol and ozone forcings are modelled to have changed up to 1930, 1980 and 2000. Substantial industrial coal-burning in the early part of the 20th century occurred in the northeastern United States and western Europe, leading to large sulphate and BC forcing near those regions (Figure 8.24, left). Between 1950 and 1970, coal burning for power generation increased while coal burning for other purposes was replaced by oil and natural gas and motor vehicle usage grew rapidly in these regions, leading to more sulphate and less BC. Peak aerosol forcing in North America and Europe occurred around 1970–1980

(Figure 8.24, second column), while Asian development led to increased biofuel and fossil fuel sources of aerosols and ozone precursors toward the end of the century. During the final decades of the century, desulphurization controls reduced sulphur emissions from North America and Europe, resulting in reduced negative forcing in these regions and positive Arctic aerosol forcing. The SH ozone hole developed during the final three decades, with negative forcing over high latitudes. Biomass burning generated ozone and carbonaceous aerosol emissions in NH high-latitude early in the century, with increased tropical burning from mid to late century.

Aerosol AF grew rapidly from 1930 to 1980, as did aerosol RFari, with a spatial structure reflecting both the influence of direct forcing and cloud responses that are especially strong over pollution outflow regions and over areas with high surface albedo. From 1980 to 2000, aerosol AF continued to become more negative even as negative aerosol RFari grew weaker, with the spatial pattern showing strengthening of aerosol AF over Asia and weakening of aerosol AF over North America and Europe.

[INSERT FIGURE 8.24 HERE]

Figure 8.24: Multi-model mean direct effect (RFari) of all aerosols, carbonaceous aerosols, ozone, and aerosol AF (W m^{-2}) for the indicated times based on the ACCMIP simulations. Global area-weighted means are given in the upper right.

Soil dust has changed since the pre-industrial due to land disturbance (a forcing) and to changes in climate (a feedback). Mahowald et al. (2010) showed approximate doubling in dust loading over the 20th century (–0.1 W m^{-2}, consistent with the best estimate in Section 8.3.4.2), with largest increase from the 1950s to the 1980s (–0.3 W m^{-2}), followed by a levelling, primarily from the Saharan and Middle Eastern deserts. The increased dustiness reduced model precipitation within the Saharan source region, improving agreement with observed precipitation.

Aerosol loading changes during the past century have had corresponding impacts on radiation at the surface (Section 2.5.3), with peak reductions in North America and Europe in the 1980s, and ongoing reduction in South and East Asia (Wild, 2009). The AR4 models simulated these trends but underestimated their magnitude, the decadal temperature variations and the diurnal temperature range over land (Wild, 2009).

Changes in spatial patterns of species and their forcing over the century are difficult to validate due to lack of observations of short-lived species, other than sparse observations in ice core records. Some confidence may be derived from validation of current-day models as well as from late-century trends from satellite and some surface-based site measurements; however the emissions estimates for historical species are very uncertain, especially for carbonaceous aerosols and dust. Therefore, the *confidence* in the historical forcing pattern changes is low for aerosol RF and ozone, and very low for AF, carbonaceous aerosols and dust.

8.6.2.2 Relationship Between Regional Forcing Patterns and Climate Response During the Industrial Era

In AR4 (Forster et al., 2007; Knutti et al., 2008) it was argued that the spatial pattern of forcing is not indicative of the pattern of climate response. Rather, the response is linked more closely to TOA flux resulting from the climate feedback spatial patterns (Boer and Yu, 2003; Taylor et al., 2011), with the lapse rate, surface albedo and cloud feedbacks explaining most of the temperature response. Yet Crook and Forster (2011) showed that both the spatial distribution of climate feedbacks and of heterogeneous forcing played important roles in the patterns of 20th century temperature changes. Other studies since AR4 have probed relationships between forcing patterns and climate responses. Attribution of regional climate change to any forcing is challenging and uncertain due to the large internal variability within particular regions (Chapter 10). Attribution of regional climate change to regionally varying forcing is particularly challenging and attempts to do so remain exploratory.

Broad links between forcing and climate response have been identified. Shindell et al. (2010) used multiple models to show that surface temperature changes are much more sensitive to latitudinal than longitudinal variations in forcing. Shindell et al. (2009) showed that NH aerosol reduction was associated with over 70% of Arctic warming from the 1970s to the 2000s, and that Arctic and much of the SH surface temperature changes are strongly affected by remote forcing changes. Voulgarakis and Shindell (2010) defined a regional transient temperature sensitivity parameter, or temperature response per unit forcing for each four-degree

latitude band. Using observed surface air temperature changes they showed that the parameter is best constrained from 50°S to 25°N, where the value is 0.35 C $(W\ m^{-2})^{-1}$, smaller than at northern higher latitudes, and 35% smaller than in AR4 models.

Some aerosol model studies have demonstrated highly localized climate response to regional forcing. For example, significant regional cooling and hydrological shifts in the Eastern U.S. and in Eastern Asia during the last half the 20th century were modelled and attributed to local aerosols (Chang et al., 2009; Leibensperger et al., 2008; Leibensperger et al., 2012). Historical surface temperature changes due to anthropogenic non-WMGHG forcing in CMIP5 models do not closely correspond to the forcing pattern, however (Shindell et al., 2012d).

Since AR4, there has been new research on aerosol forcing influences on the hydrologic cycle. An increase in aerosol loading, with greater reduction in surface energy flux (Figure 8.22) in the NH has been implicated in the observed southward shift of the intertropical convergence zone (ITCZ) towards the hemisphere with smaller surface energy reduction: southward up to the 1980s with a reversal since (e.g., Denman et al., 2007; Rotstayn et al., 2000; Zhang et al., 2007). Ming et al. (2007) showed an associated reduction in NH precipitation and Williams et al. (2001) showed associated shifts in the meridional streamfunction and the Hadley circulation. The ITCZ shift may in turn be responsible for a broad set of regional precipitation changes, including drying of the Sahel (e.g., Biasutti and Giannini, 2006; Ackerley et al., 2011; Kawase et al., 2010) and northwestern Brazil (e.g., Cox et al., 2008), which also peaked in the 1980s (e.g., Rotstayn and Lohmann, 2002). These hemispheric asymmetric ITCZ effects are overlaid on thermodynamic aerosol effects which moisten subtropical regions in both hemispheres, countering greenhouse gas drying of these regions (Ming et al., 2011). Studies indicate that aerosols have a larger effect on precipitation shifts than equivalent WMGHG forcing, and that historical trends in several areas cannot be explained without including aerosol forcing (Bollasina et al., 2011; Booth et al., 2012; Shindell et al., 2012b; Shindell et al., 2012c).

Absorbing aerosols are also responsible for shifting cloud distributions. For example, absorbing aerosols influence precipitation in monsoon regions. Stephens et al. (2004) and Miller et al. (2004) used models to show that dust absorption over Africa can enhance low-level convergence and increase vertical velocities so that local monsoon circulation and precipitation are enhanced. On the other hand, Kawase et al. (2011) and Kawase et al. (2010) showed that biomass burning black carbon may cause the decreasing precipitation trend in tropical Africa during austral summer, due to reduction in evaporation and enhanced subsidence. The aerosol effects on the Indian monsoon are similarly complex, and have been the subject of numerous studies (e.g., Lau et al., 2006; Wang et al., 2009; Wang et al., 2009; Chung and Ramanathan, 2006; Ramanathan et al., 2005; Bollasina et al., 2011), but a clear picture of how the regional aerosol forcing correlates with responses has not yet fully emerged. Attribution of changes in monsoon to human influence generally has low confidence (Section 10.3).

Stratospheric ozone loss has been modelled to affect SH surface temperatures similarly to increased greenhouse gases, cooling stratospheric temperatures, strengthening the polar vortex and shifting the westerly jet poleward, but cooling Antarctic surface temperatures, with larger influence on austral summer conditions (McLandress et al., 2011; Son et al., 2009; Thompson et al., 2011; see also Section 10.3.3.1). Tropospheric ozone has contributed proportionally more to warming of the NH and notably to the Arctic during winter than its global impact, mainly during the second half of the twentieth century (Shindell et al., 2006b).

Forcing from heterogeneous land surface albedo changes has impacted regional climate patterns. The spatial distribution of the land use, land cover change effect on AF as it evolved from 1750 to the late 20th century, assuming constant global mean snow cover, is shown in Figure 8.11. As discussed in Section 8.3.5, the surface albedo brightened on the one hand due to a shift from forest to brighter croplands, causing local cooling (e.g., Eliseev and Mokhov, 2011; Lee et al., 2011), but also darkened due to the re-expansion of forests to higher latitudes (Esper and Schweingruber, 2004) and increased vegetation height in snowy regions (Bonfils et al., 2012).

In addition to land use and climate-induced vegetation changes, CO_2 effects vegetation forcing indirectly, reducing evapotranspiration from plants as stomata open less with increasing CO_2, resulting in atmospheric

drying and warming. These are not included in the standard RF (Section 8.1) and may be considered feedbacks (Section 8.3.2). This is modelled to be largest over the Amazon, the central African forest, and to some extent over boreal and temporal forests (Andrews et al., 2011). In the coupled climate modelling study of Lawrence and Chase (2010), the vegetation changes caused significant reduction in evapotranspiration, drying and warming in tropical and subtropical regions, with insignificant cooling at higher latitudes. Dynamic vegetation models have also indicated increased vegetation in both boreal and subtropical regions from plant physiological changes due to increased CO_2, resulting in reduced albedo and positive feedbacks in both regions (O'ishi et al., 2010). Overall, vegetation changes may have caused modest cooling at high latitudes and warming at low latitudes, but the uncertainties are large and confidence is very low.

Loss of snow and ice darken the land surface, reduce albedo, and enhanced climate warming. For example, substantial snow-cover reduction of North America leads to warmer North American summertime temperature in models having a strong snow albedo feedback. These forcings can also have non-local impacts that result from enhanced land-ocean temperature contrast, increasing surface convergence over land and divergence over oceans. A poleward intensification of the high pressure patterns and subtropical jet may also result (Fletcher et al., 2009). BC contributions to darkening of snow reduces snow cover, however the magnitude of the effect is very uncertain. Two model studies calculated BC-albedo reduction to cause 20–50% Arctic snow/ice cover reduction and around 20% of Arctic warming over the previous century (Koch et al., 2011; Shindell et al., 2010). However, reductions in Arctic soot during the past two decades (e.g., Hegg et al., 2009) have likely reversed that trend (e.g., Koch et al., 2011; Skeie et al., 2011b). Cryospheric feedbacks and atmospheric dynamical responses are probably responsible for a poleward shift in the temperature response to aerosol-cloud effects (Chen et al., 2010; Koch et al., 2009a; Kristjansson et al., 2005).

Solar irradiance variations induce ozone responses, and the resulting differential heating can drive circulation anomalies which lead to regional temperature and precipitation changes (Frame and Gray, 2010; Gray et al., 2010; Haigh, 1999; Shindell et al., 2006a). Solar forcing can also influence the state of natural modes of circulation such as the Northern Annular Mode (e.g., Ineson et al., 2011; Shindell et al., 2001), the South Asian Summer Monsoon (Fan et al., 2009), the Southern Annular Mode (Kuroda and Kodera, 2005; Roscoe and Haigh, 2007) or potentially the ENSO (Mann et al., 2005). The pattern of temperature response is less uniform than the forcing, for example, warming in the NH, but little response in the SH due to temperature moderation by wind speed enhancement effects on ocean circulation (Swingedouw et al., 2011). Regional responses to solar forcing are mediated by the stratosphere, so that reproducing such change requires spectrally varying solar forcing rather than TSI forcing (see Section 8.3.1.6).

Stratospheric aerosol clouds from tropical eruptions spread poleward and can cover an entire hemisphere or the globe, depending on the initial latitudinal spread. The aerosol eruption clouds from the 1963 Agung was confined mainly to the SH; the 1982 El Chichón mainly to the NH; and the 1991 Pinatubo covered the globe, all with an *e*-folding lifetime of about 1 year (e.g., Antuña et al., 2003). High-latitude eruptions produce aerosol clouds that stay confined to the mid- high-latitudes of hemisphere of the eruption, with *e*-folding lifetimes of 2–4 months (Kravitz and Robock, 2011). Volcanic aerosols primarily scatter solar radiation back to space, but also absorb longwave radiation with the former larger by an order of magnitude. Stratospheric aerosol absorption heats the layer where they reside and produces distinct vertical and horizontal distributions of the heating rate. The temperature and chemical effects of the aerosols also enhance ozone destruction, which somewhat counteracts the radiative heating (Stenchikov et al., 2002). For tropical eruptions, this affects atmospheric dynamics, with a stronger polar vortex, a positive mode of the Arctic Oscillation, and winter warming over NH continents (Robock, 2000). Climate responses to solar and volcanic forcings are further discussed in the context of detection and attribution of millennial climate change (Section 10.7).

The study of how climate responds to regionally varying patterns of forcing is critical for understanding how local activities impact regional climate, however the studies are quite uncertain and exploratory and so far generally evoke very low *confidence*. However there is medium to high *confidence* in some qualitative but robust features, such as the damped cooling of the NH and shifting of the ITCZ from aerosols, and positive feedbacks from high-latitude snow and ice albedo changes.

8.6.3 Spatial Evolution of Radiative Forcing and Response for the Future

It is in general expected that air quality regulations will result in decreased emissions of aerosols and ozone precursors over the next centuries. All RCP emission scenarios for aerosols and aerosol/ozone precursors used by the CMIP5/AR5 models estimate reduction in air pollution toward the end of this century (except nitrate aerosol) though some species will reach the maximum amounts of emissions around the mid-21st century (Figure 8.2). On the other hand, the emission scenarios for TAR and AR4, which was based on Special Report on Emissions Scenarios (SRES), had less optimistic future projections for air pollution, at least for some scenarios and current policies do not lead to the low emissions envisioned in the RCPs (Pozzer et al., 2012). However it is not expected that carbonaceous aerosols will substantially increase in the future (e.g., Streets et al., 2004), though wildfires may increase or keep high occurrence as indicated in Section 7.3.6.2.3.

Figure 8.25 shows the global distributions of changes in aerosol and ozone forcings in 2030 and 2100 relative to 2000 for RCP2.6 and 8.5. Both scenarios indicate reduced aerosol loading, and then positive forcing over Europe, North America and Asia where RF is above +0.5 W m^{-2} because of substantial reduction of scattering aerosols. The global means are estimated to be +0.12 and +0.08 W m^{-2} for RCP2.6 and 8.5, respectively, in 2100. Though the RF by total anthropogenic aerosols is positive, reduced BC contributes substantial negative forcing especially over the similar regions. The global mean carbonaceous RF including both the effects of BC and OC is estimated to be –0.20 and –0.11 W m^{-2} for RCP2.6 and 8.5, respectively, in 2100. Early in the century, on the other hand, both scenarios indicate increased negative all aerosol forcing over South Asia, with reversal between 2030 and 2100. As shown in Figure 8.2, emissions of BC, OC, and SO_2 will reach their maximums early and middle in the century for RCP2.6 and 8.5, respectively in India. In RCP6, a large amount of SO_2 emission in China will continue until the mid-21st century (Figure 8.2), and then it is predicted to keep a high negative RF over East Asia. The carbonaceous aerosol RF is positive over East and South Asia in 2030 relative to 2000 for RCP8.5 because BC emission is also larger in 2030. Over central and southern Africa, a change in the future aerosols RF based on RCPs is not clear mainly because wildfires are not estimated to decrease in this century as mentioned above. The global mean net direct aerosol RF in the future is rather small due to offsetting effects, with reductions in BC, increases in nitrate aerosols, and reductions in scattering aerosols causing substantially more forcing than the net.

Emissions and atmospheric loadings of natural aerosols are affected by climate change. There are, however, no agreements among studies on future trends of their changes for major natural aerosols, mineral dust and sea salt, as indicated in Section 7.3.6.2.1. A robust trend is an increase in sea salt emission in the high-latitudes because of a decrease in sea ice cover with global warming, which can results in atmospheric cooling through scattering sunlight and increasing cloud albedo with acting as cloud condensation nuclei. SOA loading may greatly increase due to changes in atmospheric oxidation conditions (Tsigaridis and Kanakidou, 2007). More studies are needed to obtain reliable estimates on future atmospheric natural aerosols considering paleoclimatic records discussed in Section 5.2.2.3 as well as recent trends.

The simulations applying the RCPs indicate that the maximum latitude of air pollution, and therefore of RF, is projected to shift somewhat southward for the next few decades (in 2030 of Figure 8.25). The shift of aerosol distributions southward is expected to cause the ITCZ to continue to shift northward. This, in combination with warming and drying over tropical land, has been modelled to lead to greatly enhanced drought conditions in the Amazon (Cox et al., 2008). On the other hand, if the low-latitude aerosol is sufficiently absorbing, broadening of the ITCZ convergence region and enhanced cloud cover could result, as modelled for dust (Perlwitz and Miller, 2010).

The reduction in high-latitude BC is expected to contribute to reducing Arctic warming (e.g., Koch et al., 2011), due to reduction in BC deposition on snow as well as in absorption of sunlight over bright surface. On the other hand, reduction in mid-high-latitude scattering aerosols is expected to lead to warming (Koch et al., 2011; Shindell et al., 2010). Levy et al. (2008) indicates that increased warming over the continental US will result from aerosol emissions reduction in Asia in the late 21st century.

Figure 8.25 also shows the ozone RF in 2030 and 2100 relative to 2000, which includes both changes in tropospheric and stratospheric ozone. Recovery of ozone in the stratosphere in the 21st century will result in

positive forcing in the southern high-latitudes in comparison with the year 2000 for both the pathways. This is because of the reduced emissions of ozone-depleting substances controlled under the Montreal Protocol, with a small additional effect from the slowing down of the ozone loss cycles due to stratospheric cooling with increasing greenhouse gases (Kawase et al., 2011; Lamarque et al., 2011). In the troposphere, on the other hand, a large difference in the methane emissions between RCP8.5 and the other pathways shown in Figure 8.2 leads to a the different RF trend outside the southern high-latitudes. Ozone recovery in the stratosphere and ozone increase in the troposphere leads to a positive RF all over the globe in RCP8.5 with a mean of +0.26 W m^{-2} in 2100. The cancellation between warming by ozone increase in the stratosphere and cooling by ozone decrease in the troposphere results in a global mean RF of –0.12 W m^{-2} in RCP2.6.

Figure 8.25 also shows the global distributions of changes in aerosol AF both due to the aerosol-radiation interaction and the aerosol-cloud-interaction in 2030 and 2100 relative to 2000 for RCP8.5. Although the AF includes rapid adjustments on the radiation balance and therefore its perturbation of the spatial pattern is somewhat larger than that of RF, the general trend is similar to RF. The AF in 2100 indicates to recover to the preindustrial levels affected by getting clean air especially in North America, Europe, and Asia.

[INSERT FIGURE 8.25 HERE]
Figure 8.25: Multi-model mean RF (W m^{-2}) by the direct effect of all anthropogenic aerosols (first and second rows) and anthropogenic carbonaceous (BC+OC) aerosols (third and fourth rows), and total ozone (fifth and sixth rows) in 2030 (left) and 2100 (right) relative to 2000 for RCP2.6 (top each) and RCP8.5 (bottom each) based on the ACCMIP simulation. The seventh row shows multi-model mean AF (W m^{-2}) by all anthropogenic aerosols in 2030 (left) and 2100 (right) relative to 2000 for RCP8.5. Global area-weighted means are given in the upper right of each panel.

8.7 Emission Metrics

8.7.1 Metric Concepts

8.7.1.1 Introduction

To quantify and compare the climate impacts of various emissions, it is necessary to choose a climate impact (or end point) by which to measure the effects. Thus, various choices as well as types of (sub) models are needed for the steps down the cause-effect chain (Figure 8.26 and Box 8.1). For assessments and evaluation one may – as an alternative to models that explicitly include physical processes resulting in forcing and responses – apply simpler measures or *metrics* that are based on results from complex models. Metrics are used to quantify the contributions to climate change of emissions of different substances and can thus act as 'exchange rates' in multi-component policies or comparisons of emissions from regions/countries or sources/sectors. Metrics are also used extensively in Life Cycle Assessments (e.g., by IPCC WGIII).

[INSERT FIGURE 8.26 HERE]
Figure 8.26: The cause-effect chain from emissions to climate change and impacts showing how metrics can be used to estimate responses to emissions (left side) and for development of multi-component mitigation (right side). Adapted from Fuglestvedt et al. (2003) and Plattner et al. (2009).

Metrics can be given in absolute terms (e.g., K/kg) or in relative terms by normalizing to a reference gas – usually CO_2 (see Section 8.7.1.4). To transform the effects of different emissions to a common scale – often called (somewhat misleadingly) 'CO_2 equivalent emissions' – the emission (E_i) of component *i* can be multiplied with the adopted normalized metric (M_i): $M_i \times E_i = CO_2\text{-}eq_i$. Ideally, the climate effects should be the same regardless of composition of the equivalent CO_2 emissions, but different components have different physical properties, and a metric that establishes equivalence with regard to one effect cannot guarantee equivalence with regard to other effects, e.g., O'Neill (2000); Smith and Wigley (2000), Fuglestvedt et al., (2003).

Metrics do not define goals and policy – they are tools that enable evaluation and implementation of multi-component policies (i.e., which emissions to abate). The most appropriate metric will depend on which aspects of climate change are most important to a particular application, and different climate policy goals may lead to different conclusions about what is the most suitable metric with which to implement that policy (Plattner et al., 2009; Tol et al., 2012). Metrics that have been proposed include purely physical metrics as well as more comprehensive metrics that account for both physical and economic dimensions (see 8.7.1.5).

[START BOX 8.2 HERE]

Box 8.2: Choices Required when using Emission Metrics

Time frames: One can apply a *backward-looking* or a *forward-looking* perspective, and in the latter case one may use pulses, sustained emissions or scenarios. All choices of emission perturbations are somewhat artificial and different choices serve different purposes.

Impact or end-point: RF, ΔT, or sea level change, for example, could be examined (Figure 8.26). This choice is also related to what is considered to be 'dangerous anthropogenic interference with the climate system' (UNFCCC Article 2). Metrics may also include socioeconomic damages. One may use the *level* (e.g., degrees Celsius) or *rate* of change (e.g., degrees Celsius per decade). Furthermore, the impacts may be estimated at a particular time, be integrated over time, or discounting of future effects may be introduced (i.e., a weighting of effects over time). Impacts may also depend non-linearly on physical changes, e.g., environmental and societal impacts might be formulated to vary with temperature change raised to some exponent, or only occur when thresholds are exceeded, e.g., Boucher (2012).

Spatial dimension for emission and response: Equal-mass emissions of NTCFs from different regions can induce varying global-mean climate responses, and the climate response also has a regional component irrespective of the regional variation in emissions.

Some of the choices involved in metrics are scientific (e.g., type of model, and how processes are included or parameterized in the models). Choices of time frames and climate impact are policy-related and cannot be based on science alone, but scientific studies can be used to analyse different approaches and policy choices.

[END BOX 8.2 HERE]

8.7.1.2 The GWP Concept

The Global Warming Potential (GWP) is defined as the time-integrated radiative forcing due to a pulse emission of a given gas, relative to a pulse emission of an equal mass of CO_2 (Figure 8.27a). The GWP was presented in The First IPCC Assessment (Houghton et al., 1990) stating '*It must be stressed that there is no universally accepted methodology for combining all the relevant factors into a single global warming potential ... A simple approach has been adopted here to illustrate the difficulties inherent in the concept ...*' The GWP for a time horizon of 100 years was later adopted as a metric to implement the multi-gas approach embedded in the UNFCCC and made operational in the Kyoto Protocol. It has become the default metric for transferring emissions of different gases to a common scale; usually called 'CO_2 equivalent emissions' (e.g., Shine, 2009). It is usually integrated over 20, 100 or 500 years though according to Houghton et al. (1990) these time horizons were '*presented as candidates for discussion and should not be considered as having any special significance*'.

The choice of time horizon has a strong effect on the GWP values – and thus also on the calculated effects and contributions of emissions by component, sector or nation. There is no conclusive scientific argument that can defend 100 years, the most frequently used horizon, compared to other choices (Fuglestvedt et al., 2003; Shine, 2009). The choice is value-based since it depends on the relative value assigned to effects at different times.

For some gases the variation in GWP with time horizon mainly reflects properties of the reference gas, not the gas for which the GWP is calculated. The GWP for CH_4 decreases with increasing time horizon, since GWP is defined with the integrated RF of CO_2 in the denominator. As shown in Figure 8.28a, after ca 5 decades the development in the GWP is purely determined by CO_2. However, for long-lived gases (e.g., SF_6) the development in GWP is controlled by both the increasing integrals of RF from the long-lived gas and CO_2 (Figure 8.28b).

[INSERT FIGURE 8.27 HERE]

Figure 8.27: (a) The GWP is calculated by integrating the RF due to pulses over chosen time horizons; e.g., 20 and 100 years. The blue hatched field represents the integrated RF from a pulse of CO_2, while the green and red fields represent gases with 1.5 and 13 years lifetimes, respectively. (b) The GTP is based on the temperature response for selected years after emission; e.g., 20 or 100 years. See Supplementary Material for equations for calculations of GWP and GTP.

The GWP is an indicator of the magnitude of RF over time (which is the total energy added to the climate system) but it does not translate directly into any climatic response parameter. Even though the term 'CO_2 equivalent emissions' is often used when GWP_{100} is applied, the only thing that is equivalent is the integrated RF over 100 years, and the equivalence is weaker or non-existent with regard to many other relevant climatic end-points (Fuglestvedt et al., 2000; Fuglestvedt et al., 2003; O'Neill, 2000; Smith and Wigley, 2000; Tanaka et al., 2009).

There have been several attempts to interpret the GWP. O'Neill (2000) and Shine et al. (2005b) show that as the time horizon becomes large, the GWP of a species converges to the ratio of the equilibrium temperature response due to a sustained emission of the species and CO_2. Since the temperature response of a sustained emission at time *t* is equivalent to the integrated temperature response up to time *t* to a pulse emission in linear systems (Peters et al., 2011a), it follows that the GWP of a species converges to the integrated temperature response for a pulse emission of a species normalized to that of CO_2. Peters et al. (2011a) and Azar and Johansson (2012) confirm this for a wide range of time horizons and species (except for NTCF).

Given that the GWP is a measure of the integrated RF, the name may lead to misperception of the physical impacts. 'Relative cumulative forcing index' would be a more appropriate name. The GWP is influenced by the background atmosphere on which the GWP calculations are superimposed, and the way indirect effects and feedbacks are included (see 8.7.1.4).

[INSERT FIGURE 8.28 HERE]

Figure 8.28: a) Development of AGWP-CO_2, AGWP-CH_4 and GWP-CH_4 with time horizon. b) Same but for SF_6.

8.7.1.3 The GTP Concept

The Global Temperature change Potential (GTP) (Shine et al., 2005a) goes one step further down the cause-effect chain (Figure 8.26) and is defined as the *change in global mean surface temperature at a chosen point in time* in response to a pulse or step change in emission – relative to that of CO_2. While GWP is integrated in time (Figure 8.27a), GTP is based on temperature change for a selected year, *t*, (Figure 8.27b). Like for the GWP, the impact from CO_2 is normally used as reference, hence, for a component *i*, $GTP(t)_i = AGTP(t)_i / AGTP(t)_{CO2} = \Delta T(t)_i / \Delta T(t)_{CO2}$, where AGTP is the absolute GTP giving temperature change per unit emission (see Supplementary Material for equations and parameter values). Shine et al. (2005a) presented the GTP for both pulse and sustained emissions based on an energy balance model as well as analytical equations. A modification was later introduced (Shine et al., 2007) in which the time horizon is determined by the proximity to a target year (see Section 8.7.1.5).

The AGTP can be used to calculate the temperature change due to any given emission scenario (assuming linearity) by integrating over pulse emissions multiplied by the absolute temperature change potential ($AGTP_i$):

$$\Delta T(t_H) = \sum_i \int_{t_e=0}^{t_H} em_i(t_e) \cdot AGTP_i(t_H - t_e) dt_e$$

where *i* is component, and t_e is time of emission (Berntsen and Fuglestvedt, 2008; Peters et al., 2011b; Shindell et al., 2011).

By accounting for the climate sensitivity and the exchange of heat between the atmosphere and the ocean, the GTP includes more physical processes than does the GWP. The GTP accounts for the slow response of the (deep) ocean, thereby prolonging the response to emissions beyond what is controlled by the decay time of the atmospheric concentration. Thus the GTP includes both the atmospheric adjustment timescale of the component considered and the response timescale of the climate system.

The GWP and GTP are fundamentally different by construction and different numerical values can be expected. In particular, the GWPs for NTCF are higher due to the integrative nature of the metric. The GTP values can be significantly affected by assumptions about the climate sensitivity and heat-uptake by the ocean (Peters et al., 2011a; Shine et al., 2005a). Thus, the relative uncertainty ranges are wider for the GTP compared to GWP. The additional uncertainty is a typical tradeoff when moving to an impact of greater relevance (Figure 8.26). Since the formulation of the ocean response in the GTP has a significant impact on the values its characterization also represents a trade-off between simplicity and accuracy. The GTP is influenced by the background atmosphere, and the way indirect effects and feedbacks are included (see Section 8.7.1.4).

8.7.1.4 Uncertainties and Limitations

Uncertainties in the values of emission metrics in general can be classified as *structural* and *scientific*. (Plattner et al., 2009; Shine et al., 2005b). *Structural uncertainties* refer to the consequences of using different types of metrics, or to choices about key aspects of a metric such as the climate impact considered, background conditions, time horizon and whether discounting is applied. *Scientific uncertainties* refer to the range of values that can be calculated for a given metric due to incomplete knowledge of processes from emissions to climate change and impacts.[6]

For the AGWP, uncertainties in adjustment times and radiative efficiency determine the *scientific uncertainty*. Inclusion of indirect effects increases uncertainty in metric values. For the reference gas CO_2, the scientific uncertainty is dominated by uncertainties in the *impulse response function* (IRF) that describes the development in atmospheric concentration that follows an emission pulse (Joos et al., 2012; see Box 6.2 and Supplementary Material). The IRF is sensitive to both scientific uncertainties (e.g., representation of the carbon cycle) and structural uncertainties (e.g., background concentration of CO_2). Joos et al. (2012) estimate the uncertainty in the integrated IRF_CO_2 for a 100 year time horizon as 49% (5–95% confidence intervals). Assuming quadratic error propagation, and 10% uncertainty in RE, the uncertainty range in $AGWP_{100}$_CO_2 is 50%. This affects all metrics that use CO_2 as reference. Reisinger et al. (2010) and Joos et al. (2012) show that these uncertainties increase with time horizon because of uncertainties in long-term carbon cycle responses to both the additional atmospheric CO_2 and the resulting climate change.

The same factors contribute to uncertainties in the GTP, with an additional contribution from the parameters describing the ocean heat uptake and climate sensitivity. In the first presentation of the GTP, Shine et al. (2005a) used one time-constant for the climate response in their analytical expression. Improved approaches were used by Boucher and Reddy (2008), Collins et al. (2010), and Berntsen and Fuglestvedt (2008) that include more explicit representations of the deep ocean which increased the long-term response to a pulse forcing. Boucher and Reddy (2008) used an impulse response function for temperature with two time-constants that represents both the fast response of the land and upper ocean as well as the slower response of the deep ocean. The more detailed climate response can greatly change the GTP values of short-lived components (Shine et al., 2005a; Peters et al., 2011a). The climate sensitivity parameter (λ) (see definition in 8.1) is present in both the numerator and denominator of the GTP, and hence (unlike AGTP) the GTP is less sensitive to variations in λ. Nonetheless, over a range of likely climate sensitivities, GTP_{50} for BC was found to vary by a factor of 2, the methane GTP_{50} varied by ~50%, while for N_2O essentially no dependence was found (Fuglestvedt et al., 2010). This indicates that a better quantification of the climate impulse response functions is needed to reduce the uncertainty in the numerical values of the GTPs (Olivié and Peters, 2012; Olivié et al., 2012).

Structural uncertainties such as the time horizon can greatly affect the numerical values obtained for CO_2 equivalents. For a change in time horizon from 20 to 100 years, the GWP for methane decreases by a factor of ~3 and its GTP by more than a factor of 10. In general, emission profiles with large contributions from components that are removed on timescales very different from that of CO_2 will be most sensitive to these choices, e.g., sources/sectors with emissions of CH_4 and BC or some transport sectors (Berntsen and Fuglestvedt, 2008; Azar and Johansson, 2011). Some approaches have removed the time horizon from the

[6] These terms are used for consistency with literature in this field and differ from the uncertainty language used elsewhere in this report.

metrics (e.g., Boucher, 2012), but discounting is usually introduced instead which means that a discount rate r (for the weighting function e^{-rt}) must be chosen instead.

Another type of structural uncertainty is what processes are included in the definition of a metric. Ideally all indirect effects (Sections 8.2 and 8.3.2) should be taken into account in the calculation of metrics. The indirect effects of CH_4 on its own lifetime, tropospheric ozone and stratospheric water have been traditionally included in its GWP. Boucher et al. (2009) have quantified an indirect effect on CO_2 when fossil fuel methane is oxidised in the atmosphere. Shindell et al. (2009) estimated the impact of reactive species emissions on both gaseous and aerosol forcing species and found that ozone precursors, including methane, had an additional substantial climate effect because they increased or decreased the rate of oxidation of SO_2 to sulphate aerosol. Studies with different formulations of sulphur cycle have found lower sensitivity (Collins et al., 2010; Fry et al., 2012). Collins et al. (2010) calculated that ozone precursors had an additional component to their GWP and GTP metrics due to the decreased productivity of plants under higher levels of surface ozone. This was of the same magnitude as the O_3 and CH_4 effects, but has so far only been calculated with one model.

Gillett and Matthews (2010) included climate-carbon feedbacks in calculations of GWP for CH_4 and N_2O and found that this increased the values by 20%. They used numerical models for their studies and suggest that these effects should be considered and parameterized when used in simple models to derive metrics. Collins et al. (2012) parameterize the carbon-climate feedback based on Friedlingstein et al. (2006) and find that this more than doubles the GTP_{100} for methane. Enhancement of methane's GTP due to carbon-climate feedback is also found by Reisinger et al. (2010).

The inclusion of indirect effects and feedbacks in metric values has been inconsistent in the IPCC reports. In SAR, a carbon model without a coupling to a climate model was used for calculation of IRF_CO_2 (Joos et al., 1996), while in TAR and AR4 carbon-climate feedbacks are included (Joos et al., 2001; Plattner et al., 2008). The CH_4 GWP from SAR (adopted by the Kyoto Protocol) does include indirect effects of methane on atmospheric gaseous chemistry, but does not include other indirect effects or feedbacks (such as temperature) on methane itself nor temperature feedbacks on CO_2. The $AGWP_{100}$ for CO_2 is 13–15% lower when carbon cycle-climate feedback is not included (Joos et al., 2012). This means that the GWPs presented in TAR, AR4 and AR5 have a bias towards CO_2 and thus underestimate the relative importance of non-CO_2 gases. The different inclusions of indirect effects and feedbacks partially represents the current-state of knowledge, but also inconsistent and ambiguous definitions.

Emission metrics can be estimated based on a constant or variable background climate and this influences both the adjustment times and the concentration-forcing-temperature relationships. Peters et al. (2012) compared variable and constant background climates and found that using a variable background decreases the CO_2 AGWPs by 2% for RCP3PD and 15% for RCP85. Since the background climate continues to change, AGWP values will change if recalculated at future times. Reisinger et al. (2011) found that GWP_{100} for CH_4 would increase up to 20% under the lowest Representative Concentration Pathway (RCP) scenario by 2100 but would decrease by up to 10% by mid-century under the highest RCP. Peters et al. (2012) show that pulse emissions in 2000 compared to 2100 decrease the AGWP_CO_2 by 35% for RCP85 up to 2100 following a constant background, and 45% for a RCP85 background, while changes are in the order of a few percent for RCP3PD. While these studies have focused on the background for CO_2, the same issues apply for temperature. Olivié et al. (2012) and Olivié and Peters (2012) also find different temperature IRFs depending on the background climate and experimental set up.

It is generally assumed that for emission metrics the emissions of different components and of different magnitudes are additive and the response scales linearly with emissions. The robustness of these assumptions has not been explored.

For NTCF the metric values also depend on the location of emission and whether regional or global metrics are used for these gases is also a choice for the users. Metrics are usually calculated for pulses, but some studies also give metric values that assume constant emissions over the full time horizon (e.g., Shine et al., 2005a; Jacobson, 2010). It is important to be aware of the strong assumption about constant future emissions (or change in emissions) of the gas being considered if sustained metrics are used.

Reisinger et al. (2011) estimated the uncertainty in the GWP for CH_4 and found an uncertainty of –30/40% for the GWP_{100} and –50/75% for GTP_{100} of CH_4 (for 5–95% of the spread). Boucher (2012) performed a Monte Carlo analysis with uncertainties in lifetime, RE and IRFs and for GWP_{100} for CH_4, he found –19/+21%, and –51/+66 for GTP_{100} (for 5–95% of the spread). Olivié and Peters (2012) explore the sensitivity of the GWP and GTP to model spread in CO_2 IRFs. They find that relative uncertainty in the GWP is independent of species and not very dependent on time horizon, and for IRFs of both CO_2 and temperature the uncertainty on the CH_4 GTP was –18/+28 and –59/+68% for 20 and 100 years, respectively (for 10–90% of the spread). Reisinger et al. (2011) also consider uncertainties in N_2O and Olivié and Peters (2012) additionally consider BC, N_2O, and SF_6. While each study considers different types of uncertainty, the assessed uncertainty for methane are of the order of 20–40% for GWP_{100} and 60–75% for GTP_{100}.

8.7.1.5 New Metric Concepts

The use of physical metrics, in particular GWPs, in policy contexts has been criticized by economists (Bradford, 2001; De Cara et al., 2008; Reilly, 1992). A prominent use of metrics is to set relative prices of GHG when implementing a multi-gas emissions reduction policy. In these applications, metrics play a fundamentally economic role, and theoretically appropriate metrics include economic dimensions such as mitigation costs, damage costs, and discount rates.

If mitigation policy is set within a *cost-effectiveness* framework with the aim of making the least cost mix of emissions reductions across gases to meet a global temperature target, the appropriate emissions metric is the 'price ratio' (Manne and Richels, 2001). The price ratio, also called the Global Cost Potential (GCP; Tol et al., 2012) or the cost effective trade off ratio (CETO; Azar and Johansson, 2011), is defined as the ratio of the shadow price of a gas to the shadow price of CO_2 within a scenario that meets the target at least cost. The shadow price of a gas in a cost-effectiveness setting is the cost to society of a marginal increase in emissions of that gas while still meeting the target. Similarly, if policy is set within a *cost-benefit* framework, the appropriate index is the ratio of the marginal damages from the emission of a gas (i.e., the damage costs to society resulting from an incremental increase in emissions) relative to the marginal damages of an emission of CO_2, known as the Global Damage Potential (Kandlikar, 1995) or the relative damage cost (Azar and Johansson, 2011). Both types of measures are typically determined within an integrated climate-economy model, since they are affected both by the response of the climate system to emissions as well as by economic factors.

If other indexes, such as the GWP, are used instead of the most appropriate (cost-minimizing) index, costs to society will increase. Cost implications at the project or country level could be substantial under some circumstances (Godal and Fuglestvedt, 2002; Reisinger et al., 2012; Shine, 2009). However, at the global level the increase is relatively small, particularly when compared to the cost savings resulting from a multi- (as opposed to single-) gas mitigation strategy even when based on an imperfect metric (Aaheim et al., 2006; Johansson, 2012; Johansson et al., 2006; O'Neill, 2003).

Nonetheless, physical metrics remain attractive due to the added uncertainties in mitigation and damage costs, and therefore in metric values introduced by economic metrics (Boucher, 2012). Efforts have been made to view purely physical metrics such as GWPs and GTPs as approximations of more comprehensive economic indexes. GTPs, for example, can be interpreted as an approximation of a Global Cost Potential designed for use in a cost-effectiveness setting (Shine et al., 2007; Tol et al., 2012). Quantitative values for GTPs reproduce in broad terms several features of the Global Cost Potential such as the initially low value of metrics for short-lived gases until a climate policy target is approached. Figure 8.29 shows how contributions of N_2O, CH_4 and BC to warming in the target year changes over time. The contributions are given relative to CO_2 and shows the effects of emission at various times. Similarly, GWPs can be interpreted as approximations of the Global Damage Potential designed for use in a cost-benefit framework.

In both cases, a number of simplifying assumptions must be made for these approximations to hold (Tol et al., 2012). For example, in the case of the GWP, the influence of emissions on radiative forcing, and therefore implicitly on costs to society, beyond the time horizon is not taken into account. In the case of the GTP, the influence of emissions on temperature change (and therefore costs) is included only at the time the target is reached, but not before nor after. This highlights how even if one attempts to define a purely physical metric, there is an implicit economic valuation. The Cost Effective Temperature Potential (CETP;

Johansson, 2012) has been explicitly derived as an approximation to the GCP and is similar to the GTP but accounts for longer-term temperature effects. Like the GTP, it is based on the response of temperature to emissions and includes an assumption about the date at which a target is achieved. It also requires an assumption about one economic quantity, the discount rate (that is, how to value costs at different times), in order to account for longer-term temperature effects. Quantitative values for the CETP reproduce values of the GCP more closely than does the GTP (Johansson, 2012).

[INSERT FIGURE 8.29 HERE]

Figure 8.29: Global temperature change potential (GTP(t)) for methane, nitrous oxide and BC for each year from 2010 to the time at which the temperature change target is reached (2110). GTP(t) for CH_4 and N_2O on left axis; GTP(t) for BC on right axis. The (time-invariant) GWP_{100} is also shown for N_2O and CH_4 for comparison.

Metrics have also been proposed that take into account forcing or temperature effects over broader time spans than does the GTP (Manning and Reisinger, 2011; Tanaka et al., 2009). Values for these metrics derived for the historical period have been shown to differ significantly from GWP_{100} values for CH_4 and N_2O, and to behave in a way that is qualitatively similar to GCP and GTP. The metric Surface Temperature Response per unit continuous emission (STRE) was presented by Jacobson (2010) and is similar to the GTP for sustained emissions as presented by Shine et al. (2005b). However, Jacobson (2010) uses one single lifetime for CO_2 which is inconsistent with the literature (Joos et al., 2012; Archer et al., 2009; see Box 6.2).

An integrated version of the GTP is another means of accounting for effects over a broader time horizon (e.g., O'Neill, 2000; Peters et al., 2011a). Such an approach was investigated quantitatively in the derivation of a GTP based on the time-averaged temperature response to a pulse emission (Mean Global Temperature Change Potential (MGTP); Gillett and Matthews, 2010) and a GTP calculated in response to sustained emissions (Sustained Global Temperature Change Potential (SGTP); Azar and Johansson, 2012). Both measures were shown to be quantitatively similar to GWPs if the time horizon is 100 years. O'Neill (2000), Peters et al. (2011a; 2011b), and Azar and Johansson (2012) present and discuss integrated Global Temperature change Potential (iGTP) and show that the values (except for NTCF) are very close to the GWP values. The similarity between the iGTP and GWP may lead to a physical interpretation of the GWP (Peters et al., 2011a; Azar and Johansson, 2012).

Currently, biogenic emissions of CO_2 are not allocated to national emission totals on the assumption that the emissions from oxidation are compensated by biomass regrowth (IPCC, 1996). There is a time-lag between oxidation and regrowth, and while the CO_2 is resident in the atmosphere it causes RF. Using this concept, Cherubini et al. (2011) developed a GWP for biofuels (GWP_{bio}) which takes into account the biomass growth cycle, with values generally between zero (current default for biogenic emissions) and one (current default for fossil fuel emissions). GWP_{bio} decreases with increasing time horizon and with shorter rotation cycles. Due to the fast time scale of atmosphere-ocean CO_2 exchange, the growth cycle temporally causes a negative net RF (Cherubini et al., 2011), and hence the GTP_{bio} becomes negative dependent on the growth cycle (Cherubini et al., 2012). The GWP_{bio} uses an experimental set up where the biomass is oxidised and then grows, but the values will be different if the biomass grows before oxidation. The GWP_{bio} and GTP_{bio} have only been used in a few applications, and more research is needed to assess their robustness and applicability.

Relevant to GWP_{bio} and GTP_{bio} are biogeophysical effects, such as, albedo and evapotranspiration (Betts, 2000; Bala et al., 2007). Metrics for albedo have been proposed (Betts, 2000; Rotenberg and Yakir, 2010), but as for SLCFs regional variations are important (Claussen et al., 2001). While original studies focussed on large-scale dynamics (e.g., Bala et al., 2007), recent studies address local dynamics particularly in relation to biofuels (e.g., Bright et al., 2011; Georgescu et al., 2011; Loarie et al., 2011).

Information about regional patterns of responses is lost when global mean metrics are used. And in some cases opposing effects may cancel out in the global mean values. Shine et al. (2005b) and Lund et al. (2012) evaluate how non-linear damage functions can be used to capture information on spatial pattern of responses. Another approach is the Absolute Regional Temperature Potential (ARTP; Shindell, 2012; Collins et al., 2012) that provides estimates of impacts at a sub-global scale. It gives the time-dependent temperature response in four latitude bands as a function of the regional forcing imposed in those bands. In the tropics and the NH mid-latitudes ARTPs for land areas can be estimated by multiplying the ARTP by given factors.

Nascent work exploring regional precipitation metrics also requires additional studies to determine the robustness of such metrics (Shindell et al., 2012c).These approaches – still at an early stage – establishes a new perspective on metrics that needs further investigations.

An alternative approach for implementation of multi-component polices is to abandon the single basket approach adopted by the Kyoto Protocol and instead use a component-by-component approach or multi-basket approach (Rypdal et al., 2005, Daniel et al., 2012, Sarofim, 2012; Jackson, 2009). Smith et al. (2012) show how peak temperature change is constrained by *cumulative emissions* for gases with long lifetimes and *emissions rates* of shorter-lived gases (including CH_4). Thus, they divide GHGs in two baskets and present two metrics that can be used for estimating peak temperature for various emission scenarios. This approach uses time invariant metrics that does not account for the timing of emissions relative to the target year, and of course does not take into account any impacts other than peak warming in the distant future.

8.7.1.6 Synthesis

In the application and evaluation of metrics, it is important to distinguish between two main types of uncertainty; *structural* and *scientific*. To improve the accuracy of metrics the scientific uncertainty needs to be reduced. But one also needs to acknowledge the structural uncertainty which is linked to the application; e.g., using a different type of metric will for many components have a much larger effect than improved estimates of input parameters. The chosen metric and time horizon can have strong effects on perceived impacts and abatement strategies. While scientific choices of input data have to be made, there are value-based choices needed. For some metrics the value-based choices are not always explicit and transparent.

In addition to progress in understanding of GWP, new concepts have been introduced or further explored since AR4. Among the alternatives, the GTP concept has the broadest application. The time variant version of GTP, as well as the CETP, introduce more dynamical views of the temporal contributions that accounts for the proximity to the target (in contrast to the static GWP).

As metrics use parameters further down the cause effect chain the metrics become in general more relevant, but at the same time the uncertainties increase. Furthermore, metrics that account for regional variations in sensitivity to emissions or regional variation in response, could give a very different emphasis to various emissions. Many species, especially NTCF, produce a distinctly heterogeneous RF and temperature patterns. These aspects are not accounted for in the most commonly used metrics. The RTP is a promising new approach which could be expanded to capture the relation between patterns of emissions and responses, and also for other variables than temperature.

The GWPs suffer from inconsistent treatment of indirect effects/feedbacks. While the AR4 and AR5 values include climate-carbon feedbacks for CO_2, this was not the case for the SAR values (adopted by the Kyoto Protocol). Furthermore, for the non-CO_2 gases there are no climate feedbacks included. Such feedbacks may have significant impacts on metrics and should be treated consistently in metrics. Indirect effects and chemical feedbacks are included for some WMGHG only. More studies are needed to assess the importance of consistent treatment of indirect effects/feedbacks in metrics.

The weighting of effects over time – choice of time horizon in the case of GWP – is value based. Discounting is an alternative, which is often seen as controversial. However, the current weighting used in the GWP is a weight equal to one up to the time horizon and zero thereafter, which is not in line with common approaches for evaluation of future effects in economics (e.g., as in WGIII). Adoption of a fixed horizon of e.g., 20, 100 or 500 years will inevitably put no weight on the long-term effect of CO_2 beyond the time horizon (Figure 8.27 and Box 6.2).

The most appropriate metric depends on the particular application and which aspect of climate change is considered relevant in a given context. As pointed out in several studies (Manne and Richels, 2001; Manning and Reisinger, 2011; Shine et al., 2007; Smith et al., 2012; Tanaka et al., 2012) the time invariant GWP is not well suited for a policy context with a global concentration, forcing or temperature target. The GTP and variants may be more suitable. However, they only attempt to represent global mean temperature change, and so a more complete evaluation of the consequences of a given policy choice would require additional metrics to evaluate the effects on other aspects of climate change such as regional temperature and

precipitation changes, as well as on other environmental factors that will be influenced by these same emissions (such as air quality or ocean acidification).

To provide metrics that can be useful to the users and policymakers a more effective dialog and discussion on three topics is needed: 1) which applications particular metrics are meant to serve; 2) how comprehensive metrics need to be in terms of indirect effects and feedbacks; and – related to this; 3) how important it is to have simple and transparent metrics (given by analytical formulations) versus more complex model-based and thus model-dependent metrics. These issues are also important to consider in a wider disciplinary context (e.g., across the IPCC Working Groups). Finally, it is important to be aware that all metric choices, even 'traditional' or 'widely-used' metrics, contain implicit value judgements as well as large uncertainties.

8.7.2 Application of Metrics

8.7.2.1 Metrics for WMGHGs

Updated GWP and GTP values for WMGHG for some illustrative and tentative time horizons are given in Table 8.A.1. Metric values for CO_2, CH_4 and N_2O are calculated here while AGWP and AGTP values for the remaining components are taken from Hodnebrog et al. (2012). GWP_{100} values are also given for a selected set of ODS in Table 8.A.2. The GWP values have changed from previous assessments due to new estimates of lifetimes, impulse response functions and REs. These are updated due to improved knowledge and/or changed background levels. Since CO_2 is used as reference, any changes for this gas will affect all metrics values. This is an important element of the changes in GWP values, and Figure 8.30 shows how the values of RE, integrated IRF and consequentially AGWP-CO_2 have changed from earlier assessments relative to AR5 values. The $AGWP_{100}$_CO_2 value from AR4 is 5% lower than the AR5 value.

[INSERT FIGURE 8.30 HERE]

Figure 8.30: Changes in the radiative efficiency (RE), integrated IRF and AGWP for CO_2 from earlier IPCC Assessment Reports normalised relative to the values given in AR5. The 'original' values are calculated based on the methods explained in each IPCC Assessment Report. The 'updated' values are calculated based on the methods used in AR5. The difference is primarily in the RE, which has been updated in TAR and again in AR4. The different integrated IRF in TAR relates to a different parameterisation of the same IRF (WMO, 1999) . Changes represent both changes in scientific understanding and a changing background atmospheric CO_2 concentration (note that y-axis starts from 0.6).

From AR4 the methane GWP has changed due to changes in adjustment time, a minor change in RE, as well as change in AGWP_CO_2. The effects on tropospheric O_3 and stratospheric H_2O are accounted for by increasing the RF from methane by 48% and 15%, respectively (see Sections 8.3.3 and 8.5.1). We also present (based on Boucher et al., 2009) metric values for CH_4 of fossil origin. In applications of these values, inclusion of the CO_2 effect of fossil methane must be done with caution to avoid any double-counting since CO_2 emissions numbers are often based on total carbon content. For non-fossil CH_4 we assume balance between CO_2 taken up by the biosphere and CO_2 produced from CH_4 oxidization.

8.7.2.2 Metrics for NTCF

The GWP concept was initially used for the WMGHGs, but later for NTCF as well. There are, however, substantial challenges related to calculations of GWP (and GTP) values for these components, which is reflected in the large ranges of values in the literature. Below we present and assess the current status of knowledge and quantification of metrics for various NTCF.

8.7.2.2.1 Nitrogen oxides (NO_X)

Metric values for NO_X usually include the short-lived O_3 effect, CH_4 changes and the CH_4-controlled O_3 response. In addition, NO_X causes RF through nitrate formation, and via methane it affects stratospheric H_2O and through ozone it influences CO_2. Due to high reactivity and the many non-linear chemical interactions operating on different timescales, as well as short lifetime and heterogeneous emission patterns, calculation of *net* climate effects of NO_X is difficult. The net effect is a balance of large opposing effects with very different temporal behaviours. There is also a large spread in values between regions due to variations in chemical and physical characteristics of the atmosphere.

As shown in Table 8.A.3 the GTP and GWP values are very different. This is due the fundamentally different nature of these two metrics (see Figure 8.27) and the way they capture the temporal behaviour of the effects. Time variation of GTP for NO_X is complex, which is not directly seen by the somewhat arbitrary choices of time horizon, and the net GTP is a fine balance between the contributing terms. The general pattern for NO_X is that the short-lived ozone forcing is always positive, while the methane-induced ozone forcing and methane forcing are always negative. For the GTP, all estimates for NO_X from surface sources give a negative net effect. Collins et al. (2010) included the effect of O_3 on CO_2 levels via vegetation impacts, and found that this effect adds a large warming contribution to the net effect of NO_X. There are significant uncertainties related to the numbers, and so far there is only one study that has included this effect. Shindell et al. (2009) estimated the impact of reactive species emissions on both gaseous and aerosol forcing species and found that a substantial climate impact of ozone precursors was manifested through perturbations to the sulphur cycle in addition to ozone itself. Studies with different formulations of the sulfur cycle have found lower sensitivity (Collins et al., 2010; Fry et al., 2012). The metric estimates for NO_X reflect the level of knowledge, but they also depend on experimental design, treatment of transport processes, modelling of background levels. The multi-model study by Fry et al. (2012) shows the gaseous chemistry response to NO_X is relatively robust for European emissions, but that the uncertainty is so large that for some regions of emissions it is not possible to conclude whether NO_X causes cooling or warming.

8.7.2.2.2 Carbon monoxide (CO) and volatile organic carbons (VOC)

Emissions of carbon monoxide (CO) and volatile organic carbons (VOC) lead to production of ozone on short timescales. By affecting OH and thereby the levels of methane they also initiate a long-term O_3 effect. With its lifetime of 2–3 months, the effect of CO emissions is less dependent on location than what is the case of NO_X (see Table 8.A.4). There is also less variation across models; i.e., 25–30%. However, Collins et al. (2010) found that inclusion of vegetation effects of O_3 increased the GTP values for CO by 20–50%. By including aerosol responses Shindell et al. (2009) found an increase in GWP_{100} by a factor of ~2.5. CO of fossil origin will also have a forcing effect by contributing to CO_2 levels. This effect adds 1.4–1.6 to the GWP_{100} for CO (Daniel and Solomon, 1998; Derwent et al., 2001).

VOC is not a well-defined group of hydrocarbons. This group of gases with different lifetimes is treated differently across models by lumping or using representative key species. However, the spread in metric values in Table 8.A.5 is moderate across regions, with highest values for emissions in South-Asia (of the four regions studied). For each region the uncertainties across models are in the range 20–50%. The effects via O_3 and CH_4 cause warming, and the additional effects via interactions with aerosols and via the O_3-CO_2 link increase the warming effect further. Thus, the net effects of CO and VOC are less uncertain than for NO_X for which the net is a residual between larger terms of opposite sign.

8.7.2.2.3 Black carbon (BC) and organic carbon (OC)

Several studies have focused on the effects of emissions of BC and OC from different regions, thus making it possible to derive regional metric values (Bauer et al., 2007; Koch et al., 2007; Naik et al., 2007; Reddy and Boucher, 2007; Rypdal et al., 2009; Shindell et al., 2011). However, examination of results from these models (Fuglestvedt et al., 2010) reveals that there is not a robust relationship between the region of emission and the metric value – hence, regions that yield the highest metric value in one study, do not, in general, do so in the other studies. This could be because of differences in the representations of atmospheric processes in the models, or differences in the experimental design.

Most of the metric values for BC in the literature include the direct aerosol effect and the snow/ice albedo effect of BC, though whether external or internal mixing is used varies between the studies. Bond et al. (2011) calculate GWPs and find that when albedo effect is included the values increase by 5–15%. The RF from the albedo effect can underestimate the climate response, however.

Bond et al. (2012) assessed the current understanding of BC effects and calculated GWP and GTP for BC that include albedo, indirect and semi-direct effects. As shown in Table 8.A.6 the uncertainties are wide for both metrics (for 90% uncertainty range) reflecting the current challenges related to understanding and quantifying the various effects. The direct effect is ~55% of the total effect while the albedo effect is one third of the direct effect whereas the semi-direct effect is half of the direct effect but of opposite sign. All these values are associated with large uncertainties and are not necessarily consistent with AR5 values (see Sections 7.5, 8.3.4, 8.5.1). The GWP and GTP metrics vary with the region where BC is emitted by about

±30% (based on two studies). For larger regions of emissions, Collins et al. (2012) calculated GTPs for the direct effect of BC and found slightly lower variations between the regions.

The metric values for OC are quite consistent across studies, but fewer studies are available (see Table 8.A.6).

8.7.2.2.4 Other components

Derwent et al. (2001) report values of GWP_{100} of 3.4 for the effect of H_2 on CH_4 and 2.4 from the effect on O_3, giving a total of 5.8. For global emissions of SO_2 Fuglestvedt et al. (2010) calculated GWPs of –140 and –40 for 20 and 100 years, respectively. The GTPs are –41 and –6 for the same horizons (for both metrics the values are given on an SO_2-basis and account only for the direct effect of sulphate.). For SO_2 Shindell et al. (2009) calculated –22 ± 20 (direct only) and –76 ± 69 (direct and indirect effects) for GWP_{100}, and –78 ± 70 and –268 ± 241 for GWP_{20}. For NH_3 Shindell et al. (2009) calculated –19 ± 22 (direct only) and –15 ± 18 (direct and indirect effects) for GWP_{100}, and –65 ± 76 and –53 ± 62 for GWP_{20}. Due to competition for ammonium between nitrate and sulphate, the net aerosol forcing from either SO_2 or NH_3 emissions is the residual of larger responses of opposite signs, which leads to the high uncertainty in their numbers.

8.7.2.2.5 Summary of status of metrics for NTCF

While significant progress has been made since AR4 in our understanding of impacts of NTCF, there are still large uncertainties related to the quantifications of climate effects. The metrics provide a format for comparing the magnitudes of the various emissions (and from different studies) as well as for comparing effects of emissions from different regions. Much of the spread in results is due to differences in experimental design and how the models treat physical and chemical processes. Unlike most of the WMGHGs, many of the NTCF are tightly coupled to hydrologic cycle and atmospheric chemistry, leading to a much larger spread in results as these are highly complex processes that are difficult to validate on the requisite small spatial and short temporal scales. The scientific confidence is low for NO_X, BC and OC. For aerosols the scientific confidence in estimates are low due to lack of knowledge about cloud interactions. There are particular difficulties for NO_X, because the net impact is a small residual of opposing effects with quite different spatial distributions and temporal behaviour.

8.7.2.3 Impact by Emitted Component

We now use the metrics evaluated here to estimate climate impacts of various components (in a forward looking perspective). Figure 8.31 shows global anthropogenic emissions weighted by GWP and GTP. The time horizons are chosen merely as examples and illustrate how the perceived impacts of components – relative to the impact of the reference gas – vary strongly as function of impact parameter (integrated RF in GWP or end-point temperature in GTP) and with time horizon.

We may also calculate the temporal development of the temperature responses to pulse or sustained emissions. Figure 8.32a shows that for one-year pulses the impacts of NTCF decay quickly due to their atmospheric adjustment times even if effects are prolonged due to climate response time. In the case of constant emissions (Figure 8.32b), the effects of NTCF reach approximately constant levels since emissions are replenished every year, while components with long lifetimes accumulate causing increasing warming effect over time. Figure 8.32 also shows how some components have strong short-lived effects of both signs while CO_2 has a weaker initial effect but one that persists to create a long-lived warming effect.

These examples show that the outcome of comparisons of effects of emissions depends strongly on structural uncertainties. End-user choices will have a strong influence on the calculated contributions from NTCF vs WMGHG or non-CO_2 vs CO_2 emissions. Thus, each specific analysis should use a design chosen in light of the context and questions being asked.

[INSERT FIGURE 8.31 HERE]

Figure 8.31: Global anthropogenic emissions weighted by GWP and GTP for chosen time horizons (aerosol cloud interactions are not included.) Emission data for 2008 are taken from the Edgar database and for BC and OC from Shindell et al. (2012b).

[INSERT FIGURE 8.32 HERE]

Figure 8.32: Temperature response by component for total man-made emissions for (a) a one-year pulse (year 2000) (upper) and (b) for emissions kept constant at 2000 level (lower). 'Synthetic' includes PFCs, HCFs, HCFCs, NF_3 and SF_6. Aerosol cloud interactions (AIE) are included. From Aamaas et al. (2012).

8.7.2.4 Metrics and Impacts by Sector

While the emissions of WMGHGs vary strongly between sectors, the climate impacts of these gases are independent of sector. The latter is not the case for NTCF, due to the dependence of their impact on the emission location. Since most sectors have multiple co-emissions, and for NTCFs some of these are warming while others are cooling, the net impact of a given sector is also not obvious without explicit calculations. Since AR4 there has been significant progress in the understanding and quantification of climate impacts of NTCF from sectors such as the transport sectors, power production, biomass burning, etc. (Berntsen and Fuglestvedt, 2008; Eyring et al., 2010a; Fuglestvedt et al., 2008; Lee et al., 2010; Skeie et al., 2009; Stevenson and Derwent, 2009; Uherek et al., 2010). Many of the studies provide metrics for the components that are important for the assessment of the various sectors. Table 8.A.7 gives an overview of recent published metric values for various components by sector.

Focusing on BC, OC, NH_3 and SO_2, Henze et al. (2012) show how RF efficiencies of many individual emission perturbations differ considerably from region or sectoral averages. One important implication of their results is that RF estimates aggregated over regions or sectors may not represent the impacts of emissions changes on finer scales.

Metrics for individual land-based sectors can sometimes be similar to the global mean metric values (e.g., in Shindell et al., 2008), the BC and OC metrics for the individual land-based sectors in Asia are similar to global means.) In contrast, metrics for emissions from aviation and shipping usually show large differences from global mean metric values (Table 8.A.3 vs Table 8.A.7); especially for NO_X from shipping. Though there can sometimes be substantial variation in the impact of land-based sectors across regions, and for a particular region even from one sector to another, variability between different land-based sources is generally smaller than between land, sea and air emissions.

For NO_X from *aviation* the GWP_{20} values are positive due to the strong effect of the short-lived O_3. For GWP_{100} and GTP_{100} the values are of either sign due to the differences in balance between the individual effects modelled. Even if the models agree on net effect of NO_X, the individual contributions can differ significantly. In the multi-model study by Myhre et al. (2011) it is shown that differences in the methane response relative to the O_3 response drive much of the spread. Holmes et al. (2011) found that processes controlling the background tropospheric concentrations of NO_X are likely to be the main reason for the modelling uncertainty in climate impacts of NO_X from aviation. Köhler et al. (2012), find strong regional sensitivity of O_3 and CH_4 to NO_X particularly at cruise altitude. Generally, they find the strongest effects at low latitudes. Based on detailed studies in the literature, Fuglestvedt et al. (2010) also produced GWP and GTP for contrails, water vapor, and aviation-induced cirrus (AIC). Due to limitations in our knowledge about these components and mechanisms, there are large uncertainties connected to these metric values.

The GWP and GTPs for NO_X from *shipping* are strongly negative for all time horizons. The stronger positive effect via O_3 due to the low-NO_X environment into which ships generally emit NO_X is outweighed by the stronger effect on methane destruction at lower latitudes.

Table 8.A.7 also shows metric values for emissions of SO_2 from the sectors shipping and petroleum production in the Arctic. The direct GWP_{100} for shipping ranges from –11 to –43. The indirect GWPs and GTPs are in some cases 10 times larger than the direct values, but the uncertainty in the metrics for indirect effects is likely to be much larger than for the direct. Only one study (Lauer et al., 2007) has so far reported detailed calculations of the indirect forcing specifically for this sector. Lauer et al. also find a wide spread of values depending on the emission inventory. The values from Shindell and Faluvegi (2010) for SO_2 from power production are similar to those for shipping.

Unger et al. (2010) calculated RF for a set of components emitted from each sector. RF at chosen points in time (20 and 100 years) for *sustained* emissions was used by Unger et al. (2010) as the metric for comparison. This is approximately equal to using integrated RF up to the chosen times for *pulse* emissions

(and is thus consistent with the GWP perspective). They account for interactions and non-linearities among the emitted species. Such studies are relevant for policymaking that focuses on regulating the *total activity* of that sector or for understanding the contributions from the sector to climate change. On the other hand, the fixed mix of emissions makes it less general and relevant for different emission cases and variations in mix of emission. Alternatively, one may adopt a component-by-component view which is relevant for policies directed towards specific components (though controlling an individual pollutant in isolation is usually not practical). But this view will not capture interactions and non-linearities within the suite of components emitted by most sectors. The effects of specific emission control technologies or policies on the mix of emissions is probably the most relevant type of analysis, but there are an enormous number of possible actions and regional details that could be investigated. Comparison of perturbation response versus tagging indicates the importance of considering compensation of emissions from other sectors when analyzing the response to changes in any single sector (Grewe et al., 2012).

While the various transport sectors often are treated as one aggregate (e.g., road transport) there are important subdivisions. For instance, Bond et al. (2012) points out that among the BC-rich sectors, diesel vehicles have the most clearly positive net impact on forcing. Studies delving even further have shown substantial differences between trucks and cars, gasoline and diesel vehicles, and low-sulfur versus high-sulfur fuels. Similarly, for power production there are important differences depending on fuel type (coal, oil, gas; Shindell and Faluvegi, 2010).

In the assessment of climate impacts of *current* emissions by sectors we here apply a forward looking perspective on effects in terms of *temperature change.* Then the AGTP concept can be used to study the effects of the various components over time. Figure 8.33a shows the *net* temperature effect as function of time by sector. The effects of the sectors are summed over all the individual contributions from the various components and the figure shows that the temperature responses are of different sign and operate on very different timescales. The sectors Industry and Power production cause cooling effects during the first years after emissions (mainly due to SO_2 emissions) but change sign with a peak warming after a few decades and thereafter a long term warming, mainly from CO_2. Figure 8.33b shows the effect of assuming constant emissions. In order to see the contributions from the various components we can also look at the contributions at a particular time (see Figure 8.34; for pulse case).

Analysing climate change impacts by using the net effect of particular activities or sectors may – compared to other perspectives – provide clearer insight into how societal actions influence climate. Due to large variations in mix of short- and long-lived components, as well as cooling and warming effects, the results will also in these cases depend strongly on structural choices. Improved understanding of aerosol cloud interactions and how those are attributed to individual components is clearly necessary to refine estimates of sectoral or emitted component impacts.

[INSERT FIGURE 8.33 HERE]

Figure 8.33: (a) Net global mean temperature change by sector from total man-made emissions (one year pulse); (b) Net global mean temperature change by sector from total man-made emissions kept constant. Aerosol cloud interactions (AIE) are included. From Aamaas et al. (2012).

[INSERT FIGURE 8.34 HERE]

Figure 8.34: Net global mean temperature change by sector after 20 years (for one year pulse emissions). 'Synthetic' includes PFCs, HCFs, HCFCs, NF_3 and SF_6. Aerosol cloud interactions (AIE) are included. From Aamaas et al. (2012).

[START FAQ 8.1 HERE]

FAQ 8.1: How Important is Water Vapour to Climate Change?

As the largest contributor to the greenhouse effect, water vapour is an essential component of the Earth's climate. However, the amount of water vapour in the atmosphere is mostly controlled by air temperature, rather than by emissions. For that reason, scientists consider it a feedback, rather than a forcing to climate change. Anthropogenic emissions of water vapour through irrigation, or power plant cooling have a negligible impact on the global climate.

Water vapour is the primary greenhouse gas in the Earth's atmosphere. The contribution of water vapour to the greenhouse effect relative to that of carbon dioxide depends on the accounting method, but can be considered to be approximately two to three times greater. Additional water vapour is injected into the atmosphere from anthropogenic activities, mostly through increased evaporation from irrigated crops, but also through power plant cooling, and marginally through the combustion of fossil fuel. One may therefore question why there is so much focus on carbon dioxide, and not on water vapour, as a forcing to climate change.

Water vapour behaves differently from carbon dioxide in one fundamental way: it can condense and precipitate. When air with high humidity cools, some of the vapour condenses into water droplets or ice particles and precipitates. The typical residence time of water vapour in the atmosphere is ten days. The flux of water vapour into the atmosphere from anthropogenic sources is considerably less than from 'natural' evaporation. Therefore, it has a negligible impact on overall concentrations, and does not contribute significantly to the long-term greenhouse effect. This is the main reason why tropospheric water vapour (typically below 10 km altitude) is not considered to be an anthropogenic gas contributing to radiative forcing.

On the other hand, water vapour in the stratosphere (above 10 km altitude) is considered to be a radiative forcing agent, with measurable impacts on the greenhouse effect. Stratospheric concentrations have varied significantly in past decades. An observed increase prior to 2000 might be explained in part by the oxidation of increased concentrations of atmospheric methane from anthropogenic emissions. However, water vapour concentrations fell again after that year. The full extent of these variations is not well understood, but the contribution of stratospheric water vapour to warming is nevertheless much smaller than from methane or carbon dioxide.

The warmer air gets, the more water vapour it can hold. A typical polar air atmospheric column may contain a few kilograms of water vapour per square metre, while a tropical air mass might hold up to 100 kilograms. With every extra degree of air temperature, the atmosphere can retain around seven per cent more water vapour (see FAQ 8.1, Figure 1). This increase in concentration (with less precipitation than evaporation during the transition period) amplifies the greenhouse effect, and therefore to more warming. This process, referred to as the water vapour feedback, is well understood and quantified. It is included in all models used to estimate climate change, where its strength is consistent with observations. Although an increase in atmospheric water vapour has been observed, this change is recognised as a climate feedback (from increased atmospheric temperature) and cannot be interpreted as a radiative forcing from anthropogenic emissions.

Currently, water vapour has the largest greenhouse effect in Earth's atmosphere. However, other greenhouse gases, and primarily carbon dioxide, are necessary to sustain the presence of water vapour in the atmosphere. Indeed, if these other gases were removed from the atmosphere, its temperature would drop sufficiently to induce a decrease of water vapour, leading to a runaway drop of the greenhouse effect that would plunge the Earth into a frozen state. So greenhouse gases other than water vapour have provided the temperature structure that sustains current levels of atmospheric water vapour. Therefore, although carbon dioxide is the main anthropogenic control knob on climate, water vapour is a strong and fast feedback that amplifies any initial forcing by a typical factor of three. Water vapour is not a significant initial forcing, but is nevertheless a fundamental agent of climate change.

[INSERT FAQ 8.1, FIGURE 1 HERE]

FAQ 8.1, Figure 1: Illustration of the water cycle and its interaction with the greenhouse effect. The upper-left insert indicates the increase of potential water vapour content in the air with an increase of temperature.

[END FAQ 8.1 HERE]

[START FAQ 8.2 HERE]

FAQ 8.2: Do Improvements in Air Quality have an Effect on Climate Change?

Yes they do, but depending on which pollutant(s) they limit, they can either help cool, or warm, the climate.

Air quality is nominally a measure of airborne pollutants, such as ozone, carbon monoxide, nitrogen oxides, aerosols, and solid or liquid particulate matter, or PM. Exposure to such pollutants exacerbates respiratory and cardiovascular diseases, harms plants and even damages buildings. For these reasons, most major urban centres try to control discharges of airborne pollutants.

Unlike carbon dioxide and other long-lived greenhouse gases, tropospheric ozone and aerosols may only last in the atmosphere for a few days to a few weeks, though some indirect couplings within the Earth system can prolong their impact. These pollutants are most potent near their point of origin, which causes quite significant local or regional radiative forcing, even if the globally-averaged effect is rather small.

Therefore, surface air quality controls will have consequences for the climate, but some couplings between these short-lived pollutants and the climate are still poorly understood or quantified – some climate models do not even include them. This makes it difficult to fully quantify those consequences.

Air pollutants affect climate differently, according to their composition. Pollution-generated greenhouse gases will primarily impact climate through radiation, while aerosols can also affect climate through cloud-aerosol interactions. Sulphate particles strongly reflect sunlight, so from a purely radiative standpoint, air pollution measures to limit sulphate particle precursor emissions lead to a reduction in that reflected sunlight, and to warming.

Satellite observations have clearly shown an increase in atmospheric concentrations of sulphur dioxide (the primary precursor to sulphate aerosols) from power plants over eastern Asia during the last decade or more. Nowadays, some newer power plants use scrubbers to reduce such emissions, but the inherent irony is that this new technology, while improving air quality, might exacerbate warming.

It is unclear whether developing countries will curb sulphur emissions to the same extent as have the United States and western Europe since the 1970s, but the short-term climate cooling effect of sulphate aerosols is nevertheless important in the near future. The installation of sulphur dioxide scrubbers will not constrain the long-term warming from carbon dioxide emitted during the coal burning process.

Similarly, the interaction between hydrophilic aerosols and clouds has caused a significant net estimated cooling between pre-industrial conditions and the present day, especially during the second half of the 20th century, when anthropogenic emissions rose sharply. Controls over emissions of such aerosols and their precursors may stimulate more warming.

Black carbon, on the other hand, is a climate forcing agent which absorbs heat in the atmosphere and, when deposited on snow, reduces its albedo, or ability to reflect sunlight. Reductions of black carbon emissions can therefore have a cooling effect.

Measures to lower surface ozone—through controls on precursor emissions, such as nitrogen oxides, carbon monoxide, methane or volatile organic compounds—similarly have a cooling impact, the extent of which depends on how much those measures control ozone in the mid to upper troposphere. The consequences of changes in sector-specific emissions—from the transportation sector, for instance—can become quite complicated, because of the complex atmospheric chemistry couplings between species within the targeted sector. Nitrogen oxide emission controls, for example, should have a cooling effect because they reduce tropospheric ozone, but their impact on methane lifetime and aerosol formation is more likely instead to cause overall warming. Or smoke from biofuel combustion contains a mixture of both absorbing and scattering particles as well as ozone precursors.

There is an important twist, too, in the potential effect of climate change on air quality. Though not fully understood, an observed positive correlation between surface ozone pollution and temperature indicates that higher temperatures could worsen that pollution, a phenomenon known as a climate penalty. Models indicate that this impact could, in some regions, outstrip measures to improve air quality. This climate penalty will be regionally variable, and is difficult to assess, but better understanding, quantification and modelling of these processes will clarify the role of pollutant emissions on climate.

[INSERT FAQ 8.2, FIGURE 1 HERE]

FAQ 8.2, Figure 1: Schematic diagram of the impact of pollution controls on specific emissions and climate impact. Solid black line indicates known impact, dashed line indicates uncertain impact.

[END FAQ 8.2 HERE]

References

Aaheim, A., J. Fuglestvedt, and O. Godal, 2006: Costs savings of a flexible multi-gas climate policy. *Energy Journal*. 485-501.

Aamaas, B., G. Peters, and J. Fuglestvedt, 2012: A synthesis of climate-based emission metrics with applications. *Earth Syst. Dynam. Discuss. (submitted)*.

Abreu, J. A., J. Beer, F. Steinhilber, S. M. Tobias, and N. O. Weiss, 2008: For how long will the current grand minimum of solar activity persist? *Geophysical Research Letters*, **35**, L20109.

Ackerley, D., B. B. B. Booth, S. H. E. Knight, E. J. Highwood, D. J. Frame, M. R. Allen, and D. P. Rowell, 2011: Sensitivity of Twentieth-Century Sahel Rainfall to Sulfate Aerosol and CO2 Forcing. *Journal of Climate*, **24**, 4999-5014.

Allan, W., H. Struthers, and D. C. Lowe, 2007: Methane carbon isotope effects caused by atomic chlorine in the marine boundary layer: Global model results compared with Southern Hemisphere measurements. *Journal of Geophysical Research-Atmospheres*, **112**.

Ammann, C. M., and P. Naveau, 2003: Statistical analysis of tropical explosive volcanism occurrences over the last 6 centuries. *Geophysical Research Letters*, **30**, 4.

——, 2010: A statistical volcanic forcing scenario generator for climate simulations. *Journal of Geophysical Research-Atmospheres*, **115**.

Anchukaitis, K. J., B. M. Buckley, E. R. Cook, B. I. Cook, R. D. D'Arrigo, and C. M. Ammann, 2010: Influence of volcanic eruptions on the climate of the Asian monsoon region. *Geophysical Research Letters*, **37**.

Andersen, M., D. Blake, F. Rowland, M. Hurley, and T. Wallington, 2009: Atmospheric Chemistry of Sulfuryl Fluoride: Reaction with OH Radicals, CI Atoms and O-3, Atmospheric Lifetime, IR Spectrum, and Global Warming Potential. *Environmental Science & Technology*. doi:DOI 10.1021/es802439f, 1067-1070.

Andrews, T., and P. M. Forster, 2008: CO2 forcing induces semi-direct effects with consequences for climate feedback interpretations. *Geophysical Research Letters*, **35**.

Andrews, T., M. Doutriaux-Boucher, O. Boucher, and P. M. Forster, 2011: A regional and global analysis of carbon dioxide physiological forcing and its impact on climate. *Climate Dynamics*, **36**, 783-792.

Andrews, T., J. Gregory, M. Webb, and K. Taylor, 2012a: Forcing, feedbacks and climate sensitivity in CMIP5 coupled atmosphere-ocean climate models. *Geophysical Research Letters*, **39**.

Andrews, T., P. Forster, O. Boucher, N. Bellouin, and A. Jones, 2010: Precipitation, radiative forcing and global temperature change. *Geophysical Research Letters*. doi:ARTN L14701, 10.1029/2010GL043991, -.

Andrews, T., M. Ringer, M. Doutriaux-Boucher, M. Webb, and W. Collins, 2012b: Sensitivity of an Earth system climate model to idealized radiative forcing. *Geophysical Research Letters*, **39**.

Antuna, J. C., A. Robock, G. Stenchikov, J. Zhou, C. David, J. Barnes, and L. Thomason, 2003: Spatial and temporal variability of the stratospheric aerosol cloud produced by the 1991 Mount Pinatubo eruption. *Journal of Geophysical Research-Atmospheres*, **108**.

Archer, D., et al., 2009: Atmospheric Lifetime of Fossil Fuel Carbon Dioxide. *Annual Review of Earth and Planetary Sciences*, **37**, 117-134.

Archibald, A. T., M. E. Jenkin, and D. E. Shallcross, 2010: An isoprene mechanism intercomparison. *Atmospheric Environment*, **44**, 5356-5364.

Archibald, A. T., et al., 2011: Impacts of HO(x) regeneration and recycling in the oxidation of isoprene: Consequences for the composition of past, present and future atmospheres. *Geophysical Research Letters*, **38**.

Arora, V. K., and A. Montenegro, 2011: Small temperature benefits provided by realistic afforestation efforts. *Nature Geoscience*, **4**, 514-518.

Ashmore, M. R., 2005: Assessing the future global impacts of ozone on vegetation. *Plant Cell and Environment*, **28**, 949-964.

Azar, C., and D. Johansson, 2011: Valuing the non-CO_2 climate impacts of aviation.

Azar, C., and D. J. A. Johansson, 2012: On the relationship between metrics to compare greenhouse gases – the case of IGTP, GWP and SGTP. *Earth Syst. Dynam. Discuss.*, **3**, 113-141.

Bala, G., K. Caldeira, M. Wickett, T. J. Phillips, D. B. Lobell, C. Delire, and A. Mirin, 2007: Combined climate and carbon-cycle effects of large-scale deforestation. *Proceedings of the National Academy of Sciences of the United States of America*, **104**, 6550-6555.

BALIUNAS, S., and R. JASTROW, 1990: EVIDENCE FOR LONG-TERM BRIGHTNESS CHANGES OF SOLAR-TYPE STARS. *Nature*, **348**, 520-523.

Barnes, C. A., and D. P. Roy, 2008: Radiative forcing over the conterminous United States due to contemporary land cover land use albedo change. *Geophysical Research Letters*, **35**, -.

Bathiany, S., M. Claussen, V. Brovkin, T. Raddatz, and V. Gayler, 2010: Combined biogeophysical and biogeochemical effects of large-scale forest cover changes in the MPI earth system model. *Biogeosciences*, **7**, 1383-1399.

Bauer, S., D. Koch, N. Unger, S. Metzger, D. Shindell, and D. Streets, 2007: Nitrate aerosols today and in 2030: a global simulation including aerosols and tropospheric ozone. *Atmospheric Chemistry and Physics*, **7**, 5043-5059.

Bekki, S., J. A. Pyle, W. Zhong, R. Toumi, J. D. Haigh, and D. M. Pyle, 1996: The role of microphysical and chemical processes in prolonging the climate forcing of the Toba eruption. *Geophysical Research Letters*, **23**, 2669-2672.

Bellouin, N., J. Rae, A. Jones, C. Johnson, J. Haywood, and O. Boucher, 2011: Aerosol forcing in the Climate Model Intercomparison Project (CMIP5) simulations by HadGEM2-ES and the role of ammonium nitrate. *Journal of Geophysical Research-Atmospheres*, **116**.

Berntsen, T., and J. Fuglestvedt, 2008: Global temperature responses to current emissions from the transport sectors. *Proceedings of the National Academy of Sciences of the United States of America*. doi:DOI 10.1073/pnas.0804844105, 19154-19159.

Betts, R., 2000: Offset of the potential carbon sink from boreal forestation by decreases in surface albedo. *Nature*, **408**, 187-190.

Betts, R. A., P. D. Falloon, K. K. Goldewijk, and N. Ramankutty, 2007: Biogeophysical effects of land use on climate: Model simulations of radiative forcing and large-scale temperature change. *Agr Forest Meteorol*, **142**, 216-233.

Biasutti, M., and A. Giannini, 2006: Robust Sahel drying in response to late 20th century forcings. *Geophysical Research Letters*, **33**.

Boer, G. J., and B. Yu, 2003: Climate sensitivity and response. *Climate Dynamics*, **20**, 415-429.

Bollasina, M. A., Y. Ming, and V. Ramaswamy, 2011: Anthropogenic Aerosols and the Weakening of the South Asian Summer Monsoon. *Science*, **334**, 502-505.

Bond, T., C. Zarzycki, M. Flanner, and D. Koch, 2011: Quantifying immediate radiative forcing by black carbon and organic matter with the Specific Forcing Pulse. *Atmospheric Chemistry and Physics*, **11**, 1505-1525.

Bond, T. C., et al., 2007: Historical emissions of black and organic carbon aerosol from energy-related combustion, 1850-2000. *Glob. Biogeochem. Cycle*, **21**, 16.

Bond, T. C., et al., 2012: Bounding the role of black carbon in the climate system: A scientific assessment. *Journal of Geophysical Research*, **submitted**.

Bonfils, C., and D. Lobell, 2007: Empirical evidence for a recent slowdown in irrigation-induced cooling. *Proceedings of the National Academy of Sciences of the United States of America*, **104**, 13582-13587.

Bonfils, C. J. W., T. J. Phillips, D. M. Lawrence, P. Cameron-Smith, W. J. Riley, and Z. M. Subin, 2012: On the influence of shrub height and expansion on northern high latitude climate. *Environmental Research Letters*, **7**.

Booth, B., N. Dunstone, P. Halloran, T. Andrews, and N. Bellouin, 2012: Aerosols implicated as a prime driver of twentieth-century North Atlantic climate variability (vol 484, pg 228, 2012). *Nature*, **485**, 534-534.

Boucher, O., 2012: Comparison of physically- and economically-based CO2-equivalences for methane. *Earth Syst. Dynam.*, **3**, 49-61.

Boucher, O., and J. Haywood, 2001: On summing the components of radiative forcing of climate change. *Climate Dynamics*, **18**, 297-302.

Boucher, O., and M. Reddy, 2008: Climate trade-off between black carbon and carbon dioxide emissions. *Energy Policy*. doi:DOI 10.1016/j.enpol.2007.08.039, 193-200.

Boucher, O., P. Friedlingstein, B. Collins, and K. P. Shine, 2009: The indirect global warming potential and global temperature change potential due to methane oxidation. *Environmental Research Letters*, **4**.

Bourassa, A. E., et al., 2012: *Large volcanic aerosol load in the stratosphere linked to Asian monsoon transport*. *Science*, **337**, 78-81.

Bowman, D., et al., 2009: Fire in the Earth System. *Science*, **324**, 481-484.

Bowman, K., et al., 2012: Observational constraints on ozone radiative forcing from the Atmospheric Chemistry Climate Model Intercomparison Project (ACCMIP). *ACP/GMD Inter-Journal SI*, **Submitted**.

Bradford, D., 2001: Global change - Time, money and tradeoffs. *Nature*. 649-650.

Bright, R., A. Stromman, and G. Peters, 2011: Radiative Forcing Impacts of Boreal Forest Biofuels: A Scenario Study for Norway in Light of Albedo. *Environmental Science & Technology*, **45**, 7570-7580.

Brovkin, V., et al., 2010: Sensitivity of a coupled climate-carbon cycle model to large volcanic eruptions during the last millennium. *Tellus Series B-Chemical and Physical Meteorology*, **62**, 674-681.

BRUECKNER, G., K. EDLOW, L. FLOYD, J. LEAN, and M. VANHOOSIER, 1993: THE SOLAR ULTRAVIOLET SPECTRAL IRRADIANCE MONITOR (SUSIM) EXPERIMENT ON BOARD THE UPPER-ATMOSPHERE RESEARCH SATELLITE (UARS). *Journal of Geophysical Research-Atmospheres*, **98**, 10695-10711.

Campra, P., M. Garcia, Y. Canton, and A. Palacios-Orueta, 2008: Surface temperature cooling trends and negative radiative forcing due to land use change toward greenhouse farming in southeastern Spain. *Journal of Geophysical Research-Atmospheres*, **113**, -.

Carlton, A. G., R. W. Pinder, P. V. Bhave, and G. A. Pouliot, 2010: To What Extent Can Biogenic SOA be Controlled? *Environmental Science & Technology*, **44**, 3376-3380.

Carslaw, K. S., O. Boucher, D. V. Spracklen, G. W. Mann, J. G. L. Rae, S. Woodward, and M. Kulmala, 2010: A review of natural aerosol interactions and feedbacks within the Earth system. *Atmospheric Chemistry and Physics*, **10**, 1701-1737.

Chang, W. Y., H. Liao, and H. J. Wang, 2009: Climate Responses to Direct Radiative Forcing of Anthropogenic Aerosols, Tropospheric Ozone, and Long-Lived Greenhouse Gases in Eastern China over 1951-2000. *Advances in Atmospheric Sciences*, **26**, 748-762.

Chen, W. T., A. Nenes, H. Liao, P. J. Adams, J. L. F. Li, and J. H. Seinfeld, 2010: Global climate response to anthropogenic aerosol indirect effects: Present day and year 2100. *Journal of Geophysical Research-Atmospheres*, **115**.

Cherubini, F., G. Guest, and A. Strømman, 2012: Application of probablity distributions to the modelleing of biogenic CO2 fluxes in life cycle assessment. *Global Change Biol*, **doi: 10.1111/j.1757-1707.2011.01156.x**.

Cherubini, F., G. Peters, T. Berntsen, A. Stromman, and E. Hertwich, 2011: CO2 emissions from biomass combustion for bioenergy: atmospheric decay and contribution to global warming. *Global Change Biology Bioenergy*, **3**, 413-426.

Chung, C. E., and V. Ramanathan, 2006: Weakening of North Indian SST gradients and the monsoon rainfall in India and the Sahel. *Journal of Climate*, **19**, 2036-2045.

Cionni, I., et al., 2011: Ozone database in support of CMIP5 simulations: results and corresponding radiative forcing. *Atmospheric Chemistry and Physics*, **11**, 11267-11292.

CLARKE, A., and K. NOONE, 1985: SOOT IN THE ARCTIC SNOWPACK - A CAUSE FOR PERTURBATIONS IN RADIATIVE-TRANSFER. *Atmospheric Environment*, **19**, 2045-2053.

Claussen, M., V. Brovkin, and A. Ganopolski, 2001: Biogeophysical versus biogeochemical feedbacks of large-scale land cover change. *Geophysical Research Letters*, **28**, 1011-1014.

COLLINS, W., R. DERWENT, C. JOHNSON, and D. STEVENSON, 2002: The oxidation of organic compounds in the troposphere and their global warming potentials. *CLIMATIC CHANGE*, **52**, 453-479.

Collins, W., M. Fry, J. Fuglestvedt, Y. Hongbin, D. Shindell, and J. West, 2012: Global and regional temperature-change potentials for near-term climate forcers. *Atmospheric Chemistry and Physics Discuss.*, (submitted).

Collins, W. D., et al., 2006: Radiative forcing by well-mixed greenhouse gases: Estimates from climate models in the Intergovernmental Panel on Climate Change (IPCC) Fourth Assessment Report (AR4). *Journal of Geophysical Research-Atmospheres*, **111**.

Collins, W. J., S. Sitch, and O. Boucher, 2010: How vegetation impacts affect climate metrics for ozone precursors. *Journal of Geophysical Research-Atmospheres*, **115**.

Conley, A. J., J.-F. Lamarque, F. Vitt, W. D. Collins, and J. Kiehl, 2012: PORT, A CESM tool for the Diagnosis of Radiative Forcing. *Geos. Model Devel.*, **Submitted**.

Cooper, O. R., et al., 2010: Increasing springtime ozone mixing ratios in the free troposphere over western North America. *Nature*, **463**, 344-348.

Cox, P. M., et al., 2008: Increasing risk of Amazonian drought due to decreasing aerosol pollution. *Nature*, **453**, 212-U217.

Crook, J., and P. Forster, 2011: A balance between radiative forcing and climate feedback in the modeled 20th century temperature response. *Journal of Geophysical Research-Atmospheres*, **116**, -.

Daniel, J., and S. Solomon, 1998: On the climate forcing of carbon monoxide. *Journal of Geophysical Research-Atmospheres*, **103**, 13249-13260.

DANIEL, J., S. SOLOMON, and D. ALBRITTON, 1995: ON THE EVALUATION OF HALOCARBON RADIATIVE FORCING AND GLOBAL WARMING POTENTIALS. *Journal of Geophysical Research-Atmospheres*, **100**, 1271-1285.

Daniel, J., E. Fleming, R. Portmann, G. Velders, C. Jackman, and A. Ravishankara, 2010: Options to accelerate ozone recovery: ozone and climate benefits. *Atmospheric Chemistry and Physics*, **10**, 7697-7707.

Daniel, J., S. Solomon, T. Sanford, M. McFarland, J. Fuglestvedt, and P. Friedlingstein, 2012: Limitations of single-basket trading: lessons from the Montreal Protocol for climate policy. *Climatic Change*, **111**, 241-248.

Davin, E. L., and N. de Noblet-Ducoudre, 2010: Climatic Impact of Global-Scale Deforestation: Radiative versus Nonradiative Processes. *Journal of Climate*, **23**, 97-112.

Davin, E. L., N. de Noblet-Ducoudre, and P. Friedlingstein, 2007: Impact of land cover change on surface climate: Relevance of the radiative forcing concept. *Geophysical Research Letters*, **34**, -.

De Cara, S., E. Galko, and P. Jayet, 2008: The Global Warming Potential Paradox: Implications for the Design of Climate Policy. *Design of Climate Policy*. 359-384.

de Noblet-Ducoudre, N., et al., 2012: Determining Robust Impacts of Land-Use-Induced Land Cover Changes on Surface Climate over North America and Eurasia: Results from the First Set of LUCID Experiments. *Journal of Climate*, **25**, 3261-3281.

DeAngelis, A., F. Dominguez, Y. Fan, A. Robock, M. D. Kustu, and D. Robinson, 2010: Evidence of enhanced precipitation due to irrigation over the Great Plains of the United States. *Journal of Geophysical Research-Atmospheres*, **115**.

DeLand, M. T., and R. P. Cebula, 2012: Solar UV variations during the decline of Cycle 23. *J. Atm. Solar-Terr. Phys.*, **77**, 225-234.

Delaygue, G., and E. Bard, 2011: An Antarctic view of Beryllium-10 and solar activity for the past millennium. *Climate Dynamics*, **36**, 2201-2218.

Deligne, N. I., S. G. Coles, and R. S. J. Sparks, 2010: Recurrence rates of large explosive volcanic eruptions. *Journal of Geophysical Research-Solid Earth*, **115**.

Denman, K. L., et al., 2007: Couplings Between Changes in the Climate System and Biogeochemistry. *Climate Change 2007: The Physical Science Basis. Contribution of Working Group I to the Fourth Assessment Report of the Intergovernmental Panel on Climate Change*, Cambridge University Press.

DERWENT, R., W. COLLINS, C. JOHNSON, and D. STEVENSON, 2001: Transient behaviour of tropospheric ozone precursors in a global 3-D CTM and their indirect greenhouse effects. *CLIMATIC CHANGE*, **49**, 463-487.

Dewitte, S., D. Crommelynck, S. Mekaoui, and A. Joukoff, 2004: Measurement and uncertainty of the long-term total solar irradiance trend. *Solar Physics*, **224**, 209-216.

Doutriaux-Boucher, M., M. Webb, J. Gregory, and O. Boucher, 2009: Carbon dioxide induced stomatal closure increases radiative forcing via a rapid reduction in low cloud. *Geophysical Research Letters*. doi:ARTN L02703, 10.1029/2008GL036273, -.

Eliseev, A. V., and Mokhov, II, 2011: Effect of including land-use driven radiative forcing of the surface albedo of land on climate response in the 16th-21st centuries. *Izvestiya Atmospheric and Oceanic Physics*, **47**, 15-30.

Engel, A., et al., 2009: Age of stratospheric air unchanged within uncertainties over the past 30 years. *Nature Geoscience*, **2**, 28-31.

Erlykin, A., and A. Wolfendale, 2011: Cosmic ray effects on cloud cover and their relevance to climate change. *Journal of Atmospheric and Solar-Terrestrial Physics*, **73**, 1681-1686.

Esper, J., and F. H. Schweingruber, 2004: Large-scale treeline changes recorded in Siberia. *Geophysical Research Letters*, **31**.

Eyring, V., et al., 2010a: Transport impacts on atmosphere and climate: Shipping. *Atmospheric Environment*, **44**, 4735-4771.

Eyring, V., et al., 2010b: Sensitivity of 21st century stratospheric ozone to greenhouse gas scenarios. *Geophysical Research Letters*, **37**.

Eyring, V., et al., 2012: Long-term changes in tropospheric and stratospheric ozone and associated climate impacts in CMIP5 simulations. *J. Geophys. Res.*, **Submitted**.

Eyring, V., et al., 2010c: Multi-model assessment of stratospheric ozone return dates and ozone recovery in CCMVal-2 models. *Atmospheric Chemistry and Physics*, **10**, 9451-9472.

Fan, F. X., M. E. Mann, and C. M. Ammann, 2009: Understanding Changes in the Asian Summer Monsoon over the Past Millennium: Insights from a Long-Term Coupled Model Simulation. *Journal of Climate*, **22**, 1736-1748.

FAO, 2010: *Global Forest Resources Assessment 2010.*

Feng, X., and F. Zhao, 2009: Effect of changes of the HITRAN database on transmittance calculations in the near-infrared region. *Journal of Quantitative Spectroscopy & Radiative Transfer*, **110**, 247-255.

Feng, X., F. Zhao, and W. Gao, 2007: Effect of the improvement of the HITIRAN database on the radiative transfer calculation. *Journal of Quantitative Spectroscopy & Radiative Transfer*, **108**, 308-318.

Findell, K. L., E. Shevliakova, P. C. D. Milly, and R. J. Stouffer, 2007: Modeled impact of anthropogenic land cover change on climate. *Journal of Climate*, **20**, 3621-3634.

Fiore, A. M., et al., 2009: Multimodel estimates of intercontinental source-receptor relationships for ozone pollution. *Journal of Geophysical Research-Atmospheres*, **114**.

Fischer, E. M., J. Luterbacher, E. Zorita, S. F. B. Tett, C. Casty, and H. Wanner, 2007: European climate response to tropical volcanic eruptions over the last half millennium. *Geophysical Research Letters*, **34**.

Flanner, M. G., C. S. Zender, J. T. Randerson, and P. J. Rasch, 2007: Present-day climate forcing and response from black carbon in snow. *Journal of Geophysical Research-Atmospheres*, **112**.

Fletcher, C. G., P. J. Kushner, A. Hall, and X. Qu, 2009: Circulation responses to snow albedo feedback in climate change. *Geophysical Research Letters*, **36**.

Fomin, B. A., and V. A. Falaleeva, 2009: Recent progress in spectroscopy and its effect on line-by-line calculations for the validation of radiation codes for climate models. *Atmos. Oceanic Opt.*, **22**, 626-629.

Forster, P., and K. Shine, 1997: Radiative forcing and temperature trends from stratospheric ozone changes. *Journal of Geophysical Research-Atmospheres*, **102**, 10841-10855.

Forster, P., and K. Taylor, 2006: Climate forcings and climate sensitivities diagnosed from coupled climate model integrations. *Journal of Climate*, **19**, 6181-6194.

Forster, P., et al., 2005: Resolution of the uncertainties in the radiative forcing of HFC-134a. *Journal of Quantitative Spectroscopy & Radiative Transfer*, **93**, 447-460.

Forster, P., et al., 2007: Changes in Atmospheric Constituents and in Radiative Forcing. *Climate Change 2007: The Physical Science Basis. Contribution of Working Group I to the Fourth Assessment Report of the Intergovernmental Panel on Climate Change*, Cambridge University Press.

Forster, P., et al., 2011a: Evaluation of radiation scheme performance within chemistry climate models. *Journal of Geophysical Research-Atmospheres*, **116**, -.

Forster, P. M., T. Andrews, P. Good, J. Gregory, L. Jackson, and M. Zelinka, 2012: Evaluating adjusted forcing and model spread for historical and future scenarios in the CMIP5 generation of climate models. *J. Geophys. Res.*, **submitted**.

Forster, P. M., et al., 2011b: Stratospheric changes and climate, Chapter 4 in *Scientific Assessment of Ozone Depletion: 2010. Global Ozone Research and Monitoring Project–Report, No. 52*, 516.

Fortuin, J. P. F., and H. Kelder, 1998: An ozone climatology based on ozonesonde and satellite measurements. *Journal of Geophysical Research-Atmospheres*, **103**, 31709-31734.

Foukal, P., C. Frohlich, H. Spruit, and T. Wigley, 2006: Variations in solar luminosity and their effect on the Earth's climate. *Nature*, **443**, 161-166.

Frame, T., and L. Gray, 2010: The 11-Yr Solar Cycle in ERA-40 Data: An Update to 2008. *Journal of Climate*, **23**, 2213-2222.
Friedlingstein, P., et al., 2006: Climate-carbon cycle feedback analysis: Results from the C(4)MIP model intercomparison. *Journal of Climate*, **19**, 3337-3353.
Frohlich, C., 2006: Solar irradiance variability since 1978 - Revision of the PMOD composite during solar cycle 21. *Space Science Reviews*, **125**, 53-65.
——, 2009: Evidence of a long-term trend in total solar irradiance. *Astronomy & Astrophysics*, **501**, L27-U508.
Fry, M., et al., 2012: The influence of ozone precursor emissions from four world regions on tropospheric composition and radiative climate forcing. *Journal of Geophysical Research-Atmospheres*, **117**.
Fuglestvedt, J., T. Berntsen, O. Godal, and T. Skodvin, 2000: Climate implications of GWP-based reductions in greenhouse gas emissions. *Geophysical Research Letters*. 409-412.
Fuglestvedt, J., T. Berntsen, G. Myhre, K. Rypdal, and R. Skeie, 2008: Climate forcing from the transport sectors. *Proceedings of the National Academy of Sciences of the United States of America*. doi:DOI 10.1073/pnas.0702958104, 454-458.
Fuglestvedt, J., T. Berntsen, O. Godal, R. Sausen, K. Shine, and T. Skodvin, 2003: Metrics of climate change: Assessing radiative forcing and emission indices. *Climatic Change*. 267-331.
Fuglestvedt, J. S., et al., 2010: Transport impacts on atmosphere and climate: Metrics. *Atmospheric Environment*, **44**, 4648-4677.
Gaillard, M. J., et al., 2010: Holocene land-cover reconstructions for studies on land cover-climate feedbacks. *Clim Past*, **6**, 483-499.
Gao, C., A. Robock, and C. Ammann, 2008: Volcanic forcing of climate over the past 1500 years: An improved ice core-based index for climate models. *Journal of Geophysical Research-Atmospheres*, **113**.
Garcia, R. R., W. J. Randel, and D. E. Kinnison, 2011: On the Determination of Age of Air Trends from Atmospheric Trace Species. *J. Atmos. Sci.*, **68**, 139-154.
Georgescu, M., D. Lobell, and C. Field, 2011: Direct climate effects of perennial bioenergy crops in the United States. *Proceedings of the National Academy of Sciences of the United States of America*, **108**, 4307-4312.
Gerlach, T., 2011: Volcanic versus anthropogenic carbon dioxide. *Eos*, **92**.
Gettelman, A., J. Holton, and K. Rosenlof, 1997: Mass fluxes of O-3, CH4, N2O and CF2Cl2 in the lower stratosphere calculated from observational data. *Journal of Geophysical Research-Atmospheres*, **102**, 19149-19159.
Gillett, N., and H. Matthews, 2010: Accounting for carbon cycle feedbacks in a comparison of the global warming effects of greenhouse gases. *Environmental Research Letters*, **5**, -.
Godal, O., and J. Fuglestvedt, 2002: Testing 100-year global warming potentials: Impacts on compliance costs and abatement profile. *Climatic Change*, **52**, 93-127.
Goosse, H., et al., 2006: The origin of the European "Medieval Warm Period". *Clim Past*, **2**, 99-113.
Granier, C., et al., 2011: Evolution of anthropogenic and biomass burning emissions of air pollutants at global and regional scales during the 1980-2010 period. *Climatic Change*, **109**, 163-190.
Gray, L., S. Rumbold, and K. Shine, 2009: Stratospheric Temperature and Radiative Forcing Response to 11-Year Solar Cycle Changes in Irradiance and Ozone. *J. Atmos. Sci.*, **66**, 2402-2417.
Gray, L., et al., 2010: SOLAR INFLUENCES ON CLIMATE. *Reviews of Geophysics*, **48**, -.
Gregory, J., and M. Webb, 2008: Tropospheric adjustment induces a cloud component in CO2 forcing. *Journal of Climate*, **21**, 58-71.
Gregory, J., et al., 2004: A new method for diagnosing radiative forcing and climate sensitivity. *Geophysical Research Letters*, **31**, -.
Grewe, V., K. Dahlmann, S. Matthes, and W. Steinbrecht, 2012: Attributing ozone to NOx emissions: Implications for climate mitigation measures. *Atmospheric Environment*, **59**, 102-107.
Gusev, A. A., 2008: Temporal structure of the global sequence of volcanic eruptions: Order clustering and intermittent discharge rate. *Physics of the Earth and Planetary Interiors*, **166**, 203-218.
HAIGH, J., 1994: THE ROLE OF STRATOSPHERIC OZONE IN MODULATING THE SOLAR RADIATIVE FORCING OF CLIMATE. *Nature*, **370**, 544-546.
——, 1999: A GCM study of climate change in response to the 11-year solar cycle. *Quarterly Journal of the Royal Meteorological Society*, **125**, 871-892.
Hall, J., and G. Lockwood, 2004: The chromospheric activity and variability of cycling and flat activity solar-analog stars. *Astrophysical Journal*, **614**, 942-946.
Hallquist, M., et al., 2009: The formation, properties and impact of secondary organic aerosol: current and emerging issues. *Atmospheric Chemistry and Physics*, **9**, 5155-5236.
Hansen, J., and L. Nazarenko, 2004: Soot climate forcing via snow and ice albedos. *Proceedings of the National Academy of Sciences of the United States of America*, **101**, 423-428.
Hansen, J., et al., 2002: Climate forcings in Goddard Institute for Space Studies SI2000 simulations. *Journal of Geophysical Research-Atmospheres*, **107**.
Hansen, J., et al., 2005: Efficacy of climate forcings. *Journal of Geophysical Research-Atmospheres*, **110**.
Hansen, J., et al., 2007: Climate simulations for 1880-2003 with GISS modelE. *Climate Dynamics*, **29**, 661-696.
Harder, J., J. Fontenla, P. Pilewskie, E. Richard, and T. Woods, 2009: Trends in solar spectral irradiance variability in the visible and infrared. *Geophysical Research Letters*, **36**, -.

Harrison, R. G., and M. H. P. Ambaum, 2010: Observing Forbush decreases in cloud at Shetland. *J. Atm. Solar-Terr. Phys.*, **72**, 1408-1414.
Hauglustaine, D. A., J. Lathiere, S. Szopa, and G. A. Folberth, 2005: Future tropospheric ozone simulated with a climate-chemistry-biosphere model. *Geophysical Research Letters*, **32**.
Haywood, J., and M. Schulz, 2007: Causes of the reduction in uncertainty in the anthropogenic radiative forcing of climate between IPCC (2001) and IPCC (2007). *Geophysical Research Letters*, **34**.
Haywood, J. M., et al., 2010: Observations of the eruption of the Sarychev volcano and simulations using the HadGEM2 climate model. *Journal of Geophysical Research-Atmospheres*, **115**.
Hegg, D. A., S. G. Warren, T. C. Grenfell, S. J. Doherty, T. V. Larson, and A. D. Clarke, 2009: Source Attribution of Black Carbon in Arctic Snow. *Environmental Science & Technology*, **43**, 4016-4021.
Hegglin, M. I., and T. G. Shepherd, 2009: Large climate-induced changes in ultraviolet index and stratosphere-to-troposphere ozone flux. *Nature Geoscience*, **2**, 687-691.
Henze, D. K., et al., 2012: Spatially refined aersol direct radiative forcing efficiencies. *Environ. Sci. Tech.*, **(submitted)**.
Hodnebrog, Ø., M. Etminan, J. Fuglestvedt, G. Marston, G. Myhre, K. P. Shine, and T. J. Wallington, 2012: Global Warming Potentials and Radiative Efficiencies of Halocarbons and Related Compounds: A Comprehensive Review. *Reviews of Geophysics*. (submitted).
Hofmann, D., J. Barnes, M. O'Neill, M. Trudeau, and R. Neely, 2009: Increase in background stratospheric aerosol observed with lidar at Mauna Loa Observatory and Boulder, Colorado. *Geophysical Research Letters*, **36**.
Holmes, C., Q. Tang, and M. Prather, 2011: Uncertainties in climate assessment for the case of aviation NO. *Proceedings of the National Academy of Sciences of the United States of America*, **108**, 10997-11002.
Horowitz, L. W., 2006: Past, present, and future concentrations of tropospheric ozone and aerosols: Methodology, ozone evaluation, and sensitivity to aerosol wet removal. *Journal of Geophysical Research-Atmospheres*, **111**.
Houghton, J. T., G. J. Jenkins, and J. J. Ephraums, 1990: *Climate Change. The IPCC Scientific Assessment*, 364 pp pp.
Hoyle, C., et al., 2011: A review of the anthropogenic influence on biogenic secondary organic aerosol. *Atmospheric Chemistry and Physics*, **11**, 321-343.
Hsu, J., and M. J. Prather, 2009: Stratospheric variability and tropospheric ozone. *Journal of Geophysical Research-Atmospheres*, **114**.
Huang, J., Q. Fu, W. Zhang, X. Wang, R. Zhang, H. Ye, and S. Warren, 2011: DUST AND BLACK CARBON IN SEASONAL SNOW ACROSS NORTHERN CHINA. *Bulletin of the American Meteorological Society*, **92**, 175-+.
Huijnen, V., et al., 2010: The global chemistry transport model TM5: description and evaluation of the tropospheric chemistry version 3.0. *Geoscientific Model Development*, **3**, 445-473.
Hurtt, G., et al., 2011: Harmonization of land-use scenarios for the period 1500-2100: 600 years of global gridded annual land-use transitions, wood harvest, and resulting secondary lands. *Climatic Change*, **109**, 117-161.
Hurtt, G. C., et al., 2006: The underpinnings of land-use history: three centuries of global gridded land-use transitions, wood-harvest activity, and resulting secondary lands. *Global Change Biol*, **12**, 1208-1229.
Iacono, M. J., J. S. Delamere, E. J. Mlawer, M. W. Shephard, S. A. Clough, and W. D. Collins, 2008: Radiative forcing by long-lived greenhouse gases: Calculations with the AER radiative transfer models. *Journal of Geophysical Research-Atmospheres*, **113**.
Ineson, S., A. A. Scaife, J. R. Knight, J. C. Manners, N. J. Dunstone, L. J. Gray, and J. D. Haigh, 2011: Solar forcing of winter climate variability in the Northern Hemisphere. *Nature Geoscience*, **4**, 753-757.
IPCC, 1996: Revised 1996 IPCC Guidelines for National Greenhouse Gas Inventories.
Isaksen, I., et al., 2009: Atmospheric composition change: Climate-Chemistry interactions. *Atmospheric Environment*. doi:DOI 10.1016/j.atmosenv.2009.08.003, 5138-5192.
Ito, A., and J. E. Penner, 2005: Historical emissions of carbonaceous aerosols from biomass and fossil fuel burning for the period 1870-2000. *Glob. Biogeochem. Cycle*, **19**.
Jackson, S., 2009: Parallel Pursuit of Near-Term and Long-Term Climate Mitigation. *Science*, **326**, 526-527.
Jacobson, M., 2010: Short-term effects of controlling fossil-fuel soot, biofuel soot and gases, and methane on climate, Arctic ice, and air pollution health. *Journal of Geophysical Research-Atmospheres*, **115**, -.
——, 2012: Investigating cloud absorption effects: Global absorption properties of black carbon, tar balls, and soil dust in clouds and aerosols. *Journal of Geophysical Research-Atmospheres*, **117**.
Jin, M. L., R. E. Dickinson, and D. L. Zhang, 2005: The footprint of urban areas on global climate as characterized by MODIS. *Journal of Climate*, **18**, 1551-1565.
Jin, Y., and D. P. Roy, 2005: Fire-induced albedo change and its radiative forcing at the surface in northern Australia. *Geophysical Research Letters*, **32**, -.
Johansson, D., 2012: Economics- and physical-based metrics for comparing greenhouse gases. *Climatic Change*, **110**, 123-141.
Johansson, D., U. Persson, and C. Azar, 2006: The cost of using global warming potentials: Analysing the trade off between CO2, CH4 and N2O. *Climatic Change*. doi:DOI 10.1007/s10584-006-9054-1, 291-309.
Jones, G., M. Lockwood, and P. Stott, 2012: What influence will future solar activity changes over the 21st century have on projected global near-surface temperature changes? *Journal of Geophysical Research-Atmospheres*, **117**.
Jones, G. S., J. M. Gregory, P. A. Stott, S. F. B. Tett, and R. B. Thorpe, 2005: An AOGCM simulation of the climate response to a volcanic super-eruption. *Climate Dynamics*, **25**, 725-738.

Joos, F., M. Bruno, R. Fink, U. Siegenthaler, T. Stocker, and C. LeQuere, 1996: An efficient and accurate representation of complex oceanic and biospheric models of anthropogenic carbon uptake. *Tellus Series B-Chemical and Physical Meteorology*, **48**, 397-417.

Joos, F., et al., 2001: Global warming feedbacks on terrestrial carbon uptake under the Intergovernmental Panel on Climate Change (IPCC) emission scenarios. *Glob. Biogeochem. Cycle*, **15**, 891-907.

Joos, F., et al., 2012: Carbon dioxide and climate impulse response functions for the computation of greenhouse gas metrics: A multi-model analysis.

Joshi, M. M., and G. S. Jones, 2009: The climatic effects of the direct injection of water vapour into the stratosphere by large volcanic eruptions. *Atmospheric Chemistry and Physics*, **9**, 6109-6118.

KANDLIKAR, M., 1995: THE RELATIVE ROLE OF TRACE GAS EMISSIONS IN GREENHOUSE ABATEMENT POLICIES. *Energy Policy*. 879-883.

Kaplan, J. O., K. M. Krumhardt, E. C. Ellis, W. F. Ruddiman, C. Lemmen, and K. K. Goldewijk, 2011: Holocene carbon emissions as a result of anthropogenic land cover change. *Holocene*, **21**, 775-791.

Kasischke, E. S., and J. E. Penner, 2004: Improving global estimates of atmospheric emissions from biomass burning. *Journal of Geophysical Research-Atmospheres*, **109**.

Kawase, H., T. Nagashima, K. Sudo, and T. Nozawa, 2011: Future changes in tropospheric ozone under Representative Concentration Pathways (RCPs). *Geophysical Research Letters*, **38**.

Kawase, H., M. Abe, Y. Yamada, T. Takemura, T. Yokohata, and T. Nozawa, 2010: Physical mechanism of long-term drying trend over tropical North Africa. *Geophysical Research Letters*, **37**.

Kazil, J., K. Zhang, P. Stier, J. Feichter, U. Lohmann, and K. O´Brien, 2012: The present-day decadal solar cycle modulation of Earth's radiative forcing via charged H2SO4/H2O aerosol nucleation. *Geophys. Res. Lett.*, **39**, L02805.

Kirkby, J., et al., 2011: Role of sulphuric acid, ammonia and galactic cosmic rays in atmospheric aerosol nucleation. *Nature*, **476**, 429-435.

Kleinman, L. I., P. H. Daum, Y. N. Lee, L. J. Nunnermacker, S. R. Springston, J. Weinstein-Lloyd, and J. Rudolph, 2001: Sensitivity of ozone production rate to ozone precursors. *Geophysical Research Letters*, **28**, 2903-2906.

Knutti, R., et al., 2008: A review of uncertainties in global temperature projections over the twenty-first century. *Journal of Climate*, **21**, 2651-2663.

Koch, D., and A. D. Del Genio, 2010: Black carbon semi-direct effects on cloud cover: review and synthesis. *Atmospheric Chemistry and Physics*, **10**, 7685-7696.

Koch, D., T. Bond, D. Streets, N. Unger, and G. van der Werf, 2007: Global impacts of aerosols from particular source regions and sectors. *Journal of Geophysical Research-Atmospheres*, **112**, -.

Koch, D., S. Menon, A. Del Genio, R. Ruedy, I. Alienov, and G. A. Schmidt, 2009a: Distinguishing Aerosol Impacts on Climate over the Past Century. *Journal of Climate*, **22**, 2659-2677.

Koch, D., et al., 2011: Coupled Aerosol-Chemistry-Climate Twentieth-Century Transient Model Investigation: Trends in Short-Lived Species and Climate Responses. *Journal of Climate*, **24**, 2693-2714.

Koch, D., et al., 2009b: Evaluation of black carbon estimations in global aerosol models. *Atmospheric Chemistry and Physics*, **9**, 9001-9026.

Koffi, B., et al., 2012: Application of the CALIOP layer product to evaluate the vertical distribution of aerosols estimated by global models: AeroCom phase I results. *Journal of Geophysical Research-Atmospheres*, **117**.

Köhler, M. O., G. Rädel, K. P. Shine, R. H. L., and P. J. A., 2012: The latitudinal variation of the effect of aviation NOx emissions on atmospheric ozone and methane and related climate metrics. *Atmos. Environ.*, **Submitted**.

Kopp, G., and J. Lean, 2011: A new, lower value of total solar irradiance: Evidence and climate significance. *Geophysical Research Letters*, **38**, -.

Kratz, D., 2008: The sensitivity of radiative transfer calculations to the changes in the HITRAN database from 1982 to 2004. *Journal of Quantitative Spectroscopy & Radiative Transfer*, **109**, 1060-1080.

Kravitz, B., and A. Robock, 2011: Climate effects of high-latitude volcanic eruptions: Role of the time of year. *Journal of Geophysical Research-Atmospheres*, **116**, -.

Kravitz, B., A. Robock, and A. Bourassa, 2010: Negligible climatic effects from the 2008 Okmok and Kasatochi volcanic eruptions. *Journal of Geophysical Research-Atmospheres*, **115**.

Kravitz, B., et al., 2011: Simulation and observations of stratospheric aerosols from the 2009 Sarychev volcanic eruption. *Journal of Geophysical Research-Atmospheres*, **116**, -.

Kristjansson, J. E., T. Iversen, A. Kirkevag, O. Seland, and J. Debernard, 2005: Response of the climate system to aerosol direct and indirect forcing: Role of cloud feedbacks. *Journal of Geophysical Research-Atmospheres*, **110**.

Krivova, N., L. Vieira, and S. Solanki, 2010: Reconstruction of solar spectral irradiance since the Maunder minimum. *Journal of Geophysical Research-Space Physics*, **115**, -.

Kueppers, L. M., M. A. Snyder, and L. C. Sloan, 2007: Irrigation cooling effect: Regional climate forcing by land-use change. *Geophysical Research Letters*, **34**, -.

Kuroda, Y., and K. Kodera, 2005: Solar cycle modulation of the southern annular mode. *Geophysical Research Letters*, **32**.

Kvalevag, M. M., G. Myhre, G. Bonan, and S. Levis, 2010: Anthropogenic land cover changes in a GCM with surface albedo changes based on MODIS data. *Int J Climatol*, **30**, 2105-2117.

Lacis, A. A., and J. E. Hansen, 1974: PARAMETERIZATION FOR ABSORPTION OF SOLAR-RADIATION IN EARTHS ATMOSPHERE. *J. Atmos. Sci.*, **31**, 118-133.
Lamarque, J.-F., et al., 2012: The Atmospheric Chemistry and Climate Model Intercomparison Project (ACCMIP): Overview and description of models, simulations and climate diagnostics. *ACP/GMD Inter-Journal SI*, **Submitted**.
Lamarque, J., et al., 2011: Global and regional evolution of short-lived radiatively-active gases and aerosols in the Representative Concentration Pathways. *Climatic Change*, **109**, 191-212.
Lamarque, J., et al., 2010: Historical (1850-2000) gridded anthropogenic and biomass burning emissions of reactive gases and aerosols: methodology and application. *Atmospheric Chemistry and Physics*. doi:DOI 10.5194/acp-10-7017-2010, 7017-7039.
Lau, K. M., M. K. Kim, and K. M. Kim, 2006: Asian summer monsoon anomalies induced by aerosol direct forcing: the role of the Tibetan Plateau. *Climate Dynamics*, **26**, 855-864.
Lauer, A., V. Eyring, J. Hendricks, P. Jockel, and U. Lohmann, 2007: Global model simulations of the impact of ocean-going ships on aerosols, clouds, and the radiation budget. *Atmospheric Chemistry and Physics*, **7**, 5061-5079.
Lawrence, P. J., and T. N. Chase, 2010: Investigating the climate impacts of global land cover change in the community climate system model. *Int J Climatol*, **30**, 2066-2087.
Lean, J., and M. DeLand, 2012: How Does the Sun's Spectrum Vary?. *J. Climate*, **25**, 2555-2560.
Lean, J. L., 2000: Evolution of the Sun´s spectral irradiance since the Maunder Minimum. *Geophysical Research Letters*, **27**, 2425-2428.
Lee, D., et al., 2009: Aviation and global climate change in the 21st century. *Atmospheric Environment*. doi:DOI 10.1016/j.atmosenv.2009.04.024, 3520-3537.
Lee, D. S., et al., 2010: Transport impacts on atmosphere and climate: Aviation. *Atmospheric Environment*, **44**, 4678-4734.
Lee, X., et al., 2011: Observed increase in local cooling effect of deforestation at higher latitudes. *Nature*, **479**, 384-387.
Lee, Y., et al., 2012: Evaluation of preindustrial to present-day black carbon aerosols and its albedo forcing from ACCMIP (Atmospheric Chemistry and Climate Model Intercomparison Project). *ACP/GMD Inter-Journal SI*, **Submitted**.
Legras, B., O. Mestre, E. Bard, and P. Yiou, 2010: A critical look at solar-climate relationships from long temperature series. *Clim Past*, **6**, 745-758.
Leibensperger, E. M., L. J. Mickley, and D. J. Jacob, 2008: Sensitivity of US air quality to mid-latitude cyclone frequency and implications of 1980-2006 climate change. *Atmospheric Chemistry and Physics*, **8**, 7075-7086.
Leibensperger, E. M., et al., 2012: Climatic effects of 1950-2050 changes in US anthropogenic aerosols - Part 2: Climate response. *Atmospheric Chemistry and Physics*, **12**, 3349-3362.
Lelieveld, J., et al., 2008: Atmospheric oxidation capacity sustained by a tropical forest. *Nature*, **452**, 737-740.
Levy, H., M. Schwarzkopf, L. Horowitz, V. Ramaswamy, and K. Findell, 2008: Strong sensitivity of late 21st century climate to projected changes in short-lived air pollutants. *Journal of Geophysical Research-Atmospheres*, **113**.
LI, D., K. SHINE, and L. GRAY, 1995: THE ROLE OF OZONE-INDUCED DIABATIC HEATING ANOMALIES IN THE QUASI-BIENNIAL OSCILLATION. *Quarterly Journal of the Royal Meteorological Society*, **121**, 937-943.
Liao, H., W. T. Chen, and J. H. Seinfeld, 2006: Role of climate change in global predictions of future tropospheric ozone and aerosols. *Journal of Geophysical Research-Atmospheres*, **111**.
Loarie, S., D. Lobell, G. Asner, Q. Mu, and C. Field, 2011: Direct impacts on local climate of sugar-cane expansion in Brazil. *Nature Climate Change*, **1**, 105-109.
Lockwood, M., 2010: Solar change and climate: an update in the light of the current exceptional solar minimum. *Proceedings of the Royal Society a-Mathematical Physical and Engineering Sciences*, **466**, 303-329.
Lockwood, M., and C. Frohlich, 2008: Recent oppositely directed trends in solar climate forcings and the global mean surface air temperature. II. Different reconstructions of the total solar irradiance variation and dependence on response time scale. *Proceedings of the Royal Society a-Mathematical Physical and Engineering Sciences*, **464**, 1367-1385.
Lockwood, M., A. Rouillard, and I. Finch, 2009: THE RISE AND FALL OF OPEN SOLAR FLUX DURING THE CURRENT GRAND SOLAR MAXIMUM. *Astrophysical Journal*, **700**, 937-944.
Logan, J. A., 1999: An analysis of ozonesonde data for the troposphere: Recommendations for testing 3-D models and development of a gridded climatology for tropospheric ozone. *Journal of Geophysical Research-Atmospheres*, **104**, 16115-16149.
Logan, J. A., et al., 2012: Changes in ozone over Europe: Analysis of ozone measurements from sondes, regular aircraft (MOZAIC) and alpine surface sites. *Journal of Geophysical Research-Atmospheres*, **117**, 23.
Lohila, A., et al., 2010: Forestation of boreal peatlands: Impacts of changing albedo and greenhouse gas fluxes on radiative forcing. *J Geophys Res-Biogeo*, **115**, -.
Lohmann, U., et al., 2010: Total aerosol effect: radiative forcing or radiative flux perturbation? *Atmospheric Chemistry and Physics*, **10**, 3235-3246.
Long, D. J., and M. Collins, 2012: Deviations from linearity in quantifying global climate response, feedbacks and forcings. *Clim. Dyn.*, **submitted**.

Lu, Z., Q. Zhang, and D. G. Streets, 2011: Sulfur dioxide and primary carbonaceous aerosol emissions in China and India, 1996-2010. *Atmospheric Chemistry and Physics*, **11**, 9839-9864.
Lund, M., T. Berntsen, J. Fuglestvedt, M. Ponater, and K. Shine, 2012: How much information is lost by using global-mean climate metrics? an example using the transport sector. *Climatic Change*, **113**, 949-963.
MacMynowski, D., H. Shin, and K. Caldeira, 2011: The frequency response of temperature and precipitation in a climate model. *Geophysical Research Letters*, **38**, -.
Mader, J. A., J. Staehelin, T. Peter, D. Brunner, H. E. Rieder, and W. A. Stahel, 2010: Evidence for the effectiveness of the Montreal Protocol to protect the ozone layer. *Atmospheric Chemistry and Physics*, **10**, 12161-12171.
Mahowald, N. M., et al., 2010: Observed 20th century desert dust variability: impact on climate and biogeochemistry. *Atmospheric Chemistry and Physics*, **10**, 10875-10893.
Mann, M., M. Cane, S. Zebiak, and A. Clement, 2005: Volcanic and solar forcing of the tropical Pacific over the past 1000 years. *Journal of Climate*, **18**, 447-456.
Manne, A., and R. Richels, 2001: An alternative approach to establishing trade-offs among greenhouse gases. *Nature*. 675-677.
Manning, M., and A. Reisinger, 2011: Broader perspectives for comparing different greenhouse gases. *Philosophical Transactions of the Royal Society a-Mathematical Physical and Engineering Sciences*, **369**, 1891-1905.
Marenco, A., H. Gouget, P. Nedelec, J. P. Pages, and F. Karcher, 1994: EVIDENCE OF A LONG-TERM INCREASE IN TROPOSPHERIC OZONE FROM PIC DU MIDI DATA SERIES - CONSEQUENCES - POSITIVE RADIATIVE FORCING. *Journal of Geophysical Research-Atmospheres*, **99**, 16617-16632.
McComas, D., R. Ebert, H. Elliott, B. Goldstein, J. Gosling, N. Schwadron, and R. Skoug, 2008: Weaker solar wind from the polar coronal holes and the whole Sun. *Geophysical Research Letters*, **35**, -.
McLandress, C., T. G. Shepherd, J. F. Scinocca, D. A. Plummer, M. Sigmond, A. I. Jonsson, and M. C. Reader, 2011: Separating the Dynamical Effects of Climate Change and Ozone Depletion. Part II Southern Hemisphere Troposphere. *Journal of Climate*, **24**, 1850-1868.
Meinshausen, M., T. Wigley, and S. Raper, 2011a: Emulating atmosphere-ocean and carbon cycle models with a simpler model, MAGICC6-Part 2: Applications. *Atmospheric Chemistry and Physics*, **11**, 1457-1471.
Meinshausen, M., et al., 2011b: The RCP greenhouse gas concentrations and their extensions from 1765 to 2300. *Climatic Change*, **109**, 213-241.
Mercado, L. M., N. Bellouin, S. Sitch, O. Boucher, C. Huntingford, M. Wild, and P. M. Cox, 2009: Impact of changes in diffuse radiation on the global land carbon sink. *Nature*, **458**, 1014-U1087.
Merikanto, J., D. V. Spracklen, G. W. Mann, S. J. Pickering, and K. S. Carslaw, 2009: Impact of nucleation on global CCN. *Atm. Chem. Phys.*, **9**, 8601-8616.
Meure, C., et al., 2006: Law Dome CO2, CH4 and N2O ice core records extended to 2000 years BP. *Geophysical Research Letters*. doi:ARTN L14810, 10.1029/2006GL026152, -.
Miller, G. H., et al., 2012: Abrupt onset of the Little Ice Age triggered by volcanism and sustained by sea-ice/ocean feedbacks. *Geophysical Research Letters*, **39**.
Miller, R. L., I. Tegen, and J. Perlwitz, 2004: Surface radiative forcing by soil dust aerosols and the hydrologic cycle. *Journal of Geophysical Research-Atmospheres*, **109**.
Mills, M. J., O. B. Toon, R. P. Turco, D. E. Kinnison, and R. R. Garcia, 2008: Massive global ozone loss predicted following regional nuclear conflict. *Proceedings of the National Academy of Sciences of the United States of America*, **105**, 5307-5312.
Ming, Y., V. Ramaswamy, and G. Persad, 2010: Two opposing effects of absorbing aerosols on global-mean precipitation. *Geophysical Research Letters*, **37**, -.
Ming, Y., V. Ramaswamy, and G. Chen, 2011: A Model Investigation of Aerosol-Induced Changes in Boreal Winter Extratropical Circulation. *Journal of Climate*, **24**, 6077-6091.
Ming, Y., V. Ramaswamy, L. J. Donner, V. T. J. Phillips, S. A. Klein, P. A. Ginoux, and L. W. Horowitz, 2007: Modeling the interactions between aerosols and liquid water clouds with a self-consistent cloud scheme in a general circulation model. *J. Atmos. Sci.*, **64**, 1189-1209.
Mirme, S., A. Mirme, A. Minikin, A. Petzold, U. Horrak, V.-M. Kerminen, and M. Kulmala, 2010: Atmospheric sub-3 nm particles at high altitudes. *Atm. Chem. Phys.*, **10**, 437-451.
Montzka, S. A., E. J. Dlugokencky, and J. H. Butler, 2011a: Non-CO(2) greenhouse gases and climate change. *Nature*, **476**, 43-50.
Montzka, S. A., M. Krol, E. Dlugokencky, B. Hall, P. Jockel, and J. Lelieveld, 2011b: Small Interannual Variability of Global Atmospheric Hydroxyl. *Science*, **331**, 67-69.
Muhle, J., et al., 2009: Sulfuryl fluoride in the global atmosphere (vol 114, D05306, 2009). *Journal of Geophysical Research-Atmospheres*. doi:ARTN D10303, 10.1029/2009JD012306, -.
Mulitza, S., et al., 2010: Increase in African dust flux at the onset of commercial agriculture in the Sahel region. *Nature*, **466**, 226-228.
Murphy, D., and D. Fahey, 1994: An estimate of the flux of stratospheric reactive nitrogen and ozone into the troposphere. *Journal of Geophysical Research-Atmospheres*, **99**, 5325-5332.
Myhre, G., M. M. Kvalevag, and C. B. Schaaf, 2005a: Radiative forcing due to anthropogenic vegetation change based on MODIS surface albedo data. *Geophysical Research Letters*, **32**, -.

Myhre, G., Y. Govaerts, J. M. Haywood, T. K. Berntsen, and A. Lattanzio, 2005b: Radiative effect of surface albedo change from biomass burning. *Geophysical Research Letters*, **32**, -.
Myhre, G., J. Nilsen, L. Gulstad, K. Shine, B. Rognerud, and I. Isaksen, 2007: Radiative forcing due to stratospheric water vapour from CH4 oxidation. *Geophysical Research Letters*. doi:ARTN L01807, 10.1029/2006GL027472, -.
Myhre, G., et al., 2011: Radiative forcing due to changes in ozone and methane caused by the transport sector. *Atmospheric Environment*, **45**, 387-394.
Nagai, T., B. Liley, T. Sakai, T. Shibata, and O. Uchino, 2010: Post-Pinatubo Evolution and Subsequent Trend of the Stratospheric Aerosol Layer Observed by Mid-Latitude Lidars in Both Hemispheres. *Sola*, **6**, 69-72.
Naik, V., D. L. Mauzerall, L. W. Horowitz, M. D. Schwarzkopf, V. Ramaswamy, and M. Oppenheimer, 2007: On the sensitivity of radiative forcing from biomass burning aerosols and ozone to emission location. *Geophysical Research Letters*, **34**.
Nair, U. S., D. K. Ray, J. Wang, S. A. Christopher, T. J. Lyons, R. M. Welch, and R. A. Pielke, 2007: Observational estimates of radiative forcing due to land use change in southwest Australia. *Journal of Geophysical Research-Atmospheres*, **112**, -.
O'ishi, R., A. Abe-Ouchi, I. Prentice, and S. Sitch, 2009: Vegetation dynamics and plant CO2 responses as positive feedbacks in a greenhouse world. *Geophysical Research Letters*, **36**.
O'Neill, B., 2000: The jury is still out on global warming potentials. *Climatic Change*. 427-443.
——, 2003: Economics, natural science, and the costs of global warming potentials - An editorial comment. *Climatic Change*. 251-260.
Ødemark, K., S. Dalsøren, B. Samset, T. Berntsen, J. Fuglestvedt, and G. Myhre, 2011: Short lived climate forcers from current shipping and petroleum activities in the Artic.
Oleson, K. W., G. B. Bonan, and J. Feddema, 2010: Effects of white roofs on urban temperature in a global climate model. *Geophysical Research Letters*, **37**.
Olivié, D., and G. Peters, 2012: Impact of model variation in CO2 and temperature impulse response functions on emission metrics. *Earth Syst. Dynam. Discuss*. (submitted).
Olivié, D. J. L., G. Peters, and D. Saint-Martin, 2012: Calibration of a linear response Simple Climate Model. *J. Climate*, doi: http://dx.doi.org/10.1175/JCLI-D-11-00475.1.
Oreopoulos, L., et al., 2012: The Continual Intercomparison of Radiation Codes: Results from Phase I. *Journal of Geophysical Research-Atmospheres*, **117**.
Osterman, G. B., et al., 2008: Validation of Tropospheric Emission Spectrometer (TES) measurements of the total, stratospheric, and tropospheric column abundance of ozone. *Journal of Geophysical Research-Atmospheres*, **113**.
Ottera, O. H., M. Bentsen, H. Drange, and L. L. Suo, 2010: External forcing as a metronome for Atlantic multidecadal variability. *Nature Geoscience*, **3**, 688-694.
Parrella, J. P., et al., 2012: Tropospheric bromine chemistry: implications for present and pre-industrial ozone and mercury. *Atmos. Chem. Phys.*, **12**, 6723-6740.
Parrish, D. D., D. B. Millet, and A. H. Goldstein, 2009: Increasing ozone in marine boundary layer inflow at the west coasts of North America and Europe. *Atmospheric Chemistry and Physics*, **9**, 1303-1323.
Pechony, O., and D. Shindell, 2010: Driving forces of global wildfires over the past millennium and the forthcoming century. *Proceedings of the National Academy of Sciences of the United States of America*, **107**, 19167-19170.
Penner, J., L. Xu, and M. Wang, 2011: Satellite methods underestimate indirect climate forcing by aerosols. *Proceedings of the National Academy of Sciences of the United States of America*, **108**, 13404-13408.
Penner, J., et al., 2006: Model intercomparison of indirect aerosol effects. *Atmospheric Chemistry and Physics*, **6**, 3391-3405.
Perlwitz, J., and R. L. Miller, 2010: Cloud cover increase with increasing aerosol absorptivity: A counterexample to the conventional semidirect aerosol effect. *Journal of Geophysical Research-Atmospheres*, **115**.
Persad, G. G., Y. Ming, and V. Ramaswamy, 2012: Tropical Tropospheric-Only Responses to Absorbing Aerosols. *Journal of Climate*, **25**, 2471-2480.
Peters, G., B. Aamaas, T. Berntsen, and J. Fuglestvedt, 2011a: The integrated global temperature change potential (iGTP) and relationships between emission metrics. *Environmental Research Letters*, **6**.
Peters, G., A. Reisinger, J. Fuglestvedt, and M. Meinshausen, 2012: Dependence of Global Warming Potentials on constant and variable background concentrations. *Environmental Research Letters*. (submitted).
Peters, G., B. Aamaas, M. Lund, C. Solli, and J. Fuglestvedt, 2011b: Alternative "Global Warming" Metrics in Life Cycle Assessment: A Case Study with Existing Transportation Data. *Environmental Science & Technology*, **45**, 8633-8641.
Pierce, J. R., and P. J. Adams, 2009: Can cosmic rays affect cloud condensation nuclei by altering new particle formation rates? *Geophys. Res. Lett.*, **36**, L09820.
Pinto, J. P., R. P. Turco, and O. B. Toon, 1989: Self-limiting physical and chemical effects in volcanic-eruption clouds. *Journal of Geophysical Research-Atmospheres*, **94**, 11165-11174.
Pitman, A. J., et al., 2009: Uncertainties in climate responses to past land cover change: First results from the LUCID intercomparison study. *Geophysical Research Letters*, **36**, -.
Plattner, G.-K., T. Stocker, P. Midgley, and M. Tignor, 2009: IPCC Expert Meeting on the Science of Alternative Metrics: Meeting Report. IPCC Working Group I, Technical Support Unit.

Plattner, G. K., et al., 2008: Long-term climate commitments projected with climate-carbon cycle models. *Journal of Climate*, **21**, 2721-2751.
Pongratz, J., C. Reick, T. Raddatz, and M. Claussen, 2008: A reconstruction of global agricultural areas and land cover for the last millennium. *Glob. Biogeochem. Cycle*, **22**, -.
Pongratz, J., C. H. Reick, T. Raddatz, and M. Claussen, 2010: Biogeophysical versus biogeochemical climate response to historical anthropogenic land cover change. *Geophysical Research Letters*, **37**, -.
Pongratz, J., T. Raddatz, C. H. Reick, M. Esch, and M. Claussen, 2009: Radiative forcing from anthropogenic land cover change since AD 800. *Geophysical Research Letters*, **36**, -.
Pozzer, A., et al., 2012: Effects of business-as-usual anthropogenic emissions on air quality. *Atmos. Chem. Phys.*, **12**, 6915-6937.
Prather, M., and J. Hsu, 2010: Coupling of Nitrous Oxide and Methane by Global Atmospheric Chemistry. *Science*, **330**, 952-954.
Prather, M. J., C. D. Holmes, and J. Hsu, 2012: Reactive greenhouse gas scenarios: Systematic exploration of uncertainties and the role of atmospheric chemistry. *Geophysical Research Letters*, **39**.
Puma, M. J., and B. I. Cook, 2010: Effects of irrigation on global climate during the 20th century. *Journal of Geophysical Research-Atmospheres*, **115**, -.
Quaas, J., O. Boucher, N. Bellouin, and S. Kinne, 2011: Which of satellite- or model-based estimates is closer to reality for aerosol indirect forcing? *Proceedings of the National Academy of Sciences of the United States of America*, **108**, E1099-E1099.
Quaas, J., et al., 2009: Aerosol indirect effects - general circulation model intercomparison and evaluation with satellite data. *Atmospheric Chemistry and Physics*, **9**, 8697-8717.
Ramanathan, V., and G. Carmichael, 2008: Global and regional climate changes due to black carbon. *Nature Geoscience*, **1**, 221-227.
Ramanathan, V., et al., 2005: Atmospheric brown clouds: Impacts on South Asian climate and hydrological cycle. *Proceedings of the National Academy of Sciences of the United States of America*, **102**, 5326-5333.
Ramaswamy, V., et al., 2001: Radiative Forcing of Climate Change. *Climate Change 2001: The Scientific Basis. Contribution of Working Group I to the Third Assessment Report of the Intergovernmental Panel on Climate Change*, Cambridge University Press.
Randel, W., and F. Wu, 2007: A stratospheric ozone profile data set for 1979-2005: Variability, trends, and comparisons with column ozone data. *Journal of Geophysical Research-Atmospheres*. doi:ARTN D06313, 10.1029/2006JD007339, -.
Randles, C. A., and V. Ramaswamy, 2008: Absorbing aerosols over Asia: A Geophysical Fluid Dynamics Laboratory general circulation model sensitivity study of model response to aerosol optical depth and aerosol absorption. *Journal of Geophysical Research-Atmospheres*, **113**.
Rasch, P. J., et al., 2008: An overview of geoengineering of climate using stratospheric sulphate aerosols. *Philosophical Transactions of the Royal Society a-Mathematical Physical and Engineering Sciences*, **366**, 4007-4037.
Ravishankara, A. R., J. S. Daniel, and R. W. Portmann, 2009: Nitrous Oxide (N(2)O): The Dominant Ozone-Depleting Substance Emitted in the 21st Century. *Science*, **326**, 123-125.
Rechid, D., T. Raddatz, and D. Jacob, 2009: Parameterization of snow-free land surface albedo as a function of vegetation phenology based on MODIS data and applied in climate modelling. *Theor Appl Climatol*, **95**, 245-255.
Reddy, M., and O. Boucher, 2007: Climate impact of black carbon emitted from energy consumption in the world's regions. *Geophysical Research Letters*. doi:ARTN L11802, 10.1029/2006GL028904, -.
REILLY, J., 1992: CLIMATE-CHANGE DAMAGE AND THE TRACE-GAS-INDEX ISSUE. *Economic Issues in Global Climate Change*. 72-88.
Reisinger, A., M. Meinshausen, and M. Manning, 2011: Future changes in global warming potentials under representative concentration pathways. *Environmental Research Letters*, **6**, -.
Reisinger, A., M. Meinshausen, M. Manning, and G. Bodeker, 2010: Uncertainties of global warming metrics: CO2 and CH4. *Geophysical Research Letters*, **37**, -.
Reisinger, A., P. Havlik, K. Riahi, O. van Vliet, M. Obersteiner, and M. Herrerro, 2012: Implications of alternative metrics for global mitigation costs and greenhouse gas emissions from agriculture. *Climatic Change, submitted*.
Rigozo, N., E. Echer, L. Vieira, and D. Nordemann, 2001: Reconstruction of Wolf sunspot numbers on the basis of spectral characteristics and estimates of associated radio flux and solar wind parameters for the last millennium. *Solar Physics*, **203**, 179-191.
Rigozo, N., D. Nordemann, E. Echer, M. Echer, and H. Silva, 2010: Prediction of solar minimum and maximum epochs on the basis of spectral characteristics for the next millennium. *Planetary and Space Science*, **58**, 1971-1976.
Robock, A., 2000: Volcanic eruptions and climate. *Reviews of Geophysics*, **38**, 191-219.
Robock, A., 2010: New START, Eyjafjallajökull, and Nuclear Winter. *Eos*, **91**, 444-445.
Robock, A., L. Oman, and G. L. Stenchikov, 2007a: Nuclear winter revisited with a modern climate model and current nuclear arsenals: Still catastrophic consequences. *Journal of Geophysical Research-Atmospheres*, **112**.
Robock, A., L. Oman, and G. L. Stenchikov, 2008: Regional climate responses to geoengineering with tropical and Arctic SO_2 injections. *Journal of Geophysical Research-Atmospheres*, **113**.
Robock, A., L. Oman, G. L. Stenchikov, O. B. Toon, C. Bardeen, and R. P. Turco, 2007b: Climatic consequences of regional nuclear conflicts. *Atmospheric Chemistry and Physics*, **7**, 2003-2012.

Robock, A., C. M. Ammann, L. Oman, D. Shindell, S. Levis, and G. Stenchikov, 2009: Did the Toba volcanic eruption of similar to 74 ka BP produce widespread glaciation? *Journal of Geophysical Research-Atmospheres*, **114**.
Roscoe, H. K., and J. D. Haigh, 2007: Influences of ozone depletion, the solar cycle and the QBO on the Southern Annular Mode. *Quarterly Journal of the Royal Meteorological Society*, **133**, 1855-1864.
Rotenberg, E., and D. Yakir, 2010: Contribution of Semi-Arid Forests to the Climate System. *Science*, **327**, 451-454.
Rothman, L., 2010: The evolution and impact of the HITRAN molecular spectroscopic database. *Journal of Quantitative Spectroscopy & Radiative Transfer*, **111**, 1565-1567.
Rothman, L., et al., 2009: The HITRAN 2008 molecular spectroscopic database. *Journal of Quantitative Spectroscopy & Radiative Transfer*, **110**, 533-572.
Rotstayn, L., and J. Penner, 2001: Indirect aerosol forcing, quasi forcing, and climate response. *Journal of Climate*, **14**, 2960-2975.
Rotstayn, L. D., and U. Lohmann, 2002: Tropical rainfall trends and the indirect aerosol effect. *Journal of Climate*, **15**, 2103-2116.
Rotstayn, L. D., B. F. Ryan, and J. E. Penner, 2000: Precipitation changes in a GCM resulting from the indirect effects of anthropogenic aerosols. *Geophysical Research Letters*, **27**, 3045-3048.
Rottman, G., 2006: Measurement of total and spectral solar irradiance. *Space Science Reviews*, **125**, 39-51.
ROTTMAN, G., T. WOODS, and T. SPARN, 1993: SOLAR-STELLAR IRRADIANCE COMPARISON EXPERIMENT-1 .1. INSTRUMENT DESIGN AND OPERATION. *Journal of Geophysical Research-Atmospheres*, **98**, 10667-10677.
Russell, C., J. Luhmann, and L. Jian, 2010: HOW UNPRECEDENTED A SOLAR MINIMUM? *Reviews of Geophysics*, **48**, -.
Rypdal, K., N. Rive, T. Berntsen, Z. Klimont, T. Mideksa, G. Myhre, and R. Skeie, 2009: Costs and global impacts of black carbon abatement strategies. *Tellus Series B-Chemical and Physical Meteorology*. doi:DOI 10.1111/j.1600-0889.2009.00430.x, 625-641.
Rypdal, K., et al., 2005: Tropospheric ozone and aerosols in climate agreements: scientific and political challenges. *Environmental Science & Policy*, **8**, 29-43.
Salby, M. L., E. A. Titova, and L. Deschamps, 2012: Changes of the Antarctic ozone hole: Controlling mechanisms, seasonal predictability, and evolution. *Journal of Geophysical Research-Atmospheres*, **117**.
Sarofim, M., 2012: The GTP of Methane: Modeling Analysis of Temperature Impacts of Methane and Carbon Dioxide Reductions. *Environmental Modeling & Assessment*, **17**, 231-239.
Sato, M., J. E. Hansen, M. P. McCormick, and J. B. Pollack, 1993: STRATOSPHERIC AEROSOL OPTICAL DEPTHS, 1850-1990. *Journal of Geophysical Research-Atmospheres*, **98**, 22987-22994.
Schaaf, C., et al., 2002: First operational BRDF, albedo nadir reflectance products from MODIS. *Remote Sensing of Environment*, **83**, 135-148.
Schmidt, A., K. S. Carslaw, G. W. Mann, M. Wilson, T. J. Breider, S. J. Pickering, and T. Thordarson, 2010: The impact of the 1783-1784 AD Laki eruption on global aerosol formation processes and cloud condensation nuclei. *Atmospheric Chemistry and Physics*, **10**, 6025-6041.
Schmidt, A., et al., 2012: Importance of tropospheric volcanic aerosol for indirect radiative forcing of climate. *Atmos. Chem. Phys. Discuss.*, **12**, 8009-8051.
Schmidt, G., et al., 2011: Climate forcing reconstructions for use in PMIP simulations of the last millennium (v1.0). *Geoscientific Model Development*, **4**, 33-45.
Schneider, D. P., C. M. Ammann, B. L. Otto-Bliesner, and D. S. Kaufman, 2009: Climate response to large, high-latitude and low-latitude volcanic eruptions in the Community Climate System Model. *Journal of Geophysical Research-Atmospheres*, **114**.
Schultz, M. G., et al., 2008: Global wildland fire emissions from 1960 to 2000. *Glob. Biogeochem. Cycle*, **22**.
Seinfeld, J. H., and S. N. Pandis, 2006: *Atmospheric chemistry and physics: from air pollution to climate change.* Wiley.
Self, S., and S. Blake, 2008: Consequences of explosive supereruptions. *Elements*, **4**, 41-46.
Sharma, S., D. Lavoue, H. Cachier, L. Barrie, and S. Gong, 2004: Long-term trends of the black carbon concentrations in the Canadian Arctic. *Journal of Geophysical Research-Atmospheres*, **109**, -.
Shibata, K., and K. Kodera, 2005: Simulation of radiative and dynamical responses of the middle atmosphere to the 11-year solar cycle. *Journal of Atmospheric and Solar-Terrestrial Physics*, **67**, 125-143.
Shindell, D., and G. Faluvegi, 2009: Climate response to regional radiative forcing during the twentieth century. *Nature Geoscience*, **2**, 294-300.
——, 2010: The net climate impact of coal-fired power plant emissions. *Atmospheric Chemistry and Physics*, **10**, 3247-3260.
Shindell, D., G. Faluvegi, N. Bell, and G. Schmidt, 2005: An emissions-based view of climate forcing by methane and tropospheric ozone. *Geophysical Research Letters*, **32**, -.
Shindell, D., G. Schmidt, M. Mann, D. Rind, and A. Waple, 2001: Solar forcing of regional climate change during the maunder minimum. *Science*, **294**, 2149-2152.
Shindell, D., G. Faluvegi, R. Miller, G. Schmidt, J. Hansen, and S. Sun, 2006a: Solar and anthropogenic forcing of tropical hydrology. *Geophysical Research Letters*, **33**.

Shindell, D., G. Faluvegi, A. Lacis, J. Hansen, R. Ruedy, and E. Aguilar, 2006b: Role of tropospheric ozone increases in 20th-century climate change. *Journal of Geophysical Research-Atmospheres*. doi:ARTN D08302, 10.1029/2005JD006348, -.

Shindell, D., M. Schulz, Y. Ming, T. Takemura, G. Faluvegi, and V. Ramaswamy, 2010: Spatial scales of climate response to inhomogeneous radiative forcing. *Journal of Geophysical Research-Atmospheres*, **115**.

Shindell, D., et al., 2008: Climate forcing and air quality change due to regional emissions reductions by economic sector. *Atmospheric Chemistry and Physics*, **8**, 7101-7113.

Shindell, D., et al., 2011: Climate, health, agricultural and economic impacts of tighter vehicle-emission standards. *Nature Climate Change*, **1**, 59-66.

Shindell, D., et al., 2012a: Attribution of historical whole atmosphere ozone forcing. *Nature Climatic Change*, **(submitted)**.

Shindell, D., et al., 2012b: Simultaneously Mitigating Near-Term Climate Change and Improving Human Health and Food Security. *Science*, **335**, 183-189.

Shindell, D. T., 2012: Evaluation of the absolute regional temperature potential. *Atmos. Chem. Phys. Discuss.*, **12**, 13813-13825.

Shindell, D. T., A. Voulgarakis, G. Faluvegi, and G. Milly, 2012c: Precipitation response to regional radiative forcing. *Atmos. Chem. Phys.*, **12**, 6969-6982.

Shindell, D. T., G. Faluvegi, D. M. Koch, G. A. Schmidt, N. Unger, and S. E. Bauer, 2009: Improved Attribution of Climate Forcing to Emissions. *Science*, **326**, 716-718.

Shindell, D. T., et al., 2006c: Simulations of preindustrial, present-day, and 2100 conditions in the NASA GISS composition and climate model G-PUCCINI. *Atmospheric Chemistry and Physics*, **6**, 4427-4459.

Shindell, D. T., et al., 2012d: Radiative forcing in the ACCMIP historical and future climate simulations. *ACP/GMD Inter-Journal SI*, **submitted**.

Shine, K., 2009: The global warming potential-the need for an interdisciplinary retrial. *Climatic Change*. doi:DOI 10.1007/s10584-009-9647-6, 467-472.

Shine, K., J. Fuglestvedt, K. Hailemariam, and N. Stuber, 2005a: Alternatives to the global warming potential for comparing climate impacts of emissions of greenhouse gases. *Climatic Change*. 281-302.

Shine, K., T. Berntsen, J. Fuglestvedt, and R. Sausen, 2005b: Scientific issues in the design of metrics for inclusion of oxides of nitrogen in global climate agreements. *Proceedings of the National Academy of Sciences of the United States of America*. doi:DOI 10.1073/pnas.0506865102, 15768-15773.

Shine, K., T. Berntsen, J. Fuglestvedt, R. Skeie, and N. Stuber, 2007: Comparing the climate effect of emissions of short- and long-lived climate agents. *Philosophical Transactions of the Royal Society a-Mathematical Physical and Engineering Sciences*. doi:DOI 10.1098/rsta.2007.2050, 1903-1914.

Siddaway, J. M., and S. V. Petelina, 2011: Transport and evolution of the 2009 Australian Black Saturday bushfire smoke in the lower stratosphere observed by OSIRIS on Odin. *Journal of Geophysical Research-Atmospheres*, **116**.

Sitch, S., P. M. Cox, W. J. Collins, and C. Huntingford, 2007: Indirect radiative forcing of climate change through ozone effects on the land-carbon sink. *Nature*, **448**, 791-U794.

Skeie, R., T. Berntsen, G. Myhre, K. Tanaka, M. Kvalevag, and C. Hoyle, 2011a: Anthropogenic radiative forcing time series from pre-industrial times until 2010. *Atmospheric Chemistry and Physics*, **11**, 11827-11857.

Skeie, R., T. Berntsen, G. Myhre, C. Pedersen, J. Strom, S. Gerland, and J. Ogren, 2011b: Black carbon in the atmosphere and snow, from pre-industrial times until present. *Atmospheric Chemistry and Physics*, **11**, 6809-6836.

Skeie, R. B., J. Fuglestvedt, T. Berntsen, M. T. Lund, G. Myhre, and K. Rypdal, 2009: Global temperature change from the transport sectors: Historical development and future scenarios. *Atmospheric Environment*, **43**, 6260-6270.

Smith, E., and A. Balogh, 2008: Decrease in heliospheric magnetic flux in this solar minimum: Recent Ulysses magnetic field observations. *Geophysical Research Letters*, **35**, -.

Smith, S., and M. Wigley, 2000: Global warming potentials: 1. Climatic implications of emissions reductions. *Climatic Change*. 445-457.

Smith, S. M., J. A. Lowe, N. H. A. Bowerman, L. K. Gohar, C. Huntingford, and M. R. Allen, 2012: Equivalence of greenhouse-gas emissions for peak temperature limits. *Nature Clim. Change*, **2**, 535-538.

Snow-Kropla, E. J., J. R. Pierce, D. M. Wesrervelt, and W. Trivitayanurak, 2011: Cosmic rays, aerosol formation and cloud-condensation nuclei: Sensitivities to model uncertainties. *Atm. Chem. Phys.*, **11**, 4001-4013.

Solomon, S., 1999: Stratospheric ozone depletion: A review of concepts and history. *Reviews of Geophysics*, **37**, 275-316.

Solomon, S., J. S. Daniel, R. R. Neely, J. P. Vernier, E. G. Dutton, and L. W. Thomason, 2011: The Persistently Variable "Background" Stratospheric Aerosol Layer and Global Climate Change. *Science*, **333**, 866-870.

Solomon, S., K. Rosenlof, R. Portmann, J. Daniel, S. Davis, T. Sanford, and G. Plattner, 2010: Contributions of Stratospheric Water Vapor to Decadal Changes in the Rate of Global Warming. *Science*. doi:DOI 10.1126/science.1182488, 1219-1223.

Son, S. W., N. F. Tandon, L. M. Polvani, and D. W. Waugh, 2009: Ozone hole and Southern Hemisphere climate change. *Geophysical Research Letters*, **36**.

Soukharev, B., and L. Hood, 2006: Solar cycle variation of stratospheric ozone: Multiple regression analysis of long-term satellite data sets and comparisons with models. *Journal of Geophysical Research-Atmospheres*, **111**.
Sovde, O., C. Hoyle, G. Myhre, and I. Isaksen, 2011: The HNO3 forming branch of the HO2 + NO reaction: pre-industrial-to-present trends in atmospheric species and radiative forcings. *Atmospheric Chemistry and Physics*, **11**, 8929-8943.
Steinhilber, F., J. Beer, and C. Frohlich, 2009: Total solar irradiance during the Holocene. *Geophysical Research Letters*, **36**, -.
Stenchikov, G., A. Robock, V. Ramaswamy, M. D. Schwarzkopf, K. Hamilton, and S. Ramachandran, 2002: Arctic Oscillation response to the 1991 Mount Pinatubo eruption: Effects of volcanic aerosols and ozone depletion. *Journal of Geophysical Research-Atmospheres*, **107**.
Stenchikov, G., T. L. Delworth, V. Ramaswamy, R. J. Stouffer, A. Wittenberg, and F. R. Zeng, 2009: Volcanic signals in oceans. *Journal of Geophysical Research-Atmospheres*, **114**.
Stephens, G. L., N. B. Wood, and L. A. Pakula, 2004: On the radiative effects of dust on tropical convection. *Geophysical Research Letters*, **31**.
Stevenson, D., and R. Derwent, 2009: Does the location of aircraft nitrogen oxide emissions affect their climate impact? *Geophysical Research Letters*. doi:ARTN L17810, 10.1029/2009GL039422, -.
Stevenson, D. S., et al., 2012: Tropospheric ozone changes, attribution to emissions and radiative forcing in the Atmospheric Chemistry and Climate Model Inter-comparison Project (ACCMIP). *ACP/GMD Inter-Journal SI*, **Submitted**.
Stevenson, D. S., et al., 2006: Multimodel ensemble simulations of present-day and near-future tropospheric ozone. *Journal of Geophysical Research-Atmospheres*, **111**.
Stiller, G. P., et al., 2012: Observed temporal evolution of global mean age of stratospheric air for the 2002 to 2010 period. *Atmospheric Chemistry and Physics*, **12**, 3311-3331.
Stothers, R. B., 2007: Three centuries of observation of stratospheric transparency. *Climatic Change*, **83**, 515-521.
Streets, D. G., T. C. Bond, T. Lee, and C. Jang, 2004: On the future of carbonaceous aerosol emissions. *Journal of Geophysical Research-Atmospheres*, **109**.
Swann, A. L. S., I. Y. Fung, and J. C. H. Chiang, 2012: Mid-latitude afforestation shifts general circulation and tropical precipitation. *Proceedings of the National Academy of Sciences of the United States of America*, **109**, 712-716.
Swingedouw, D., L. Terray, C. Cassou, A. Voldoire, D. Salas-Melia, and J. Servonnat, 2011: Natural forcing of climate during the last millennium: fingerprint of solar variability. *Climate Dynamics*, **36**, 1349-1364.
Tanaka, K., D. Johansson, B. O'Neill, and J. Fuglestvedt, 2012: Emission metrics under the 2°C climate stabilization. *Climatic Change Letters*. (submitted).
Tanaka, K., B. O'Neill, D. Rokityanskiy, M. Obersteiner, and R. Tol, 2009: Evaluating Global Warming Potentials with historical temperature. *Climatic Change*. doi:DOI 10.1007/s10584-009-9566-6, 443-466.
Taylor, P. C., R. G. Ellingson, and M. Cai, 2011: Seasonal Variations of Climate Feedbacks in the NCAR CCSM3. *Journal of Climate*, **24**, 3433-3444.
Textor, C., et al., 2006: Analysis and quantification of the diversities of aerosol life cycles within AeroCom. *Atmospheric Chemistry and Physics*, **6**, 1777-1813.
Thomason, L., and T. Peter, 2006: Assessment of Stratospheric Aerosol Properties (ASAP).
Thompson, D. W. J., S. Solomon, P. J. Kushner, M. H. England, K. M. Grise, and D. J. Karoly, 2011: Signatures of the Antarctic ozone hole in Southern Hemisphere surface climate change. *Nature Geoscience*, **4**, 741-749.
Thonicke, K., A. Spessa, I. C. Prentice, S. P. Harrison, L. Dong, and C. Carmona-Moreno, 2010: The influence of vegetation, fire spread and fire behaviour on biomass burning and trace gas emissions: results from a process-based model. *Biogeosciences*, **7**, 1991-2011.
Tilmes, S., et al., 2011: Ozonesonde climatology between 1995 and 2009: description, evaluation and applications. 28747-28796.
Timmreck, C., 2012: Modeling the climatic effects of large large volcanic eruptions. *WIREs Climate Change*, **submitted**.
Timmreck, C., et al., 2010: Aerosol size confines climate response to volcanic super-eruptions. *Geophysical Research Letters*, **37**, -.
Tol, R. S. J., T. K. Berntsen, B. C. O'Neill, J. S. Fuglestvedt, and K. P. Shine, 2012: A UNIFYING FRAMEWORK FOR METRICS FOR AGGREGATING THE CLIMATE EFFECT OF DIFFERENT EMISSIONS. *Environmental Research Letters*. (submitted).
Toon, O. B., A. Robock, and R. P. Turco, 2008: Environmental consequences of nuclear war. *Physics Today*, **61**, 37-42.
Trenberth, K. E., and A. Dai, 2007: Effects of Mount Pinatubo volcanic eruption on the hydrological cycle as an analog of geoengineering. *Geophysical Research Letters*, **34**.
Tsigaridis, K., and M. Kanakidou, 2007: Secondary organic aerosol importance in the future atmosphere. *Atmospheric Environment*, **41**, 4682-4692.
Uherek, E., et al., 2010: Transport impacts on atmosphere and climate: Land transport. *Atmospheric Environment*. doi:DOI 10.1016/j.atmosenv.2010.01.002, 4772-4816.
UNEP, 2011: Near-term Climate Protection and Clean Air Benefits: Actions for Controlling Short-Lived Climate Forcers. United Nations Environment Programme (UNEP), 78 pp.

Unger, N., T. C. Bond, J. S. Wang, D. M. Koch, S. Menon, D. T. Shindell, and S. Bauer, 2010: Attribution of climate forcing to economic sectors. *Proceedings of the National Academy of Sciences of the United States of America*, **107**, 3382-3387.
Usoskin, I., S. Solanki, M. Schussler, K. Mursula, and K. Alanko, 2003: Millennium-scale sunspot number reconstruction: Evidence for an unusually active Sun since the 1940s. *Physical Review Letters*, **91**, -.
van der Molen, M. K., B. J. J. M. van den Hurk, and W. Hazeleger, 2011: A dampened land use change climate response towards the tropics. *Climate Dynamics*, **37**, 2035-2043.
van der Werf, G. R., et al., 2010: Global fire emissions and the contribution of deforestation, savanna, forest, agricultural, and peat fires (1997-2009). *Atmospheric Chemistry and Physics*, **10**, 11707-11735.
van Vuuren, D., J. Edmonds, M. Kainuma, K. Riahi, and J. Weyant, 2011: A special issue on the RCPs. *Climatic Change*, **109**, 1-4.
Velasco-Herrera, V. M., B. Mendoza, and G. Velasco-Herrera, 2012: Estimations of the Total Solar Irradiance from the Spoerer minimum to 21st century. *Astronomy and Astrophysics*, **submitted**.
Vernier, J. P., et al., 2011: Major influence of tropical volcanic eruptions on the stratospheric aerosol layer during the last decade. *Geophysical Research Letters*, **38**, 8.
Vieira, L., S. Solanki, N. Krivova, and I. Usoskin, 2011: Evolution of the solar irradiance during the Holocene. *Astronomy & Astrophysics*, **531**.
Volz, A., and D. Kley, 1988: EVALUATION OF THE MONTSOURIS SERIES OF OZONE MEASUREMENTS MADE IN THE 19TH-CENTURY. *Nature*, **332**, 240-242.
Voulgarakis, A., and D. T. Shindell, 2010: Constraining the Sensitivity of Regional Climate with the Use of Historical Observations. *Journal of Climate*, **23**, 6068-6073.
Voulgarakis, A., et al., 2012: Multimodel simulations of present-day and future OH and methane lifetime. *Atmos. Phys. Chem. Discussion*, **Submitted**.
Wang, C., D. Kim, A. Ekman, M. Barth, and P. Rasch, 2009: Impact of anthropogenic aerosols on Indian summer monsoon. *Geophysical Research Letters*, **36**, -.
Wang, M., and J. E. Penner, 2009: Aerosol indirect forcing in a global model with particle nucleation. *Atmospheric Chemistry and Physics*, **9**, 239-260.
Wang, Y., J. Lean, and N. Sheeley, 2005: Modeling the sun's magnetic field and irradiance since 1713. *Astrophysical Journal*, **625**, 522-538.
WARREN, S., and W. WISCOMBE, 1980: A MODEL FOR THE SPECTRAL ALBEDO OF SNOW .2. SNOW CONTAINING ATMOSPHERIC AEROSOLS. *J. Atmos. Sci.*, **37**, 2734-2745.
Weiss, R., J. Muhle, P. Salameh, and C. Harth, 2008: Nitrogen trifluoride in the global atmosphere. *Geophysical Research Letters*. doi:ARTN L20821, 10.1029/2008GL035913, -.
Wenzler, T., S. Solanki, N. Krivova, and C. Frohlich, 2006: Reconstruction of solar irradiance variations in cycles 21-23 based on surface magnetic fields. *Astronomy & Astrophysics*, **460**, 583-595.
Wild, M., 2009: How well do IPCC-AR4/CMIP3 climate models simulate global dimming/brightening and twentieth-century daytime and nighttime warming? *Journal of Geophysical Research-Atmospheres*, **114**.
Wild, O., 2007: Modelling the global tropospheric ozone budget: exploring the variability in current models. *Atmospheric Chemistry and Physics*, **7**, 2643-2660.
Wild, O., and P. I. Palmer, 2008: How sensitive is tropospheric oxidation to anthropogenic emissions? *Geophysical Research Letters*, **35**.
Wild, O., M. Prather, and H. Akimoto, 2001: Indirect long-term global radiative cooling from NOx emissions. *Geophysical Research Letters*, **28**, 1719-1722.
Williams, K. D., A. Jones, D. L. Roberts, C. A. Senior, and M. J. Woodage, 2001: The response of the climate system to the indirect effects of anthropogenic sulfate aerosol. *Climate Dynamics*, **17**, 845-856.
Willson, R., and A. Mordvinov, 2003: Secular total solar irradiance trend during solar cycles 21-23. *Geophysical Research Letters*, **30**, -.
WMO, 1999: Scientific Assessment of Ozone Depletion: 1998, Global Ozone Research and Monitoring Project. World Meteorological Organization, Report No. 44,.
——, 2010: *Scientific Assessment of Ozone Depletion 2010.* Vol. 52, World Meteorological Organisation.
Worden, H., K. Bowman, J. Worden, A. Eldering, and R. Beer, 2008: Satellite measurements of the clear-sky greenhouse effect from tropospheric ozone. *Nature Geoscience*. doi:DOI 10.1038/ngeo182, 305-308.
Wright, J. T., 2004: Do we know of any Maunder minimum stars? *Astronomical J.*, **128**, 1273-1278.
Wu, S. L., L. J. Mickley, D. J. Jacob, J. A. Logan, R. M. Yantosca, and D. Rind, 2007: Why are there large differences between models in global budgets of tropospheric ozone? *Journal of Geophysical Research-Atmospheres*, **112**.
Young, P. J., et al., 2012: Pre-industrial to end 21st century projections of tropospheric ozone from the Atmospheric Chemistry and Climate Model Intercomparison Project (ACCMIP). *ACP/GMD Inter-Journal SI*, **Submitted**.
Zanchettin, D., A. Rubino, and J. H. Jungclaus, 2010: Intermittent multidecadal-to-centennial fluctuations dominate global temperature evolution over the last millennium. *Geophysical Research Letters*, **37**.
Zarzycki, C. M., and T. C. Bond, 2010: How much can the vertical distribution of black carbon affect its global direct radiative forcing? *Geophysical Research Letters*, **37**.
Zeng, G., J. A. Pyle, and P. J. Young, 2008: Impact of climate change on tropospheric ozone and its global budgets. *Atmospheric Chemistry and Physics*, **8**, 369-387.

Zeng, G., O. Morgenstern, P. Braesicke, and J. A. Pyle, 2010: Impact of stratospheric ozone recovery on tropospheric ozone and its budget. *Geophysical Research Letters*, **37**.

Zhang, H., G. Y. Shi, and Y. Liu, 2005: A Comparison Between the Two Line-by-Line Integration Algorithms. *Chinese Journal of Atmospheric Sciences*, **29**, 581-593.

Zhang, H., G. Shi, and Y. Liu, 2008: The effects of line-wing cutoff in LBL integration on radiation calculations. *Acta Meteorologica Sinica*, **22**, 248-255.

Zhang, H., J. Wu, and P. Luc, 2011: A study of the radiative forcing and global warming potentials of hydrofluorocarbons. *Journal of Quantitative Spectroscopy & Radiative Transfer*, **112**, 220-229.

Zhang, X. B., et al., 2007: Detection of human influence on twentieth-century precipitation trends. *Nature*, **448**, 461-U464.

Zhong, Y., G. H. Miller, B. L. Otto-Bliesner, M. M. Holland, D. A. Bailey, D. P. Schneider, and A. Geirsdottir, 2011: Centennial-scale climate change from decadally-paced explosive volcanism: a coupled sea ice-ocean mechanism. *Climate Dynamics*, **37**, 2373-2387.

Ziemke, J. R., S. Chandra, G. J. Labow, P. K. Bhartia, L. Froidevaux, and J. C. Witte, 2011: A global climatology of tropospheric and stratospheric ozone derived from Aura OMI and MLS measurements. *Atmospheric Chemistry and Physics*, **11**, 9237-9251.

Appendix 8.A

Table 8.A.1: Radiative efficiencies (RE), lifetimes/adjustment times, AGWP and GWP values for 20 and 100 years, and AGTP and GTP values for 20, 50 and 100 years. Metric values for CO_2, CH_4 and N_2O are calculated here while AGWP and AGTP values for the remaining components are taken from Hodnebrog et al. (2012). Indirect effects of methane on tropospheric ozone and stratospheric H_2O are included. Indirect effects of selected Ozone Depleting Substances (ODS) are given in Table 8.A.2. Impact on own lifetime is included for CH_4 and N_2O. Climate-carbon feedbacks are included for CO_2 while no climate feedbacks are included for the other components. See also notes below the table. [PLACEHOLDER FOR FINAL DRAFT: Number of significant digits will be adjusted].

			Radiative	AGWP	GWP	AGWP	GWP	AGTP	GTP	AGTP	GTP	AGTP	GTP
Industrial Designation	**Chemical**	**Lifetime**	**Efficiency**	20-yr		100-yr		20-yr		50-yr		100-yr	
or Common name	**Formula**	(years)	(W m-2 ppb-1)	Wm-2 yr kg-1		Wm-2 yr kg-1		Kelvin / kg		Kelvin / kg		Kelvin / kg	
Carbon dioxide	CO_2	See below [*]	1.37E-05	2.50E-14	**1**	9.18E-14	**1**	6.85E-16	**1**	6.17E-16	**1**	5.48E-16	**1**
Methane (non-fossil)	CH_4	12.2	3.63E-04	2.04E-12	**82**	2.54E-12	**28**	4.49E-14	**65**	8.28E-15	**13**	2.26E-15	**4**
Methane (fossil) [§] (preliminary)	CH_4	12.2	3.63E-04		**82.7-83.5**		**29.2-30.5**		**66-66.9**				**5.4-6.8**
Nitrous oxide	N_2O	121	3.03E-03	7.15E-12	**286**	2.64E-11	**288**	2.06E-13	**301**	1.89E-13	**306**	1.39E-13	**254**
Chlorofluorocarbons													
CFC-11	CCl3F	45	0.263	1.74E-10	**6957**	4.32E-10	**4702**	4.76E-12	**6942**	3.04E-12	**4931**	1.29E-12	**2353**
CFC-12	CCl2F2	100	0.32	2.70E-10	**10814**	9.42E-10	**10257**	7.73E-12	**11278**	6.77E-12	**10976**	4.63E-12	**8458**
CFC-13	CClF3	640	0.25	2.65E-10	**10623**	1.25E-09	**13585**	7.82E-12	**11415**	8.58E-12	**13908**	8.52E-12	**15559**
CFC-113	CCl2FCClF2	85	0.3	1.61E-10	**6432**	5.30E-10	**5771**	4.57E-12	**6665**	3.82E-12	**6193**	2.43E-12	**4430**
CFC-114	CClF2CClF2	190	0.315	1.97E-10	**7886**	8.07E-10	**8786**	5.73E-12	**8364**	5.70E-12	**9229**	4.79E-12	**8740**
CFC-115	CClF2CF3	1020	0.206	1.49E-10	**5947**	7.14E-10	**7780**	4.39E-12	**6404**	4.89E-12	**7925**	4.99E-12	**9105**
Hydrochlorofluorocarbons													
HCFC-21	CHCl2F	1.7	0.14	1.30E-11	**521**	1.30E-11	**142**	1.26E-13	**184**	1.53E-14	**25**	1.07E-14	**20**
HCFC-22	CHClF2	11.9	0.2	1.26E-10	**5049**	1.55E-10	**1687**	2.75E-12	**4009**	4.91E-13	**796**	1.37E-13	**250**
HCFC-123	CHCl2CF3	1.3	0.149	7.11E-12	**285**	7.11E-12	**77**	6.56E-14	**96**	8.26E-15	**13**	5.86E-15	**11**
HCFC-124	CHClFCF3	5.9	0.192	4.52E-11	**1811**	4.68E-11	**510**	7.40E-13	**1079**	7.23E-14	**117**	3.91E-14	**71**
HCFC-141b	CH3CCl2F	9.2	0.152	5.97E-11	**2390**	6.74E-11	**734**	1.19E-12	**1737**	1.57E-13	**255**	5.72E-14	**104**
HCFC-142b	CH3CClF2	17.2	0.186	1.23E-10	**4939**	1.79E-10	**1948**	2.96E-12	**4316**	8.33E-13	**1349**	1.91E-13	**349**
HCFC-225ca	CHCl2CF2CF3	1.9	0.211	1.11E-11	**446**	1.11E-11	**121**	1.11E-13	**162**	1.32E-14	**21**	9.19E-15	**17**
HCFC-225cb	CHClFCF2CClF2	5.9	0.278	4.39E-11	**1760**	4.55E-11	**495**	7.19E-13	**1049**	7.02E-14	**114**	3.79E-14	**69**
	trans-CF3CH=CHCl	0.0712	0.053	1.62E-13	**6**	1.62E-13	**2**	1.29E-15	**2**	1.82E-16	**0**	1.33E-16	**0**
Hydrofluorocarbons													
HFC-23	CHF3	222	0.176	2.70E-10	**10817**	1.14E-09	**12386**	7.89E-12	**11504**	7.99E-12	**12953**	6.95E-12	**12688**
HFC-32	CH2F2	5.2	0.11	6.06E-11	**2425**	6.19E-11	**674**	9.29E-13	**1355**	8.90E-14	**144**	5.15E-14	**94**
HFC-41	CH3F	2.8	0.022	1.00E-11	**402**	1.01E-11	**110**	1.14E-13	**166**	1.23E-14	**20**	8.32E-15	**15**
HFC-125	CHF2CF3	28.2	0.219	1.47E-10	**5886**	2.81E-10	**3061**	3.84E-12	**5595**	1.78E-12	**2876**	5.12E-13	**934**
HFC-134	CHF2CHF2	9.7	0.187	8.72E-11	**3492**	9.99E-11	**1088**	1.77E-12	**2588**	2.48E-13	**402**	8.53E-14	**156**
HFC-134a	CH2FCF3	13.4	0.159	9.09E-11	**3641**	1.17E-10	**1277**	2.05E-12	**2993**	4.26E-13	**690**	1.08E-13	**197**
HFC-143	CH2FCHF2	3.5	0.123	2.88E-11	**1152**	2.89E-11	**314**	3.60E-13	**526**	3.67E-14	**59**	2.39E-14	**44**
HFC-143a	CH3CF3	47.1	0.159	1.74E-10	**6959**	4.42E-10	**4816**	4.78E-12	**6969**	3.13E-12	**5076**	1.37E-12	**2509**
HFC-152	CH2FCH2F	0.4	0.043	1.47E-12	**59**	1.47E-12	**16**	1.22E-14	**18**	1.66E-15	**3**	1.21E-15	**2**
HFC-152a	CH3CHF2	1.5	0.094	1.20E-11	**479**	1.20E-11	**130**	1.13E-13	**165**	1.40E-14	**23**	9.87E-15	**18**
HFC-161	CH3CH2F	0.1808	0.016	3.48E-13	**14**	3.48E-13	**4**	2.81E-15	**4**	3.92E-16	**1**	2.86E-16	**1**
HFC-227ca	CF3CF2CHF2	28.2	0.265	1.26E-10	**5030**	2.40E-10	**2616**	3.28E-12	**4781**	1.52E-12	**2458**	4.37E-13	**798**
HFC-227ea	CF3CHFCF3	38.9	0.257	1.33E-10	**5319**	3.05E-10	**3324**	3.59E-12	**5240**	2.11E-12	**3412**	7.93E-13	**1448**
HFC-236cb	CH2FCF2CF3	13.1	0.224	8.52E-11	**3410**	1.09E-10	**1184**	1.91E-12	**2785**	3.85E-13	**624**	9.91E-14	**181**
HFC-236ea	CHF2CHFCF3	11	0.3	1.02E-10	**4098**	1.22E-10	**1331**	2.18E-12	**3174**	3.53E-13	**571**	1.06E-13	**194**
HFC-236fa	CF3CH2CF3	242	0.244	1.73E-10	**6944**	7.40E-10	**8060**	5.07E-12	**7395**	5.19E-12	**8409**	4.59E-12	**8376**
HFC-245ca	CH2FCF2CHF2	6.5	0.23	5.99E-11	**2398**	6.28E-11	**684**	1.03E-12	**1499**	1.04E-13	**168**	5.25E-14	**96**
HFC-245cb	CF3CF2CH3	47.1	0.231	1.58E-10	**6333**	4.02E-10	**4383**	4.35E-12	**6342**	2.85E-12	**4619**	1.25E-12	**2283**
HFC-245fa	CHF2CH2CF3	7.7	0.233	6.96E-11	**2787**	7.52E-11	**819**	1.29E-12	**1883**	1.45E-13	**234**	6.32E-14	**115**
HFC-272ca	CH3CF2CH3	2.6	0.069	1.26E-11	**506**	1.26E-11	**138**	1.39E-13	**203**	1.54E-14	**25**	1.04E-14	**19**
HFC-329p	CHF2CF2CF2CF3	28.4	0.304	1.12E-10	**4466**	2.14E-10	**2332**	2.91E-12	**4249**	1.36E-12	**2197**	3.93E-13	**717**
HFC-365mfc	CH3CF2CH2CF3	8.7	0.21	6.25E-11	**2502**	6.95E-11	**756**	1.22E-12	**1779**	1.52E-13	**246**	5.87E-14	**107**
HFC-43-10mee	CF3CHFCHFCF2CF3	16.1	0.4	1.02E-10	**4096**	1.44E-10	**1563**	2.42E-12	**3527**	6.29E-13	**1019**	1.46E-13	**267**
	CF3CF=CHF(Z)	0.0233	0.031	3.06E-14	**1**	3.06E-14	**0**	2.43E-16	**0**	3.43E-17	**0**	2.51E-17	**0**
	CF3CF=CHF(E)	0.0134	0.02	1.14E-14	**0**	1.14E-14	**0**	9.07E-17	**0**	1.28E-17	**0**	9.37E-18	**0**
	CF3CH=CHF(Z)	0.0274	0.027	3.63E-14	**1**	3.63E-14	**0**	2.89E-16	**0**	4.07E-17	**0**	2.98E-17	**0**
HFO-1234yf	CF3CF=CH2	0.0288	0.031	4.44E-14	**2**	4.44E-14	**0**	3.54E-16	**1**	4.98E-17	**0**	3.64E-17	**0**
(E)-HFO-1234ze	trans-CF3CH=CHF	0.0449	0.05	1.11E-13	**4**	1.11E-13	**1**	8.89E-16	**1**	1.25E-16	**0**	9.15E-17	**0**
HFC-1243zf	CF3CH=CH2	0.0192	0.018	2.02E-14	**1**	2.02E-14	**0**	1.61E-16	**0**	2.27E-17	**0**	1.66E-17	**0**
HFO-1345zfc	C2F5CH=CH2	0.0208	0.021	1.68E-14	**1**	1.68E-14	**0**	1.34E-16	**0**	1.89E-17	**0**	1.38E-17	**0**
	C4F9CH=CH2	0.0208	0.038	1.82E-14	**1**	1.82E-14	**0**	1.45E-16	**0**	2.04E-17	**0**	1.49E-17	**0**
	C6F13CH=CH2	0.0208	0.043	1.44E-14	**1**	1.44E-14	**0**	1.15E-16	**0**	1.62E-17	**0**	1.19E-17	**0**
	C8F17CH=CH2	0.0208	0.047	1.24E-14	**0**	1.24E-14	**0**	9.91E-17	**0**	1.40E-17	**0**	1.02E-17	**0**
Chlorocarbons													
Methyl chloroform	CH3CCl3	5	0.069	1.42E-11	**570**	1.45E-11	**158**	2.14E-13	**312**	2.05E-14	**33**	1.21E-14	**22**
Carbon tetrachloride	CCl4	26	0.175	8.96E-11	**3588**	1.63E-10	**1780**	2.31E-12	**3373**	9.97E-13	**1616**	2.70E-13	**493**
Methyl chloride	CH3Cl	1	0.01	1.12E-12	**45**	1.12E-12	**12**	9.91E-15	**14**	1.28E-15	**2**	9.18E-16	**2**
Methylene chloride	CH2Cl2	0.3945	0.03	7.85E-13	**31**	7.85E-13	**9**	6.50E-15	**9**	8.89E-16	**1**	6.45E-16	**1**
	CHCl3	0.4082	0.076	1.47E-12	**59**	1.47E-12	**16**	1.22E-14	**18**	1.66E-15	**3**	1.21E-15	**2**
	CH2ClCH2Cl	0.1781	0.009	8.76E-14	**4**	8.76E-14	**1**	7.09E-16	**1**	9.87E-17	**0**	7.19E-17	**0**
Bromocarbons and Halons													
Methyl bromide	CH3Br	0.8	0.004	2.07E-13	**8**	2.07E-13	**2**	1.80E-15	**3**	2.37E-16	**0**	1.70E-16	**0**
	CH2Br2	0.337	0.008	9.21E-14	**4**	9.21E-14	**1**	7.58E-16	**1**	1.04E-16	**0**	7.57E-17	**0**
Halon-1201	CHBrF2	5.2	0.149	3.27E-11	**1309**	3.34E-11	**364**	5.01E-13	**731**	4.80E-14	**78**	2.78E-14	**51**
Halon-1211	CBrClF2	16	0.3	1.17E-10	**4669**	1.63E-10	**1776**	2.75E-12	**4014**	7.11E-13	**1152**	1.65E-13	**302**
Halon-1301	CBrF3	65	0.32	2.08E-10	**8339**	6.18E-10	**6725**	5.85E-12	**8530**	4.45E-12	**7214**	2.44E-12	**4452**
Halon-2311 / Halothane	CHBrClCF3	1	0.121	3.46E-12	**139**	3.46E-12	**38**	3.08E-14	**45**	3.99E-15	**6**	2.85E-15	**5**
Halon-2402	CBrF2CBrF2	20	0.33	9.04E-11	**3619**	1.42E-10	**1547**	2.23E-12	**3260**	7.45E-13	**1207**	1.75E-13	**319**

Halogenated Alcohols and Ethers													
HFE-125	CHF2OCF3	119	0,406	3,09E-10	**12387**	1,14E-09	**12380**	8,91E-12	**12992**	8,14E-12	**13188**	5,96E-12	**10883**
HFE-134 (HG-00)	CHF2OCHF2	24,4	0,559	3,64E-10	**14575**	6,40E-10	**6969**	9,30E-12	**13574**	3,79E-12	**6137**	9,82E-13	**1792**
HFE-143a	CH3OCF3	4,8	0,172	4,57E-11	**1830**	4,64E-11	**506**	6,72E-13	**981**	6,45E-14	**104**	3,86E-14	**70**
HFE-227	CF3CHFOCF3	51,6	0,44	2,21E-10	**8836**	5,88E-10	**6403**	6,11E-12	**8909**	4,20E-12	**6800**	1,97E-12	**3597**
HCFE-235ca2 (enflurane)	CHF2OCF2CHFCl	4,3	0,393	5,11E-11	**2045**	5,16E-11	**562**	7,10E-13	**1035**	6,89E-14	**112**	4,28E-14	**78**
HCFE-235da2 (isoflurane)	CHF2OCHClCF3	3,5	0,405	4,31E-11	**1726**	4,32E-11	**471**	5,40E-13	**788**	5,49E-14	**89**	3,58E-14	**65**
HFE-236 (desflurane)	CHF2OCHFCF3	10,8	0,446	1,36E-10	**5450**	1,61E-10	**1758**	2,88E-12	**4195**	4,56E-13	**739**	1,40E-13	**255**
HFE-236fa	CF3CH2OCF3	7,5	0,34	7,95E-11	**3183**	8,54E-11	**930**	1,46E-12	**2125**	1,60E-13	**259**	7,17E-14	**131**
HFE-245cb2	CF3CF2OCH3	4,9	0,32	5,78E-11	**2316**	5,88E-11	**641**	8,60E-13	**1255**	8,24E-14	**133**	4,89E-14	**89**
HFE-245fa1	CHF2CH2OCF3	6,6	0,3	7,07E-11	**2831**	7,43E-11	**809**	1,22E-12	**1782**	1,24E-13	**201**	6,21E-14	**113**
HFE-245fa2	CHF2OCH2CF3	5,5	0,349	7,02E-11	**2809**	7,21E-11	**785**	1,11E-12	**1616**	1,07E-13	**173**	6,00E-14	**110**
	CF3CF2CH2OH	0,33	0,14	1,73E-12	**69**	1,73E-12	**19**	1,42E-14	**21**	1,96E-15	**3**	1,42E-15	**3**
HFE-254cb2	CH3OCF2CHF2	2,5	0,245	2,61E-11	**1043**	2,61E-11	**284**	2,83E-13	**413**	3,16E-14	**51**	2,15E-14	**39**
HFE-263fb2	CF3CH2OCH3	0,063	0,047	1,46E-13	**6**	1,46E-13	**2**	1,17E-15	**2**	1,65E-16	**0**	1,20E-16	**0**
R-E-143a	CF3OCH2CH3	0,43	0,124	2,63E-12	**105**	2,63E-12	**29**	2,19E-14	**32**	2,98E-15	**5**	2,16E-15	**4**
	CF3CH2CH2OH	0,033	0,029	4,80E-14	**2**	4,80E-14	**1**	3,83E-16	**1**	5,40E-17	**0**	3,94E-17	**0**
HFE-329	CHF2CF2OCF2CF3	22,5	0,49	1,55E-10	**6200**	2,60E-10	**2830**	3,91E-12	**5701**	1,47E-12	**2384**	3,63E-13	**663**
HFE-338 isomer	(CF3)2CHOCHF2	21,2	0,41	1,37E-10	**5487**	2,22E-10	**2422**	3,42E-12	**4995**	1,21E-12	**1966**	2,91E-13	**531**
HFE-338mcf2	CF3CH2OCF2CF3	7,5	0,43	7,75E-11	**3102**	8,33E-11	**907**	1,42E-12	**2072**	1,56E-13	**253**	6,99E-14	**128**
HFE-347 isomer (sevoflurane)	(CF3)2CHOCH2F	2,2	0,306	1,89E-11	**757**	1,89E-11	**206**	1,97E-13	**287**	2,26E-14	**37**	1,56E-14	**29**
HFE-347mcc (HFE-7000)	CH3OCF2CF2CF3	5	0,331	4,57E-11	**1830**	4,65E-11	**507**	6,87E-13	**1002**	6,58E-14	**107**	3,87E-14	**71**
HFE-347mcf2	CHF2CH2OCF2CF3	6,6	0,41	7,25E-11	**2902**	7,61E-11	**829**	1,25E-12	**1827**	1,27E-13	**206**	6,37E-14	**116**
HFE-347pcf2	CHF2CF2OCH2CF3	6	0,25	4,07E-11	**1630**	4,22E-11	**460**	6,71E-13	**979**	6,59E-14	**107**	3,52E-14	**64**
	(CF3)2CFOCH3	3,7	0,31	3,21E-11	**1287**	3,23E-11	**352**	4,14E-13	**603**	4,15E-14	**67**	2,68E-14	**49**
HFE-356mec3	CH3OCF2CHFCF3	3,8	0,3	3,51E-11	**1404**	3,52E-11	**384**	4,57E-13	**667**	4,56E-14	**74**	2,92E-14	**53**
HFE-356mff2	CF3CH2OCH2CF3	0,2877	0,172	1,53E-12	**61**	1,53E-12	**17**	1,26E-14	**18**	1,73E-15	**3**	1,26E-15	**2**
HFE-356pcf2	CHF2CH2OCF2CHF2	5,7	0,37	6,33E-11	**2533**	6,52E-11	**710**	1,02E-12	**1483**	9,86E-14	**160**	5,44E-14	**99**
HFE-356pcf3	CHF2OCH2CF2CHF2	3,5	0,39	4,21E-11	**1684**	4,22E-11	**460**	5,27E-13	**769**	5,36E-14	**87**	3,50E-14	**64**
HFE-356pcc3	CH3OCF2CF2CHF2	3,8	0,33	3,86E-11	**1544**	3,88E-11	**422**	5,03E-13	**734**	5,01E-14	**81**	3,22E-14	**59**
HFE-356mmz	(CF3)2CHOCH3	0,266	0,154	1,27E-12	**51**	1,27E-12	**14**	1,04E-14	**15**	1,43E-15	**2**	1,04E-15	**2**
HFE-365mcf3	CF3CF2CH2OCH3	0,053	0,058	1,05E-13	**4**	1,05E-13	**1**	8,40E-16	**1**	1,18E-16	**0**	8,64E-17	**0**
	CF3CF2OCH2CH3	0,59	0,254	5,14E-12	**206**	5,14E-12	**56**	4,35E-14	**64**	5,85E-15	**9**	4,23E-15	**8**
HFE-374pc2	CHF2CF2OCH2CH3	5	0,25	4,73E-11	**1893**	4,82E-11	**525**	7,11E-13	**1037**	6,80E-14	**110**	4,01E-14	**73**
	CF3(CH2)2CH2OH	0,011	0,008	2,82E-15	**0**	2,82E-15	**0**	2,24E-17	**0**	3,17E-18	**0**	2,32E-18	**0**
	-(CF2)4CH(OH)-	0,3	0,3	2,20E-12	**88**	2,20E-12	**24**	1,81E-14	**26**	2,49E-15	**4**	1,81E-15	**3**
HFE-43-10pccc124 (H-Galden 1040x, HG-11)	CHF2OCF2OC2F4OCHF	13,5	1,002	1,96E-10	**7855**	2,54E-10	**2763**	4,43E-12	**6470**	9,29E-13	**1505**	2,34E-13	**427**
HFE-449sl (HFE-7100)	C4F9OCH3	4,7	0,353	3,68E-11	**1474**	3,73E-11	**407**	5,36E-13	**781**	5,14E-14	**83**	3,10E-14	**57**
HFE-569sf2 (HFE-7200)	C4F9OC2H5	0,8	0,3	5,12E-12	**205**	5,12E-12	**56**	4,44E-14	**65**	5,86E-15	**9**	4,21E-15	**8**
HFE-236ca12 (HG-10)	CHF2OCF2OCHF2	25	0,647	2,72E-10	**10909**	4,86E-10	**5290**	6,99E-12	**10197**	2,91E-12	**4716**	7,67E-13	**1399**
HFE-338pcc13 (HG-01)	CHF2OCF2CF2OCHF2	12,9	0,843	2,06E-10	**8255**	2,62E-10	**2849**	4,60E-12	**6714**	9,10E-13	**1475**	2,37E-13	**433**
	(CF3)2CHOH	1,9	0,28	1,78E-11	**714**	1,78E-11	**194**	1,78E-13	**259**	2,11E-14	**34**	1,47E-14	**27**
HG-02	HF2C–(OCF2CF2)2–OC	12,9	1,224	1,93E-10	**7744**	2,45E-10	**2672**	4,32E-12	**6298**	8,54E-13	**1383**	2,22E-13	**406**
HG-03	HF2C–(OCF2CF2)3–OC	12,9	1,732	2,02E-10	**8097**	2,57E-10	**2794**	4,51E-12	**6586**	8,93E-13	**1446**	2,33E-13	**425**
HG-20	HF2C–(OCF2)2–OCF2H	25	0,913	2,70E-10	**10815**	4,82E-10	**5244**	6,93E-12	**10109**	2,89E-12	**4675**	7,60E-13	**1387**
HG-21	HF2C–OCF2CF2OCF2O	13,5	1,688	2,71E-10	**10842**	3,50E-10	**3814**	6,12E-12	**8931**	1,28E-12	**2077**	3,23E-13	**590**
HG-30	HF2C–(OCF2)3–OCF2H	25	1,637	3,73E-10	**14936**	6,65E-10	**7242**	9,57E-12	**13961**	3,98E-12	**6456**	1,05E-12	**1916**
	CF3CF2CF2OCH2CH3	0,75	0,269	5,31E-12	**212**	5,31E-12	**58**	4,58E-14	**67**	6,07E-15	**10**	4,37E-15	**8**
Fluoroxene	CF3CH2OCH=CH2	0,01	0,018	8,24E-15	**0**	8,24E-15	**0**	6,55E-17	**0**	9,25E-18	**0**	6,77E-18	**0**
	CH2FOCF2CF2H	6,2	0,333	7,45E-11	**2982**	7,75E-11	**845**	1,25E-12	**1821**	1,24E-13	**201**	6,48E-14	**118**
	CF3CFHCF2OCF2H	3,957	0,45	4,57E-11	**1829**	4,60E-11	**501**	6,08E-13	**887**	6,00E-14	**97**	3,81E-14	**70**
PFPMIE (perfluoropolymethylisopropyl)	CF3OCF(CF3)CF2OCF2(	800	0,65	1,87E-10	**7497**	8,91E-10	**9705**	5,53E-12	**8065**	6,12E-12	**9909**	6,16E-12	**11245**
	HCOOCF3	3,6	0,301	5,33E-11	**2132**	5,35E-11	**582**	6,76E-13	**987**	6,83E-14	**111**	4,43E-14	**81**
	HCOOCF2CF3	3,6	0,427	5,25E-11	**2102**	5,27E-11	**574**	6,67E-13	**973**	6,73E-14	**109**	4,37E-14	**80**
	HCOOCF2CF2CF3	2,6	0,482	3,30E-11	**1320**	3,30E-11	**359**	3,63E-13	**530**	4,01E-14	**65**	2,73E-14	**50**
	HCOOCF2CF2CF2CF3	3	0,539	3,44E-11	**1378**	3,45E-11	**375**	4,02E-13	**586**	4,27E-14	**69**	2,85E-14	**52**
	HCOOCH2CF3	0,44	0,154	2,98E-12	**119**	2,98E-12	**32**	2,48E-14	**36**	3,38E-15	**5**	2,45E-15	**4**
	HCOOCH2CH2CF3	0,3	0,134	1,59E-12	**64**	1,59E-12	**17**	1,30E-14	**19**	1,79E-15	**3**	1,30E-15	**2**
	HCOOCHFCF3	3,2	0,335	4,12E-11	**1651**	4,13E-11	**450**	4,95E-13	**723**	5,16E-14	**84**	3,42E-14	**62**
	HCOOCH(CF3)2	3,2	0,32	2,92E-11	**1171**	2,93E-11	**319**	3,51E-13	**513**	3,66E-14	**59**	2,43E-14	**44**
	CH3COOCF2CF2CF2CF3	0,06	0,152	1,85E-13	**7**	1,85E-13	**2**	1,48E-15	**2**	2,08E-16	**0**	1,52E-16	**0**
	CH3COOCF2CF2CF3	0,06	0,13	1,93E-13	**8**	1,93E-13	**2**	1,54E-15	**2**	2,17E-16	**0**	1,59E-16	**0**
	CH3COOCF2CF3	0,06	0,121	2,30E-13	**9**	2,30E-13	**3**	1,83E-15	**3**	2,58E-16	**0**	1,89E-16	**0**
	CH3COOCF3	0,06	0,088	2,32E-13	**9**	2,32E-13	**3**	1,85E-15	**3**	2,60E-16	**0**	1,90E-16	**0**
	FCOOCH3	1,8	0,064	8,36E-12	**335**	8,36E-12	**91**	8,23E-14	**120**	9,86E-15	**16**	6,90E-15	**13**
	FCOOCF2CH3	0,33	0,168	2,43E-12	**97**	2,43E-12	**26**	2,00E-14	**29**	2,75E-15	**4**	2,00E-15	**4**
	CF3COOCF2CH3	0,33	0,268	2,79E-12	**112**	2,79E-12	**30**	2,30E-14	**34**	3,16E-15	**5**	2,30E-15	**4**
	CF3COOCH2CH3	0,06	0,064	1,53E-13	**6**	1,53E-13	**2**	1,22E-15	**2**	1,72E-16	**0**	1,26E-16	**0**
	CF3COOCH2CF3	0,15	0,155	6,69E-13	**27**	6,69E-13	**7**	5,40E-15	**8**	7,54E-16	**1**	5,50E-16	**1**
	HCF2COOCH3	0,11	0,059	3,33E-13	**13**	3,33E-13	**4**	2,68E-15	**4**	3,75E-16	**1**	2,74E-16	**0**
	CF3COOCHF2	0,3	0,24	2,47E-12	**99**	2,47E-12	**27**	2,02E-14	**30**	2,79E-15	**5**	2,03E-15	**4**
	C3F7CH2OH	0,55	0,193	2,98E-12	**119**	2,98E-12	**32**	2,51E-14	**37**	3,39E-15	**5**	2,45E-15	**4**
	CHF2CHFOCF3	9,834	0,338	9,69E-11	**3881**	1,12E-10	**1214**	1,98E-12	**2891**	2,81E-13	**456**	9,53E-14	**174**
	CF3CHFCF2OCH2CH3	0,389	0,188	2,10E-12	**84**	2,10E-12	**23**	1,74E-14	**25**	2,37E-15	**4**	1,72E-15	**3**
	CF3CF2CF2OCHFCF3	67	0,58	1,98E-10	**7909**	5,93E-10	**6462**	5,55E-12	**8104**	4,28E-12	**6935**	2,39E-12	**4359**
	CHF2CF2CH2OH	0,25	0,113	1,20E-12	**48**	1,20E-12	**13**	9,82E-15	**14**	1,36E-15	**2**	9,89E-16	**2**
	CF3CHFCF2CH2OH	0,26	0,196	1,57E-12	**63**	1,57E-12	**17**	1,28E-14	**19**	1,78E-15	**3**	1,29E-15	**2**
	CF3CF2CF2CH2OH	0,33	0,159	1,48E-12	**59**	1,48E-12	**16**	1,22E-14	**18**	1,67E-15	**3**	1,21E-15	**2**
	CHF2CF2CH2OCH3	0,039	0,042	6,29E-14	**3**	6,29E-14	**1**	5,02E-16	**1**	7,07E-17	**0**	5,17E-17	**0**
perfluoro-2-methyl-3-pentanone	CF3CF2C(O)CF(CF3)2	0,0192	0,042	1,35E-14	**1**	1,35E-14	**0**	1,08E-16	**0**	1,52E-17	**0**	1,11E-17	**0**
	CF3CH2CHO	0,0055	0,007	1,82E-15	**0**	1,82E-15	**0**	1,44E-17	**0**	2,04E-18	**0**	1,49E-18	**0**
	CH2FCH2OH	0,0558	0,02	9,93E-14	**4**	9,93E-14	**1**	7,93E-16	**1**	1,12E-16	**0**	8,15E-17	**0**
	CHF2CH2OH	0,1096	0,041	3,08E-13	**12**	3,08E-13	**3**	2,48E-15	**4**	3,47E-16	**1**	2,53E-16	**0**
	CF3CH2OH	0,3205	0,102	1,85E-12	**74**	1,85E-12	**20**	1,52E-14	**22**	2,09E-15	**3**	1,52E-15	**3**

1

Fully Fluorinated Species													
	NF3	500	0,21	3,26E-10	**13069**	1,51E-09	**16434**	9,61E-12	**14023**	1,04E-11	**16885**	1,01E-11	**18517**
	SF6	3200	0,575	4,42E-10	**17678**	2,18E-09	**23744**	1,31E-11	**19080**	1,48E-11	**24044**	1,56E-11	**28480**
	SF5CF3	800	0,603	3,42E-10	**13694**	1,63E-09	**17727**	1,01E-11	**14732**	1,12E-11	**18101**	1,13E-11	**20540**
	SO2F2	36	0,2	1,69E-10	**6774**	3,72E-10	**4054**	4,54E-12	**6624**	2,53E-12	**4098**	8,93E-13	**1630**
PFC-14	CF4	50000	0,1	1,28E-10	**5121**	6,39E-10	**6959**	3,79E-12	**5533**	4,34E-12	**7028**	4,62E-12	**8438**
PFC-116	C2F6	10000	0,26	2,12E-10	**8484**	1,06E-09	**11492**	6,28E-12	**9164**	7,17E-12	**11615**	7,61E-12	**13892**
PFC-c216	c-C3F6	3000	0,42	3,14E-10	**12579**	1,55E-09	**16881**	9,31E-12	**13576**	1,06E-11	**17098**	1,11E-11	**20233**
PFC-218	C3F8	2600	0,282	1,68E-10	**6733**	8,28E-10	**9018**	4,98E-12	**7266**	5,64E-12	**9138**	5,91E-12	**10788**
PFC-318	c-C4F8	3200	0,32	1,80E-10	**7189**	8,87E-10	**9656**	5,32E-12	**7760**	6,04E-12	**9778**	6,35E-12	**11582**
PFC-31-10	C4F10	2600	0,369	1,74E-10	**6964**	8,56E-10	**9327**	5,15E-12	**7515**	5,83E-12	**9451**	6,11E-12	**11158**
PFC-41-12	C5F12	4100	0,41	1,60E-10	**6401**	7,92E-10	**8621**	4,74E-12	**6911**	5,38E-12	**8725**	5,68E-12	**10367**
PFC-51-14	C6F14	3100	0,449	1,49E-10	**5970**	7,36E-10	**8016**	4,42E-12	**6444**	5,01E-12	**8118**	5,27E-12	**9611**
PFC-61-16	C7F16	3000	0,51	1,47E-10	**5904**	7,28E-10	**7924**	4,37E-12	**6372**	4,95E-12	**8025**	5,20E-12	**9497**
	C8F18	3000	0,561	1,44E-10	**5752**	7,09E-10	**7720**	4,26E-12	**6208**	4,83E-12	**7819**	5,07E-12	**9253**
	C10F18	2000	0,524	1,27E-10	**5087**	6,23E-10	**6783**	3,76E-12	**5488**	4,25E-12	**6880**	4,43E-12	**8080**
	cis-C10F18	2000	0,566	1,37E-10	**5495**	6,73E-10	**7325**	4,06E-12	**5927**	4,59E-12	**7431**	4,78E-12	**8726**
	trans-C10F18	2000	0,492	1,19E-10	**4778**	5,85E-10	**6371**	3,53E-12	**5154**	3,99E-12	**6462**	4,16E-12	**7589**
PFC-1114	CF2=CF2	0,003	0,003	5,46E-16	**0**	5,46E-16	**0**	4,34E-18	**0**	6,13E-19	**0**	4,48E-19	**0**
PFC-1216	CF3CF=CF2	0,0134	0,02	1,01E-14	**0**	1,01E-14	**0**	8,04E-17	**0**	1,14E-17	**0**	8,30E-18	**0**
	CF2=CFCF=CF2	0,003	0,006	6,71E-16	**0**	6,71E-16	**0**	5,33E-18	**0**	7,53E-19	**0**	5,51E-19	**0**
	CF3CF2CF=CF2	0,0164	0,028	1,27E-14	**1**	1,27E-14	**0**	1,01E-16	**0**	1,43E-17	**0**	1,05E-17	**0**
	CF3CF=CFCF3	0,0849	0,078	1,87E-13	**7**	1,87E-13	**2**	1,50E-15	**2**	2,10E-16	**0**	1,53E-16	**0**

Notes:
The GTP values are calculated with a temperature impulse response function taken from Boucher and Reddy (2008). See also Supplementary Material.
RE values for CO_2, CH_4 and N_2O are taken from Table 8.5. AGWPs and AGTPs for the other components are taken from Hodnebrog et al. (2012).
* For emissions of fossil CO_2 we have used the impulse response function from Joos et al. (2012). See also Supplementary Material.
Adjustment times for N_2O and CH_4 based on Prather et al. (2012) and Prather and Hsu (2010).
A factor 1.63 is applied for methane to account for effects on tropospheric ozone (48% of the direct effect of methane) and stratospheric water vapour (15%; see Sections 8.3.3 and 8.5.1).
§ Preliminary adjustments of metric values for fossil fuel methane are based on Boucher et al. (2009).

Uncertainties in metric values for all non-CO_2 gases are estimated to be of the order of 20–40% for GWP100 and 60–75% for GTP100 based on uncertainty in the IRF of CO_2 and the RE and lifetime of the gases, and in addition climate sensitivity and ocean heat uptake for GTP. Inclusion of additional effects that are less well-quantified increases the range of potential metric values further, though in most cases causing systematic changes (i.e., the sign is known but uncertainty in magnitude is large). There is an estimated 20% increase in the GWPs of CH_4 and N_2O when carbon-cycle responses to the temperature changes they induce are included (analogous to the treatment of CO_2), and a 100% increase for the GTP100 of methane. GWPs and GTPs for methane increase by roughly a factor of two when ozone-CO_2 impacts are included. Oxidant-sulfate interactions may also increase the GWP100 of methane by up to 30%.

Table 8.A.2. Halocarbon indirect GWPs from ozone depletion using the EESC-based method described in WMO (2010), adapted from Daniel et al. (1995). A radiative forcing of –0.22 W m^2 relative to preindustrial times is used (see Section 8.3.3). The stated uncertainties in the indirect GWPs reflect the uncertainty in stratospheric ozone radiative forcing of 0.05 W m^2 (Section 8.3.3).

Gas	Indirect GWP (100)		
CFC-11	–3475	±	789
CFC-12	–2773	±	630
CFC-113	–2842	±	645
CFC-114	–1216	±	276
CFC-115	–298	±	68
HCFC-22	–125	±	28
HCFC-123	–50	±	11
HCFC-124	–61	±	14
HCFC-141b	–328	±	75
HCFC-142b	–206	±	47
HCFC-225ca	–54	±	12
HCFC-225cb	–79	±	18

CH_3CCl_3	–428	±	97
CCl_4	–2761	±	627
CH_3Br	–1703	±	387
Halon-1211	–24691	±	5605
Halon-1301	–58709	±	13327
Halon-2402	–41774	±	9483

Table 8.A.3: GWP and GTP for NO_X from surface sources for time horizons of 20 and 100 years from the literature. All values are on a per kg N basis. Uncertainty for numbers from Fry et al. (2012) and Collins et al. (2012) refer to 1SD. For the reference gas CO2, RE and IRF from AR4 are used in the calculations. [PLACEHOLDER FOR FINAL DRAFT: Scaling factor for updating to AR5 values will be given in the final draft].

	GWP		**GTP**	
	H = 20	**H =100**	**H = 20**	**H =100**
NO_X East Asia [a]	3.4 (±41.5)	–6.3 (±13.7)	–55.6 (±23.8)	–1.3 (±2.1)
NO_X EU+N-Africa [a]	–41.3 (±17.8)	–16.2 (±6.7)	–48.0 (±14.9)	–2.5 (±1.3)
NO_X North America [a]	–5.6 (±30.7)	–9.3 (±11.7)	–61.9 (±27.8)	–1.7 (±2.1)
NO_X South Asia [a]	–46.6 (±79.7)	–27.4 (±27.8)	–124.6 (±67.4)	–4.6 (±5.1)
NO_X 4 above regions [a]	–18.9 (±33.2)	–12.6 (±12.0)	–62.1 (±26.2)	–2.2 (±2.1)
Mid-Latitude NOx [c]	–43 to +23	–18 to +1.6	–55 to –37	–29 to –0.02
Tropical NOx [c]	43 to 130	–28 to –10	–260 to –220	–6.6 to –5.4
NO_X global [b]	19	–11	–87	–2.9
NO_X global [d]	–108 ± 35 –335 ± 110 –560 ± 279	–31 ± 10 –95 ± 31 –159 ± 79		

Notes:
(a) Fry et al. (2012) and Collins et al. (2012)
(b) Fuglestvedt et al. (2010); based on Wild et al. (2001)
(c) Fuglestvedt et al. (2010)
(d) Shindell et al. (2009). Three values are given: First, without aerosols, second, direct aerosol effect included (sulfate and nitrate), third, direct and indirect aerosol effects included. Uncertainty ranges from Shindell et al. (2009) are given for 95% confidence levels.

Table 8.A.4: GWP and GTP for CO for time horizons of 20 and 100 years from the literature. Uncertainty for numbers from Fry et al. (2012) and Collins et al. (2012) refer to 1SD. For the reference gas CO_2, RE and IRF from AR4 are used in the calculations. [PLACEHOLDER FOR FINAL DRAFT: Scaling factor for updating to AR5 values will be given in the final draft].

	GWP		**GTP**	
	H = 20	**H = 100**	**H = 20**	**H = 100**
CO East Asia [a]	5.5 (±1.8)	1.8 (±0.6)	3.5(±1.3)	0.26(±0.12)
CO EU+N-Africa [a]	5.0 (±1.3)	1.6 (±0.4)	3.2(±1.2)	0.24(±0.11)
CO North America [a]	5.7 (±1.8)	1.9 (±0.6)	3.7(±1.3)	0.27(±0.12)
CO South Asia [a]	5.8 (±1.1)	1.8 (±0.4)	3.4(±1.0)	0.27(±0.10)
CO 4 regions above [a]	5.5 (±1.5)	1.8 (±0.5)	3.5(±1.2)	0.26(±0.11)
CO global [b]	6 to 9.3	2 to 3.3	3.7 to 6.1	0.29 to 0.55
CO global [c]	7.8 ± 2.0 11.4 ± 2.9 18.6 ± 8.3	2.2 ± 0.6 3.3 ± 0.8 5.3 ± 2.3		

Notes:
(a) Fry et al. (2012) and Collins et al. (2012)
(b) Fuglestvedt et al. (2010)
(c) Shindell et al. (2009). Three values are given: First, without aerosols, second, direct aerosol effect included, third, direct and indirect aerosol effects included. Uncertainty ranges from Shindell et al. (2009) are given for 95% confidence levels.

Table 8.A.5: GWP and GTP for VOC for time horizons of 20 and 100 years from the literature. Uncertainty for numbers from Fry et al. (2012) and Collins et al. (2012) refer to 1SD. For the reference gas CO_2, RE and IRF from AR4 are used in the calculations. [PLACEHOLDER FOR FINAL DRAFT: Scaling factor for updating to AR5 values will be given in the final draft].

	GWP		GTP	
	H = 20	**H = 100**	**H = 20**	**H = 100**
VOC East Asia [a]	16.5 (±6.8)	5.1 (±2.3)	8.4 (±4.6)	0.7 (±0.4)
VOC EU+N-Africa [a]	18.2 (±8.0)	5.7 (±2.7)	9.5 (±6.5)	0.8 (±0.5)
VOC North America [a]	16.4 (±8.1)	5.1 (±2.6)	8.6 (±6.4)	0.7 (±0.5)
VOC South Asia [a]	28.2 (±9.3)	8.9 (±3.3)	15.7 (±5.0)	1.3 (±0.5)
VOC 4 regions above	18.9 (±7.7)	5.9 (±2.6)	10.0 (±5.7)	0.9 (±0.5)
VOC global [b]	14	4.5	7.5	0.66

Notes:
(a) Fry et al. (2012) and Collins et al. (2012)
(b) Fuglestvedt et al. (2010) based on Collins et al. (2002)

Table 8.A.6: GWP and GTP from the literature for BC and OC for time horizons of 20 and 100 years. For the reference gas CO_2, RE and IRF from AR4 are used in the calculations. [PLACEHOLDER FOR FINAL DRAFT: Scaling factor for updating to AR5 values will be given in the final draft].

	GWP		GTP	
	H = 20	**H = 100**	**H = 20**	**H = 100**
BC global [c]	3600 (280–7200)	1000 (80–2000)	1000 (–50–2500)	140 (–7–340)
BC (4 regions) [d]	1255 ± 688	360 ± 196	420 ± 190	56 ± 25
BC global [a]	1,600	460	470	64
BC dir+albedo Global [b]	2,900 ± 1,500	830 ± 440		
OC global [a]	–240	–69	–71	–10
OC global [b]	–160 (–60, –320)	–46 (–18, –92)		

Notes:
(a) Fuglestvedt et al. (2010)
(b) Bond et al. (2011). Uncertainties for OC are asymmetric and are presented as ranges.
(c) Bond et al. (2012)
(d) Collins et al. (2012). The 4 regions are East Asia, EU + North Africa, North America and South Asia (as also given in Fry et al., 2012). Only direct effect is included.

Table8.A.7: GWPs and GTPs for NO_X, BC, OC and SO_2 from various sectors (metrics for SO_2 are given on SO_2 basis, while for NO_X they are given on N basis). For the reference gas CO_2, RE and IRF from AR4 are used in the calculations. [PLACEHOLDER FOR FINAL DRAFT: Scaling factor for updating to AR5 values will be given in the final draft].

	GWP		GTP	
	H = 20	**H = 100**	**H = 20**	**H = 100**
Aviation				
NO_X [a]	92 to 338	–21 to 67	–396 to –121	–5.8 to 7.9
NO_X [b]	120 to 470	–2.1 to 71	–590 to –200	–9.5 to 7.6
NO_X [h]	415	75	–239	8.6
Shipping				
NO_X [b]	–76 to –31	–36 to –25	–190 to –130	–6.1 to –42
NO_X shipping [c]	–107	–73	–135	–30
Shipping SO_2 (direct) [b]	–150 to –37	–43 to –11	–44 to –11	–6.1 to –1.5
Shipping SO_2 (indirect) [b]	–1,600 to –760	–440 to –220	–450 to –220	–63 to –31
SO_2, Arctic shipping [e]	–65	–18		
Arctic shipping SO_2 (indirect) [e]	–283	–80		

OC (Shipping, Arctic) [e]	–209	–59
BC direct (shipping, Arctic) [e]	2,816	801
BC snow (shipping, Arctic) [e]	1,056	300
Energy Related		
BC direct + albedo [g]	2,800 ± 1,800	790 ± 530
OC Energy related [g]	–100 (–40,–210)	–30 (–12, –60)
Industrial/Power BC, Asia [f]	3,260	910
Household BC, Asia [f]	2,680	750
Transport BC, Asia [f]	2,640	740
Transport BC, N America [f]	3,900	1,090
Household OC, Asia [f]	–260	–72
Transport OC, Asia [f]	–180	–50
Ind/Power SO_2, Asia [f]	–106 (direct)	–30 (direct)
Ind./Power SO_2, N-America[f]	–215 (direct)	–60 (direct)
Global coalfired power, NO_X [d]	20	
Global coalfired power, SO_2 [d]	–189 (direct) –377 (dir+ind)	–53 (direct) –106 (dir + ind)
Petroleum Production		
BC direct (Arctic emissions) [e]	2,369	673
BC snow (Arctic emissions) [e]	4,104	1,166
SO_2, Arctic petroleum [e]	–64	–18
Arctic petroleum SO_2 [e] (indir)	–48	–14
OC (Arctic emissions) [e]	–152	–13
Open Biomass		
BC dir + albedo [g]	3,100 ± 1,300	880 ± 370
OC Open biomass [g]	–180 (–70, –360)	–53 (–20, –100)

Notes:
(a) Myhre et al. (2011)
(b) Fuglestvedt et al. (2010)
(c) Collins et al. (2010)
(d) Shindell & Faluvegi (2010)
(e) Ødemark et al. (2011)
(f) Shindell et al. (2008)
(g) Bond et al. (2011)
(h) Köhler et al. (2012)

Chapter 8: Anthropogenic and Natural Radiative Forcing

Coordinating Lead Authors: Gunnar Myhre (Norway), Drew Shindell (USA)

Lead Authors: François-Marie Bréon (France), William Collins (UK), Jan Fuglestvedt (Norway), Jianping Huang (China), Dorothy Koch (USA), Jean-François Lamarque (USA), David Lee (UK), Blanca Mendoza (Mexico), Teruyuki Nakajima (Japan), Alan Robock (USA), Graeme Stephens (USA), Toshihiko Takemura (Japan), Hua Zhang (China)

Contributing Authors: Olivier Boucher (France), Stig B. Dalsøren (Norway), John Daniel (USA), Piers Forster (UK), Claire Granier (France), Joanna Haigh (UK), Jed O. Kaplan (Switzerland), Brian, O'Neill (USA), Glen Peters (Norway), Julia Pongratz (Germany), Venkatachalam Ramaswamy (USA), Leon Rotstayn (Australia), Paul Young (USA), Jean-Paul Vernier (USA)

Review Editors: Daniel Jacob (USA), A.R. Ravishankara (USA), Keith Shine (UK)

Date of Draft: 5 October 2012

Notes: TSU Compiled Version

Figures

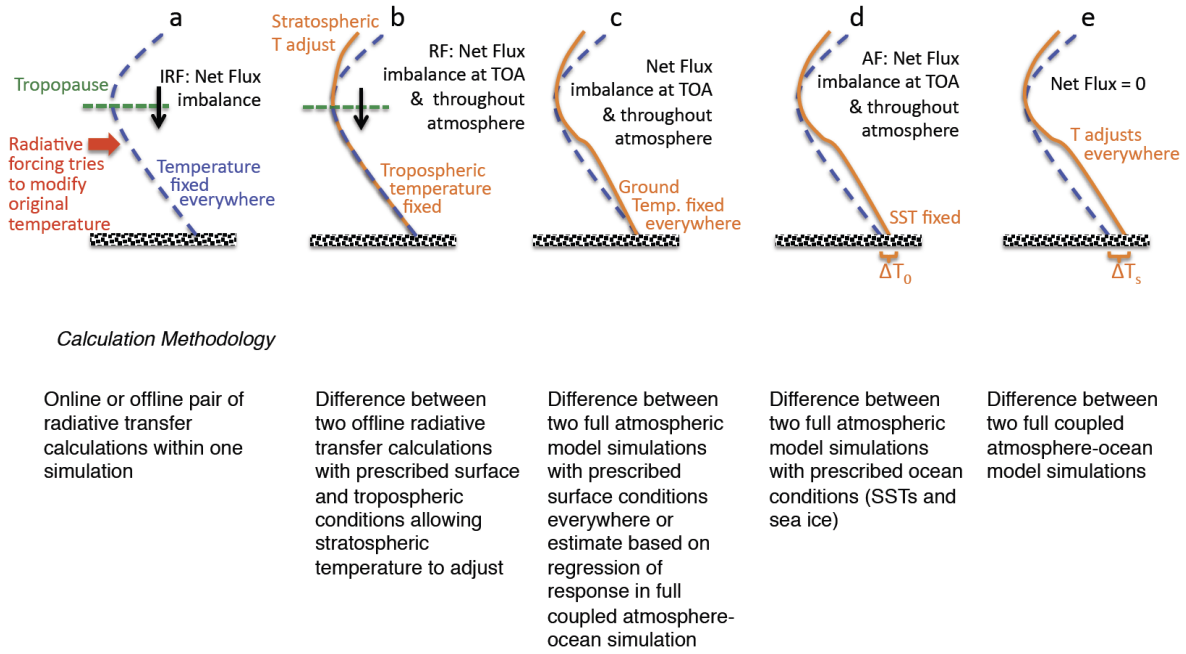

Figure 8.1: Cartoon comparing (a) instantaneous RF, (b) RF, which allows stratospheric temperature to adjust, (c) flux change when the surface temperature is fixed over the whole Earth, (d) AF, the adjusted forcing which allows atmospheric and land temperature to adjust while ocean conditions are fixed, and (e) the equilibrium response to the climate forcing agent. The methodology for calculation of each type of forcing is also outlined. dT_o represents the land temperature response, while dT_s is the full surface temperature response. Updated from Hansen et al. (2005).

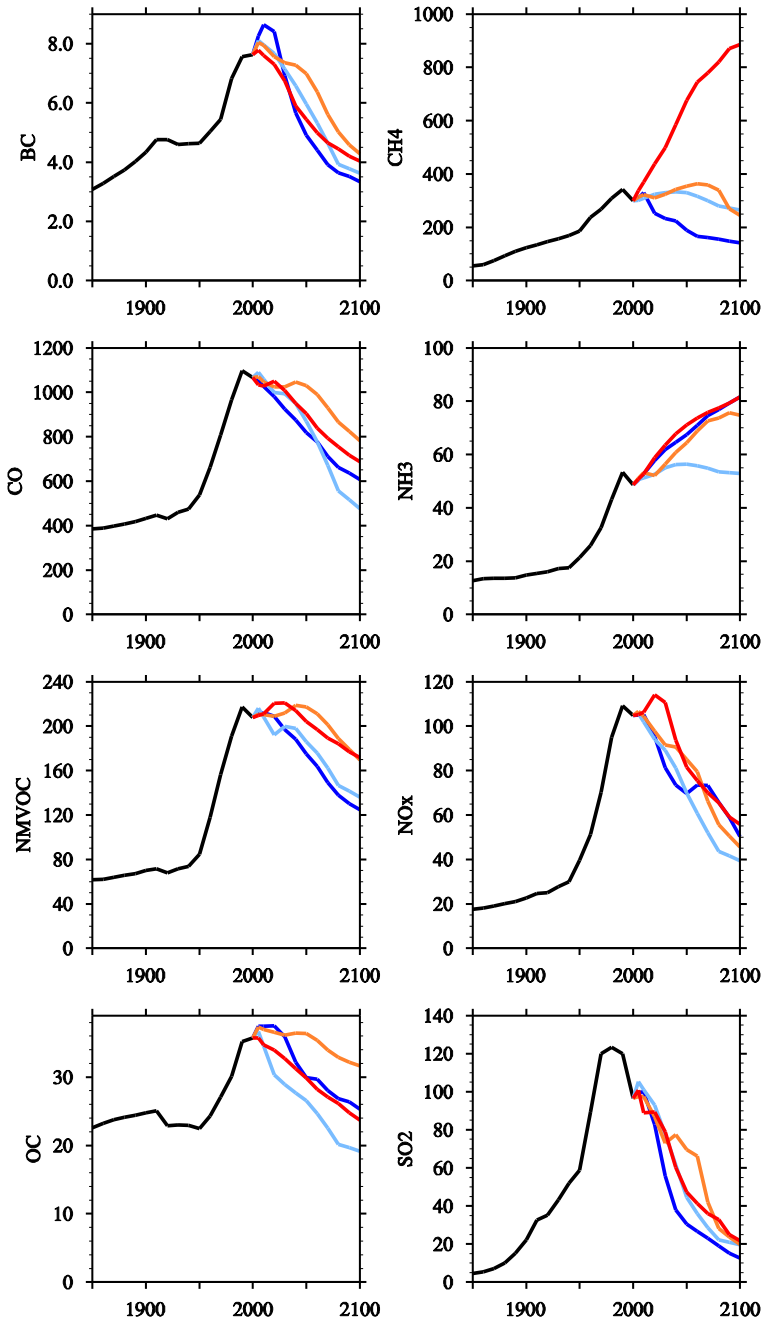

Figure 8.2: Time evolution of global anthropogenic and biomass burning emissions 1850–2100 used in CMIP5/ACCMIP following each RCP; blue (RCP2.6), light blue (RCP4.5), orange (RCP6.0) and red (RCP8.5). BC stands for black carbon (in Tg(C) yr^{-1}), OC for organic carbon (in Tg(C) yr^{-1}), NMVOC for non-methane volatile organic compounds (in Tg(C) yr^{-1}) and NO_X for nitrogen oxides (in Tg(NO_2) yr^{-1}). Other panels are in Tg(species) yr^{-1}. Historical (1850–2000) values are from (Lamarque et al., 2010). RCP values are from (van Vuuren et al., 2011). Regional estimates for Africa, China, India, North America, South America and Western Europe are shown in Supplementary Material.

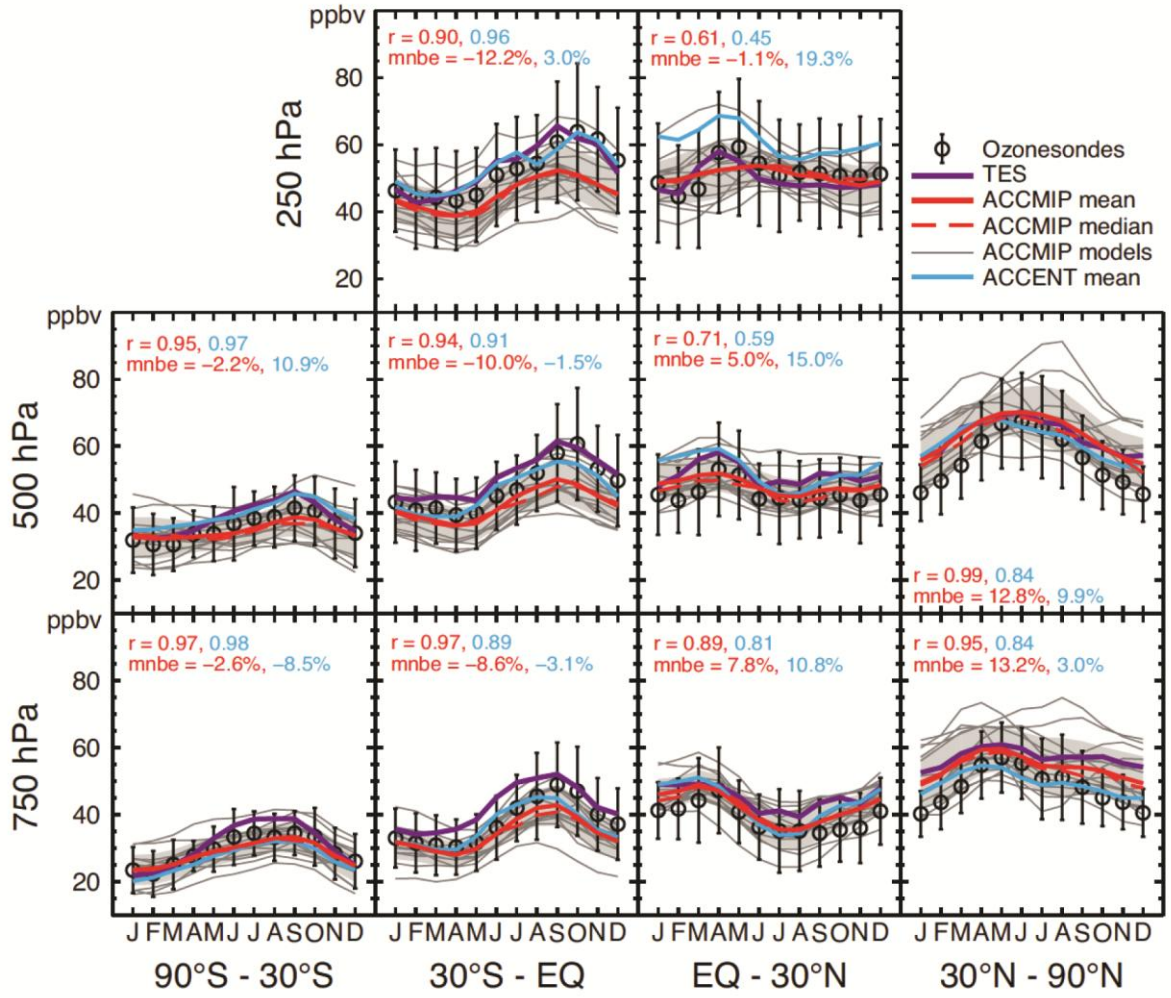

Figure 8.3: Comparisons between observations and simulations for the monthly mean ozone for ACCMIP results (Young et al., 2012). ACCENT refers to the model results in (Stevenson et al., 2006).

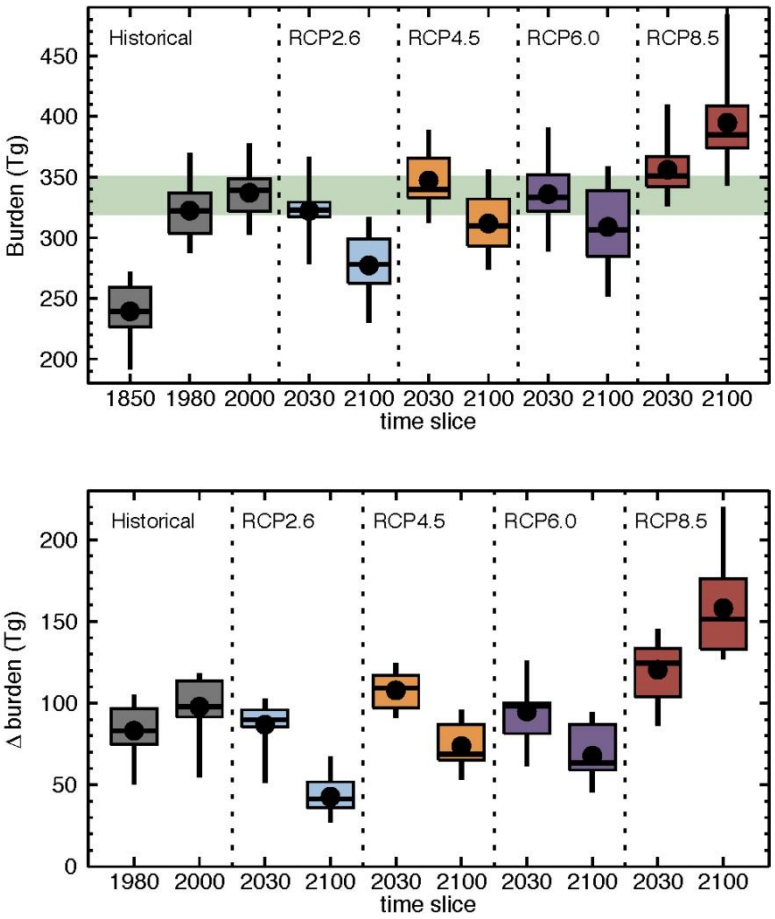

Figure 8.4: (a) Time evolution of global tropospheric ozone burden (in $Tg(O_3)$) from 1850 to 2100 from ACCMIP results. In bottom panel (b), time evolution of global tropospheric ozone burden (in $Tg(O_3)$) differenced to 1850. The box, whiskers, line and dot show the interquartile range, full range, median and mean burdens and differences, respectively. The green line indicates the range of observational estimates (Table 8.2). Adapted from Young et al. (2012).

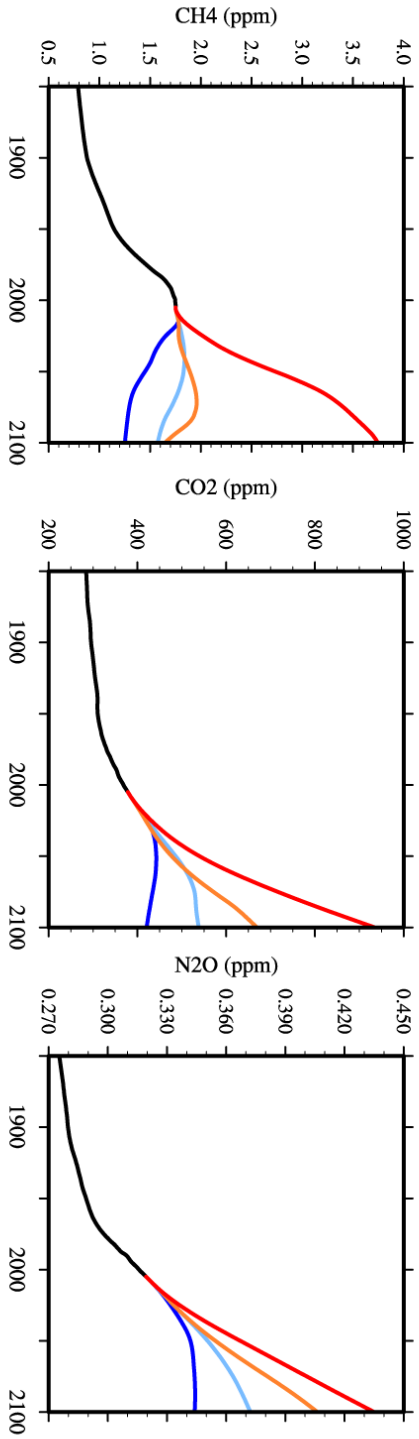

Figure 8.5: Time evolution of global-averaged mixing ratio of long-lived species1850–2100 following each RCP; blue (RCP2.6), light blue (RCP4.5), orange (RCP6.0) and red (RCP8.5). Based on Meinshausen et al. (2011b).

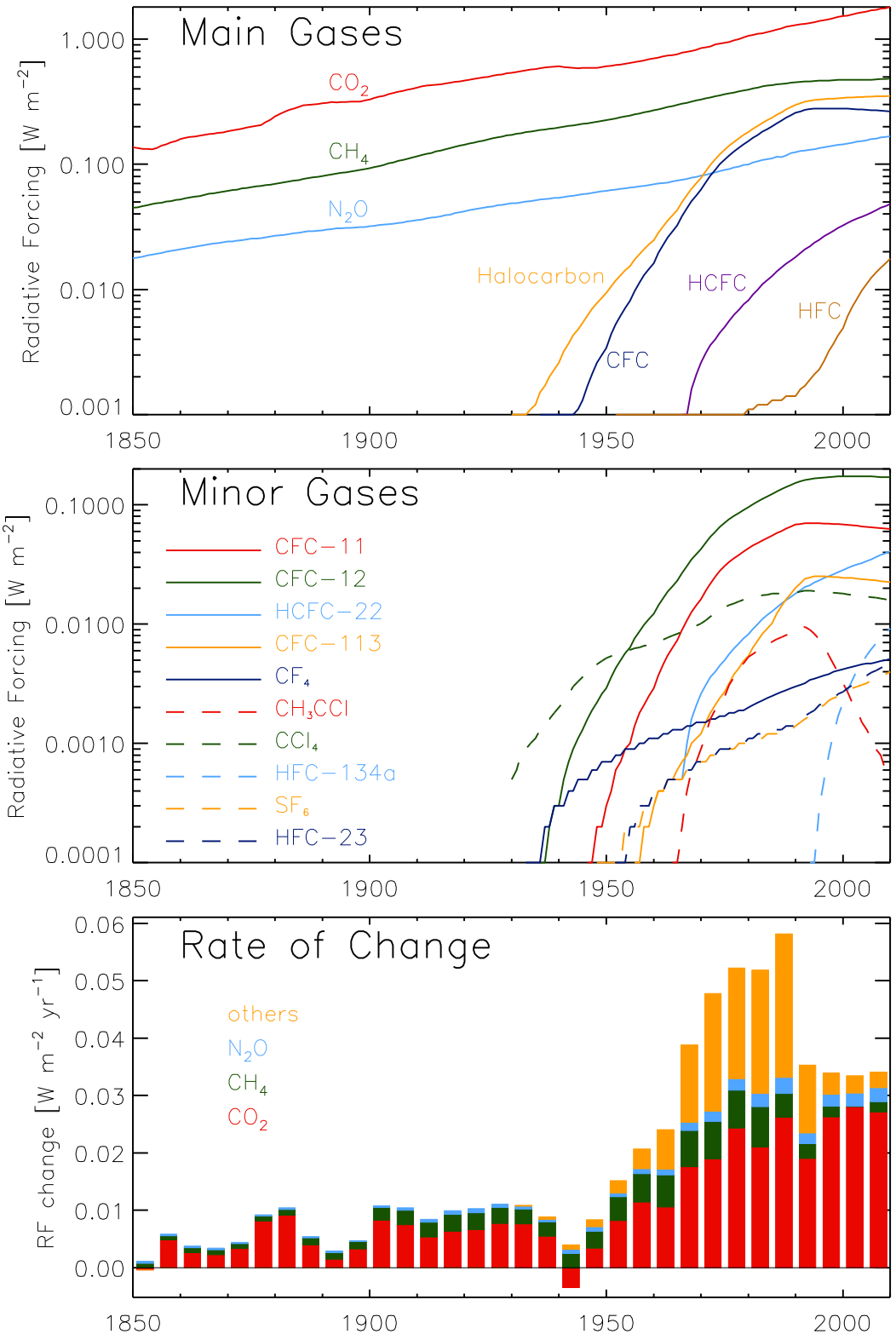

Figure 8.6: (a) Radiative forcing from the major well-mixed greenhouse gases and groups of halocarbons from 1850 to 2011 (data currently from NASA GISS http://data.giss.nasa.gov/modelforce/ghgases/). (b) Radiative forcing from the minor well-mixed greenhouse gases from 1850 to 2011. (c) Rate of change in forcing from the major well-mixed greenhouse gases and groups of halocarbons from 1850 to 2011.

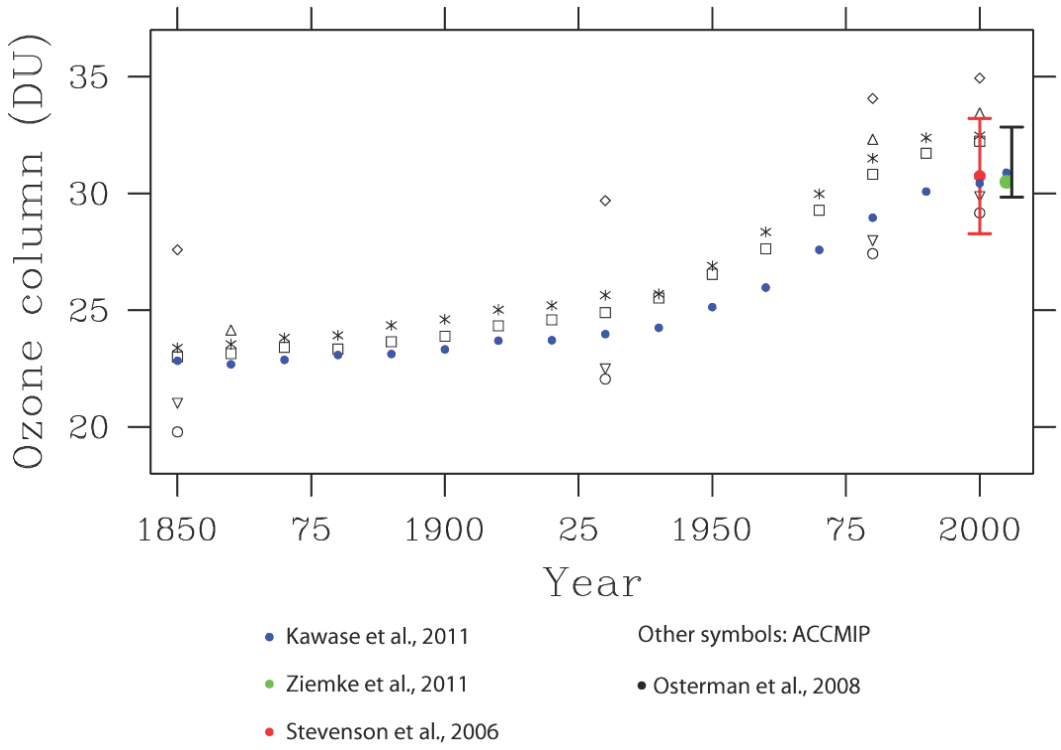

Figure 8.7: Time evolution of tropospheric ozone column (in DU) from 1850 to 2005 from ACCMIP results and (Kawase et al., 2011). The OMI-MLS (Ziemke et al., 2011) and TES (Osterman et al., 2008) satellite-based climatologies are also shown, along with the ACCENT-AR4 results.

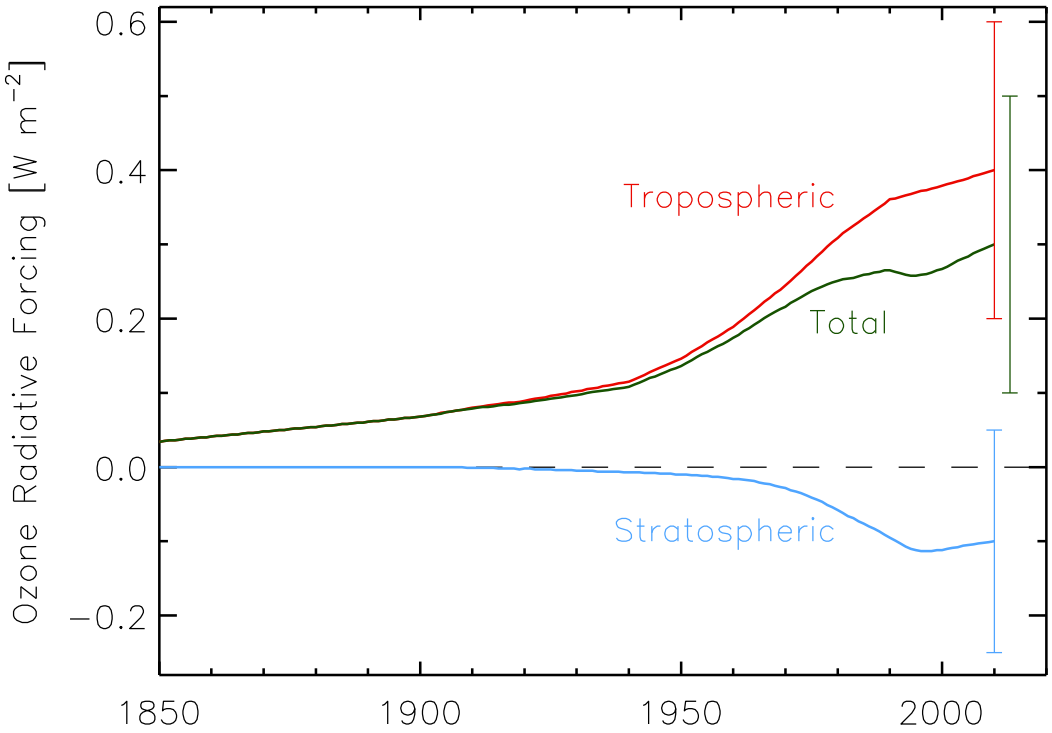

Figure 8.8: Time evolution of the radiative forcing from tropospheric and stratospheric ozone from 1850 to 2010. Tropospheric ozone data are from Skeie et al. (2011a) scaled to give 0.40 W m^{-2} at 2010, stratospheric ozone RF follow Effective Equivalent Stratospheric Chlorine (Daniel et al., 2010) scaled to give –0.10 W m^{-2} at 2010.

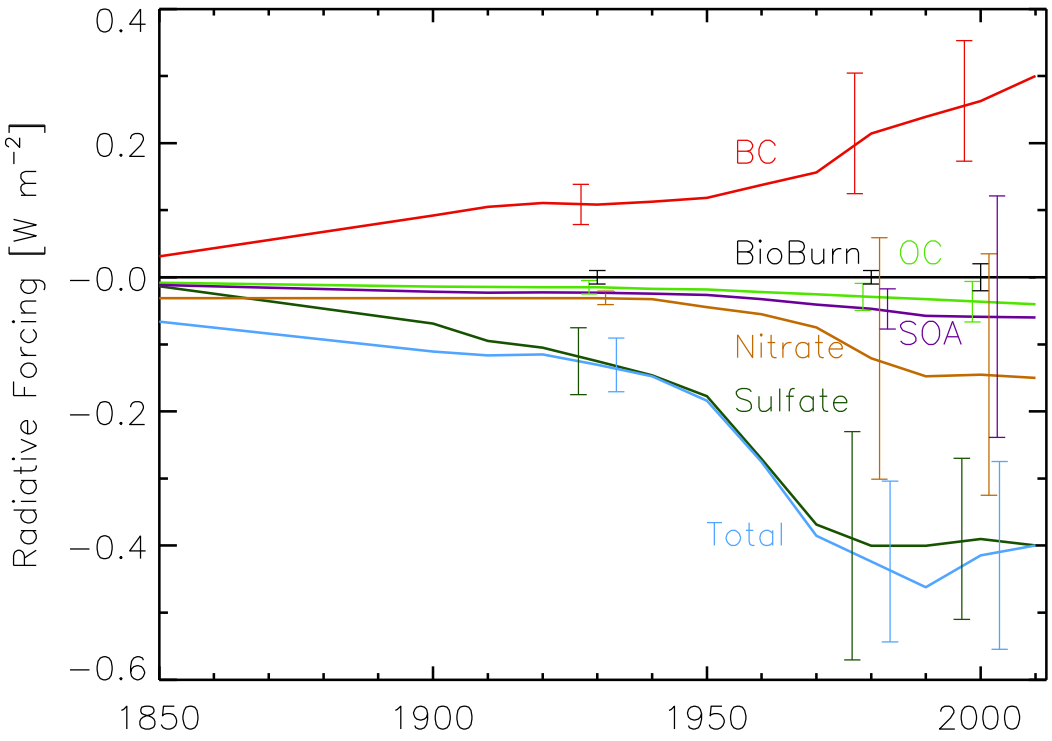

Figure 8.9: Time evolution of RF of the aerosol-radiation interaction (total as well as by components). Multi-model results for 1930, 1980, and 2000 from ACCMIP are combined with higher temporal results from the GISS-E2 and Oslo-CTM2 models. Solid lines show the mean of individual model results and one standard deviation among the ACCMIP models are shown for 1930, 1980 and 2000. The 2010 values have been scaled to the best estimates given in Table 8.7. Note that time evolution for mineral dust is not included and the total is estimated based on the total of the six other aerosol components.

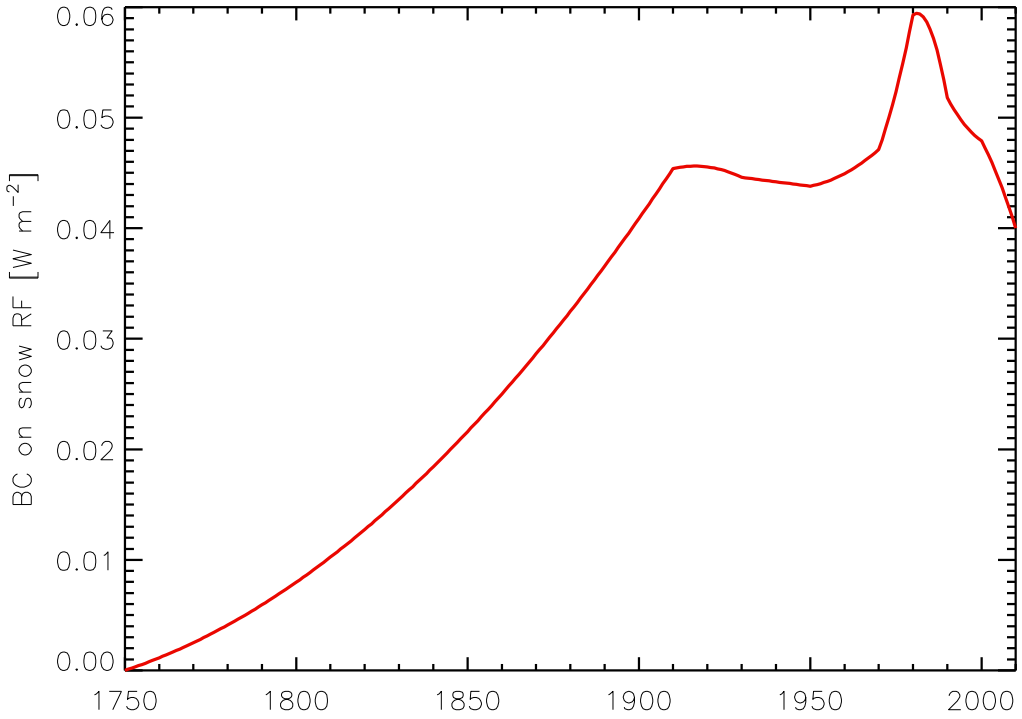

Figure 8.10: Time evolution of RF due to BC on snow and ice. The simulations are mainly based on the ACCMIP multi-model study by Lee et al. for the years 1850, 1930, 1980, and 2000. Additional simulations with one model were performed for the years 1750, 1950, 1970, 1990 and 2010. The 2010 value is scaled to the AR5 best estimate (from Lee et al., 2012).

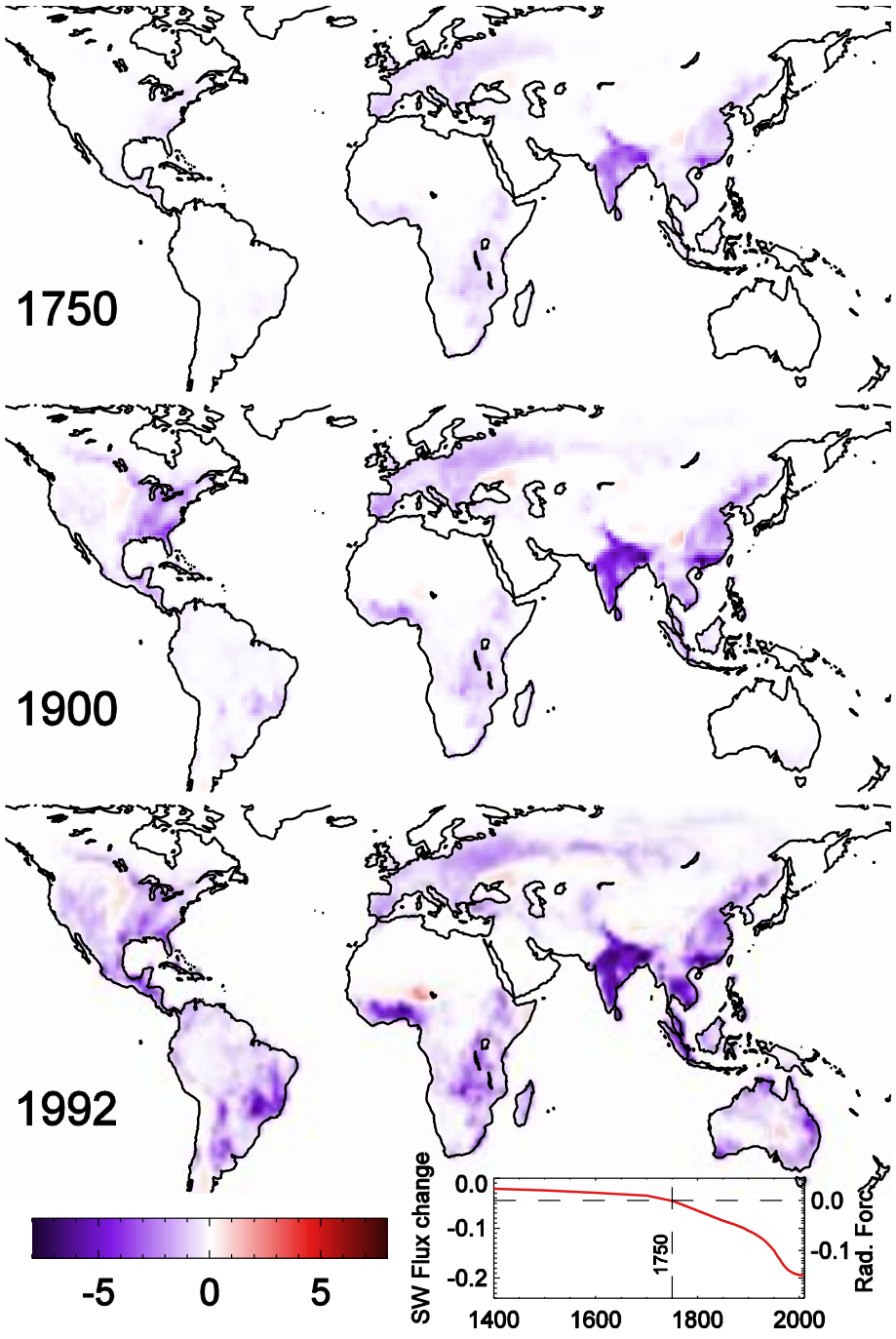

Figure 8.11: Change in TOA SW flux [W m^{-2}] following the change in albedo as a result of anthropogenic Land Use Change for three periods (1750, 1900 and 1992 from top to bottom). By definition, the RF is with respect to 1750. The lower right inset shows the globally averaged impact of the surface albedo change to the TOA SW flux (left scale) as well as the corresponding RF (right scale) after normalization to the 1750 value. Based on simulations by Pongratz et al. (2009).

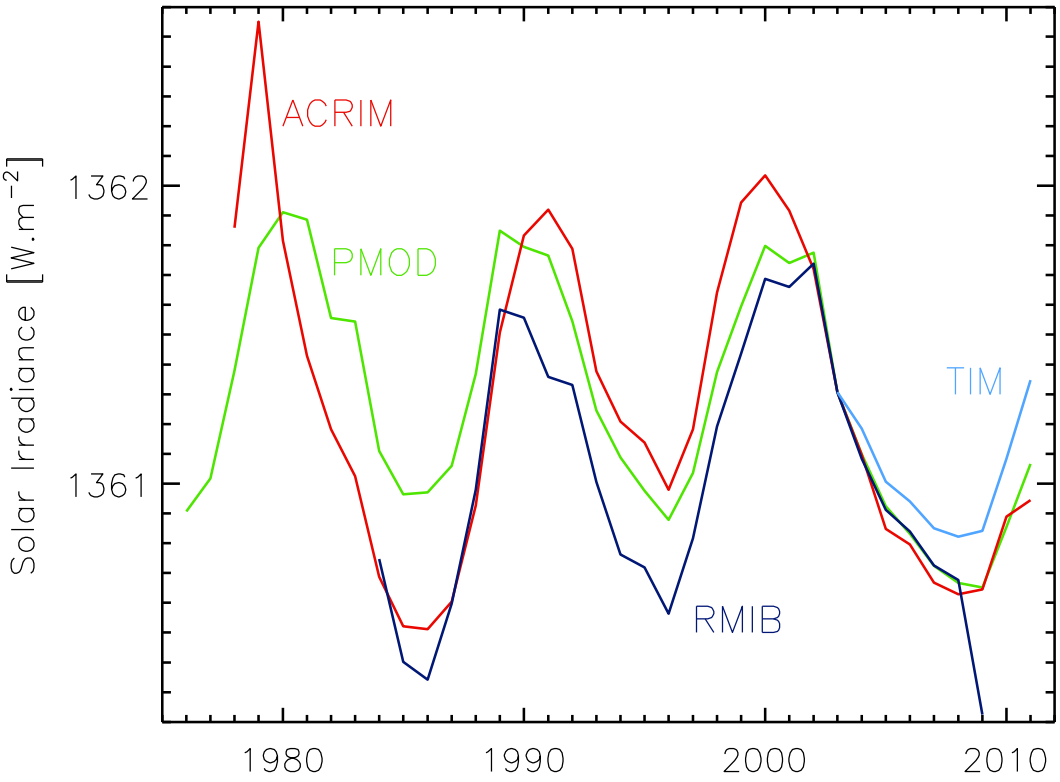

Figure 8.12: Annual average **c**omposites of measured Total Solar Irradiance: The Active Cavity Radiometer Irradiance Monitor (ACRIM) (Willson and Mordvinov, 2003), the Physikalisch-Meteorologisches Observatorium Davos (PMOD) (Frohlich, 2006) and the Royal Meteorological Institute of Belgium (RMIB) (Dewitte et al., 2004). These composites are matched at the year 2003 to the annual average of the Total Solar Irradiance Monitor (TIM) (Kopp and Lean, 2011) measurements that are also shown.

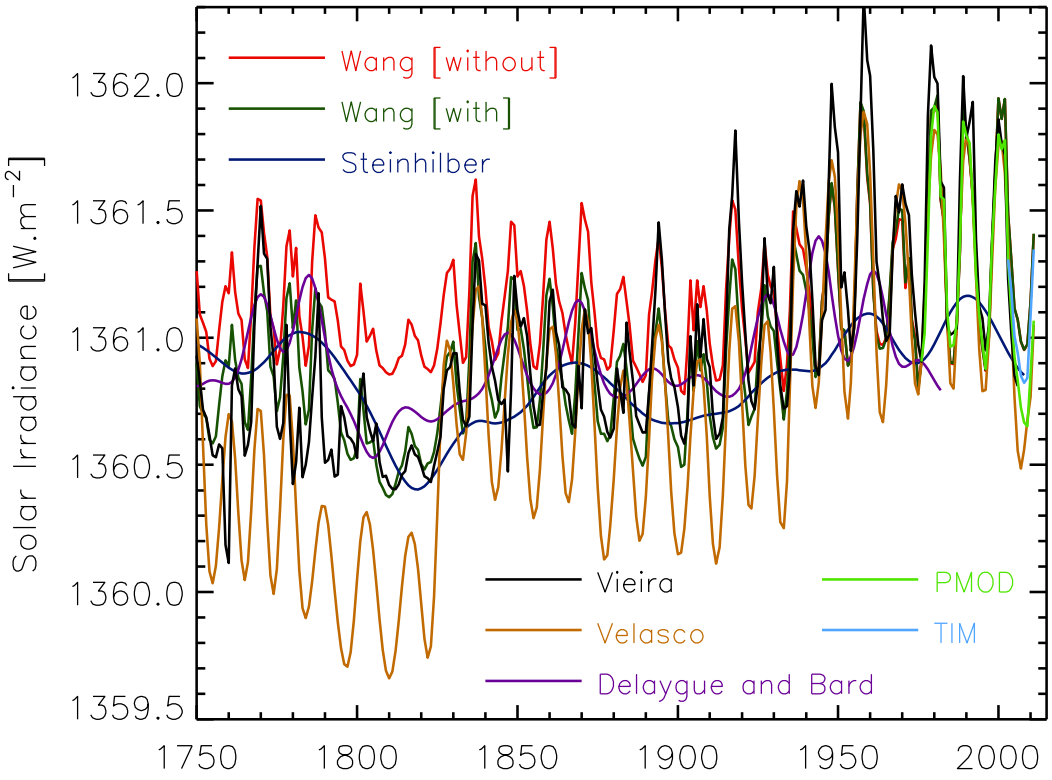

Figure 8.13: Reconstructions of Total Solar Irradiance between 1750 and 1975: Wang et al. (2005) with and without an independent change in the background level of irradiance (annual resolution series), Steinhilber et al. (2009; 5-year time resolution series), Vieira et al. (2011; annual resolution series), Delaygue and Bard (2011; 5-year time resolution series) and Velasco-Herrera et al. (2012; annual resolution series). The series are set to match PMOD at the year 1976 (PMOD is already matched to TIM at the year 2003).

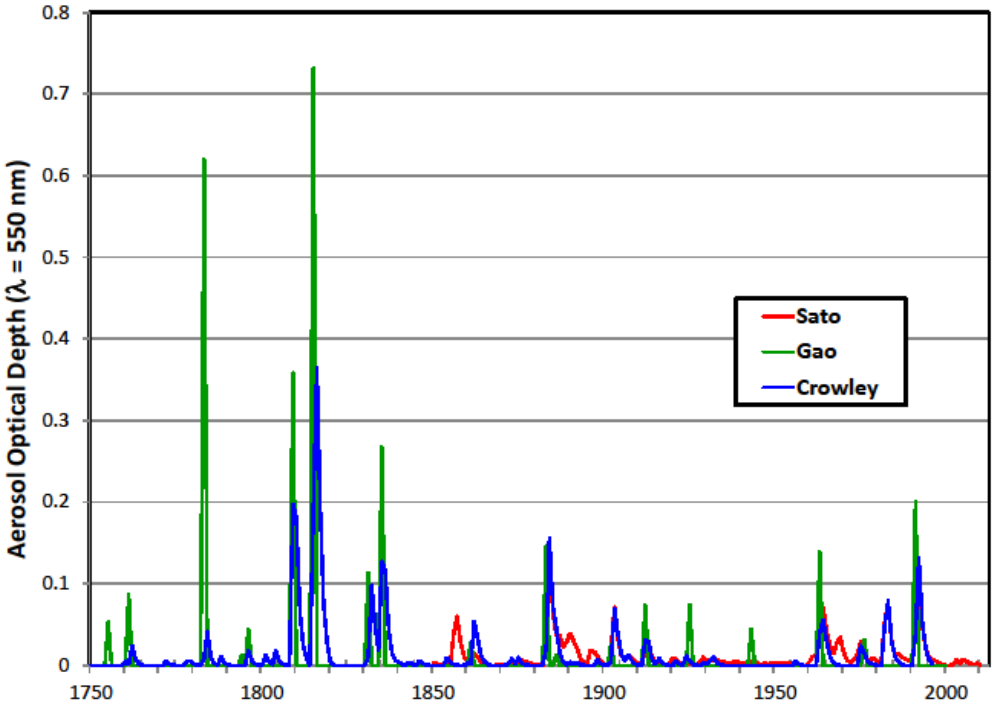

Figure 8.14: Two volcanic reconstructions of aerosol optical depth (at 550 μm) as developed for the Paleoclimate Model Intercomparison Project (top), with a comparison to the updated estimates of Sato et al. (1993). Updated from Schmidt et al. (2011).

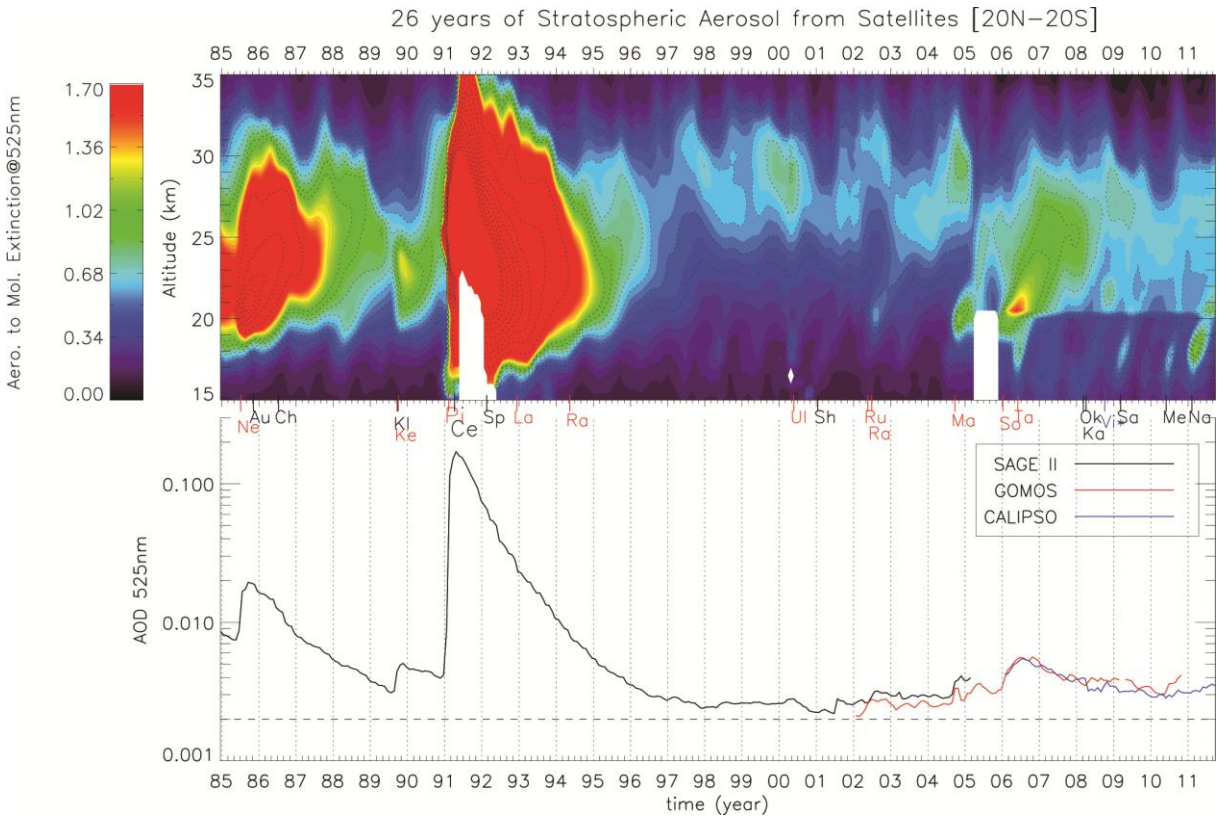

Figure 8.15: (a) Monthly mean extinction ratio (525 nm) profile evolution in the tropics [20°N–20°S] from January 1985 to June 2010 derived from (left) SAGE II extinction in 1985–2005 and (right) CALIOP scattering ratio in 2006–2011, after removing clouds below 18 km based on their wavelength dependence (SAGE II) and depolarization properties (CALIOP) compared to aerosols. Black contours represent the extinction ratio in log-scale from 0.1 to 100. The position of each volcanic eruption occurring during the period is displayed with its first two letters on the horizontal axis, where tropical eruptions are noted in red. The eruptions were Nevado del Ruiz (Ne), Augustine (Au), Chikurachki (Ch), Kliuchevskoi (Kl), Kelut (Ke), Pinatubo (Pi), Cerro Hudson (Ce), Spur (Sp), Lascar (La), Rabaul (Ra), Ulawun (Ul), Shiveluch (Sh), Ruang (Ru), Reventador (Ra), Manam (Ma), Soufrière Hills (So), Tavurvur (Ta), Chaiten (Ch), Okmok (Ok), Kasatochi (Ka), Fire/Victoria (Vi*), Sarychev (Sa), Merapi (Me), Nabro (Na). Updated from Figure 1 from Vernier et al. (2011). (b) Mean stratospheric Aerosol Optical Depth in the tropics [20°N–20°S] between 20 and 30 km since 1985 from the Stratospheric Aerosol and Gas Experiment (SAGE) II (black line), the Global Ozone Monitoring by Occultation of Stars (GOMOS) (red line), and CALIOP (blue line). Updated from Figure 5, Vernier et al. (2011).

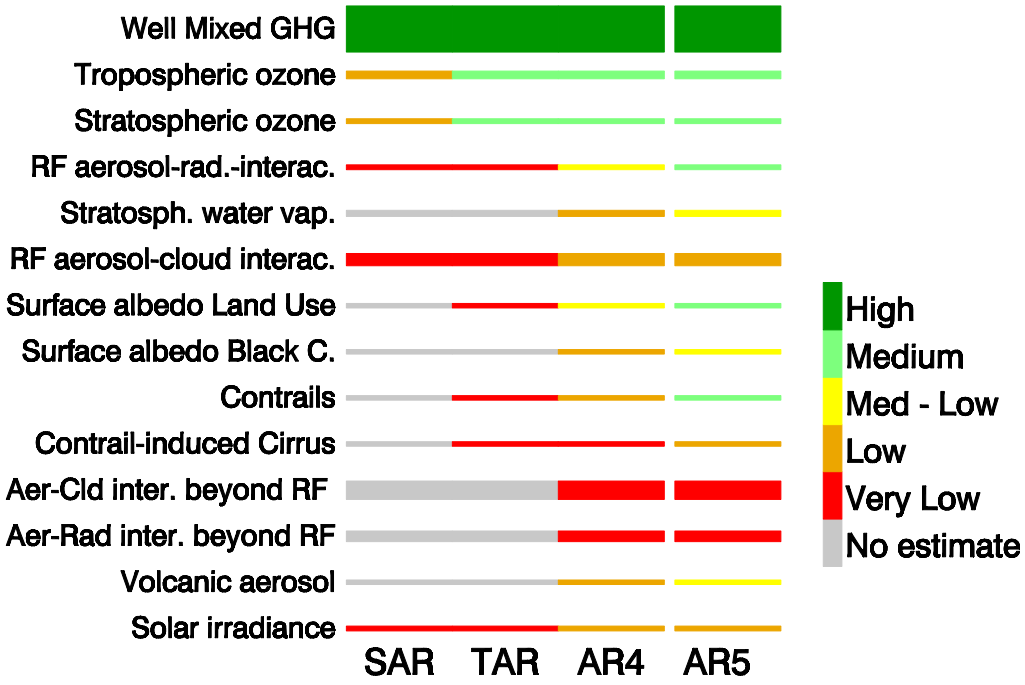

Figure 8.16: Level of scientific understanding (LOSU) of the RF mechanisms in the 4 last IPCC assessments. The LOSU terminology is not regularly used in AR5, but for comparison with previous IPCC assessments the confidence level is converted approximately to LOSU. The thickness of the bars represents the relative magnitude of the current RF (with a minimum value for clarity of presentation). LOSU for the RF mechanisms was not available in the first IPCC Assessment (Houghton et al., 1990).

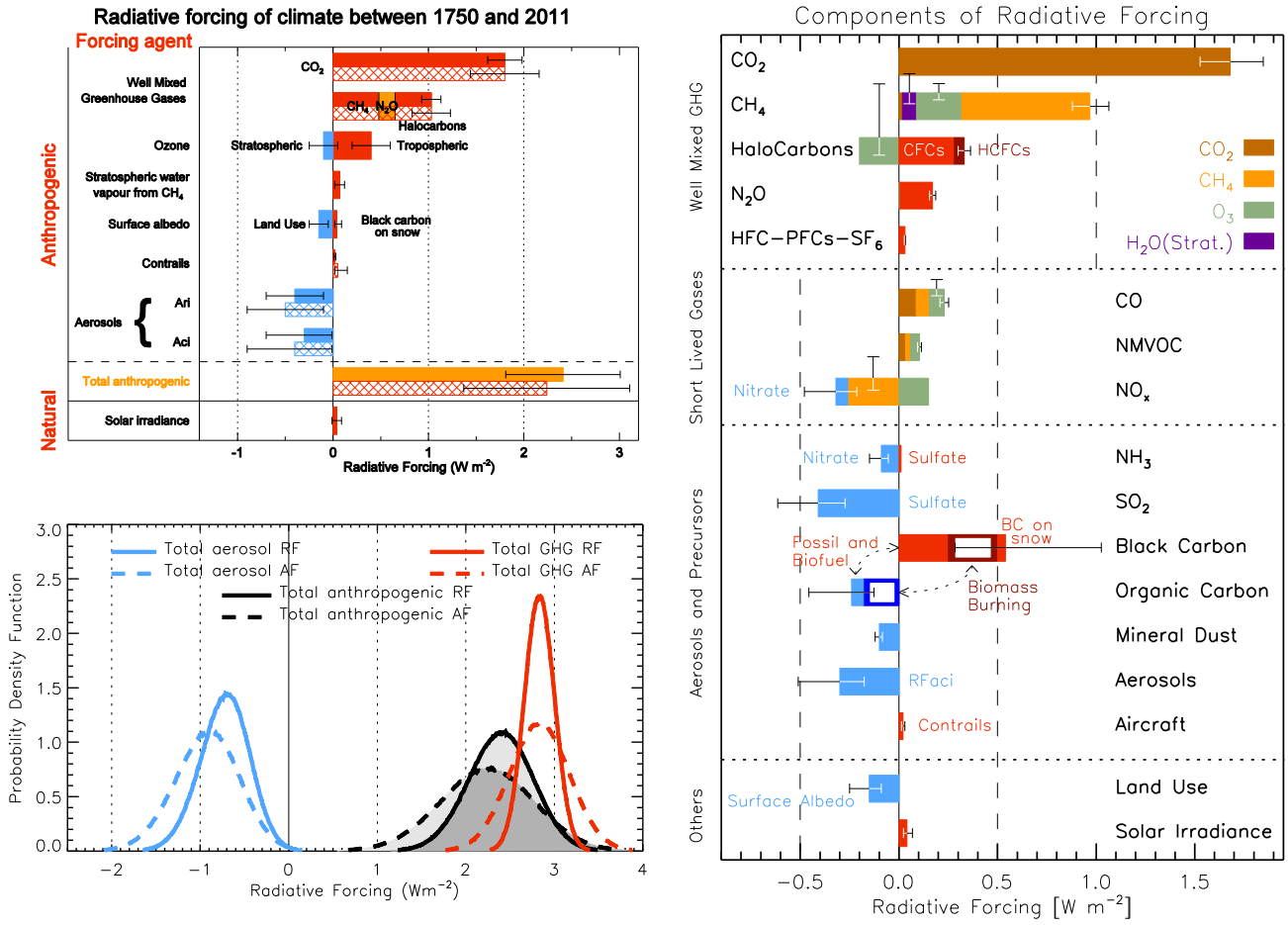

Figure 8.17: (a) Bar chart for RF (solid) and AF (hatched) for the period 1750–2011, where the total anthropogenic RF and AF are derived from panel b. (b) Probability density function (PDF) of total GHG RF, aerosol forcing, and total anthropogenic forcing. The GHG consists of WMGHG and ozone, and stratospheric water vapour. The PDFs are generated based on uncertainties provided in Table 8.7. The combination of the individual RF agents to derive total anthropogenic forcing are done by Monte Carlo simulations and based on the method in Boucher and Haywood (2001). PDF of the RF from surface albedo changes is included in the total anthropogenic forcing, but not shown as a separate PDF. The AF for GHG other than CO_2 and surface albedo change from land use change are assumed to be equal to their best estimate RF values, but with larger uncertainties. (c) RF bar chart based on emitted compounds (gases, aerosols or aerosol precursors) or other changes. Note that in this figure nitrate aerosols is only associated with NO_X emissions but ammonia (NH_3) is also important for the formation of this aerosol type. SOA has not been included since the formation depends on a variety of factors not currently sufficiently quantified.

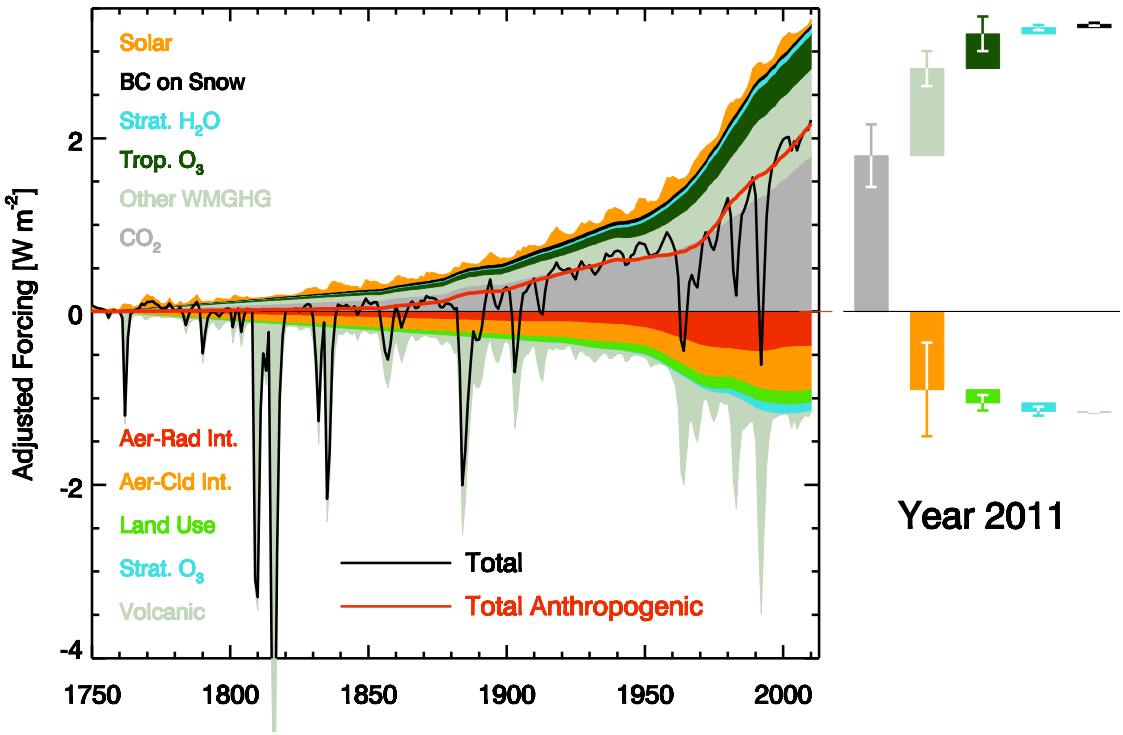

Figure 8.18: Time evolution of RF for anthropogenic and natural RF mechanisms. Bar with the RF estimate at present associated with uncertainty ranges are given to the right part of the figure. For aerosol the RF of aerosol-radiation interaction and total aerosol AF are shown.

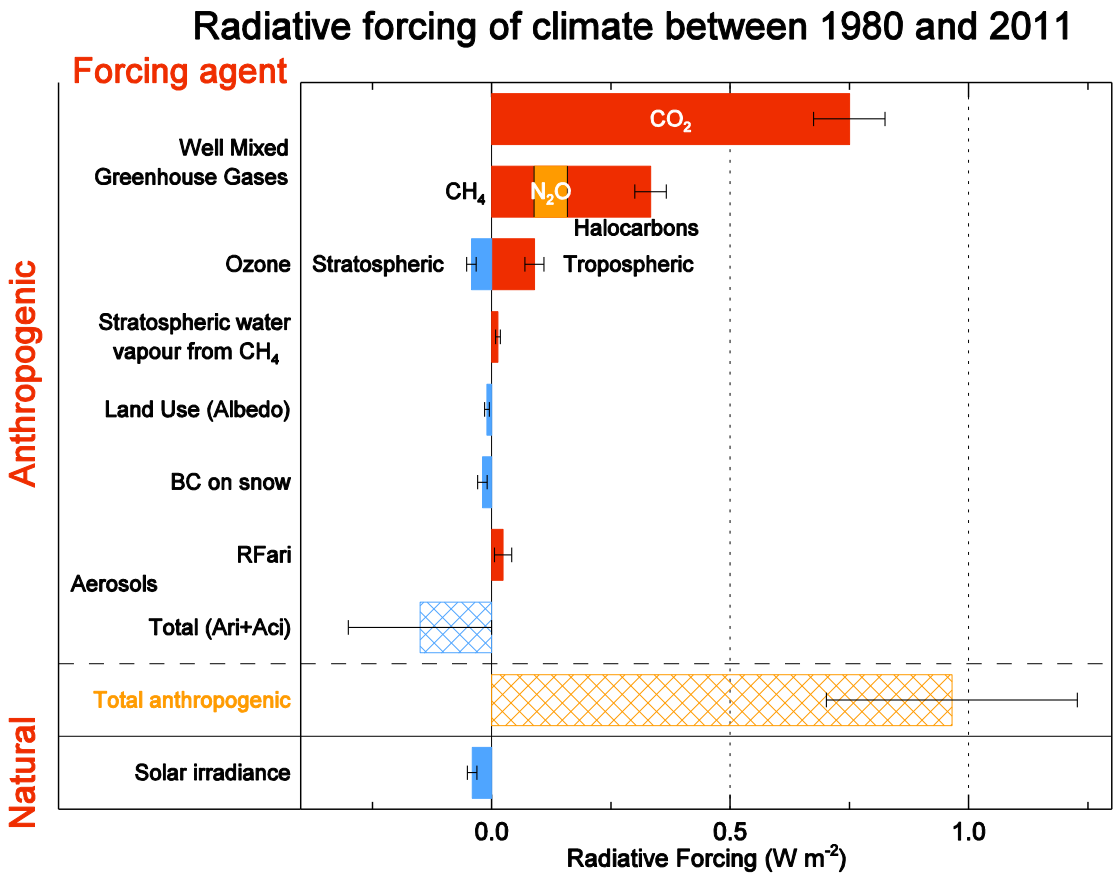

Figure 8.19: Bar chart for RF (solid) and AF (hatched) for the period 1980–2011, where the total anthropogenic AF are derived from Monte-Carlo simulations similar to Figure 17b. Total aerosol AF (ari + aci) is shown.

a)

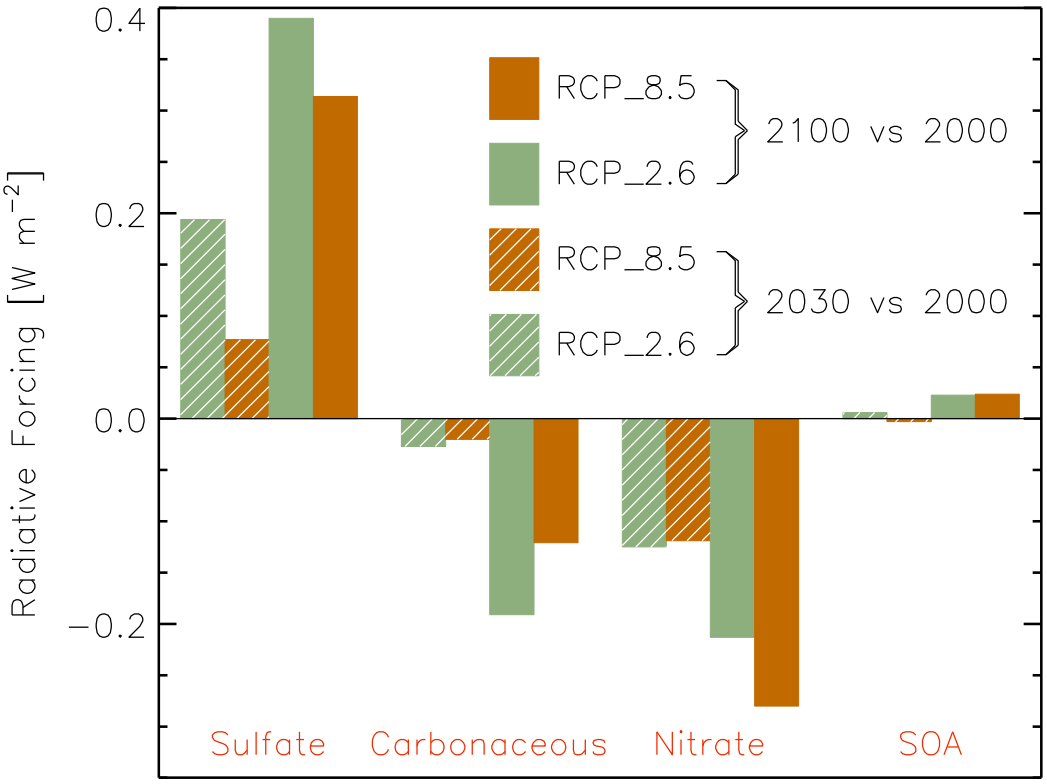

b)

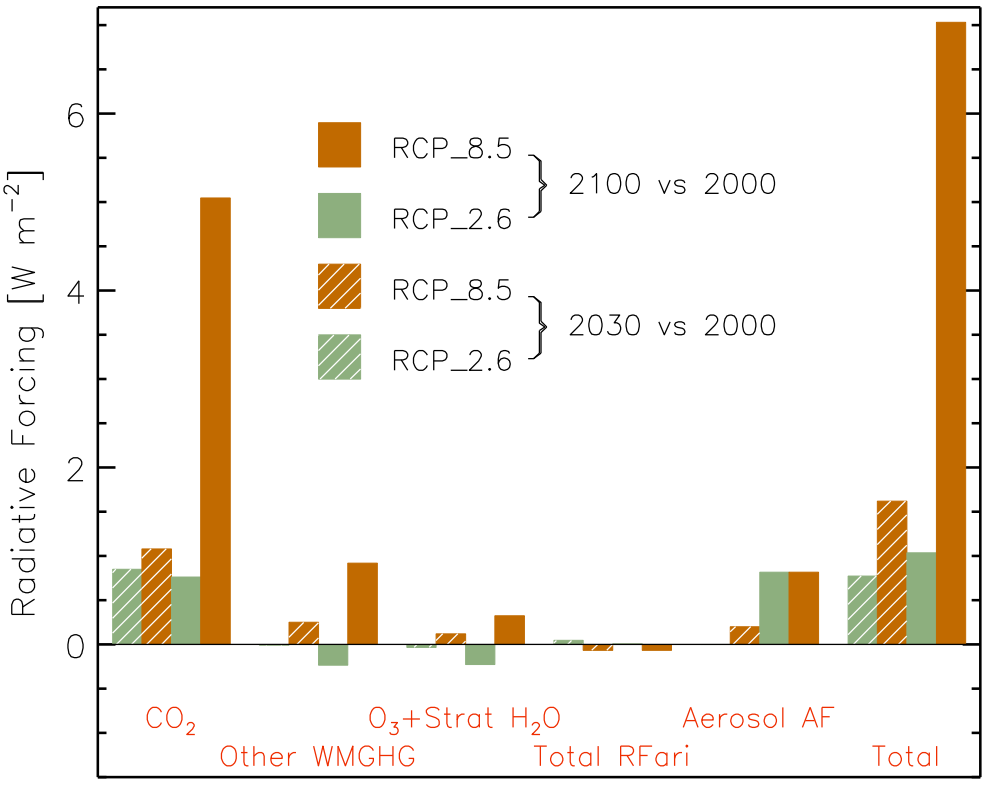

Figure 8.20: Radiative forcing relative to 2000 due to anthropogenic composition changes based on ACCMIP models for aerosols (with aerosol AF scaled to match the best estimate of present-day forcing) and total ozone and RCP WMGHG forcings. Ranges are one standard deviation in the ACCMIP models and assessed relative uncertainty for WMGHGs and stratospheric water vapor. Carbonaceous aerosols refers to primary carbonaceous, while SOA are secondary organic aerosols. Note that 2030 AF for RCP2.6 was not available, and hence the total shown for that scenario is not perfectly comparable to the other total values.

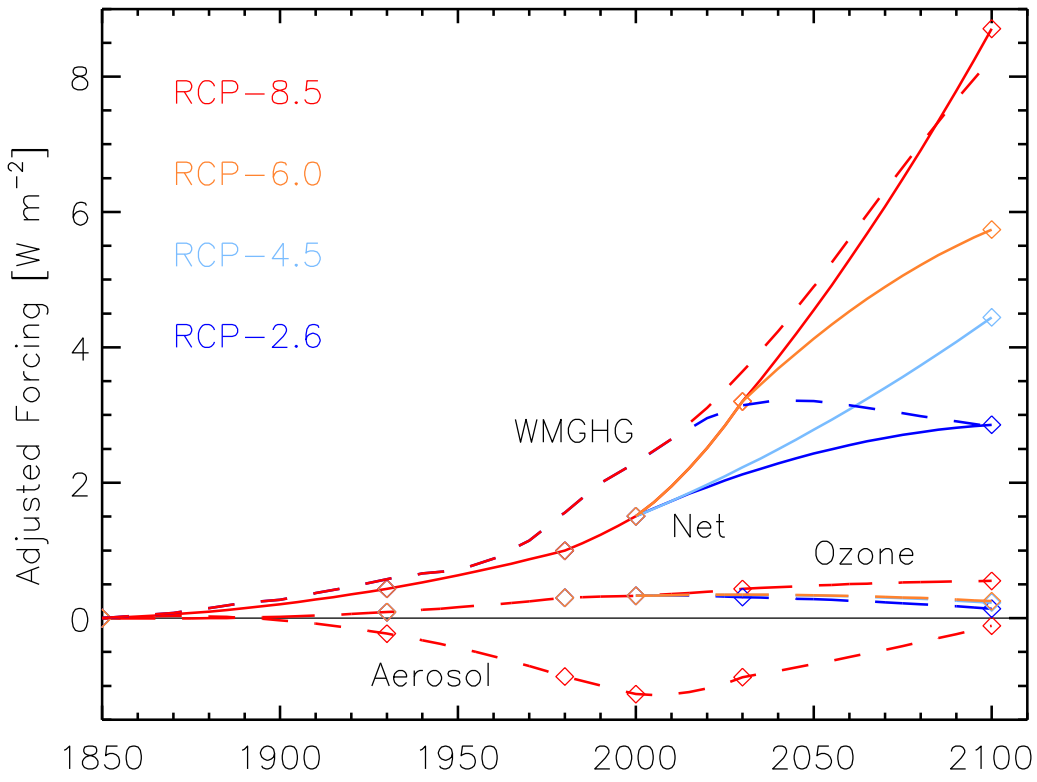

Figure 8.21: Global mean forcing with symbols indicating the times at which ACCMIP simulations were performed (solid lines with circles are net, long dashes with squares are ozone, short dashes with diamonds are aerosol, dash-dot are WMGHG, colors indicate the RCPs with red for RCP8.5, orange RCP6.0, light blue RCP4.5, and dark blue RCP2.6). RCPs 2.6, 4.5 and 6.0 net forcings at 2100 are approximate values using aerosol AF projected for RCP8.5 (modified from Shindell et al., 2012d).

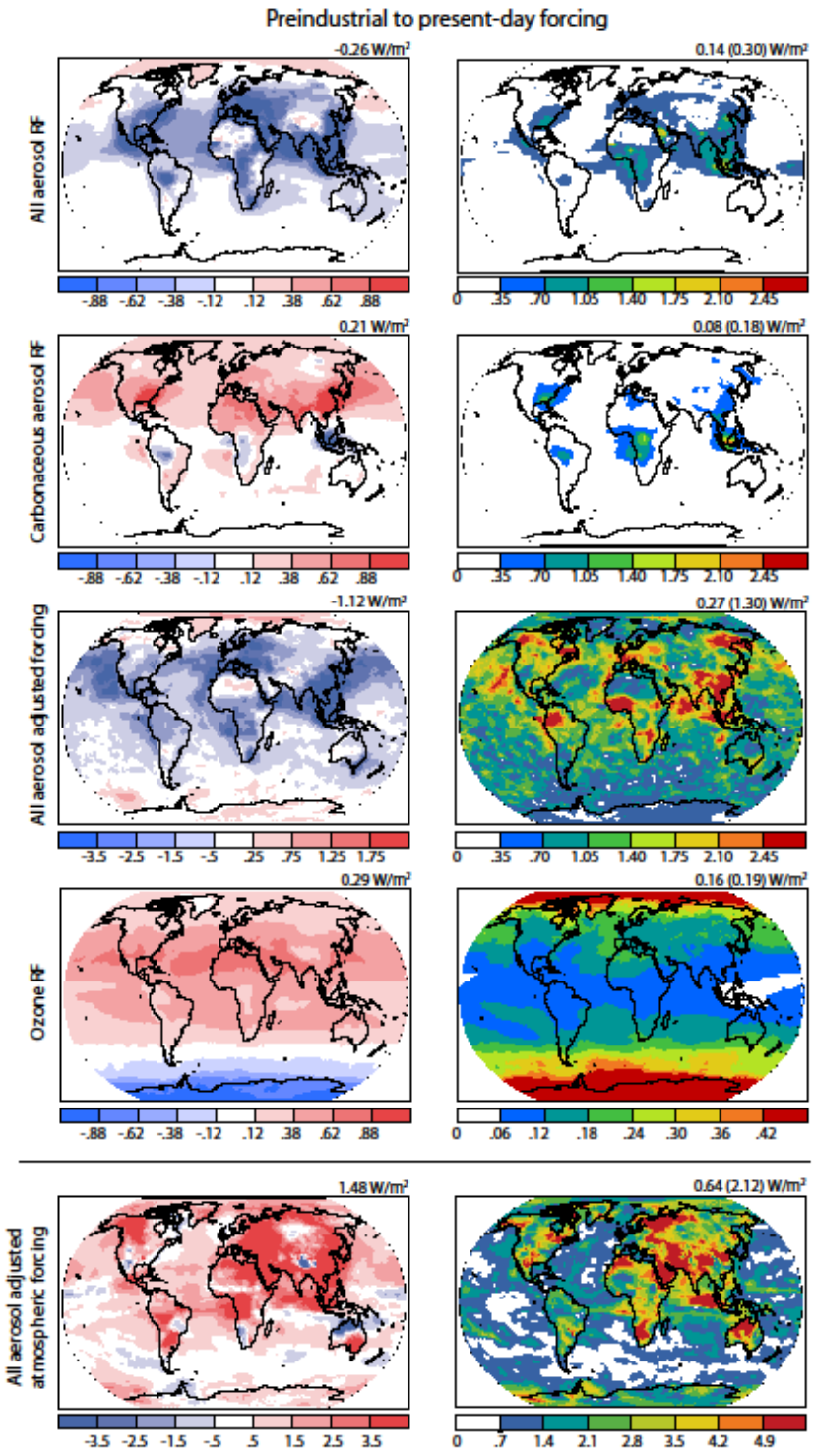

Figure 8.22: Spatial pattern of ACCMIP models preindustrial to present-day forcings, mean values (left) and standard deviation (right) for aerosols and ozone. Values above are the average of the model area-weighted global means, with the area weighted mean of the standard deviation of models at each point provided in parenthesis. Shown are net aerosol RF (top, 10 models), carbonaceous aerosol RF (2nd row, 7 models), net AF (3rd row, 8 models), ozone (4th row, 11 models), atmospheric absorption (bottom, 5 models). Note that RF and AF means are shown with different color scales, and standard deviation color scales vary among rows.

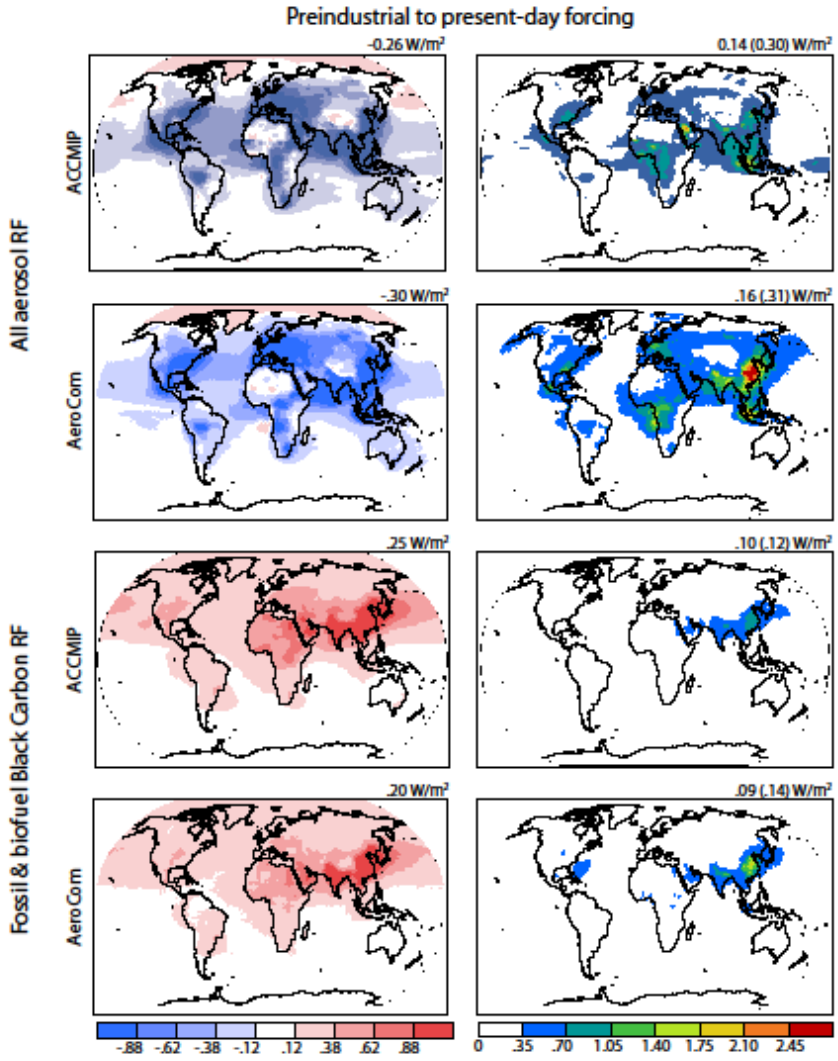

Figure 8.23: Spatial pattern of ACCMIP and 15 AeroCom models preindustrial to present-day RF, mean values (left) and standard deviation (right). Values above are the average of the model area-weighted global means, with the area weighted mean of the standard deviation of models at each point provided in parenthesis.

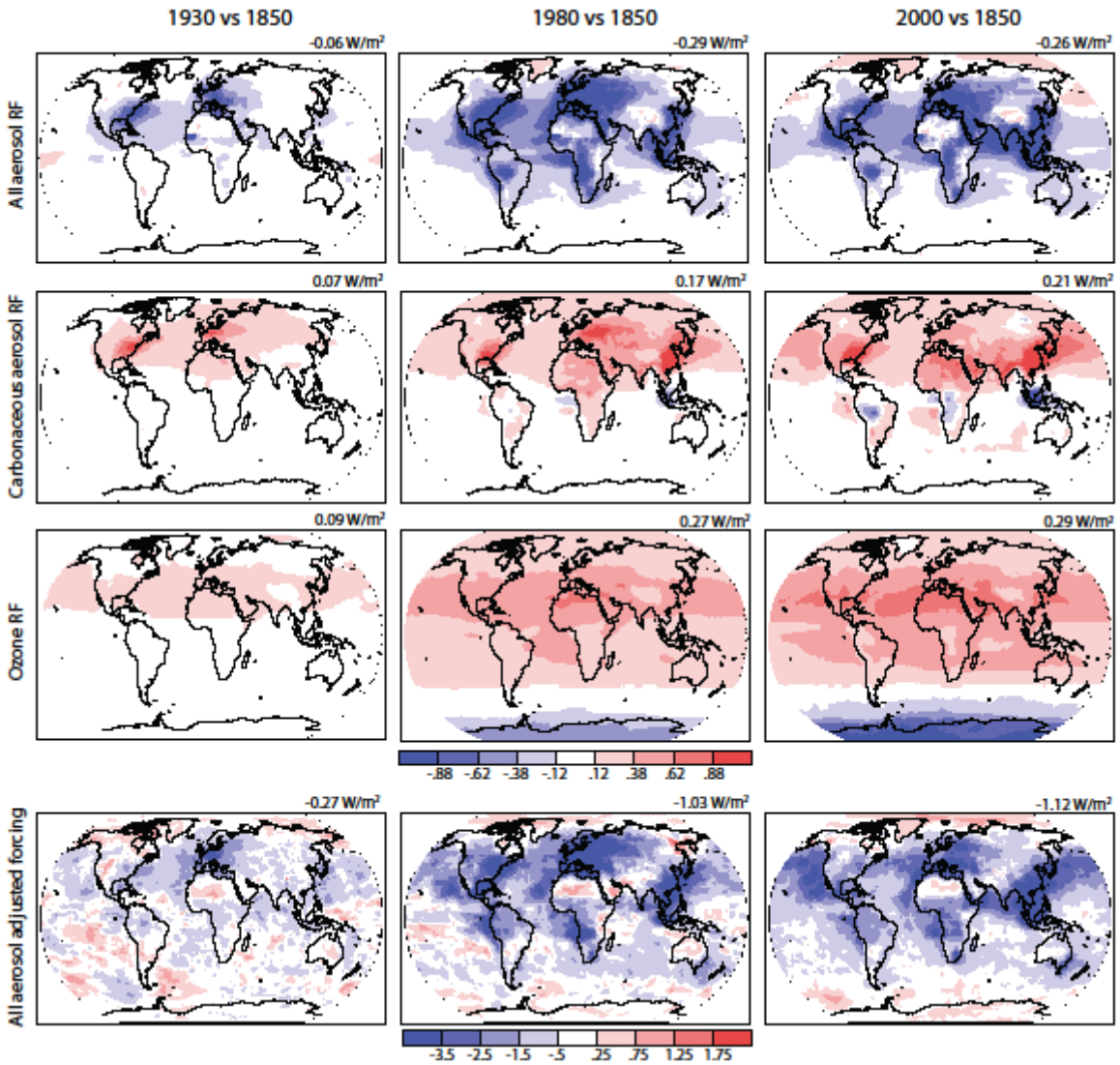

Figure 8.24: Multi-model mean direct effect (RFari) of all aerosols, carbonaceous aerosols, ozone, and aerosol AF (W m^{-2}) for the indicated times based on the ACCMIP simulations. Global area-weighted means are given in the upper right.

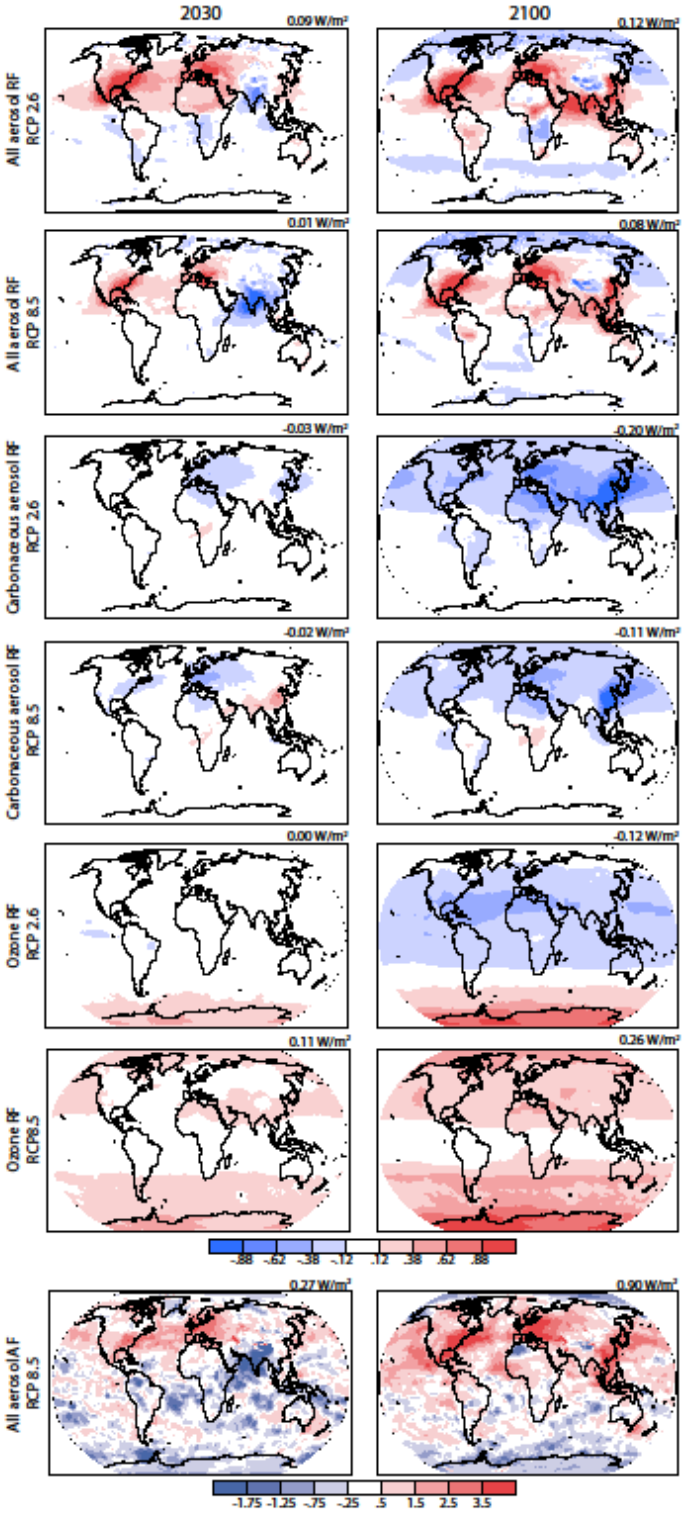

Figure 8.25: Multi-model mean RF (W m^{-2}) by the direct effect of all anthropogenic aerosols (first and second rows) and anthropogenic carbonaceous (BC+OC) aerosols (third and fourth rows), and total ozone (fifth and sixth rows) in 2030 (left) and 2100 (right) relative to 2000 for RCP2.6 (top each) and RCP8.5 (bottom each) based on the ACCMIP simulation. The seventh row shows multi-model mean AF (W m^{-2}) by all anthropogenic aerosols in 2030 (left) and 2100 (right) relative to 2000 for RCP8.5. Global area-weighted means are given in the upper right of each panel.

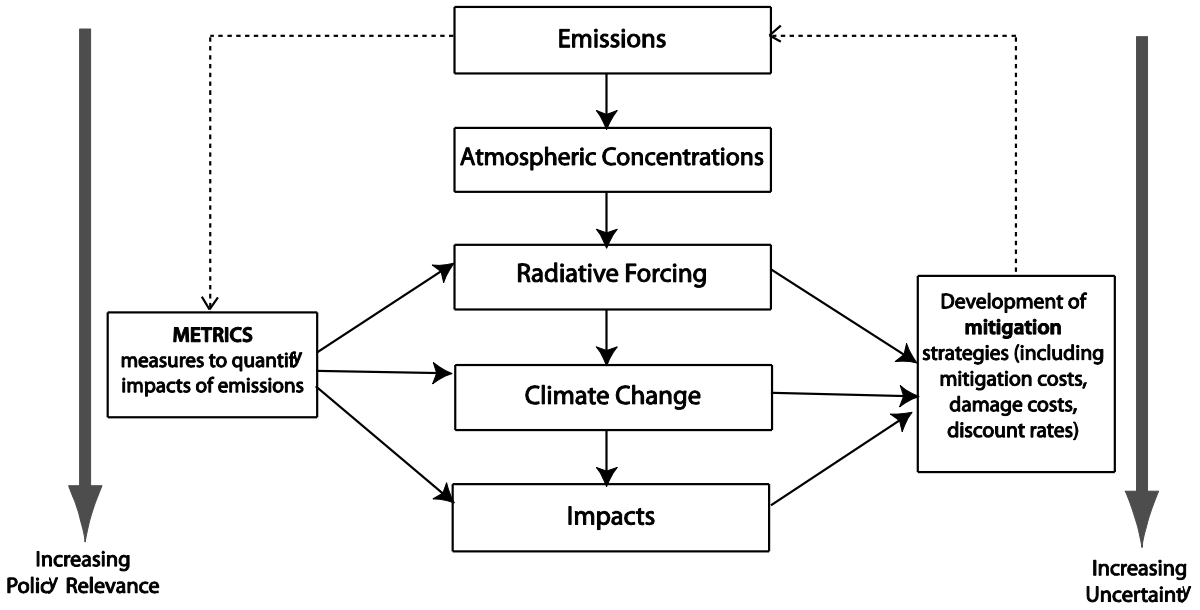

Figure 8.26: The cause-effect chain from emissions to climate change and impacts showing how metrics can be used to estimate responses to emissions (left side) and for development of multi-component mitigation (right side). Adapted from Fuglestvedt et al. (2003) and Plattner et al. (2009).

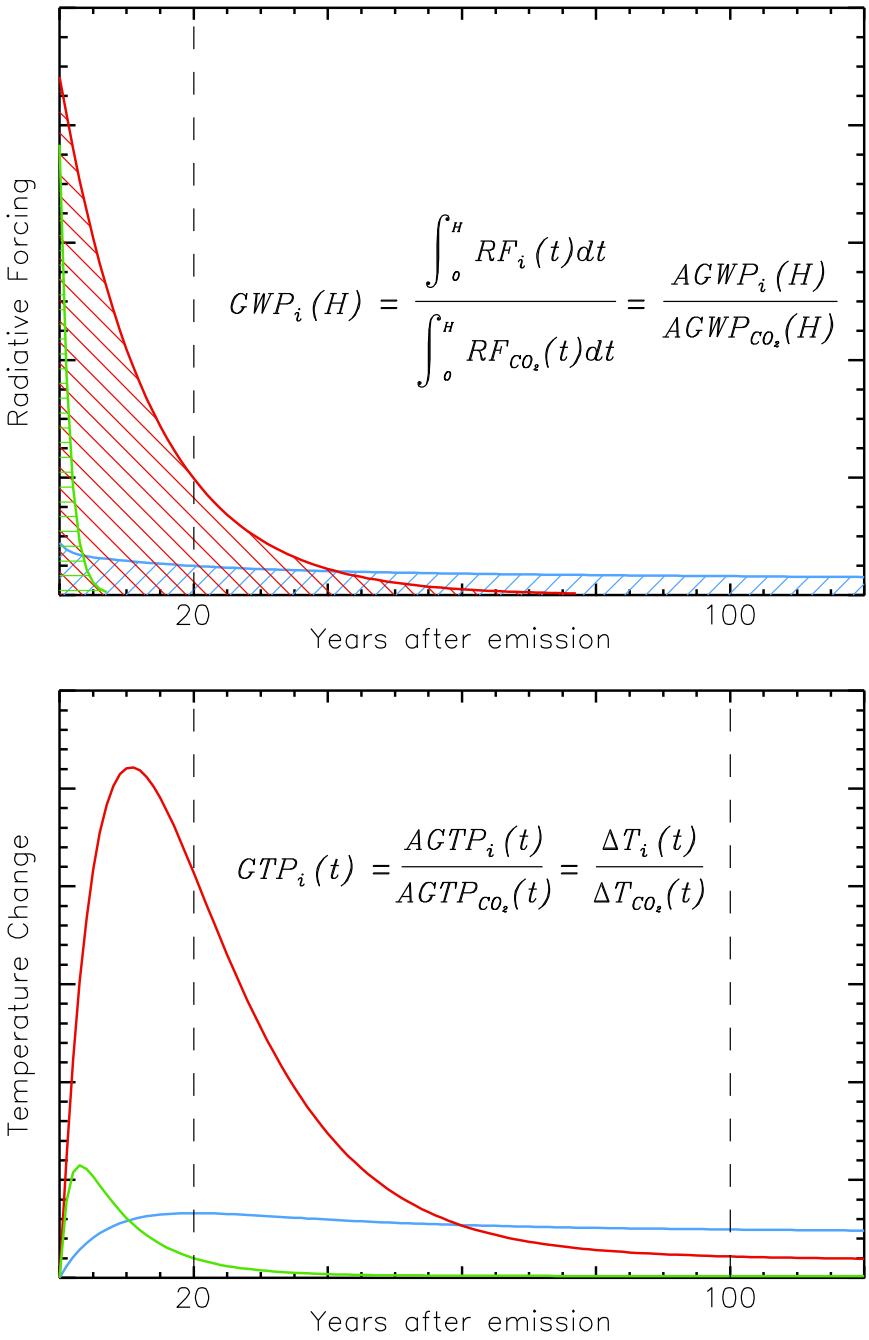

Figure 8.27: (a) The GWP is calculated by integrating the RF due to pulses over chosen time horizons; e.g., 20 and 100 years. The blue hatched field represents the integrated RF from a pulse of CO_2, while the green and red fields represent gases with 1.5 and 13 years lifetimes, respectively. (b) The GTP is based on the temperature response for selected years after emission; e.g., 20 or 100 years. See Supplementary Material for equations for calculations of GWP and GTP.

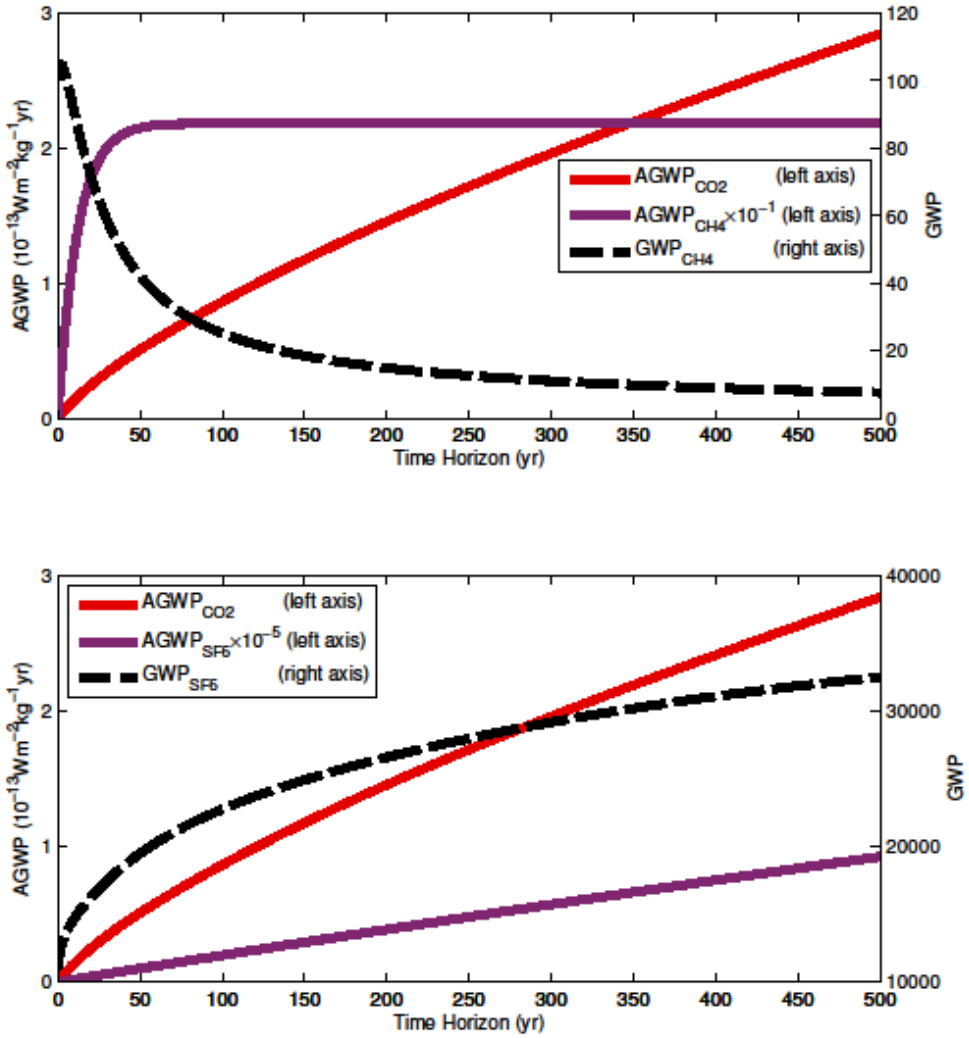

Figure 8.28: a) Development of AGWP-CO_2, AGWP-CH_4 and GWP-CH_4 with time horizon. b) Same but for SF_6.

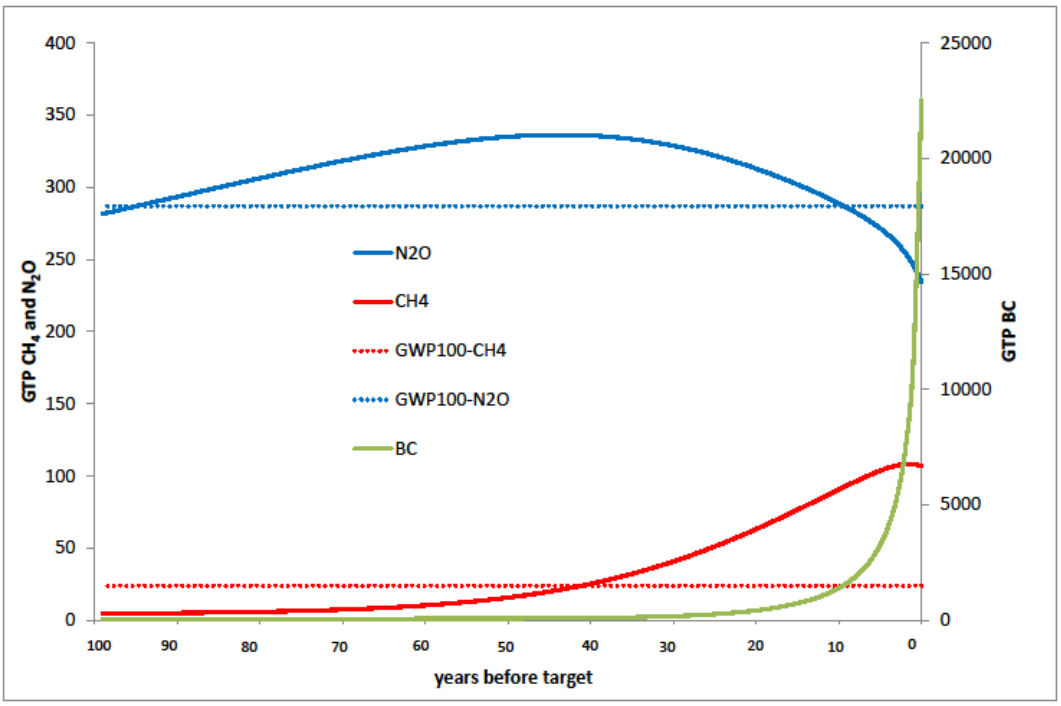

Figure 8.29: Global temperature change potential (GTP(t)) for methane, nitrous oxide and BC for each year from 2010 to the time at which the temperature change target is reached (2110). GTP(t) for CH_4 and N_2O on left axis; GTP(t) for BC on right axis. The (time-invariant) GWP_{100} is also shown for N_2O and CH_4 for comparison.

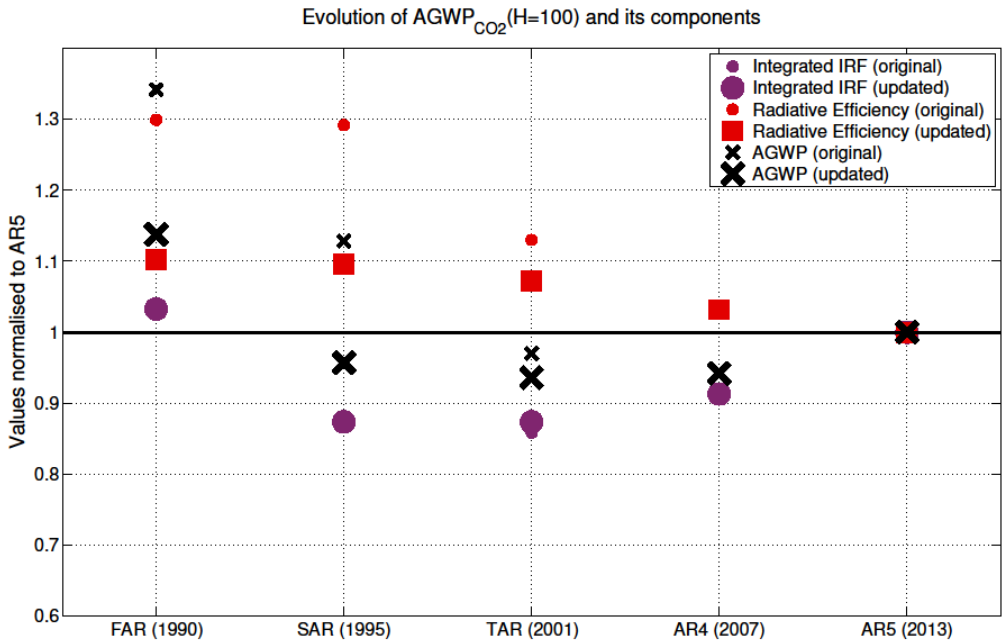

Figure 8.30: Changes in the radiative efficiency (RE), integrated IRF and AGWP for CO_2 from earlier IPCC Assessment Reports normalised relative to the values given in AR5. The 'original' values are calculated based on the methods explained in each IPCC Assessment Report. The 'updated' values are calculated based on the methods used in AR5. The difference is primarily in the RE, which has been updated in TAR and again in AR4. The different integrated IRF in TAR relates to a different parameterisation of the same IRF (WMO, 1999) . Changes represent both changes in scientific understanding and a changing background atmospheric CO_2 concentration (note that y-axis starts from 0.6).

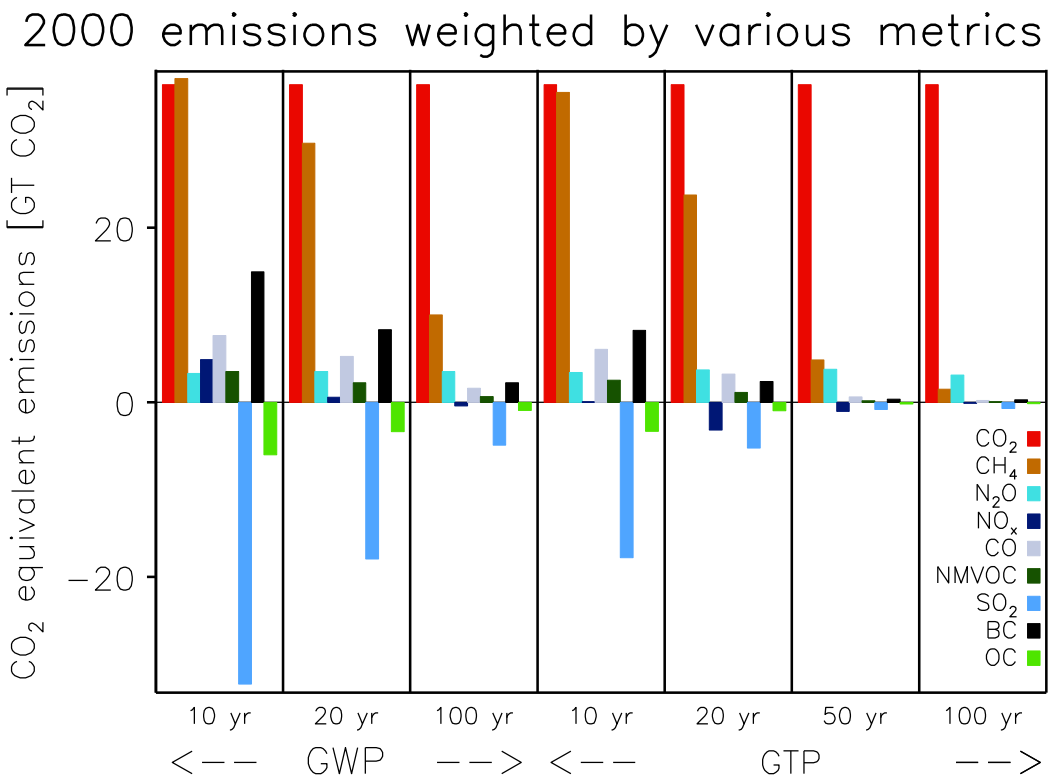

Figure 8.31: Global anthropogenic emissions weighted by GWP and GTP for chosen time horizons (aerosol cloud interactions are not included.) Emission data for 2008 are taken from the Edgar database and for BC and OC from Shindell et al. (2012b).

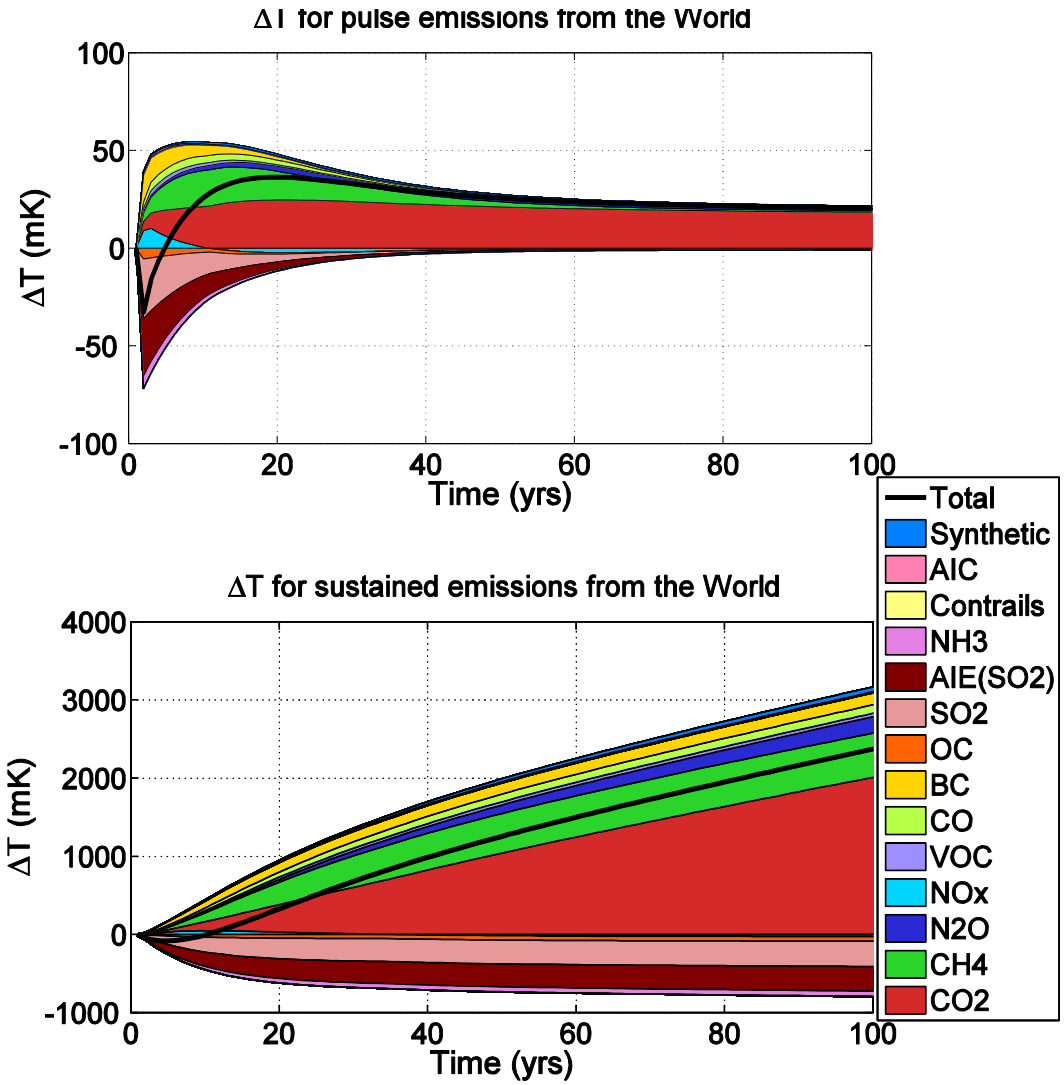

Figure 8.32: Temperature response by component for total man-made emissions for (a) a one-year pulse (year 2000) (upper) and (b) for emissions kept constant at 2000 level (lower). 'Synthetic' includes PFCs, HCFs, HCFCs, NF_3 and SF_6. Aerosol cloud interactions (AIE) are included. From Aamaas et al. (2012).

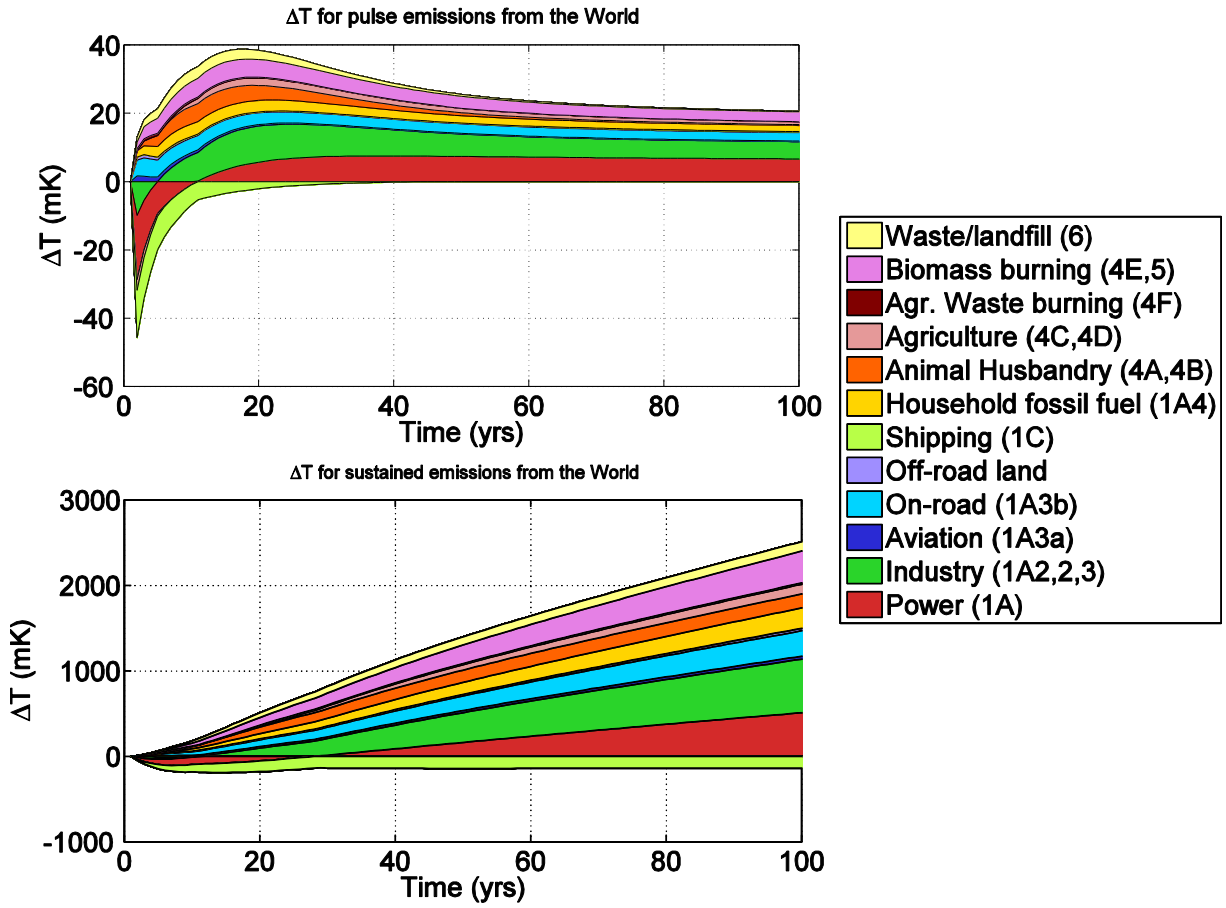

Figure 8.33: (a) Net global mean temperature change by sector from total man-made emissions (one year pulse); (b) Net global mean temperature change by sector from total man-made emissions kept constant. Aerosol cloud interactions (AIE) are included. From Aamaas et al. (2012).

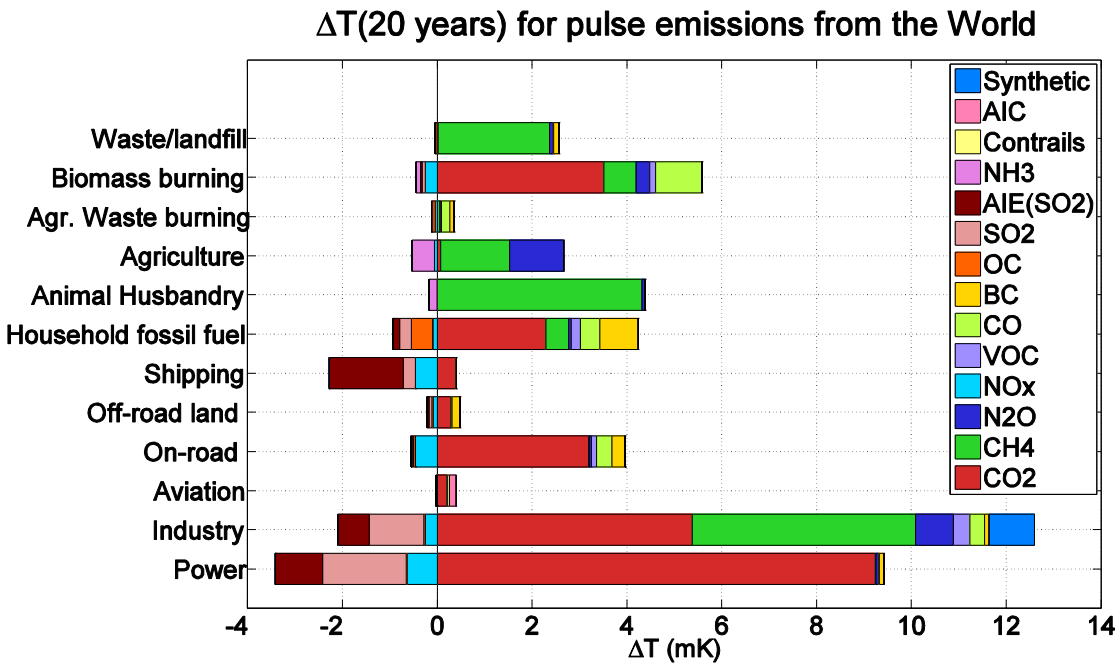

Figure 8.34: Net global mean temperature change by sector after 20 years (for one year pulse emissions). 'Synthetic' includes PFCs, HCFs, HCFCs, NF_3 and SF_6. Aerosol cloud interactions (AIE) are included. From Aamaas et al. (2012).

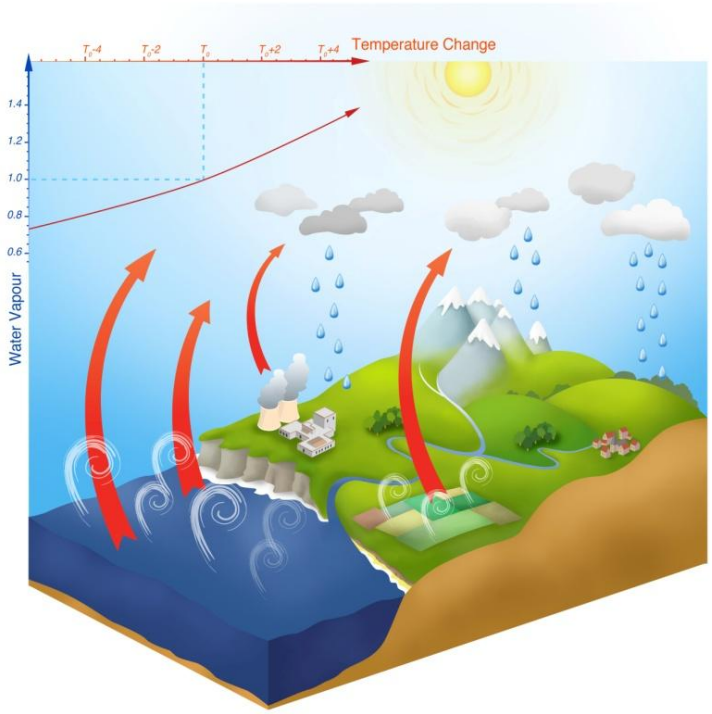

FAQ 8.1, Figure 1: Illustration of the water cycle and its interaction with the greenhouse effect. The upper-left insert indicates the increase of potential water vapour content in the air with an increase of temperature.

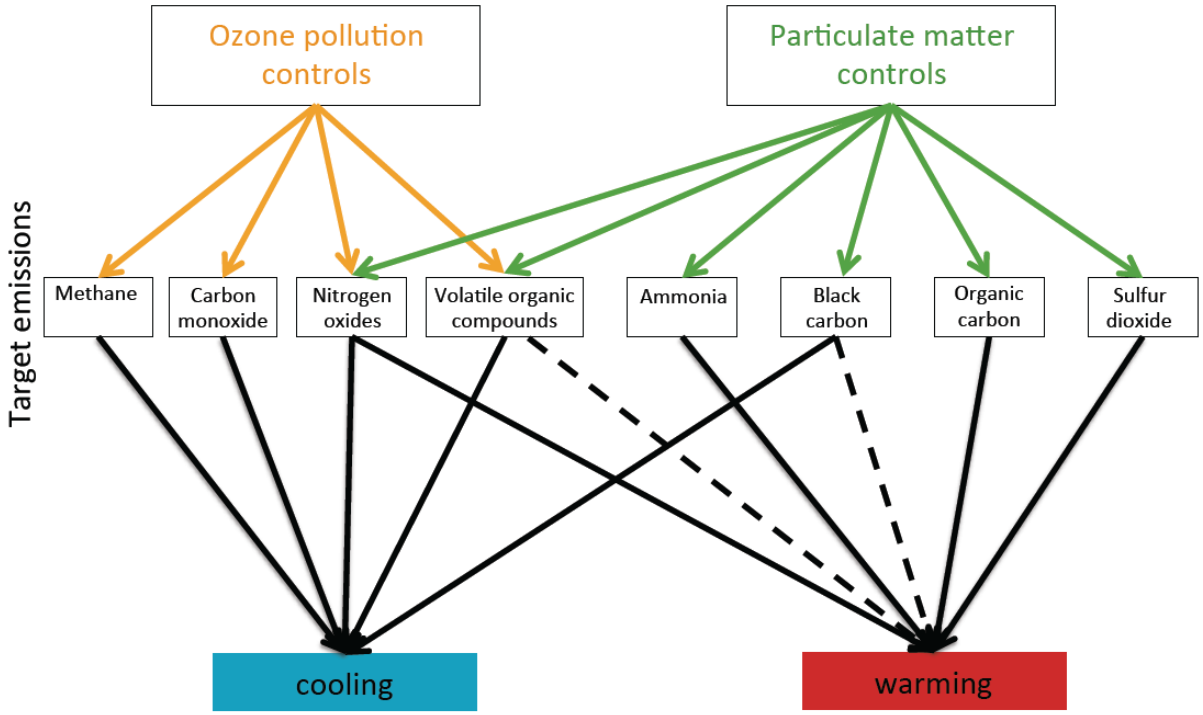

FAQ 8.2, Figure 1: Schematic diagram of the impact of pollution controls on specific emissions and climate impact. Solid black line indicates known impact, dashed line indicates uncertain impact.